2020

Design, Modeling and Optimization of Reciprocating Tubular Permanent Magnet Linear Generators for Free Piston Engine Applications

Jayaram Subramanian
West Virginia University, js0003@mix.wvu.edu

2020

Design, Modeling and Optimization of Reciprocating Tubular Permanent Magnet Linear Generators for Free Piston Engine Applications

Jayaram Subramanian

Design, Modeling and Optimization of Reciprocating Tubular Permanent Magnet Linear Generators for Free Piston Engine Applications

JAYARAM SUBRAMANIAN

Dissertation submitted to the
Benjamin M. Statler College of Engineering and Mineral Resources
At West Virginia University
in partial fulfillment of the requirements for the degree of
Doctor of Philosophy in Electrical Engineering

Parviz Famouri, PhD, Chair

Muhammad Choudhry, PhD

Dale Dzielski

Nigel N. Clark, PhD

Terence Musho, PhD

Lane Department of Computer Science and Electrical Engineering

Morgantown, West Virginia

2020

Keywords: Linear generator, Optimization, FEMM, Free piston engine, MATLAB GUI, Genetic algorithm, neural network

Abstract

Design, Modeling and Optimization of Reciprocating Tubular Permanent Magnet Linear Generators for Free Piston Engine Applications

Jayaram Subramanian

Permanent Magnet Linear Generators (PMLG) are electric generators which convert the linear motion into electricity. One of the applications of the PMLG system is with free piston engines. Here, the piston is moved by the expander using an internal combustion engine or a Stirling engine. Other applications of the PMLG are wave energy conversion, micro energy harvesters, and supercritical CO_2 expander systems. The most common technology of the electric generators is a rotary electric generator. The current technology of the engine-generators (GENSET) is of a rotary type which uses a crankshaft to convert the linear motion to rotary motion coupled to a rotary electric generator. This technology can be improved by using PMLG in the place of rotary generators by eliminating the crankshaft in the system.

This research thesis is to introduce a new design guideline and steps to design and optimize a PMLG for linear reciprocating applications. The new design guideline provides the steps and techniques to calculate the electrical and geometrical parameters of the PMLG system with experimental verification. A finite element (FE) model of the PMLG system was developed using Finite Element Method Magnetics (FEMM) software. Furthermore, two experimental prototypes of the reciprocating engine PMLG were constructed and tested. The results from the experimental prototype were compared with the FE model and errors less than 10 % were found.

One of the important aspects of the reciprocating free piston engines is to have a low moving mass of the translator to increase the frequency of the system. Therefore, using the FE model, sensitivity study of different geometric parameters such as the magnet thickness, outer diameter of the magnet, airgap, frequency, stroke length, turns, poles,

and spacer of the PMLG system was performed. It was found that the magnet thickness has a greater power / moving mass ratio compared to the other geometric parameters. Furthermore, an optimization routine was developed to optimize the PMLG system with low moving mass and low volume. Finally, a MATLAB GUI was developed for the optimization routine to simplify the process of optimization for new designers of the PMLG system.

To my Amma, Appa and Jayashri

Acknowledgements

I would like to sincerely thank my supervisor Dr.Parviz Famouri for spending his valuable time in guiding me through this research work. I would also like to acknowledge him for the detailed supervision, advice, ideas and words of encouragement which helped me complete the thesis.

I would like to thank the other members of my supervisory committee Dr.Nigel Clark, Dr.Terence Musho, Dr. Muhammad Choudhry and Mr.Dale Dzielski who have helped me throughout my thesis providing valuable suggestions and advice.

I would like to thank my lab members Mr. Mehar Bade, Mr. Greg Heiskell, Ms. Fereshteh Mahmudzadeh, Mr. Nima Zamani, Mr. Chris Ulishney, Mr. Mahdi Darzi and Mr. Al Yasin for helping me in the lab during this project.

I would to thank ARPA-E for funding this research project as a part of the GENSETS program.

I would like to thank my friends Irfan, Mehar, Hari, Saicharan, Harsha, Chandu, Utsav, Kashif, Sarojini for their continuous support throughout my degree.

Last but not the least I would like to thank my family members without whom this work never would have been possible.

Table of Contents

List of Figures

List of Tables

Abbreviations

ARPA – E – Advanced Research Project Agency

CFC - Chlorofluorocarbon

FE – Finite element

FEMM – Finite element method magnetics

FPE – Free piston engine

FPLG – Free piston engine linear generator

GA – Genetic algorithm

GENSET – Engine – generator set

GSA – Global sensitivity analysis

GUI – Graphical user interface

HCFC – Hydrochlorofluorocarbon

LG - Linear generator

LIG – Linear induction generator

LSRG – Linear switched reluctance generator

M – Moving mass of the translator

MFC – Mass flow controller

MOO – Multi objective optimization

MT – Magnet radial thickness

Mtoe – Millions of tonnes of oil equivalent

NdFeB – Neodymium iron boron

P – Output power

PMLG – Permanent magnet linear generator

OD – Outer diameter of the magnet

OAT – One at a time

SRG – Switched reluctance generator

WEC – Wave energy conversion

WSN – Wireless sensor networks

Nomenclature

F – Mechanical force (N),

$\dot{x}$ – Velocity (m/s),

v – Voltage (V), and

i – Current (A).

λ - Flux linkage

m_r – Rotor poles

H_m – Magnetic field intensity

B_g – Average airgap flux density

μ_o – Permeability of air

k_c – Carter's co-efficient

g – Airgap

k_s – Slot factor

B_{gmax} – Maximum airgap flux density

E_d – Energy density

E_g – Energy in the airgap

S – Rated output power

η – Efficiency

f_e – Rated frequency

V_{air} – Volume of air

D_s – Diameter of the stator

F_r – Rated force

u – Rated velocity

OD_m – Outer diameter of the magnet

ID_m – Inner diameter of the magnet

W_1 – Number of turns per phase

V_0 – Open circuit voltage

k_w – Winding factor

n_s – Number of turns per slot

I_r – Rated current

Vr – Rated voltage

A_{slot} – Area of the slot

K_{fill} – Fill factor

w_s – Width of the slot

h_s – Height of the slot

R_s – Resistance of the stator

L_M – Inductance of the stator

X_l – Inductive reactance

X_c – Capacitive reactance

I_l – Load current

V_l – Load voltage

S_i – Individual sobol index

S_{Ti} – Total sobol index

CHAPTER ONE

1 Introduction

Electricity consumption of the world is increasing every year. Based on a report by the British Petroleum company [1] in 2019, energy consumption has grown at a rate of 2.9% in 2018 which is almost twice the 10-year average of 1.5% per year. Furthermore, China, USA, and India have contributed to 2/3rd of the global increase in electricity consumption [1]. As of 2018, China consumes 3164 Mtoe (Millions of tonnes of oil equivalent) of energy, followed by the US – 2258 Mtoe, India – 929 Mtoe and Russia – 800 Mtoe [2]. These four countries consume 57.6% percentage of the overall energy consumption of the world. Figure 1-1 shows the energy consumption in total by regions.

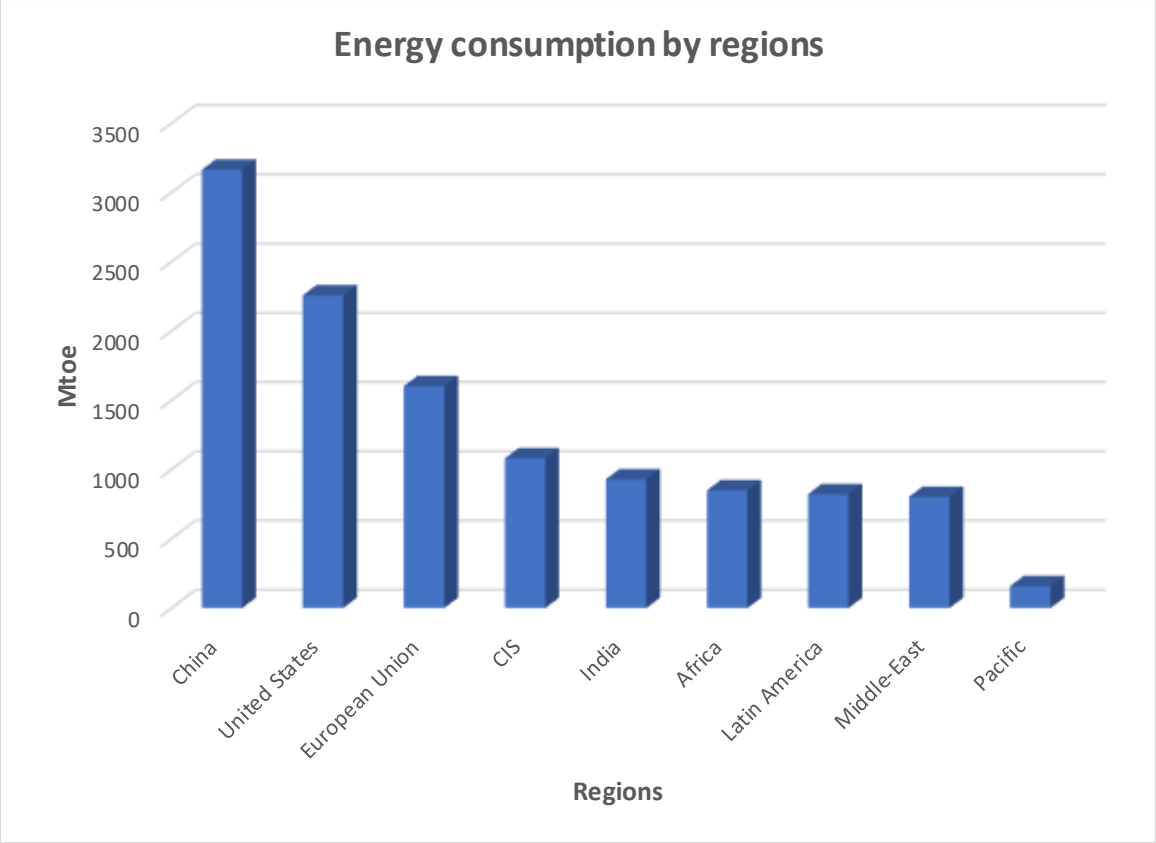

Figure 1-1 - Total energy consumption by regions (CIS refers to Kazakhstan, Russia, Ukraine and Uzbekistan).

Increasing demand for electricity increased the amount of greenhouse gas emissions. This, in turn, caused climate change with the global temperatures rising at an alarming level. Global average temperatures have increased by more than 1° C since the 1960s. The total global emission of CO_2 per year is 36 billion tonnes. China is the world's largest CO_2 emitter (> 25%) followed by US (15%), European Union (10%), India (7%) and Russia (5%) [3]. Figure 1-2 shows the contribution of CO_2 by countries between the years 1751 – 2017 [3]. Although there is a lot of development going on in renewable energy technologies, fossil fuels such as coal, natural gas, and oil remain the main source of energy for the world. Therefore, new technologies need to be developed to mitigate the effects of CO_2 emissions, increase energy production and increase the efficiencies of the existing energy systems.

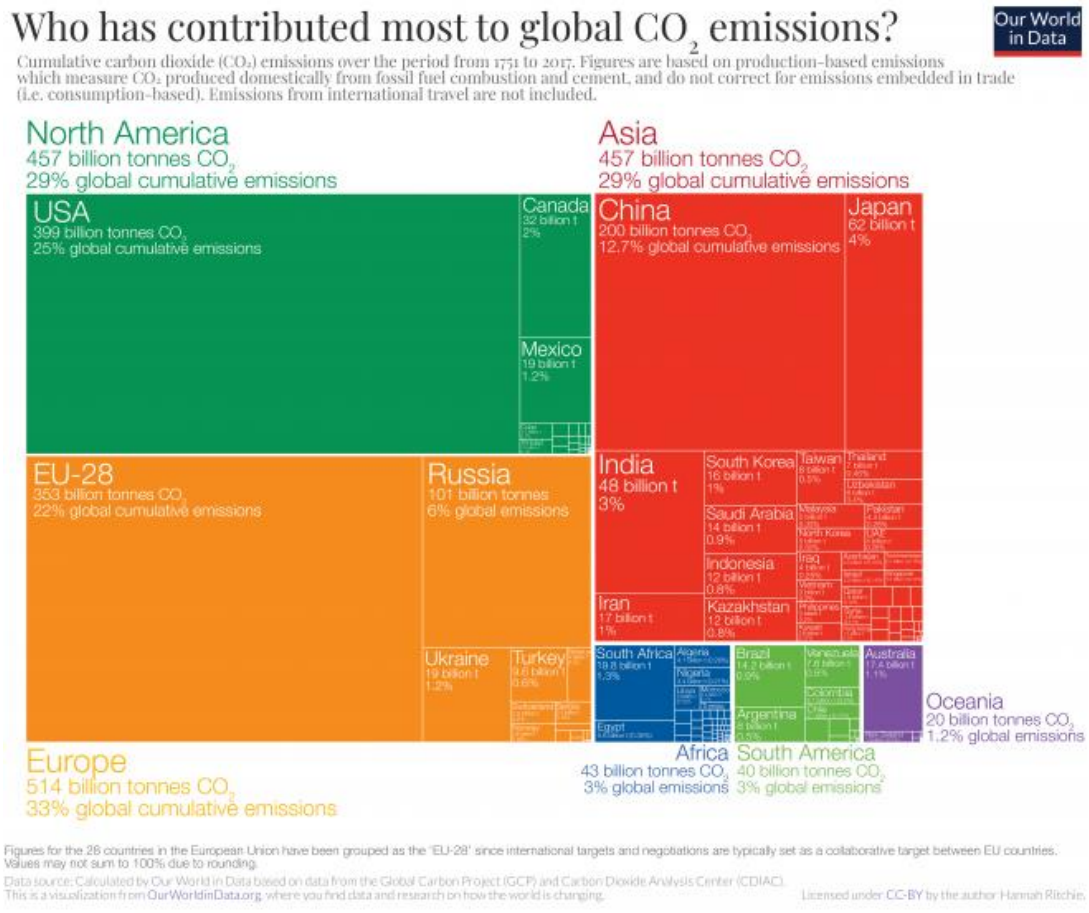

Figure 1-2 - Contribution of CO_2 emissions [3] by different countries.

One of the methods of generating electricity from fossil fuels is through an electrical generator. Electrical generators, in general, refer to rotary electric generators. Rotary electric generators are those which convert rotary motion (rotational energy) into electricity. Rotary electric generators are popular because the technology is mature (over a hundred years of research and development) and has been widely accepted by the industries. On the other hand, there is another type of electrical generator called linear generators. Linear generators are electric generators that convert the energy produced by the linear thrust force into electricity. Linear generators offer unique opportunities in terms of the utilization of renewable energy sources as well as efficient energy technologies. Some of the applications of a linear generator are 1) Free piston engines 2) Wave energy 3) Range extenders in hybrid vehicles 4) Micro-energy harvesters and 5) Supercritical CO_2 expanders.

Rotary electric generators are currently used in engine-generators (GENSET) for various applications, however primarily for backup electric power. These generators use combustion engines to convert gasoline/other fuels into electricity. The engine used for this purpose is an internal combustion engine. These engines provide a linear thrust force when the fuels combust. This linear force is converted into a rotational force by a crankshaft mechanism in crankshaft housing. Once the linear force is converted to a rotary motion, the energy is transferred to the rotary electric generators and electricity is produced. If the linear force can be directly converted to electricity, the efficiency of the GENSET can be improved by eliminating additional conversion processes with reduction in total volume. One way to do that is to use the linear generators since they require a linear thrust force to operate and produce electricity. Therefore, linear generators are advantageous in applications where the energy produced by the linear thrust force needs to be converted to electricity compared to rotary electric generators. This is shown in Figure 1-3.

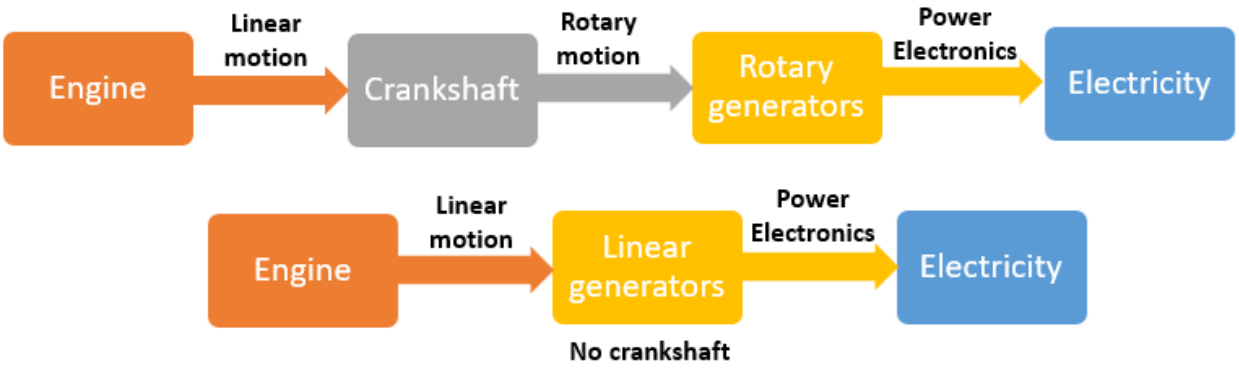

Figure 1-3 - Difference between rotary and linear electric generators in a GENSET system.

Research on linear generators has been increasing, as can be seen from papers published in IEEE Xplore™ from 1960 - 2017. Figure 1-4 shows the growing interest in linear generators.

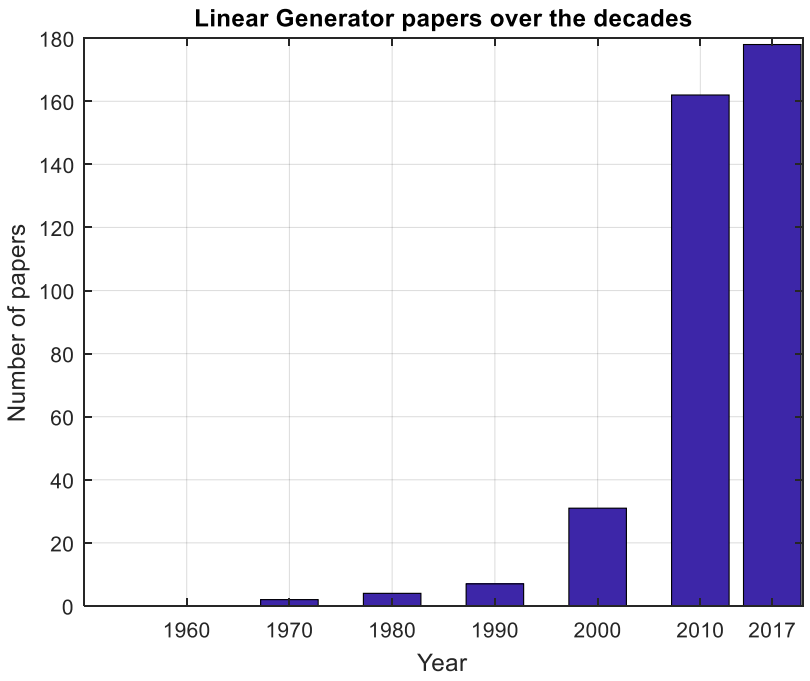

Figure 1-4 - Linear generator papers published over the decades in IEEE Xplore™.

Both rotary and linear generators work on the principle of electromechanical energy conversion. When electrical energy is converted to mechanical energy (rotary or linear), it is called as an electrical motor. When mechanical energy is converted to electrical

energy it is called an electrical generator. The energy conversion equation for a linear electrical generator is shown in equation (1-1).

$$F.\dot{x} = vi \tag{1-1}$$

where,

F – Mechanical force (N),

$\dot{x}$ – Velocity (m/s),

v – Voltage (V), and

i – Current (A).

The linear generator, in general, can be understood as a rotary generator whose stator and rotor are cut along its axis and rolled down into a sheet as shown in Figure 1-5.

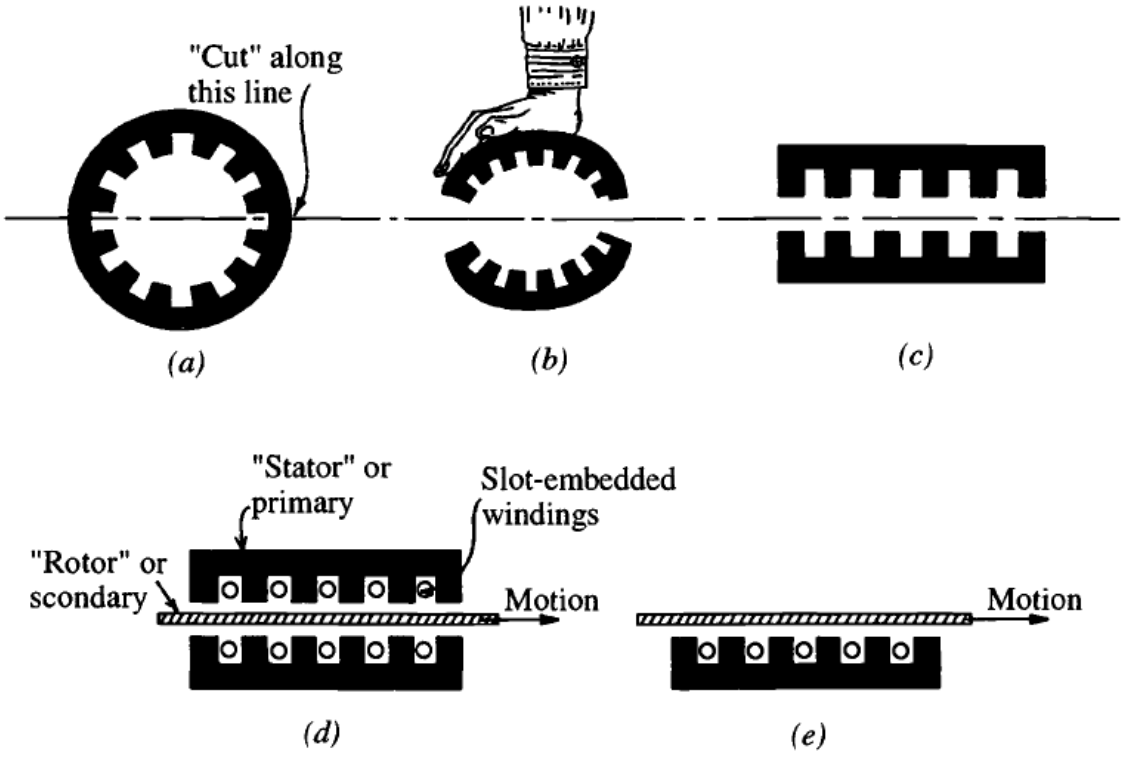

Figure 1-5 - Conversion of rotary generator to linear generator [4].

Linear generators work similar to rotary generators and operate on the principle of Faraday's law of electromagnetic induction as shown below in equation (1-2).

$$e = \frac{d\lambda}{dt} \quad (1\text{-}2)$$

Voltage (e) is induced in a coil if the flux linkage λ varies with time t.

The main objective of this dissertation research is to design, model and optimize a 1 kW tubular permanent magnet linear generator (PMLG) for free piston engine applications. Furthermore, research is focused specifically on reducing the moving mass and increasing the power density of the PMLG system.

Four sub-objectives of this research are,

1. Develop a design guideline for a single phase PMLG system,
2. Develop a finite element model and validate it with the experimental prototype built at West Virginia University,
3. Sensitivity study of the geometric parameters of the PMLG system, and
4. Optimization of the PMLG system for low moving mass of the translator and low volume of the overall system.

The outline of the dissertation is given below.

Chapter 2 deals with the literature review of different classifications of the linear generators. Following that, concepts and properties specific to linear generators were discussed. Later different applications of the linear generator were discussed in detail.

Chapter 3 discusses the design guideline for a single phase PMLG system. The equation and steps involved in calculating the geometric and electrical parameters of the PMLG were provided. In addition, a MATLAB GUI was developed to simplify the process of designing a PMLG system. Based on this design guideline, linear generators of 0.5 kW, 1 kW, 1.5 kW, and 2 kW sizes were designed.

Chapter 4 involves the finite element modeling and experimental validation of the PMLG system. Procedures involved in modeling in Finite Element Method Magnetics (FEMM) software were discussed in detail. Subsequently, the results from FEMM were compared with the experimental prototype of the PMLG system built at West Virginia University.

Chapter 5 discusses the sensitivity study of the PMLG system. Parameters such as neutral position, magnetic flux arrangement, magnet thickness, outer diameter of stator, airgap, oscillating frequency, stroke length, number of poles, and number of turns were studied over a wide spatial range of 0.5 – 2.5 kW PMLG system. The sensitivity analysis was done to investigate the effects of the different geometric parameters of the PMLG system. This study helped to identify the important parameters affecting the PMLG system.

Chapter 6 discusses the methods to optimize the PMLG system based on user specifications. Optimization was done to design the PMLG based on two criteria - 1) Power / Weight ratio 2) Power/ Volume ratio. Using these criteria, PMLG for 0.5 kW, 1 kW, 1.5 kW, and 2 kW was developed. Later a MATLAB GUI was developed to make the optimization procedure simple for future designers. The details on the optimization and the techniques used were discussed in detail in this chapter.

Chapter 7 provides the conclusion and future scope of this research. Discussion on the improvement of the design of the PMLG prototype was proposed. Furthermore, the methods to improve the finite element modeling of the PMLG system was provided.

CHAPTER TWO

2 Literature Review

Classification of linear generators, their applications and important characteristics unique to linear generators are discussed in this chapter.

2.1 Classification of linear generators

Linear generators can be classified based on major types, phase, different configurations, magnet shapes (for PMLG), stator core and overall shape of the system. The detailed classification of linear generators is shown in Figure 2-1.

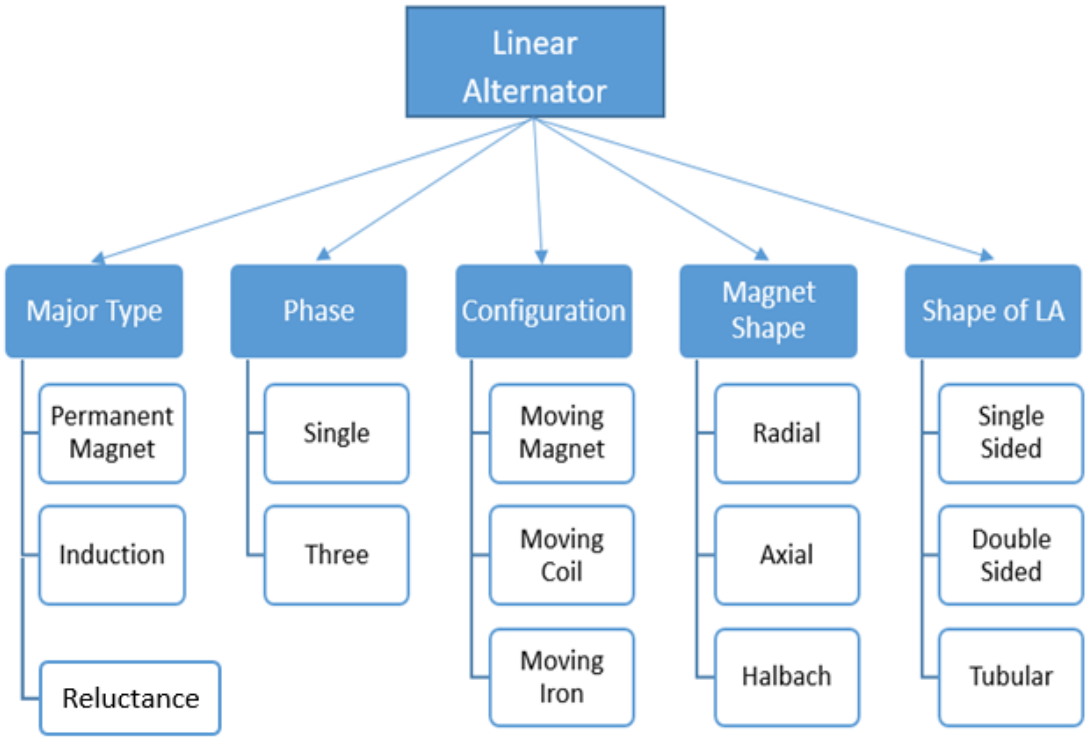

Figure 2-1 - Classification of linear generators.

From Figure 2-1, it is seen that some of the classifications of linear generators are similar to a rotary generator. Major type, phase, configuration and magnet shape are classifications similar to rotary generators (in case of PM machines).

2.2 Major Type

Linear generators are classified into three major types.

1. Permanent Magnet Linear Generator (PMLG)
2. Linear Induction Generator (LIG)
3. Linear Switched Reluctance Generator (LSRG)

2.2.1 Permanent Magnet Linear Generator (PMLG)

A permanent magnet linear generator is similar to a permanent magnet rotary generator. PMLG usually consists of a stator that is made up of copper windings and laminations. Laminations are used to reduce eddy currents losses in electric machines. The translator is made up of permanent magnets. These magnets may be either rings/cylinders/rectangular bars depending on the configuration of the PMLG system. In general, high-energy product rare earth permanent magnets are used in PMLG. They have large remnant flux densities B_r and large coercive forces H_c. Examples of some of the B-H (Magnetic flux density – Magnetic field intensity) characteristics of rare-earth magnets are shown in Figure 2-2. Details on different parameters of commercially available rare-earth magnets are attached in the Appendix. PMLG is one of the widely used linear generators both in research and development of different systems utilizing energy stored during the linear motion to convert to electricity. PMLG is being researched for applications such as wave energy conversion, Stirling engines, free-piston engines, micro energy harvesters, and supercritical CO_2 expanders.

A large body of research is being conducted on PMLG because of the following advantages.

1. High Efficiency (90% and higher) [5],
2. Small air gap compared to LIG and LSRG,
3. No external magnetization for the translator, and
4. Small size [6, 7].

Some of the disadvantages of PMLG are,

1. Magnet can be demagnetized because of thermal effects [8],
2. Cogging force in iron-core machines [9],
3. Cost and availability of high energy-dense (rare-earth) magnets [10], and
4. Stray magnetic fields especially in single-sided configurations.

PMLG has been discussed in detail in sections 2.4, 2.5 and 2.6.

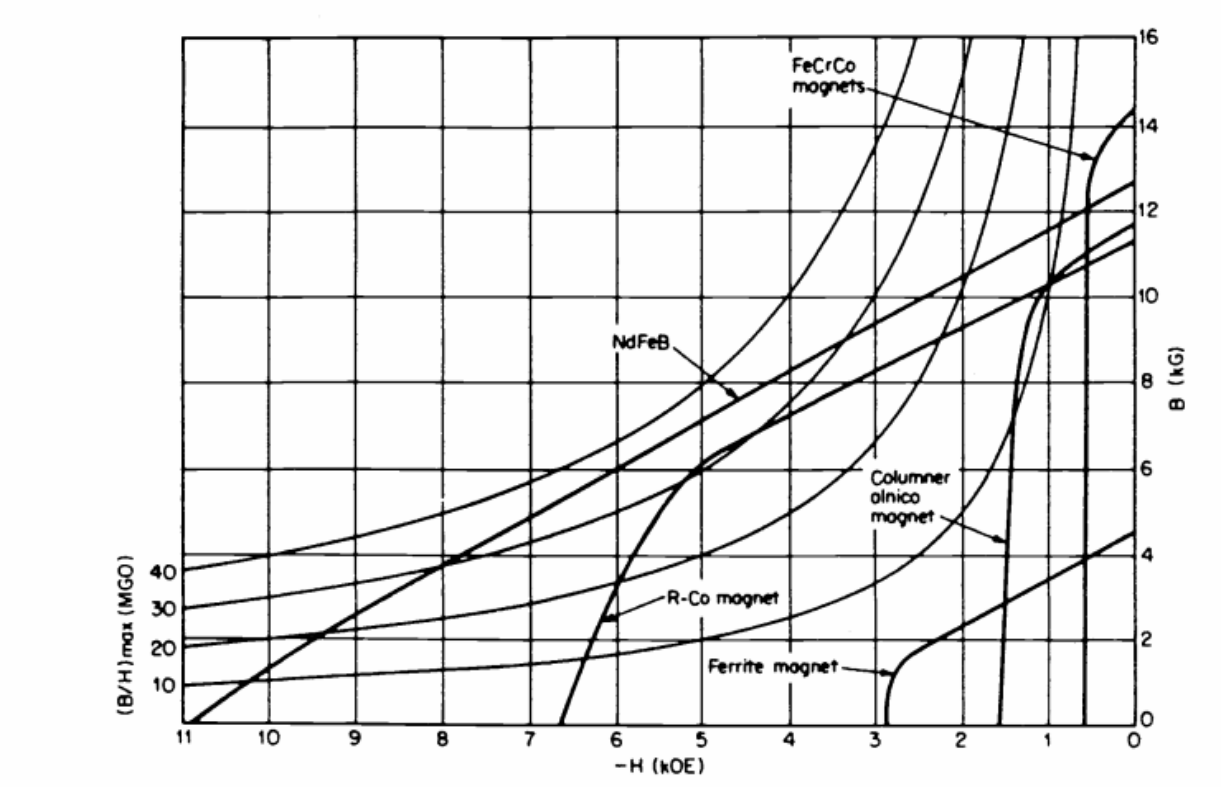

Figure 2-2 – B-H for different magnet materials [5].

2.2.2 Linear Induction Generator (LIG)

PMLG has been widely researched and studied while LIG has not been focused much by the researchers and the industry. Linear induction machines, in general, are widely used as a motor rather than a generator. Because of its high velocity, it is widely used in industrial robots and rapid launchers [11, 12]. LIG has advantages such as low maintenance cost, rigid structure, easy construction, and no cogging force. Unlike PMLG, LIG does not have magnets hence they do not have the problem of demagnetization and armature reaction at heavy loads.

Construction of LIG is similar to rotary induction generators. Conventional configurations of LIG consists of a conducting plate on solid iron as the secondary / translator. Some configurations of LIG consists of only conducting plates as the secondary / translator. Primary or the stator consists of single / three-phase windings. Laminated cores are used in the stator to reduce core losses. In LIG, the air gap needs to be small to obtain larger airgap flux density. Figure 2-3 shows a flat linear induction generator. The LIG shown in the figure consists of a conducting plate that moves with a velocity (u) and a primary/stator with coils.

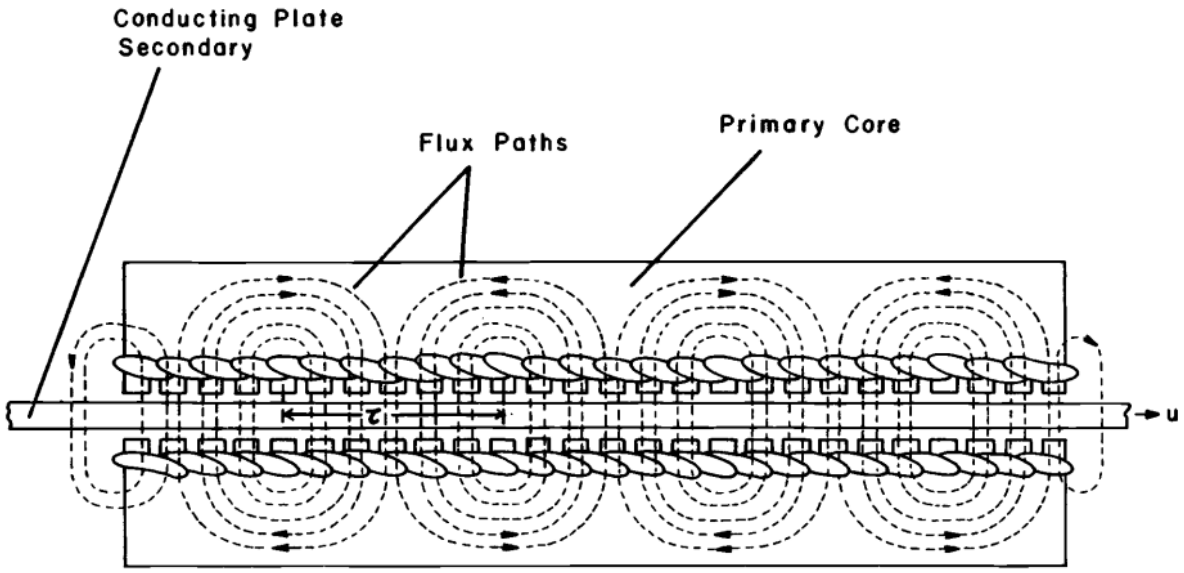

Figure 2-3 – Configuration of a flat linear induction generator [13].

Induction machine when driven mechanically will deliver electric power when the speed goes beyond the synchronous speed. This phenomenon is known since the 1900s. When an external mechanical force is applied to an induction machine, it operates as a generator if a reactive power source is available for the machine's excitation. This can be achieved by using a capacitor bank with appropriate capacitance. Linear induction machines operate in the same way as rotary induction machines and therefore when there is a suitable capacitor to provide self-excitation, the machine can operate as a generator. This process of utilizing a capacitor to self-excite has been discussed in [14]. This paper [14] provides details on modeling and experimental validation of a linear

induction generator. Finite element modeling was performed to model the linear induction generator. The application of the proposed LIG was for wave energy conversion system. Hence modeling and simulations were conducted keeping wave energy conversion parameters in mind. The LIG system used in this study consisted of 90 turns per coil, stator diameter of 114mm, 6 poles, stroke length of 84mm and speed of 1.5m /s. In general, sea waves have stroke length in the range of 1 m but since a prototype was developed in the lab, stroke length was kept smaller. In this study, a capacitance of 800μF was used to excite the stator. It was seen that the use of copper plates inside the slots increases the output power significantly in [14]. The experimental output voltage of 180V was shown in this paper. The experimental setup used in this paper is shown below in Figure 2-4. A rotary induction motor was used as a prime mover and it was connected to linear induction motor using a rotary to linear interface equipment.

Figure 2-4 - Experimental setup of linear induction generator [14].

There are two ways in which a linear induction machine could be designed either short primary (long secondary) or long primary (short secondary). Short primary induction machines are widely used in industrial equipment and transportation systems. This is because of the lower manufacturing and operating cost. If higher force density is required, the secondary needs to be short to have a lower mass. Some of the applications of short secondary linear induction machines are maglev, air-craft launchers and car crash testers [15].

LIG for hybrid vehicle applications has been discussed in [16]. It used a free piston engine (FPE) as the prime mover and linear induction generator as the electrical generator. A 1KW 3 phase LIG with a speed of 6 m/s, 218 turns / phase and output voltage of 220V was modeled using an FE software and simulated. A 150μF excitation capacitor was attached to the stator terminals. It was seen from the simulations that the machine produced unbalanced current and voltages as shown in Figure 2-5. The reason for this unbalance was attributed to the end effect in induction machines.

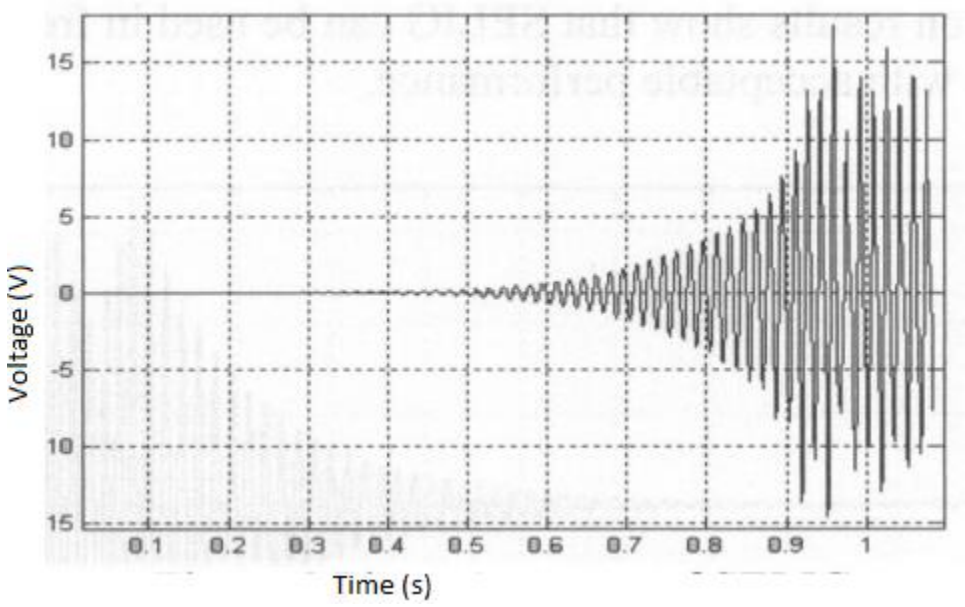

Figure 2-5 – Unbalanced phase current in an LIG [16].

As shown in [16], induction machines produce unbalanced voltage and current and hence achieving balanced voltage and current requires special control schemes. In LIG, the active length of the mover part can be made longer than the length of the stator and this causes the reduction of the leakage flux and end effects.

The mass is lower for the translator (moving part) of the induction generator which uses aluminum translator. Therefore, in applications where the prime mechanical mover provides reciprocating motion, frequency /speed will be higher. This compensates for the low thrust force density of the linear induction generators [17].

The analytical model of a linear induction generator for Stirling engine was discussed in [18]. Detailed modeling was done with two different conditions – slots and without slots.

Following this, the FE model was designed, and the flux density and force were compared with the analytical model. To calculate the resistances and inductances of the circuit, an equivalent circuit model was developed. Since this machine has to be studied for a Stirling engine, the engine was modeled based on [19]. Following that, control of the whole system was designed. Since many parameters affect the design of the system, a genetic algorithm was used to optimize the parameters to design a system with high efficiency and low losses. Subsequently, the control system was developed for the engine as well as the LIG. This is shown in Figure 2-6. Following this, global optimization of the system was done to reduce the generator losses and the size of the inverter components. Overall optimization was done to increase the generator power output. These are parameters that were optimized – mover radius, yoke, airgap, coil turns and pole pitch. These parameters were optimized using a non-dominated sorting genetic algorithm. Overall this paper [19] provides a preliminary theory for the development model of tubular LIG in FE and mathematical steps. Simplified experiments to check the thrust forces were done to validate the optimization. LIG has a low maintenance cost, rigid structure, easy construction and a wide range of applications but with a lower power density compared to PMLG.

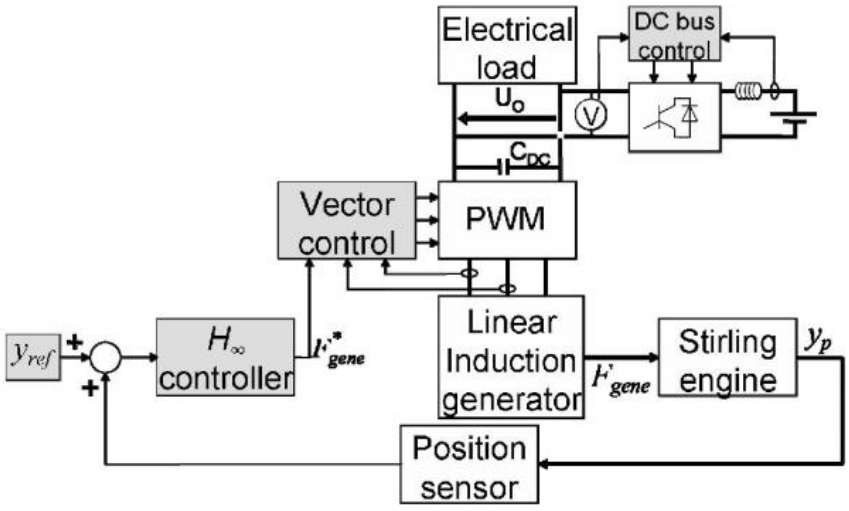

Figure 2-6 - LIG - Stirling engine Co-generator control system [18].

Theoretical modeling of LIG for Stirling engine system is discussed in [20]. Simplified modeling was done in [18] compared to [20]. In addition to modeling, a linear induction

machine was built for a 1 kW system. Testing was done to calculate the equivalent circuit parameters of the LIG system, and the measurements were compared to the theoretical results. Results were comparable with errors of less than 5%. This paper [20] performs a complete simulation of a Stirling system with LIG. The overall system of the LIG – Stirling engine system is shown in Figure 2-7.

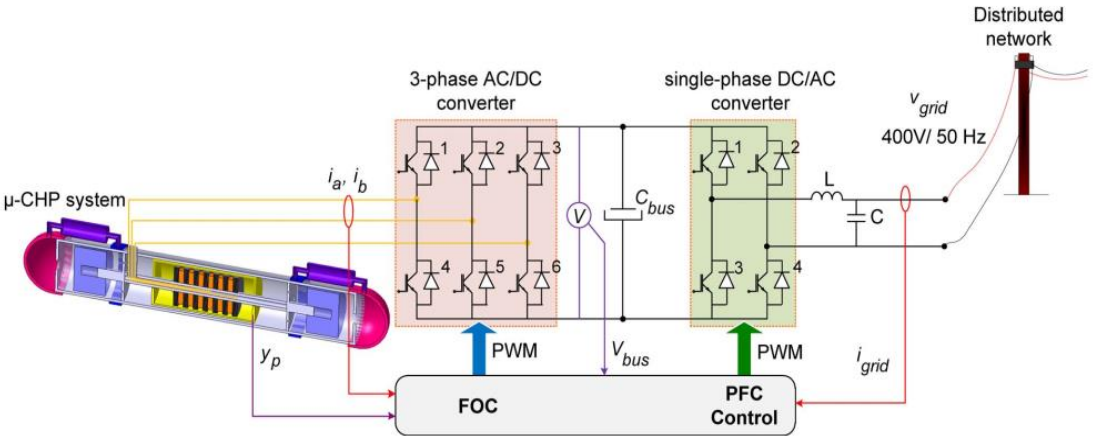

Figure 2-7 – Overall model of a Stirling engine - LIG cogeneration system [20].

Optimizations were done to reduce the size/ cost of TLIG using a genetic algorithm. The comparison table of PMLG and LIG is shown in Table 2.1.

Table 2.1 – Advantages and disadvantages of PMLG and LIG [20].

LG type	Advantages	Disadvantages
PMLG	• High efficiency • Low losses • High acceleration can be achieved with springs	• Heavy mover • Mechanical losses • Cogging Force • High cost of magnets
LIG	• Very high acceleration • Zero cogging torque • Low cost • Compact and Rugged • Less maintenance	• Large airgap • Low efficiency • Secondary joule losses

2.2.3 Linear Switched Reluctance Generator (LSRG)

Linear switched reluctance generator is similar to a rotary switched reluctance generator. LSRG does not have permanent magnets. Instead, the LSRG translator consists of salient electrical steel poles. The stator consists of current-carrying coils arranged in phases with steel laminations. The phases of the windings are energized in sequence creating a magnetic field and an aligning force between stator and translator. When the translator is pushed by the prime mover, it has to overcome the aligning force and thus the mechanical energy is converted into electrical energy [21]. When the translator moves, translator poles move out of alignment and another group of poles is moving into alignment. This process is similar to a rotary SRG. This can be achieved by having unequal pole numbers in stator and translator. Eg: 6/4 or 8/6 stator/rotor poles. One of the requirements for LSRG is a power converter circuit to create a magnetic field when the translator is moving and to deliver the current to the load.

Different configurations of LSRG were reported and studied in [22]. The different configurations of LSRG are shown below in Figure 2-8.

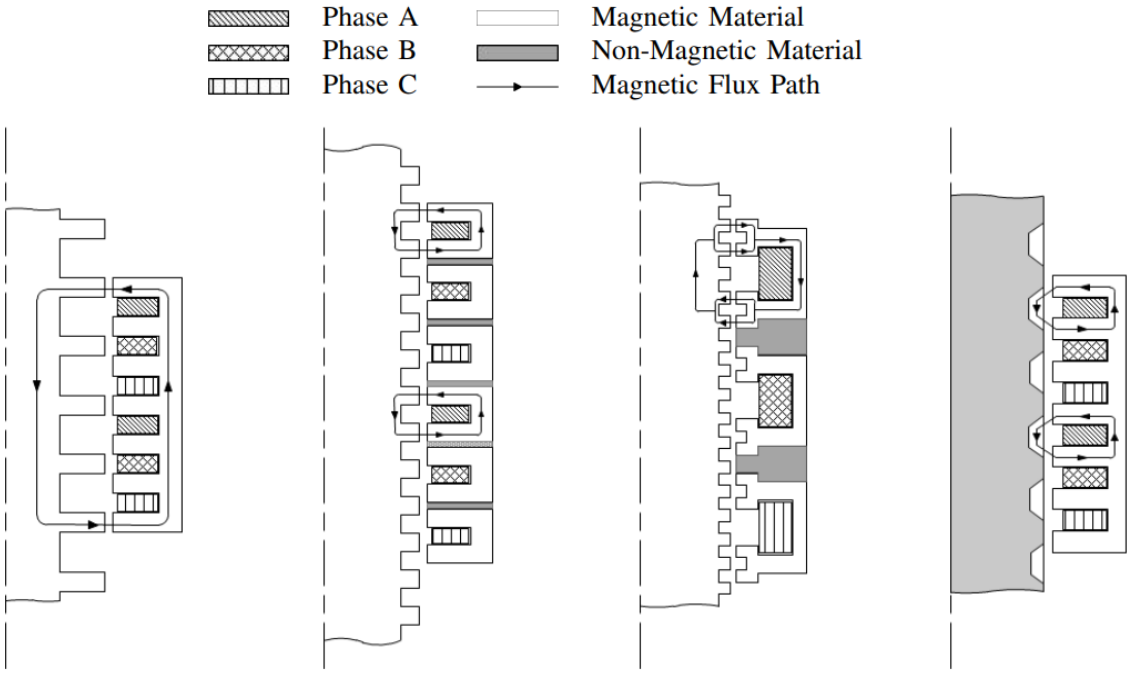

Figure 2-8 - Different configurations of LSRG [22].

The first configuration was a 3 phase generator with each phase composed of two conducting wire coils connected in series. Each coil is ring-shaped placed concentrically with the stator and the translator. Both stator and translator have ferromagnetic material to provide a path for the magnetic flux. The second configuration uses a 4 phase Switched reluctance actuator. The difference between first and second is the independent path for each coil in the second case. An independent path is achieved by using a paramagnetic material between the magnetic paths. The third configuration has a salient structure both in the primary and secondary. This has one coil per phase. Each magnetic pole has two teeth with the same dimensions as the salient profile in the secondary. The fourth configuration consists of a translator made of non-magnetic material with segments of magnetic material embedded in them. This provides the salient profile for the translator. For LSRG, if the inductance change is higher between the unaligned and aligned position, the power capability of the LSRG is high. Based on these criteria, it was found from finite element simulation that the second case provided higher inductance during aligned position and lowest inductance in unaligned position. In [22], four configurations were tested only for inductance and details were not provided in terms of power, output voltage and force. Further research needs to be conducted to make an accurate prediction compared to what has been presented in [22]. Detailed modeling for a two-sided LSRG was developed in [23]. This paper talks about the design guideline for a two-sided LSRG with 6/4 structure and 200W output power.

Some of the advantages of LSRG are no permanent magnets, easy construction, and low maintenance costs. The disadvantage of LSRG compared to permanent magnet and induction generator is the control of the winding sequence phases. The control logic for LSRG was developed and discussed in [24, 25].

2.3 Phase of linear generator

Linear generators can be of many phase configurations however the two most common types based on the number of phases are either a single-phase or a three-phase.

2.3.1 Single phase linear generator

Single-phase linear generator consists of a single-phase of windings. This results in the output voltage which will be single-phase. Single-phase linear generator is easy to construct and maintain. Single-phase generator is easier to control and produces a sinusoidal waveform as output and therefore it will have lesser harmonics compared to 3 phase linear generators (for short stators). In terms of size, Single-phase linear generator is suitable for small power applications in the range of 1 - 5 kW. For high power applications, the size of the single-phase generator becomes an issue and design needs to be changed to three-phase generators. Design of a single-phase generator is shown in Figure 2-9. Windings are shown in orange color, laminations are shown in blue color, back iron is in brown color, the aluminum drum is shown in gray color and magnets are shown in red and purple color. Windings are made up of 9 coils connected alternatively in the opposite orientation. A denotes the winding coming out and A' denotes the winding going in. There is only one set of windings in the system.

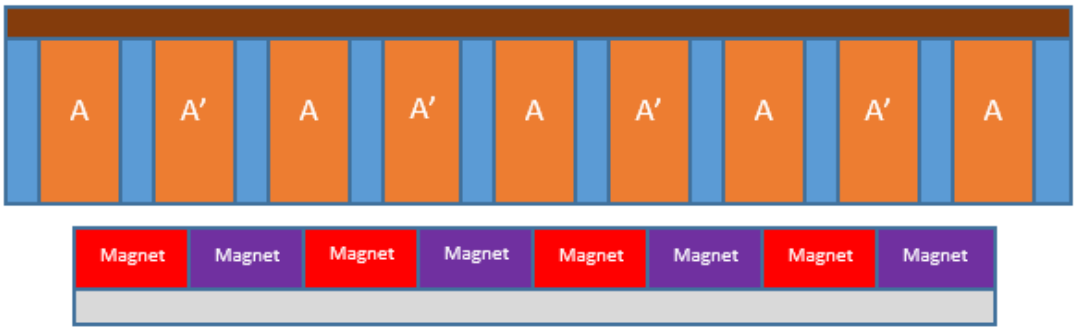

Figure 2-9 - Permanent Magnet Linear Generator - Single phase configuration.

2.3.2 Three phase linear generator

Three phase generators consist of three phase of windings A, B and C in the stator. This results in the output voltage of three phase each 120^{o} out of phase with the other two. Linear generator design of three phase windings is shown in Figure 2-10. In smaller lower power machines, three phase windings are difficult to construct compared to single phase LG. Control of 3-phase linear generator is also complicated. For oscillatory LG, 3 phase LG will not produce pure sinusoidal three phase voltage 120^{o} out of phase with the other

two as seen in [26]. The size of three phase linear generator will be smaller compared to single phase. Hence it can be used for high power applications in the range of 10kW to MW.

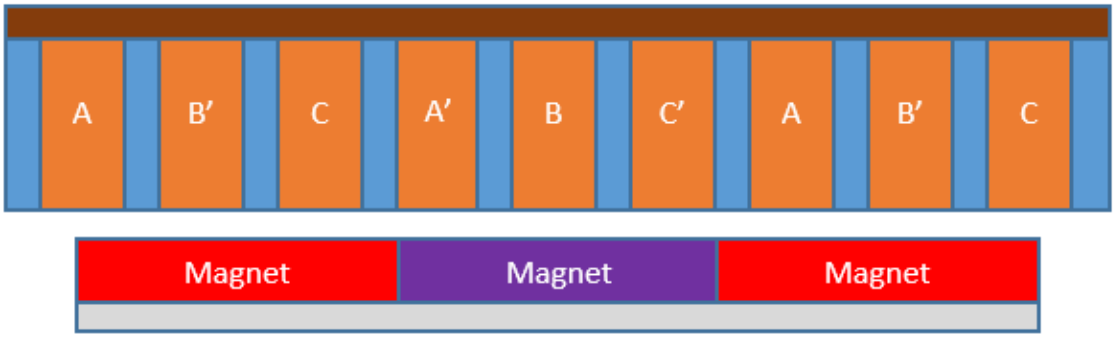

Figure 2-10 - Permanent Magnet Linear Generator - Three phase configuration.

2.4 LG Configuration

Linear generators can be of three types based on its configuration. They are,

1. Moving Magnet,
2. Moving coil, and
3. Moving Iron.

2.4.1 Moving magnet LG

A moving magnet linear generator consists of a stationary part made of copper windings and a moving part made of permanent magnets. This is the most popular linear generator design, and this resembles a common rotary permanent magnet synchronous machine. Advantages of moving magnet LG are 1) Moving mass is low 2) Construction is simple 3) Airgap can be made as small as production and assembling capability of the system. The disadvantage of moving magnet LG is 1) Leakage magnetic fields 2) Thermal and vibrational impact on demagnetization, 3) Lack of field control. Figure 2-11 shows an example of a moving coil PMLG. Multiple magnets are present in the translator constituting multiple poles in a PMLG system.

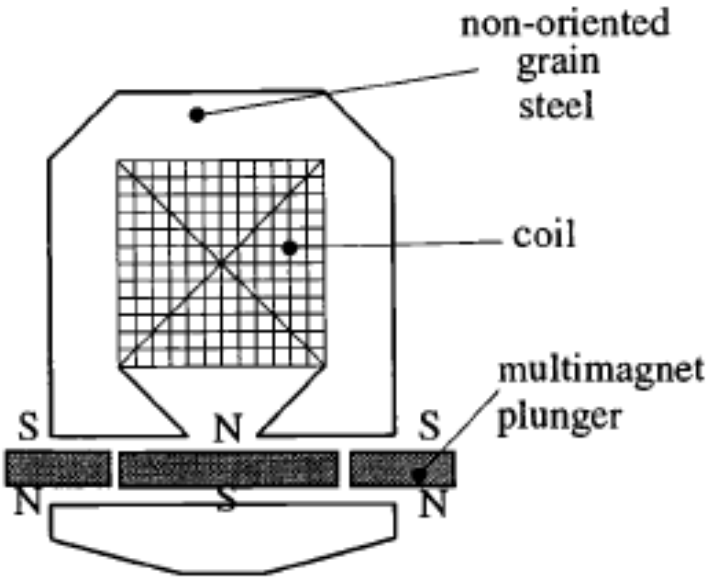

Figure 2-11 – Configuration of a moving magnet PMLG [13].

2.4.2 Moving coil LG

A moving coil linear generator consists of a stationary part made of magnets and the moving part made of windings. This is contrary to popular linear generator design where magnets are the moving portion of the machine. Advantages of moving coil LG are 1) Reduction of radial forces due to eccentricity [27] and 2) Impact force demagnetization of the magnets is reduced [28] since the magnet is stationary 3) Ability for field control. Disadvantages of moving coil LG are 1) Large air gap 2) Difficulties in energizing the moving field 3) Large sized machine construction is complicated 4) Moving mass is high. Shortcomings of the moving coil LG outweighs its limited advantages and hence moving coil LG is generally of less practical interest while designing linear generators.

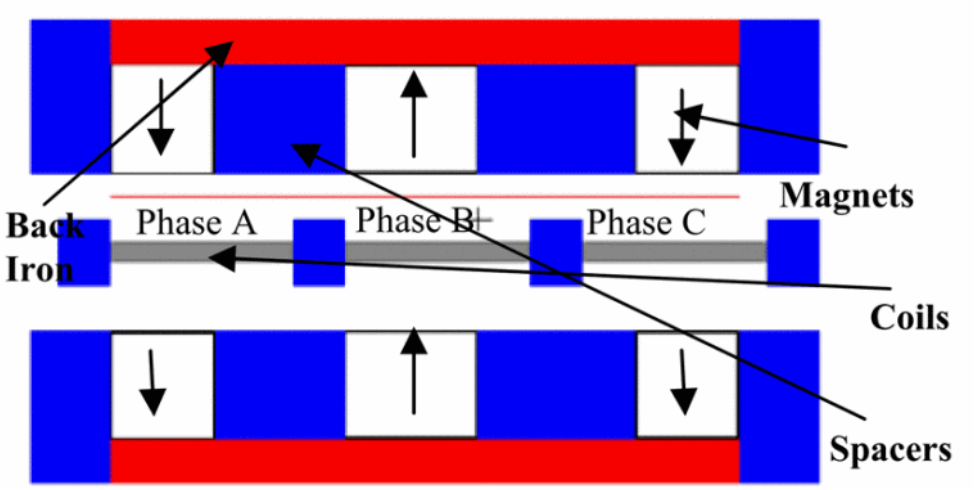

Figure 2-12 - FE Model of Moving coil LG [28].

2.4.3 Moving iron LG

Moving iron LG consists of a stationary part made of magnet and copper coils and the moving part made of iron. This is different from both moving magnet and moving coil magnets. The advantage of moving iron LG is the ability to change the flux path based on moving iron. Radial magnets will be used for the stationary magnets and they are embedded in the stator. Since only iron is moving, the system is rugged compared to a moving magnet and moving coil configuration.

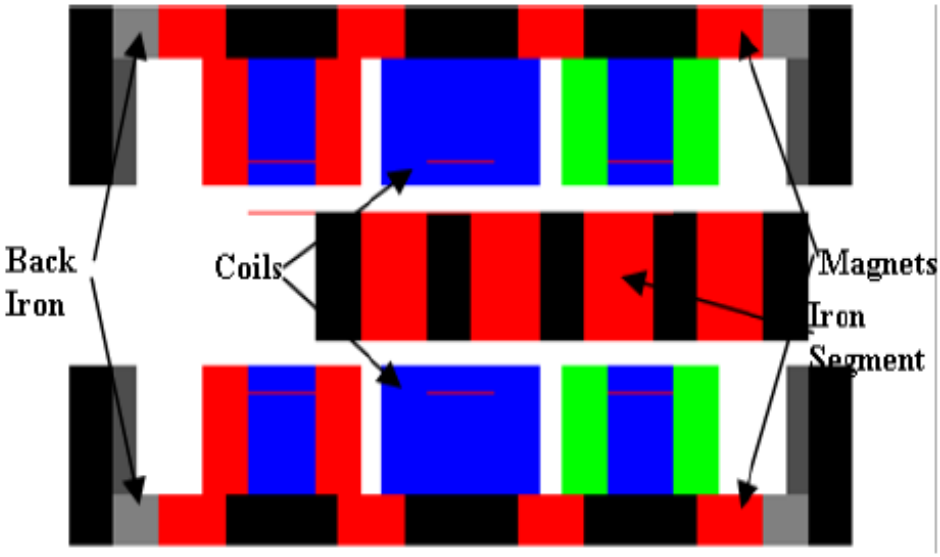

Figure 2-13 - FE Model of moving iron LG [29].

Of the three types of linear generators, construction wise moving magnet is the popular and widely used design in the industry and research.

2.5 Magnet Orientation

Permanent magnet linear generator consists of magnets in their stator or rotor. These magnets can be of

- Radial arrangement,
- Axial arrangement, and
- Halbach arrangement.

Radial arrangement uses radially magnetized magnets in the translator whereas axial magnets use axially magnetized magnet in the translator. Halbach arrangement uses a combination of radial and axial magnets to achieve a different magnet orientation for the translator. All three types of configuration are shown below in Figure 2-14. Widely used magnet orientation is radial arrangement for permanent magnet linear generators. Currently, there is research going on in utilizing axial and halbach arrangement in linear generators. Comparisons of axial and radial magnet arrangement in rotary and linear generators were discussed in [30, 31, 32, 33, 34]. It was found from these papers that the axial arrangement is better compared to the radial magnet arrangement in terms of power density and efficiency. Neumann and Homrich in [31] noted that for low-speed applications, cogging forces are higher on axial field machines compared to radial field machines and are not the best option. The advantages of the halbach magnet arrangement in linear generators for wave energy conversion systems [35, 36]. Several researchers have studied all the three arrangements individually but no comprehensive comparison of the three magnet arrangements have been done for the linear generator.

Chapter 4 presents the comparison of the three magnets arrangements for a permanent magnet tubular linear generator.

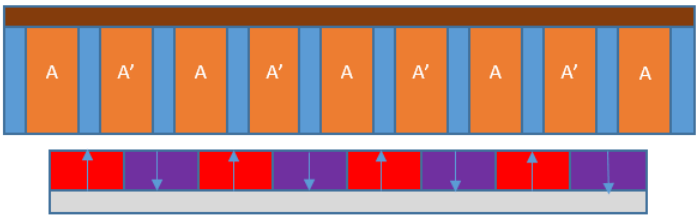

(a) – Radial arrangement

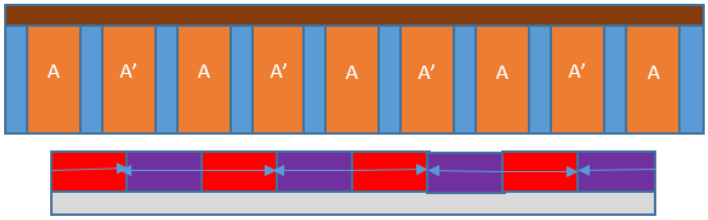

(b) – Axial arrangement

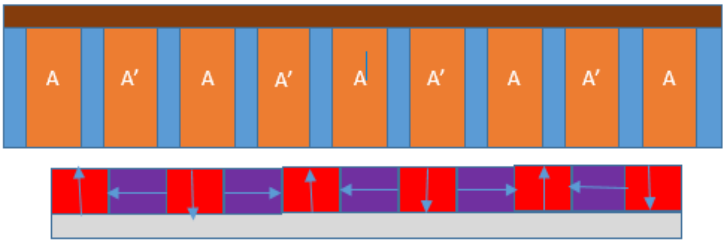

(c) – Halbach arrangement

Figure 2-14 - Magnet orientation of linear generators (a) -Axial arrangement (b) – Radial arrangement (c) – Halbach arrangement.

2.6 Shape of linear generators

The shape of the permanent magnet linear generator can be single-sided, double-sided or tubular. Single-sided LG can be imagined as a rotary generator with the stator and rolled down onto a plane [5]. Double-sided LG is similar to a single-sided linear generator except there is stator coils on either side of the rotor/translator. The tubular linear generator is similar to the single-sided linear generator with the rotor and stator rotated 360^0 along its axis thereby giving a tubular formation for the rotor and stator. Of these three types, tubular generators are considered to be more efficient because of its high power density per volume. Tubular configuration is volumetrically efficient because of its shape. One of the disadvantages of tubular topology is the complicated construction

process with high costs [4]. Figure 2-15 shows the single-sided, double-sided and tubular linear generator.

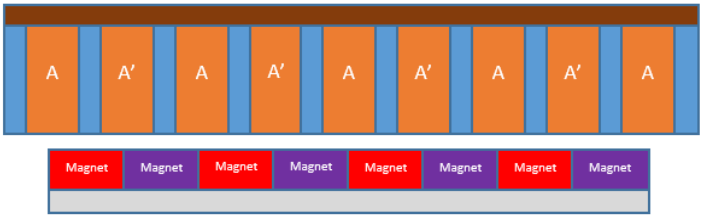

(a) Singled side PMLG

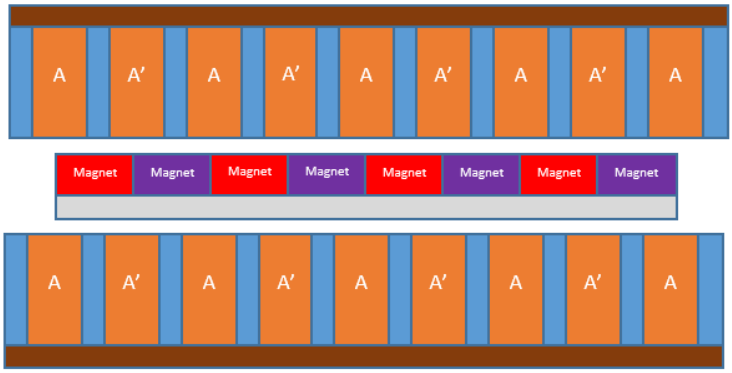

(b) Double sided PMLG

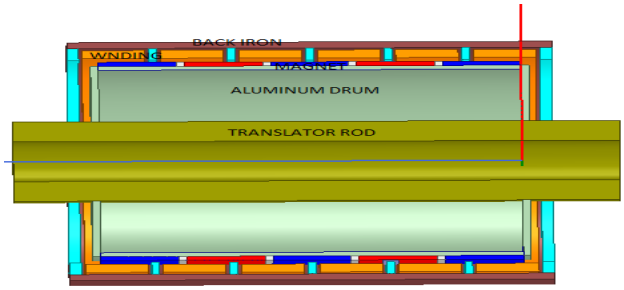

(c) Tubular PMLG

Figure 2-15 - Shapes of linear generators (a) – Single sided PMLG (b) – Double sided PMLG (c) – Tubular PMLG.

2.7 End effect in linear generators

The end effect is a concept specific to linear machines. For a rotary machine, there are no ends as the motion is circular but in the case of linear motion, there is an entry end and exit end. Because of this, there are effects on the air gap magnetic field. The end effect is shown in Figure 2-16.

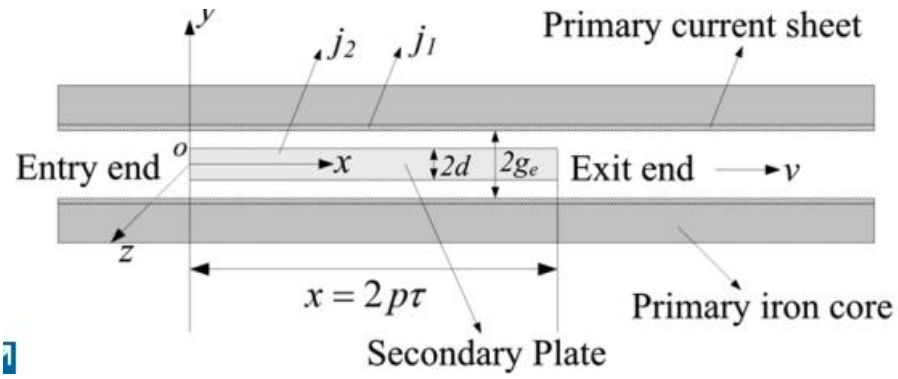

Figure 2-16 - End effect in a LIG system [37].

The analytical model of the end effects on the magnetic field and force is shown in detail in [37]. End effects are different for long stator and short stator linear generator. It can be seen that the end effects are lower for long primary stator compared to a short stator. Also, the higher the velocity of the mover, the end effect is smaller for a long stator. A lot of research has been conducted on the end effects of a linear induction motor. Further, techniques to reduce the end effects for linear induction motor was also studied. One of the techniques shown in [38] is to model a chamfered edge on end at an angle between 12^o to 78^o. Field oriented and vector control schemes have also proven to reduce end effects in linear induction machine as shown in [39, 40]. The use of auxiliary poles has also been studied to minimize the end effects [41]. In a PMLG system, end effects lower the power contribution from the magnets at the end of the translator due to high flux leakage. This can be reduced by having a longer stator and shorter translator.

2.8 Cogging Force

Cogging force is the force produced in the permanent magnet machine due to the interaction between the permanent magnets and the stator laminations. This force causes undesirable vibrations, noise, and eccentricity. For linear generators, the cogging force plays an important role and it needs to be minimized. Different techniques have been studied to reduce or minimize the cogging force. Magnet shapes (conical and sloped) [42] have been studied to minimize the PM linear generator as shown in Figure 2-17.

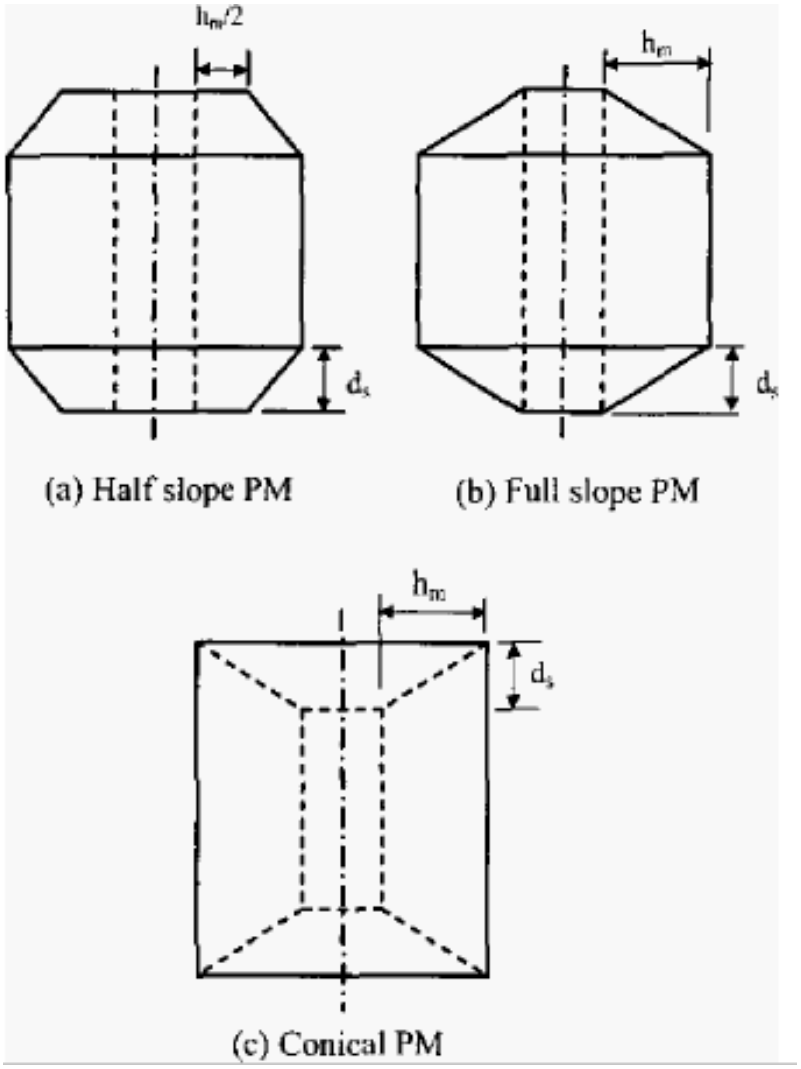

Figure 2-17 - Conical Shaped Magnets (a) – Half slope PM (b) – Full slope PM (c) – Conical PM [42].

Stator teeth width and shape can be modified to reduce the cogging force as seen in [43]. Another technique of reducing the magnet length and using skewed PM is shown in [44].

2.9 Applications of linear generators

There are several applications for linear generators. Some of the applications where research is being carried out are,

1. Wave energy conversion (WEC),
2. Free Piston Engine System (FPE),
3. Micro energy harvesting systems, and
4. Supercritical CO_2 expander systems.

2.9.1 Wave energy conversion

Fossil fuels are diminishing rapidly and there is a great movement towards renewable energy resources in the past few decades. All the countries have committed toward reducing their existing fossil fuel consumption and move towards environmentally friendly and renewable resources [45]. With that in mind, we can see that a lot of research and development has gone towards solar and wind energy. This has resulted in a tremendous improvement in developing a robust, sturdy and reliable renewable energy source [45, 46]. Although there is a great deal of development in these two areas, the cost is still higher compared to fossil fuels which have curbed its rapid growth among the customers. But it is expected that the cost would go down as more and more customers move towards renewables such as solar and wind power.

With the research in solar and wind power going at a rapid pace, there is another renewable energy source that has a huge potential in satiating the world's energy needs. That renewable energy source is called wave energy. Wave energy is a fuel-free, continuous and environmentally friendly like solar and wind power. It has been estimated that the wave power resource which is available worldwide is 2TW [47] or 8000-80000TWh/yr [48].

Waves, especially with large amplitude contains a large amount of energy. Wave energy is stored by the following process – due to solar heating of the earth, the pressure difference is created in the atmosphere. Because of this pressure difference, winds are produced creating waves. When the winds are strong, oceans create large waves near the coastlines. Figure 2-18 shows the sea wave energy distribution across the world in KW/m crest length.

Figure 2-18 - Open sea wave energy distribution, and wave power levels expressed in kW/m crest length [49].

It can be seen from Figure 2-18 that North America and the US especially has a huge potential in terms of wave energy resource. Based on [50], the estimated wave energy resource in the USA is shown in Figure 2-19. Recoverable energy from US continental shelf is 1170 TWh/yr which is split is 250TWh/yr from West coast, 160TWh/yr from East coast, 60 TWh/yr from the Gulf of Mexico, 620TWh/yr from Alaska, 8TWh/yr from Hawaii and 20TWh/yr from Puerto Rico [50] .

The process of conversion of wave energy to electricity is shown in Figure 2-20.

Table ES-1
Total Available Wave Energy Resource Breakdown by Region

Coastal Region	EPRI 2004 Estimate	Present Estimate Outer Shelf *
West Coast (WA,OR,CA)	440 TWh/yr	590 TWh/yr (34% greater)
East Coast (ME thru NC)	110 TWh/yr	200 TWh/yr (82% greater)
East Coast (SC thru FL)	NOT ESTIMATED	40 TWh/yr
Gulf of Mexico	NOT ESTIMATED	80 TWh/yr
Alaska (Pacific Ocean)	1,250 TWh/yr	1,360 TWh/yr (9% greater)
Alaska (Bering Sea)	NOT ESTIMATED	210 TWh/yr
Hawaii	300 TWh/yr	130 TWh/yr (not comparable **)
Puerto Rico	NOT ESTIMATED	30 TWh/yr
TOTAL	2,100 TWh/yr	2,640 TWh/yr (26% greater)

* Rounded to nearest 10 TWh/yr for consistent comparison with EPRI 2004 estimate.

** EPRI's 2004 estimate for Hawaii was along the northern boundary of the U.S. EEZ, as far west as the Midway Islands. The present estimate extends only as far west as Kauai, and encompassed the entire islands (not just their northern exposures).

Figure 2-19 - Wave energy resource in the USA [50].

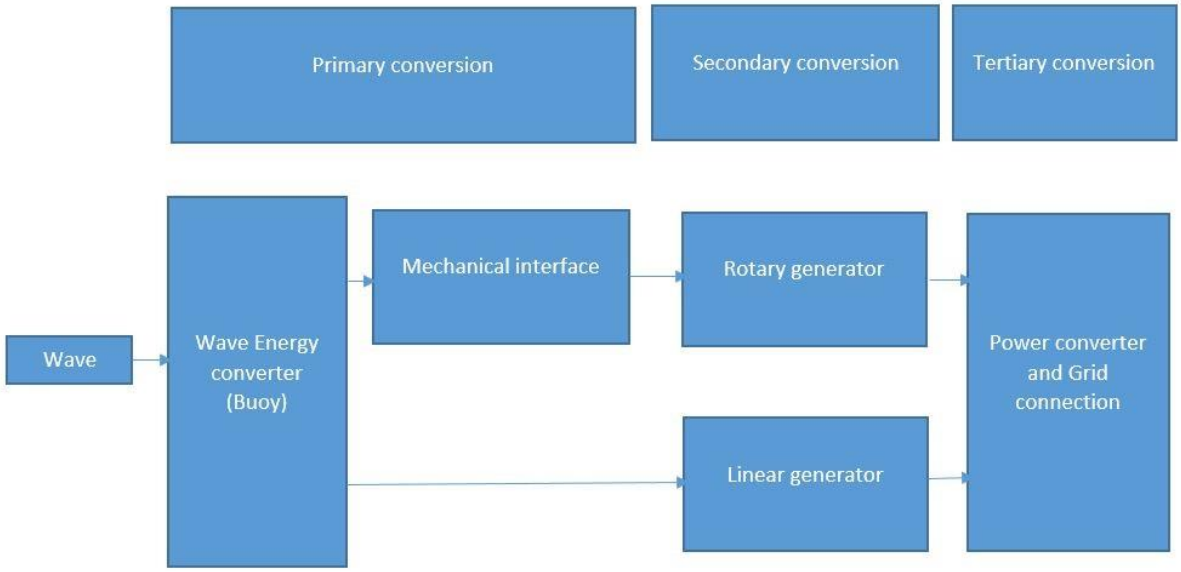

Figure 2-20 – Block diagram of a wave energy conversion system.

Several companies/academicians are working on the wave energy conversion process and technology. Some of the existing installed wave energy farms are Agucadoura wave farm [51] in Portugal, Wave hub in the UK [52], Bombora Wave power [53], CETO Wave farm [54], Oceanlinx [55] in Australia and Kaneohe Bay Oahu and Oregon Farm [56] in the USA. In terms of academicians, considerable research has started in Asia and a group in Malaysia – University Technology Petronas is working on wave energy and linear generators used in the WEC system.

Wave energy converters are of three types. They are,

- Turbine type,
- Hinged Contour type, and
- Point absorber / Buoy type.

Two prominent types of turbine type WEC are oscillating water column WEC used by Wavegen's Limpet, Oceanlinx and Orecon's MRC and overtopping wave energy converter used by Wave dragon [57]. Hinged contour devices are used by Pelamis Wave power, Salter's Duck, Aquamarine Power's Oyster, Swell Fuel, and OWEC. Buoy type devices are used by Ocean Power Technology's PowerBuoy, Sea-based AB, Finavera's AquaBuoy, AWS Ocean Power's Archimedes Wave swing and WaveBob [58]. Illustrations of the different WECs are shown in Figure 2-21 and Figure 2-22.

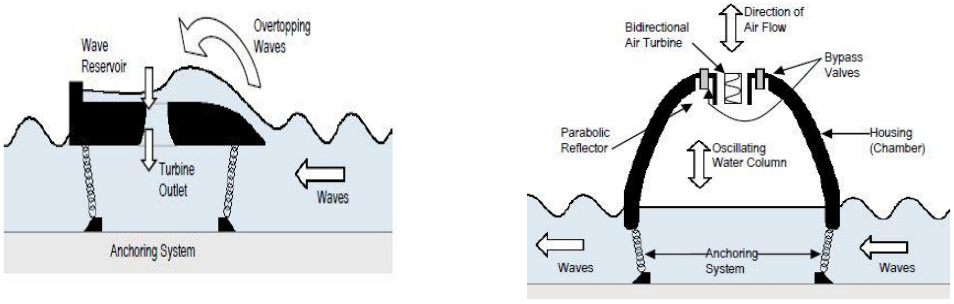

(a) (b)

Figure 2-21 - (a) - Oscillating water column device (b) – Overtopping WEC [58].

Continuous research and efforts are going on finding a suitable, robust and reliable wave energy conversion device as shown above. Another important aspect of the whole system is the conversion of the energy stored in the motion to electricity using an electrical generator. From Figure 2-20, there are two options to do the electromechanical energy conversion. One method is to go for the tried and tested rotary generator but has an additional mechanical interface for the linear to rotary conversion. Another option is to use a linear generator. This is an interesting study to see if a linear generator can work efficiently compared to a rotary generator. Therefore, several researchers have worked on the linear generator for wave energy conversion.

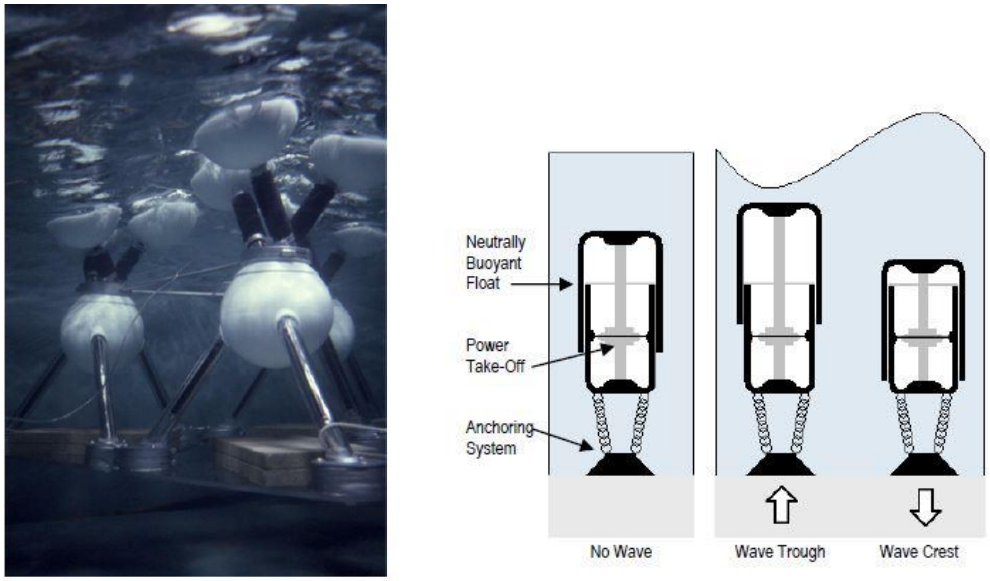

(a) (b)

Figure 2-22 - (a) – Hinged contour device (b) – Point absorber [58].

One of the important aspects of the linear generator is the cogging force associated with it. At lower frequencies or speeds, the effect of cogging force is prominent leading to jerkiness in the motion. At higher speeds, the momentum of the generator overcomes the cogging forces. Since the waves work in the order of 1Hz, the effect of the cogging force plays an important role in the design of the linear generator. Cogging force occurs because of the iron core in the stator. Hence an air-core machine in the Malaysian coast was studied for wave energy application in [59, 60]. Three unique designs were studied

in finite element simulations such as Tri core, Square core and Tri coil for the linear generator to minimize the cogging force as shown in Figure 2-23. It was found from the FE analysis that the square core was comparatively better than the other two designs. Another interesting concept for the linear generator was to keep the magnet and the winding in the primary and keeps the secondary structure simple. This leads to less end effects thereby reducing the detent force of the system. Because of the simple structure, the cogging force will also be less. This will help in improving the efficiency, voltage regulation, and performance of the system. Figure 2-24 shows the structure of the tubular primary permanent magnet linear generator.

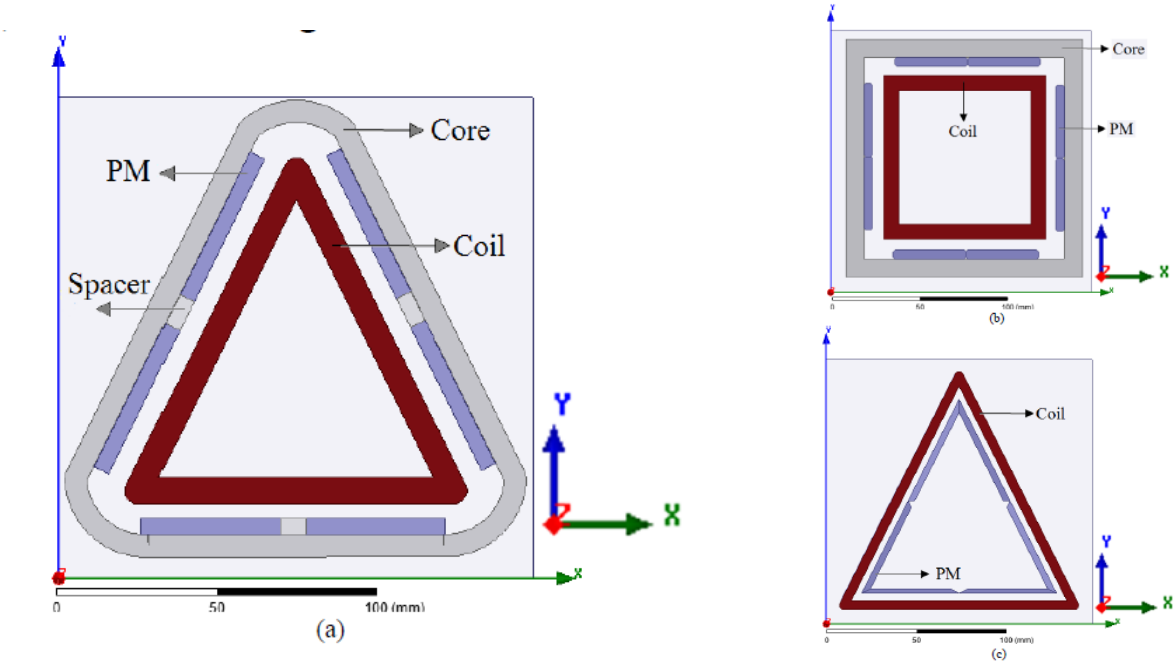

Figure 2-23 - Magnet shape for WEC PMLG (a) – Tri core (b) – Square core (c) – Tri coil [60].

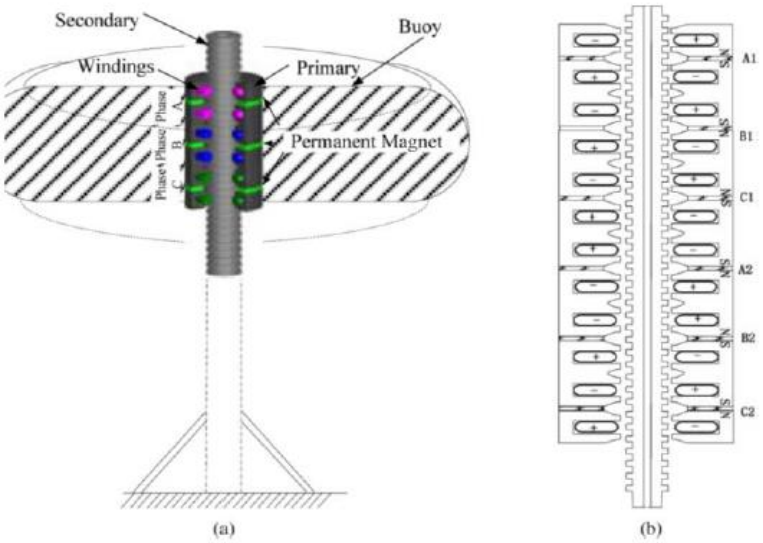

Figure 2-24 - Tubular PMLG for WEC (a) – Basic structure (b) - Cross section of the PMLG [61].

A novel linear generator where the stator windings use non-overlapped (NO) winding because the amount of copper used is less by 50% compared to normal winding. The winding factor of 0.875 can also be achieved with NO windings. The 3D view of the generator is shown in Figure 2-25.

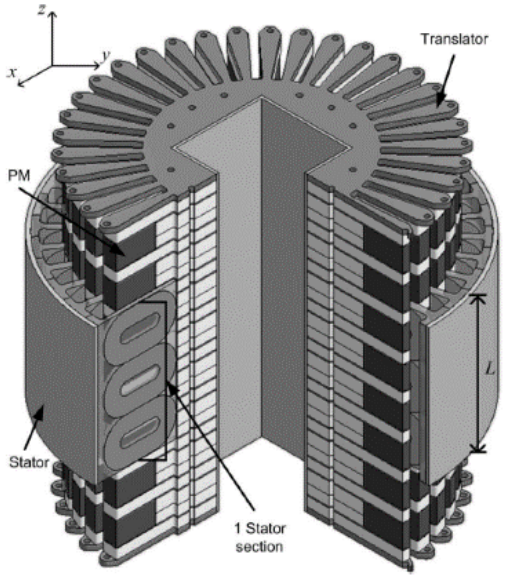

Figure 2-25 - 3D view of a non-winding in PMLG [62].

Another concept of PMLG was inner PMLG (slotted) which is normal PMLG with magnet translator (NdFeB) and stator is made of coils inside the slots with iron or air core and outer PMLG (slotless) where the magnets are on the inner diameter of the buoy and windings are located in the outer diameter of the spar (inner structure) [63]. This way, the magnet is still the mover and the coils do not feel stress because of the movement. Based on their FE study, it was found that 1) Flux density is lower in OPM than IPM 2) Cogging forces are less in OPM 3) Slotted machines generate lesser active power than slot less machine 4) Reactive power is larger in a slotted machine.

The usage of superconducting wire MgB_2 for the stator of the permanent linear generator was studied in [64]. Also, the arc-shaped structure has been proposed for the windings of the stator. It was seen that the MgB_2 has a low manufacturing cost and is isotropic. Furthermore, the current density is 10,000A/cm2 under a magnetic field condition of 2T. Also, the resistance of the superconducting wire is very low and goes to be nearly zero at 40K. Based on FE modeling and simulation, it was seen that the superconducting generator has low voltage regulation and higher efficiency compared to the typical PMFSLG. The disadvantage of superconducting windings is that it is costlier compared to copper wires and the arc type configuration would be difficult to wound compared to the linear winding configuration. The design of the superconducting PMLG is shown in Figure 2-26.

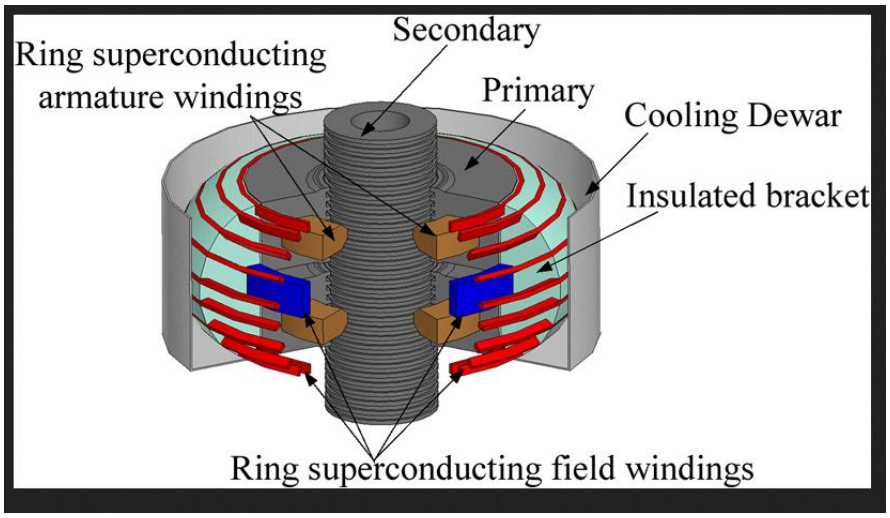

Figure 2-26 – Model of a super conducting PMLG [64].

A new design of PMLG for wave energy conversion was proposed in [65]. Figure 2-27 shows the different views of the proposed PMLG. The main novelty is the design of pole shoes to improve the rate of change of magnetic flux thereby improving the output power. The proposed PMLG has the following novelties 1) Flux switching method to generate electricity 2) Vertical velocity of the translator is kept low 3) New design of pole shoes to increase the rate of change of flux.

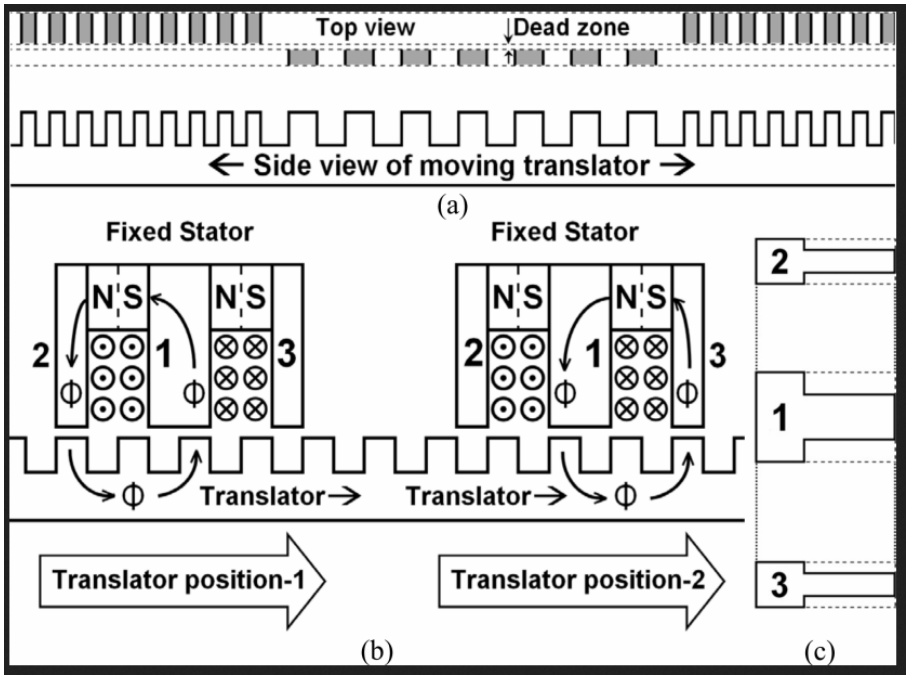

Figure 2-27 - Proposed flux switched PMLG translator (a) top view and side view of the proposed translator, (b) direction change of flux in stator when position is changed, (c) bottom view of proposed pole tips of stator [65].

The implementation of PMLG in the ocean surface and testing it and the difficulties faced in implementing the system was discussed in [66]. Some of the issues faced were corrosion because of the saltwater environment, optimizing the design for hydrodynamics and stress on the power cables.

2.9.2 Free Piston Engine System

Free piston engines have been considered a promising alternative to conventional engines in applications such as hybrid electric vehicles, standalone generators, and Stirling engines. Several groups of researchers and companies have been working in this area to develop a stable and efficient system that can work on different fuel sources.

Some of the advantages of FPE are 1) No crankshaft. Hence less friction losses because of the rotary to linear motion 2) Lesser moving parts. Most of the research has been in the development of free piston for hybrid vehicles because of the move towards the development of research and move towards efficient transportation methods.

The comparison of free piston linear generator for hybrid electric vehicles and other range extender technologies such as fuel cell, microturbine, and diesel engines was discussed in [67, 68]. The advantage of free piston engine PMLG is the ease of packaging and placement. This is shown in Figure 2-28. Thermal efficiency can be as high as 36% with optimization as shown in [67]. The cost of the system could be around $2500. Also, free piston engine PMLG systems have the flexibility of fuel that could be used.

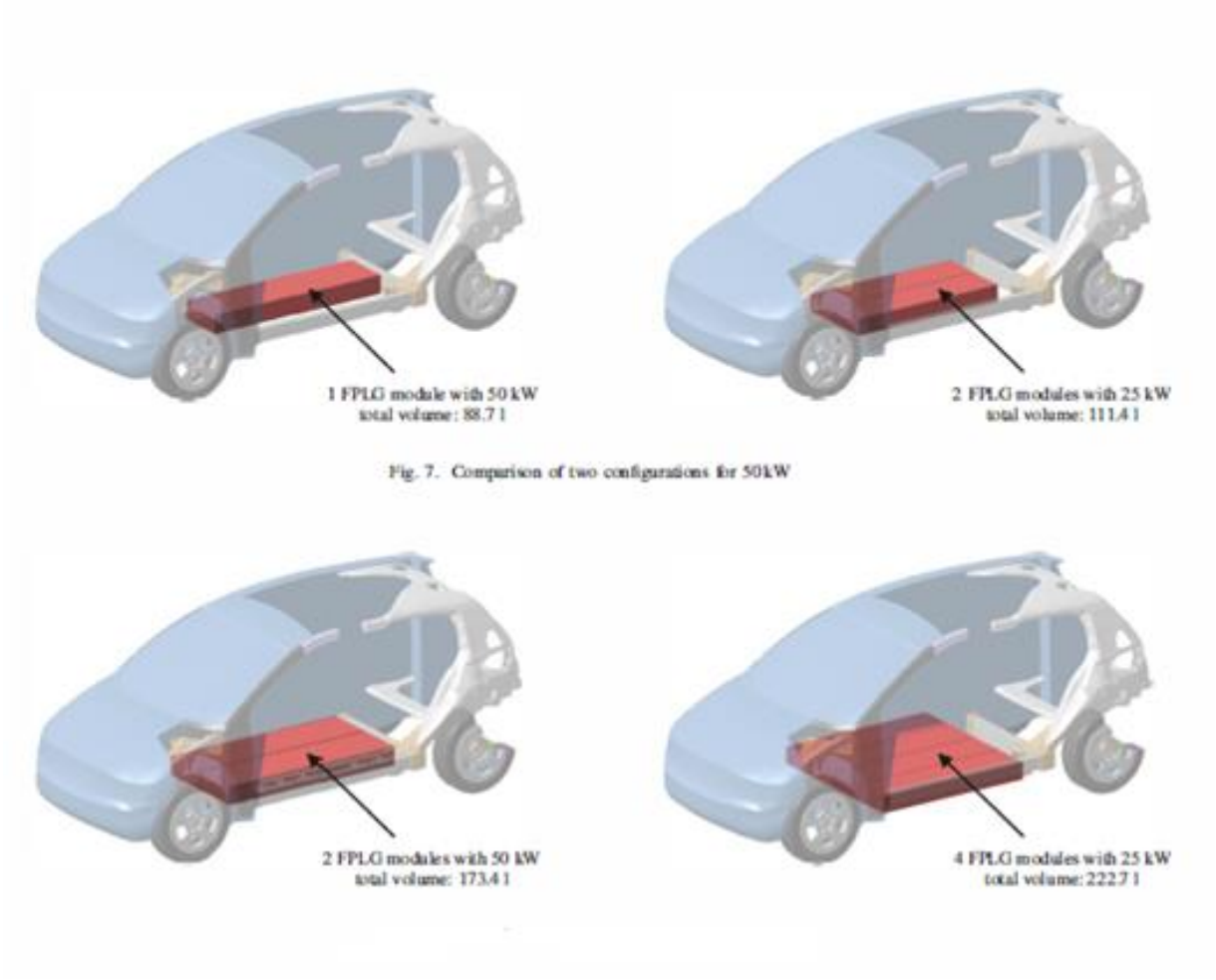

Figure 2-28 - Placement of different sizes of PMLG in a car [67].

For microturbines, free piston engine PMLG has high efficiency, faster dynamics, high power density and less strain on the battery. In comparison to ICE, high efficiency, easy integration to the vehicle. With all these advantages, free piston engine PMLG is in a position to be in the automotive vehicles soon and it is a suitable solution for range extenders until fuel cells come into picture.

Different configurations for free piston engines configurations are available. They are single cylinder, dual cylinder and opposed piston design. A single cylinder free piston engine system consists of a PMLG and a single cylinder one side of the system. This configuration requires a return stroke by springs or some other mechanism. Control is simpler in this configuration as one engine needs to be controlled. Further, if high stiff springs are used, the springs will have control over the motion and hence the control is easier in a single cylinder system. Dual cylinder free piston engine consists of a PMLG and two cylinders on either side of the system. Therefore, no springs are required as engine fires from both ends and run the system. This requires complicated control compared to single cylinder system. This is because two engines have to be controlled in terms of ignition, injection, and motion. Opposed piston engine configuration consists of a two PMLG systems and one engine in the center. This requires more precise control in terms of position between the two PMLG systems.

Depending on the space available in the vehicle and the power requirement, different free piston engine PMLG could be installed. Of these, central combustion opposed piston engine design is important as it uses only one combustion chamber for two subsystems. DLR has worked extensively on free piston engine linear generators (FPLG) for several years and has also built experimental test rigs for the complete system and the potentials of FPLG were studied [69]. This design has low noise, vibration and harshness and also the efficiency are higher compared to other schemes. This is shown in Figure 2-29.

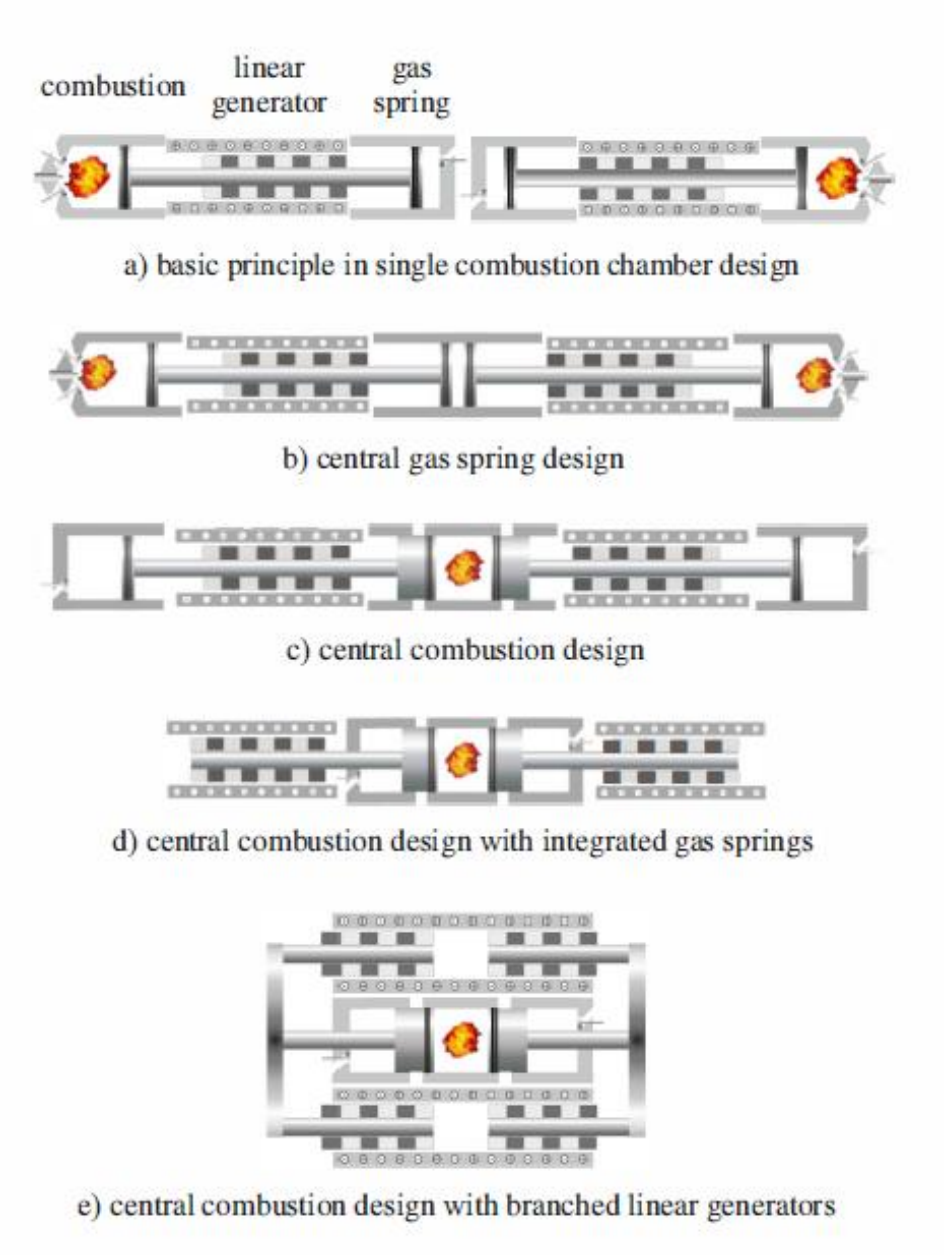

Figure 2-29 - Opposed piston design by DLR (a) Single combustion chamber design (b) Central gas spring (c) Central combustion (d) Central combustion with integrated gas springs (e) Central combustion with branched linear generators [69].

A four-stroke engine linear generator system was discussed in [67]. One of the important aspects of free piston engine PMLG is motion accuracy and control strategy of fuel delivery and electromagnetic force. This plays a role in power conversion efficiency. Simulation of the free piston engine PMLG system with control was done and 42% thermal

efficiency could be achieved. They were able to have good control of the system having fewer misfires and have a stable system for operation.

Using PMLG as a motor for starting the engine and then converting to a generator after the engine achieves stable operation was discussed in [70]. Dual piston system was chosen and the PMLG system was modeled and analyzed using ANSYS Maxwell [71, 72]. These papers have analyzed the free piston engines for hybrid vehicles and Stirling engines using Finite element methods to develop a suitable and stable working model of a free piston engines.

The groups that are researching in the area of FPE are Petronas University, New Castle University, Stanford University, Nanjing University, Tianjin University, and West Virginia University. Companies such as GM, Toyota, BMW, Honda, and Ford have filed several patents in this area [73] . GM [74] utilized bounce chambers/ air spring and electrical braking for their control schemes and introduced an electrical flywheel system to compensate the variable compression ratios in the free piston engine PMLG system. Toyota [75] has used a bounce chamber with pressure regulation to vary the stiffness of the gas spring system and worked with DLR to implement the configuration. Several patents were filed on the heat transfer design, engine cooling and coatings on the permanent magnets. Volvo [76] worked with KTH and developed a method for controlling a dual piston engine system and starting the engine system with smaller energy storage system. Ford developed the opposed the piston, opposed cylinder system. This method exploits the resonance of the mechanical system for starting and igniting the FPE system. Honda [77] developed a detailed patent on a single cylinder single piston system with a mechanical spring system. With several companies and researchers working on the FPE system, a single stable system hasn't been developed yet but with the progress happening in this area, the viability of FPE system is promising and shows the potential to be implemented in commercial systems soon. Of all the FPE systems available in the literature, the following groups have shown an experimental demonstration of the FPLG system – German Aerospace center (DLR) [78], Toyota research group [79], Sandia National Laboratories [80], and West Virginia University [81, 82, 83].

One of the experimental FPE systems at West Virginia University is shown in Figure 2-30.

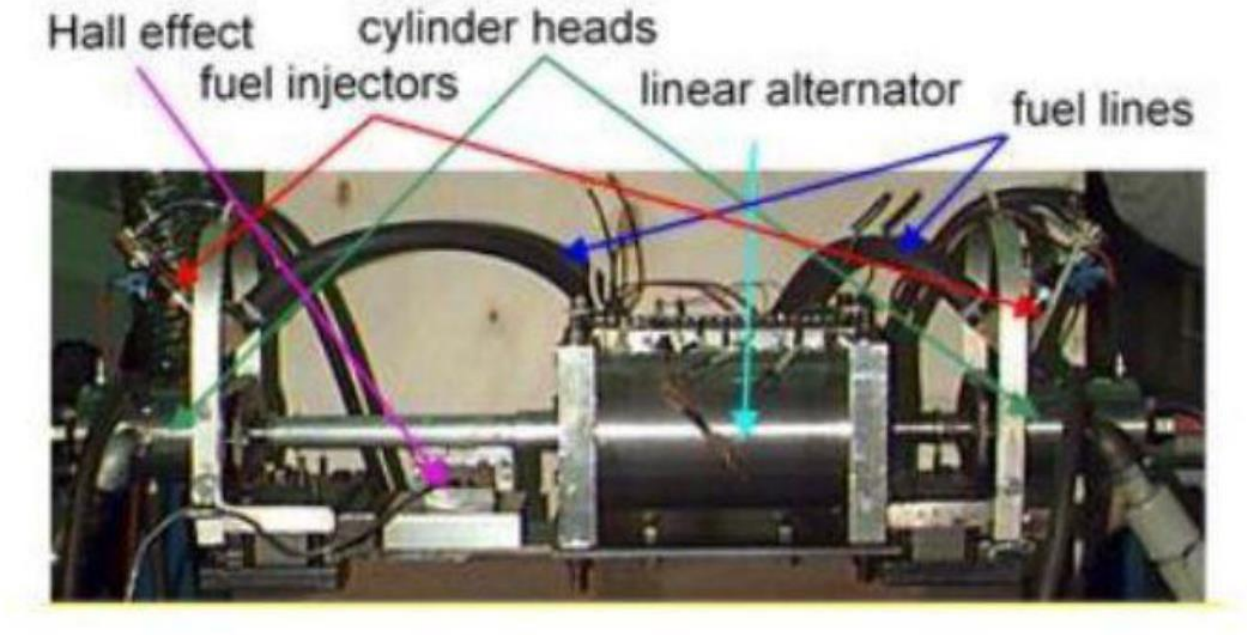

Figure 2-30 - Free Piston Engine prototype from WVU [84].

2.9.3 Energy harvesting systems

PMLG has been researched and implemented for high power applications such as hybrid vehicles and wave energy systems. Also, PMLG can be used in micro energy level applications. Some of the applications of micro PMLG devices are in vibration energy harvester for wireless sensor networks, small vibrational systems, electronics devices, and wearable energy harvesters

Utilization of PMLG for wireless sensor networks (WSN) was discussed in [85]. There is a need to power these low power electronics in an environmentally friendly way and PMLG can be used for this purpose. PMLG combined with vibrational sources can provide energy that is being wasted otherwise. Some of the existing vibration sources are air compressors, handling equipment, pumps, elevators, acoustics and building services. A design of PMLG for lower power vibration systems was discussed in [86]. These researchers have built a single sided PMLG system as shown in Figure 2-31. Voltages in the range of 1-5V were produced at a velocity of 175mm/s. Furthermore, different wire gauges such as AWG 30, 36, and 43 were tested and the results were shown. It was seen that AWG 43 produced more voltage which is expected as the number of turns

increased as the wire size decreased. But details were not provided how the output varied with respect to wire gauges. This is also important as the wire size decreases their resistances increases thereby affecting the output power.

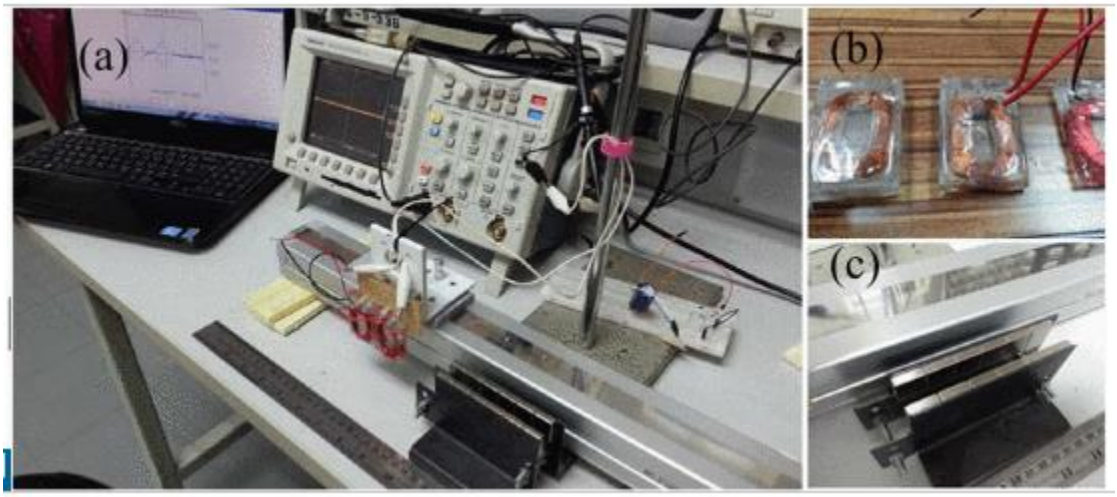

Figure 2-31 - PMLG energy harvester (a) – Overall system (b) moving coils (c) magnet slot [86].

The use of PMLG in human foot motion was discussed in [87]. Finite element modeling of PMLG for this application was developed and power in the range of 8.5mW/cm^3 could be produced. Although this seems like a novel idea, the implementation requires careful consideration of the placement and location of the PMLG system. The application of PMLG in implanted devices was studied in [88]. About 8-10% of Americans carry some form of implanted electronic devices. Powering these implanted devices is an important problem that needs to be solved. Current methods for delivering power are 1) Implanted batteries [89] 2) Percutaneous systems [90] 3) Transcutaneous systems [91] . Newer technologies require more power and therefore implanted secondary batteries were studied. Problems associated with these technologies are 1) Inefficient power transfer 2) Tissue damage 3) Need for a large internal battery. To solve these issues, the authors have suggested implanting micro PMLG inside the body. To determine where these PMLG can be implanted, two areas are suggested 1) Diaphragm muscle 2) Fascial layers of the rectus abdominus. Figure 2-32 shows the place where PMLG can be placed.

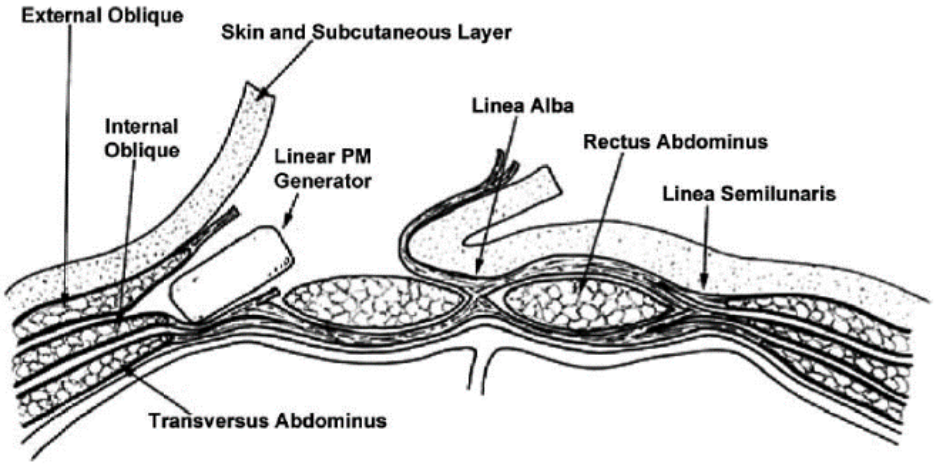

Figure 2-32 - Micro energy harvester in diaphragm muscle [88].

An experimental device that tries to utilize the vibration of vehicles was discussed in [92]. This type of energy was in the order of mill watts and could be used to power small micro electronic devices in the vehicles. A unique application on PMLG in a renewable road tunnel system where PMLG harvests the energy from running vehicles was presented in [93]. The overall system consists of a speed bump, suspension, generator and a power storage module. Preliminary testing of the prototype showed promise of its application in commercial applications. This method could provide a power source to the area where they can't be delivered economically and for intelligent transport systems.

2.9.4 Supercritical CO_2 expanders

Supercritical operation is one of the techniques to achieve high efficiency in thermodynamic systems. These supercritical systems are used to upgrade a low quality heat to upgraded heat or convert the heat to electrical power. Types of refrigerants that are available are chrlorofluorocarbons (CFC), hydrochlorofluorocarbons (HCFC), CO_2, ammonia or hydrocarbons. Of these, CO_2 is used in industrial and marine refrigeration because it is not flammable. The vapor pressure of CO_2 is higher compared to the other refrigerants and its critical temperature is 31^o C. Supercritical CO_2 power cycle operates similar to a normal turbine cycle but uses CO_2 as the working fluid instead of other fuels. Using supercritical conditions, the CO_2 does not change its phase from liquid to gas. The pressure temperature phase diagram for CO_2 is shown in Figure 2-33.

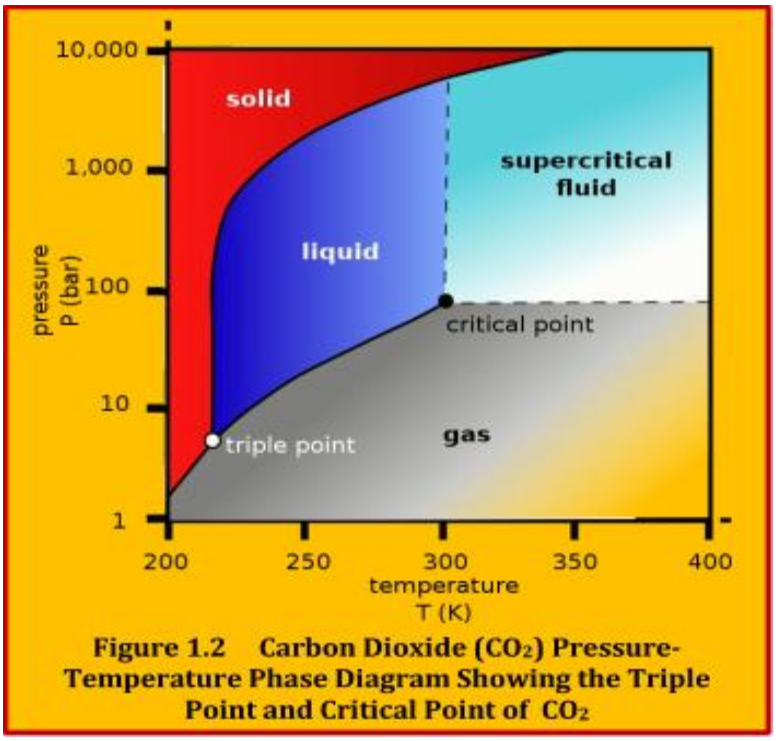

Figure 2-33 - Pressure - Temperature diagram for CO_2 [94].

Power generation from waste heat is economically feasible if the temperatures are higher than 150^0C [94]. But if supercritical cycles are used, the temperature of the waste heat can be lower or higher amount of power can be extracted for the same heat level. The advantages of CO_2 are supercritical applications are low critical point, non-toxic, non-flammable, no ozone depletion potential. Advances in the energy recovery expanders in supercritical CO_2 applications was discussed in [94]. Different energy recovery expanders are free piston expanders, rolling piston expanders, vane expander, scroll expander, screw expander and turbo expanders. Of these, piston expander is of interest for the PMLG systems. Example of a piston expander used in supercritical CO_2 applications was shown in Figure 2-34.

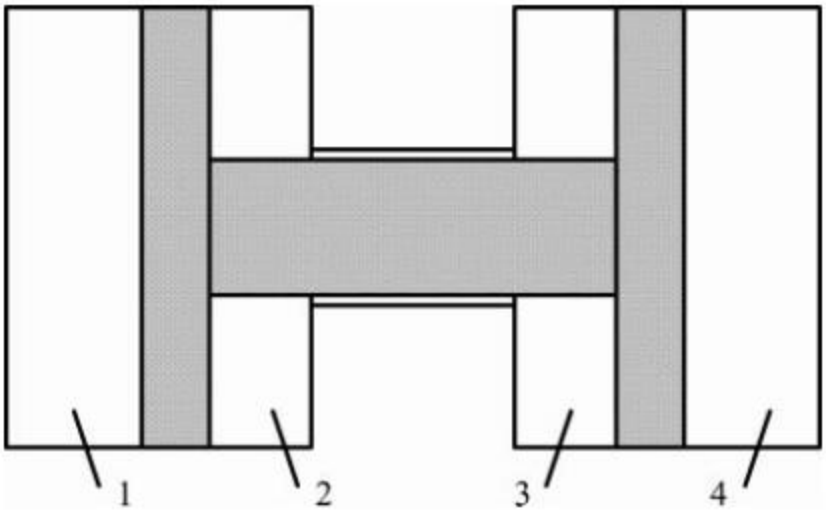

Figure 2-34 - Piston expander concept for supercritical CO_2 applications [95].

Chamber 1 and 4 represent the compression chambers and chamber 2 and 3 represent the expansion chambers. This was first suggested by Heyl et al in 1999 [95]. The central system which performs the compression and expansion can be the PMLG system. Not a lot of research is available on the use of PMLG is supercritical CO_2 application. But there is a potential in using the PMLG system in supercritical CO_2 applications.

CHAPTER THREE

3 Design guideline for a single phase tubular Permanent Magnet Linear Generator (PMLG)

Basic design guideline for a 3-Phase PMLG system was provided in [96, 97] by Boldea and Nassar. These two papers mainly focus on a 3-phase linear generator design for Stirling engine and high-power applications (greater than 10 kW). It does not account for small scale PMLG systems (around 1 kW) and does not have experimental verifications. Our current research uses a free piston engine internal combustion engine for the PMLG system. Very few free piston engine PMLG systems have been designed and fabricated in the world. As a result, certain modifications were made to the design of PMLG shown in [96, 97] to make it suitable for FPE applications and for low power PMLG systems. Furthermore, some of the design equations were modified based on the understanding of the experimental results of the PMLG system. The experimental results will be discussed in Chapter 4. Overall, this section provides a detailed design guideline for a single phase PMLG and the chosen application for this guideline was free piston engine (FPE) applications in the range of 0.5 – 2.5 kW systems. Each of the geometrical and electrical quantities was discussed and design equations were provided to build a complete PMLG from start to end.

The design guideline is presented in the order the calculations must be performed. All the notations and symbols used in this chapter are listed in the nomenclature section.

3.1 Configuration of the PMLG system

Linear generators can be either permanent magnet, induction or reluctance type. In this study, design guideline was developed for a tubular permanent magnet linear generator (PMLG). The moving part of the PMLA can be either windings (coil) or magnets. Moving coil linear generator will have a higher moving mass compared to a moving magnet linear generator and therefore lower oscillating frequency of the overall system. Moving coil also makes the connection difficult because of the need of some sort of slip strip (similar to

slip ring in rotary machines) and carbon brushes. Moving magnets has issues because of thermal demagnetization and vibrations. In this chapter, moving magnet tubular PMLG was chosen because of its low moving mass of the translator compared to moving coil PMLG. The moving magnet translator can be made of cylindrical or ring magnets. Axial magnets for PMLG are better than radial magnets as shown in [32]. Therefore, axial magnets are used for the study. The magnet length can be same as the stroke length or closer to the stroke length. Steel1010 can be used for the laminations and back iron. Based on this information, the following design considerations have been made for the single phase PMLG system.

1. Translator of the PMLG consists of permanent magnets (In this case NdFeB magnets)
2. Iron core stator consists of copper windings and steel laminations.
3. Axial magnets are used for the translator
4. The pole pitch of the linear generator is equal to its stroke length
5. PMLG is a single-phase machine
6. End effects are neglected
7. Fringing effects are neglected

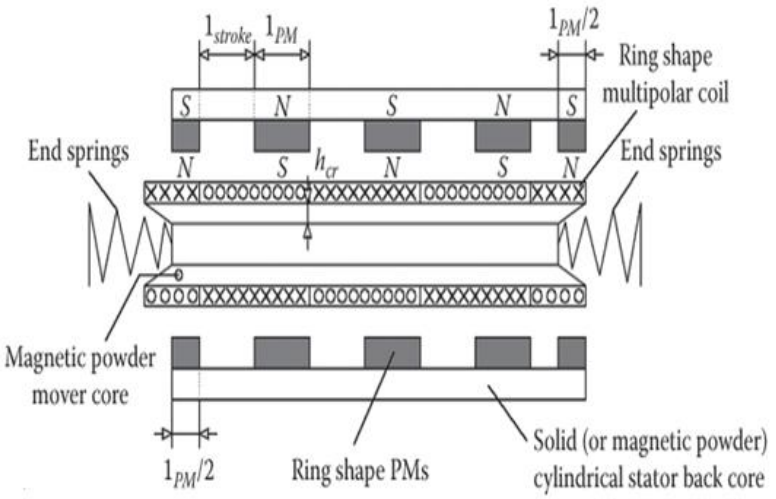

Figure 3-1 - Model of a PMLG system [5].

3.2 Design Equations

The input parameters of the PMLG are the output power, rated voltage, and efficiency. Once the basic input parameters are chosen, the number of rotor poles and, air gap flux density needs to be decided. Details on each of the geometric and electrical parameters are discussed below.

3.2.1 Step 1: Number of translator poles

The translator poles of PMLG can be either higher or lower than the stator poles. Therefore, the first thing to decide is a short translator or a short stator. It has been seen in [68] and [69] that the design chosen for the FPE application was a short translator. In [70], simulations were done to study the difference between a short translator vs a short stator for FPE applications. It was seen that the short translator provides better performance and design attributes compared to a short stator for FPE applications. Therefore, for this guideline, the number of rotor/translator poles will be less than the stator. Since the translator poles are lesser than the stator poles, only the windings overlapping the translator poles will be active when the PMLG is in operation.

The number of translator poles influences the size and volume of the PMLG system. Therefore, the volume of the system needs to be considered while deciding the number of translator poles. Also, the translator pole in combination with stroke length and magnet size determines the moving mass of the PMLG system. Therefore, translator poles need to be chosen based on application requirements.

The length of the stator can be calculated using the equation (3-1).

$$Ls = (m_r + 2) * strokeLength \quad (3\text{-}1)$$

3.2.2 Step 2: Airgap magnetic flux density

The designer has to determine the operating characteristics of the airgap magnetic flux density of the machine. Once the airgap flux density is fixed, the calculation of the permanent magnet ring thickness is performed. Mathematical modeling of the magnet radial thickness (MT) is shown here. The equations for the calculations are shown in [5].

This mathematical model will help us to get an idea of the magnet thickness required to achieve the target magnet flux density.

The equation to calculate permanent magnet ring thickness MT is given in (3-2).

$$H_m * MT + \frac{B_g}{\mu_o} k_c g(1 + k_s) = 0 \quad (3\text{-}2)$$

where k_s is to account for any additional airgap between the stator laminations and saturation.

$$k_c = \frac{1}{1 - \gamma \frac{g}{t_s}} \quad (3\text{-}3)$$

$$\gamma = (ts/g)/(5 + \left(\frac{ts}{g}\right)) \quad (3\text{-}4)$$

$$ts = 2 * tau/3 \quad (3\text{-}5)$$

$$B_m = B_r + \mu_m H_m \quad (3\text{-}6)$$

$$B_{gmax} = 4 * B_g/3.14 \quad (3\text{-}7)$$

To compare the mathematical model's accuracy, finite element modeling for the flux density was done and compared at different conditions of magnetic flux density and thickness.

Using FEMM software, the thickness of the magnets to achieve a given flux density in the air gap was found. To simplify and eliminate the need of finite element software to determine the magnet thickness, a parametric study was done by running models of magnets of varying thickness in steps of 0.1mm and their peak magnetic flux density for varying thickness was found at 0.5mm ,1mm ,1.5mm, and 2mm airgap. Figure 3-2, Figure 3-3, Figure 3-4, and Figure 3-5 show the plots of Magnetic flux density vs Magnet thickness for different airgap.

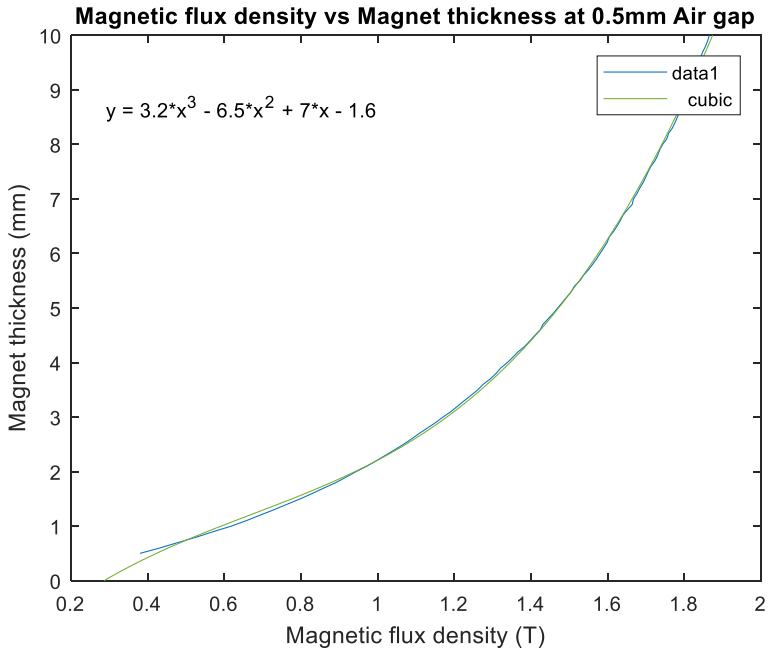

Figure 3-2 - Magnetic flux density calculations from FEMM for 0.5 mm airgap.

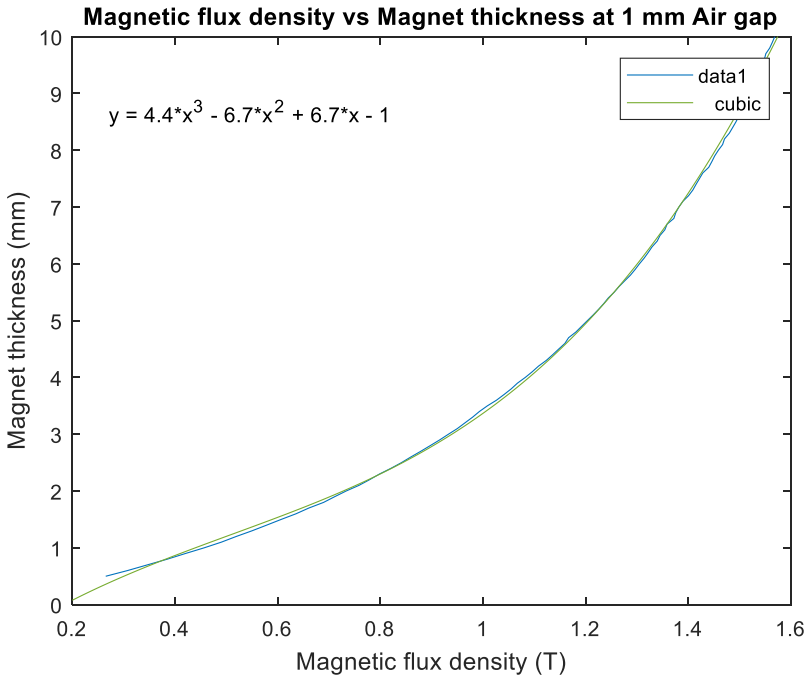

Figure 3-3 - Magnetic flux density calculations from FEMM for 1 mm airgap.

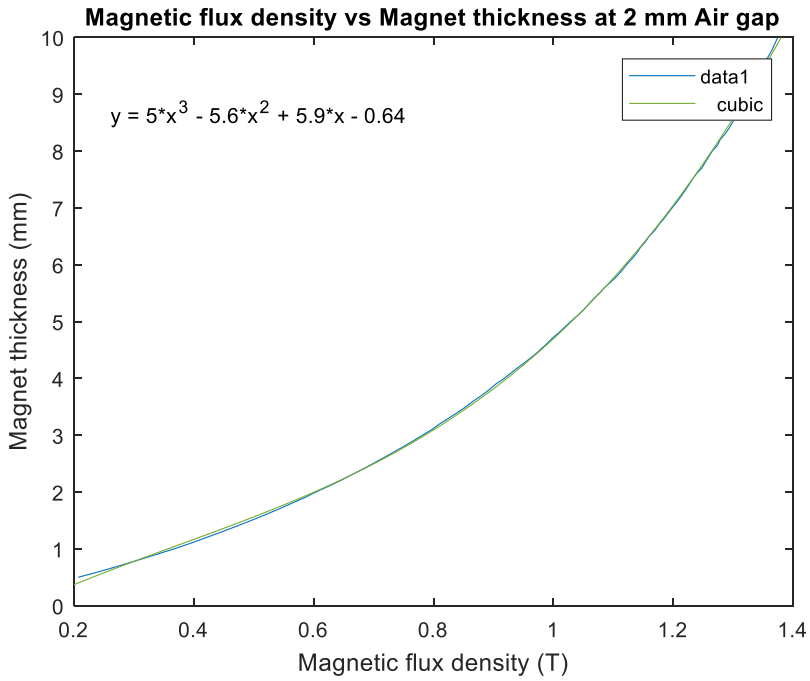

Figure 3-4 - Magnetic flux density calculations from FEMM for 1.5 mm airgap.

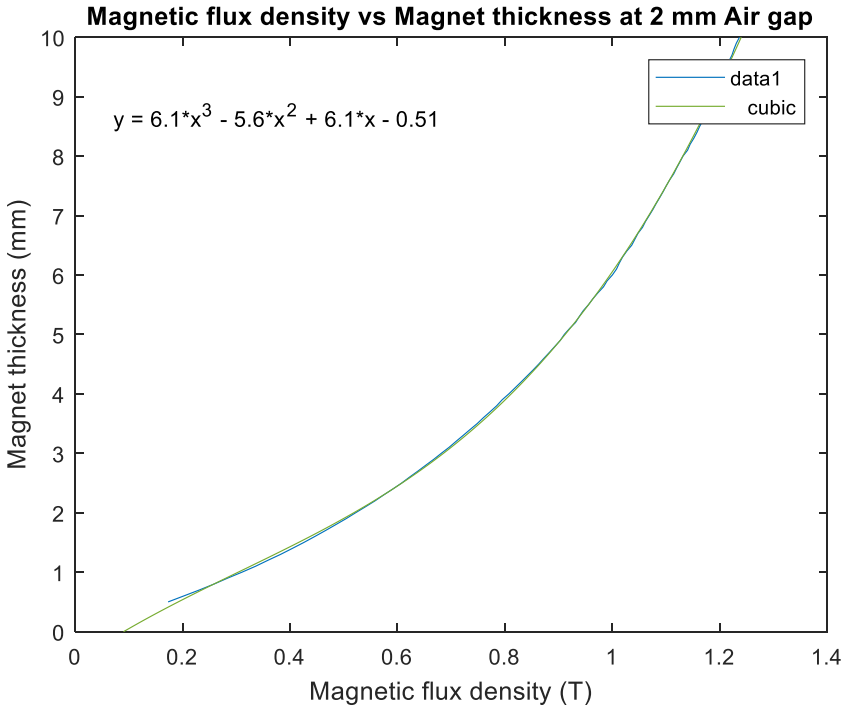

Figure 3-5 - Magnetic flux density calculations from FEMM for 2 mm airgap.

Once the values of the magnetic flux densities were known, a cubic fit was used to fit the peak magnetic flux density to the magnetic thickness.

Based on the magnetic flux density, the equations for the magnetic flux density at different air gaps are shown below.

$$MT = 3.2* B_{gmax}^3 - 6.5* B_{gmax}^2 + 7* B_{gmax} - 1.6 \quad (3\text{-}8)$$

$$MT = 4.4* B_{gmax}^3 - 6.7* B_{gmax}^2 + 6.7* B_{gmax} - 1 \quad (3\text{-}9)$$

$$MT = 5* B_{gmax}^3 - 5.6* B_{gmax}^2 + 5.9* B_{gmax} - 0.64 \quad (3\text{-}10)$$

$$MT = 6.1* B_{gmax}^3 - 5.6* B_{gmax}^2 + 6.1* B_{gmax} - 0.51 \quad (3\text{-}11)$$

Later different flux densities at 4 different air gaps were calculated based on the mathematical model and compared with the FEMM results. This is shown in Table 3-1.

Table 3-1 - Magnetic flux density error results for different airgap.

Bg (T)	0.5 mm (%)	1 mm (%)	1.5mm (%)	2 mm (%)
0.5	65	33	12	5
0.6	56	22	6	1
0.7	41	11	0	2
0.8	23	0.4	7	9
0.9	3	13	19	20
1	21	32	36	37

From the table, it is seen that the error percentages between the mathematical model and FEMM are very high. This shows that the mathematical model can be used as a starting point, but later a shift needs to be done with finite element analysis to determine the accurate magnetic flux density. Keeping that in mind, the equations derived from FEMM for the magnetic flux density was used in the future calculations shown in this chapter.

3.2.3 Step 3: Energy density in the airgap

The energy density in an airgap is given by the equation shown in (3-12).

$$E_d = \frac{Bg^2}{2*\mu_0} \quad (3\text{-}12)$$

where,

E_d – Energy density,

$\mu_0 = 4pi * 10^{-7}$, and

$B_g = 3.14 * B_{gmax}/4.$

Energy stored in the airgap is calculated using the rated output power and frequency as shown in (3-13).

$$E_g = \frac{S}{(\eta * f_e)} \quad (3\text{-}13)$$

where,

E_g – Energy stored in the airgap,

S – Rated output power,

f_e – Frequency, and

η – Efficiency.

3.2.4 Step 4: Stator inner diameter

Once, the energy density and energy stored in the airgap is known, volume of air V_{air} which stores the airgap was calculated as shown in (3-14).

$$V_{air} = \frac{E_g}{E_d} \quad (3\text{-}14)$$

From the volume of air required to store the energy is known, inner diameter of the stator was calculated using (3-15).

$$Ds = \frac{\left(\frac{V_{air}}{pi*L} - g^2\right)}{g} \quad (3\text{-}15)$$

where,

D_s – Inner diameter of the stator,

$L = (m_r + 1) * \tau$,

m_r – Translator poles,

τ – Stroke length, and

g – Airgap.

The electromagnetic thrust force of the PMLG is given by the equation (3-16).

$$F_r = \frac{S}{(u * \eta)} \quad (3\text{-}16)$$

where,

u – velocity.

The pole pitch and stroke length are equal for a single phase PMLG. Once the magnet thickness, airgap and outer diameter of the stator are known, the magnet dimensions was calculated.

$$OD_m = Ds - g \quad (3\text{-}17)$$

$$ID_m = OD_m - 2 * MT \quad (3\text{-}18)$$

where,

OD_m – Outer diameter of the magnet, and

ID_m – Inner diameter of the magnet.

Once the basic dimensions of the magnet are known, the number of turns per phase (W_1) can be determined using the equation (3-19).

$$W_1 = \frac{V_0}{(4.44 * f_e * Bg * A_f * k_w)} \quad (3\text{-}19)$$

where,

$$A_f = pi * \tau * (OD_m - ID_m) + \left(\frac{pi}{2}\right) * \left(OD_m{}^2 - ID_m{}^2\right), \quad (3\text{-}20)$$

$V_0 = 1.67 * V_r$ - Open circuit (OC) voltage, and (3-21)

$k_w = 0.9$ – Winding factor.

Number of turns per slot (n_s) was found using equation (3-22) given in [7].

$$n_s = \frac{W_1 * 2}{(m_r * q)} \quad (3\text{-}22)$$

q = slots/poles/phase.

With the rotor geometry determined, the next step is to determine the stator slot geometry.

$$I_r = \frac{S}{Vr} \quad (3\text{-}23)$$

where,

I_r – Rated current, and

V_r – Rated voltage.

Slot geometry was found using (24) shown in [1].

$$A_{slot} = \frac{n_s * I_r}{K_{fill} * J_{co}} \quad (3\text{-}24)$$

K_{fill} – Fill factor of winding in the slots.

The width of the slot depends on the flux density and saturation of the lamination in the stator. The width of the slot (w_s) for this system can be chosen between 60 – 75% of the pole pitch.

$$w_s = (0.60\ to\ 0.8) * \tau \quad (3\text{-}25)$$

Slot height (h_s) is given by equation (3-26).

$$h_s = \frac{A_{slot}}{w_s} \quad (3\text{-}26)$$

The next step is to determine the AWG wire gauge for the PMLG. With the knowledge of the current in the generator and the number of turns in the system, AWG can be chosen.

Once the winding size is known, the resistance of the generator can be found using the equation (3-27).

$$R_s = pi * (D + h_s) * n_s * slot * AWG \quad (3\text{-}27)$$

The inductance of the stator is calculated using the equation (3-28) in [1].

$$L_M = \frac{6\mu_0 (K_W W_1)^2 D_S}{P} \quad (3\text{-}28)$$

3.3 Example calculations for a 1 kW design in shown below

Design a 1 kW linear generator with 90% efficiency with a rated voltage of 120V with a stroke length of 33 mm and a frequency of 80Hz.

Parameters such as rotor poles, air gap flux density needs to be decided.

m_r (rotor / translator poles) = 4

B_g (Airgap flux density) = 0.6 T

g (Air gap) = 2 mm

With the initial parameters, first the maximum air gap flux density is calculated

B_{gmax} = 0.6 * 4/3.14 = 0.7643 T

Using the maximum airgap flux density and FEMM equation,

MT = 6.1* B_{gmax}^3 – 5.6* B_{gmax}^2 + 6.1* B_{gmax} - 0.51

MT = 3.61 mm

Energy density is calculated based on the airgap flux density.

$E_d = \frac{Bg^2}{2*\mu_0}$ = 0.6^2/ (2*4*π*10^{-7}) = 1.4324*10^5 J/m^3

$E_g = \frac{S}{(\eta * f_e)}$ = 1000 / (0.9*80) = 13.88 J

$V_{air} = \frac{E_g}{E_d}$ = (13.88 / 1.4324*10^5) = 9.6963*10^{-5} m^3

Using these values, the diameter of the stator is calculated.

$D_s = \frac{\left(\frac{V_{air}}{pi*L} - g^2\right)}{g}$ = 91.5 mm

$F_r = \frac{S}{(u*\eta)}$ = 1000 / (5.8655 * 0.9) = 189 N

Dimensions of the magnet

$OD_m = Ds - g = 91.5 - 2 = 89.5\,mm$

$ID_m = OD_m - 2 * h_m$ = 89.5 – 2*3.6 = 82.3 mm

Stator calculations:

$A_f = pi * \tau * (OD_m - ID_m) + \left(\frac{pi}{2}\right) * ({OD_m}^2 - {ID_m}^2)$ = 0.003 m^2

Number of turns per phase

$W_1 = \frac{V_0}{(4.44*f_e*Bg*A_f*k_w)}$ = 200 / (4.44 * 80 * 0.6 * 0.003 * 0.9) = 390

Number of turns per slot

$n_s = \frac{W_1*2}{(m_r*q)}$ = (390 * 2)/ (4 * 1.5) = 130

Rated current

$I_r = \frac{S}{Vr}$ = 1000 / 120 = 9.25 A

Slot area

$A_{slot} = \frac{n_s*I_r}{K_{fill}*J_{co}}$ = (117 * 9.25) / (0.8 * 4.17) = 3.2474*10^{-6} m^2

Slot width

$w_s = (0.66) * \tau$ = 0.66*33 = 22 mm

Slot height

$h_s = \frac{A_{slot}}{w_s}$ = 324.74 / 22 = 14.8 mm

Resistance of the stator

$R_s = pi * (D + h_s) * n_s * slot * AWG$

$R_s = 1.89\ \Omega$

3.3.1 Equivalent circuit of PMLG

Simplified equivalent circuit model of PMLG in open circuit is shown in Figure 3-6. PMLG was modeled as a simple E_b – R – L circuit.

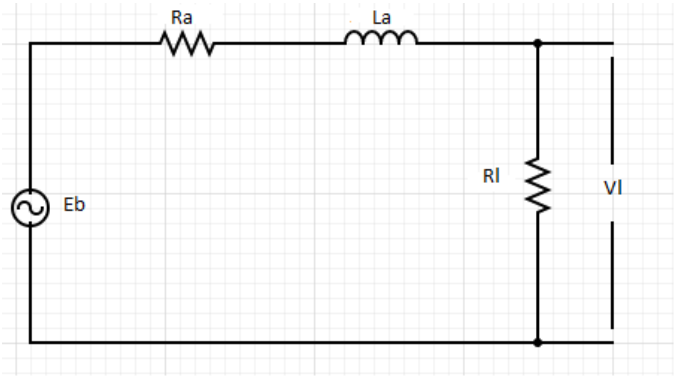

Figure 3-6 – Simplified open circuit of linear generator.

Therefore, generated voltage (E_b) of PMLG is given by (3-29).

$$E_b = V_l + V_{Ra} + V_{La} \quad (3\text{-}29)$$

where,

$V_l - Load\ voltage$,

$V_{Ra} - Voltage\ across\ the\ machine\ resistance$,

$V_{La} - Voltage\ across\ the\ machine\ inductance$,

$R_a - Machine\ resistance$,

$L_a - Machine\ inductance$, *and*

$R_l - load\ resistance.$

3.3.2 Velocity profile

Linear generator can be used in free piston engines and Stirling engines. Each of these engines has a different position and velocity profiles. Spring assisted FPE Engine has a sinusoidal waveform as a velocity profile, whereas it is trapezoidal for Stirling engines as seen in [7].

Velocity profile of a PMLG for FPE (33mm stroke and 75Hz) is shown in Figure 3-7. Position vs Velocity for FPE is shown in Figure 3-8. The equations for position and velocity for linear generator in FPE is given in (3-30) and (3-31).

$$x = \frac{l_{stroke}}{2} * sin\,(2\pi f_e t) \tag{3-30}$$

$$u = \frac{l_{stroke}}{2} * 2\pi f_e \cos\,(2\pi f_e t) \tag{3-31}$$

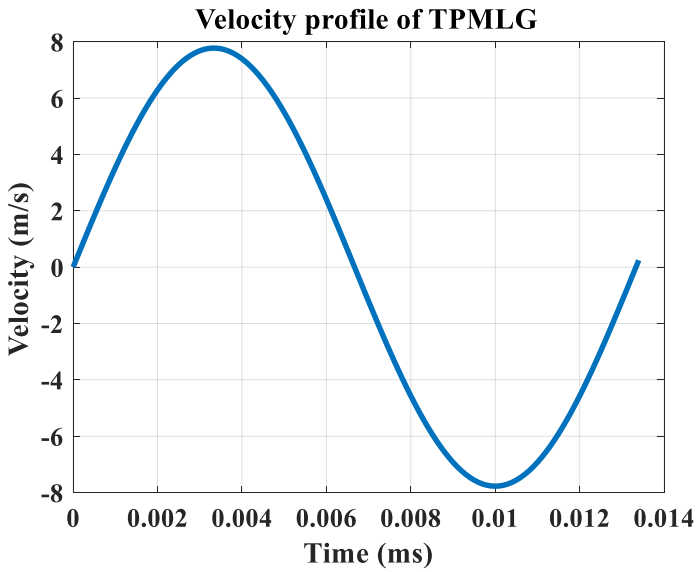

Figure 3-7 - Velocity profile for a spring assisted PMLG.

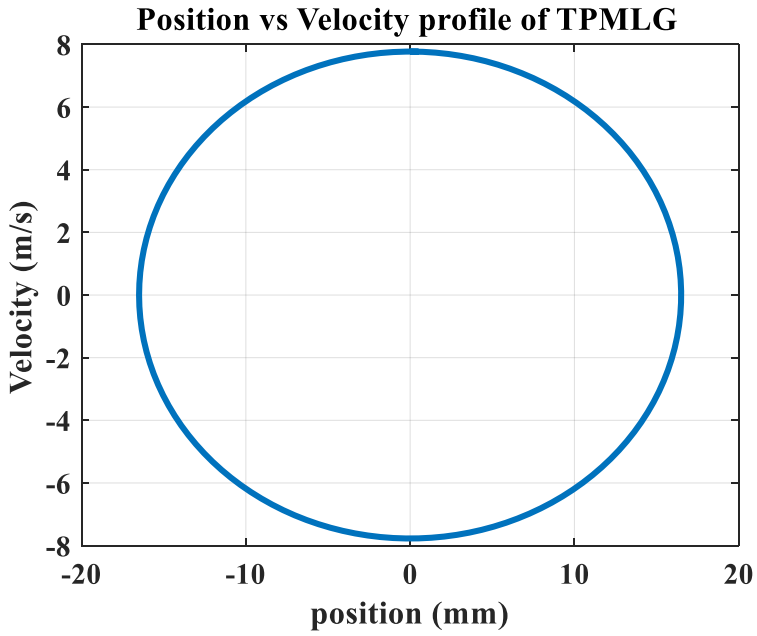

Figure 3-8 - Position vs Velocity for a spring assisted PMLG.

Table 3-2 gives the design calculation for 0.5 kW – 2.5 kW machine for an airgap of 2mm at 0.5 T, 0.6 T, 0.7 T, 0.8 T and 0.9 T.

Table 3-2 - Theoretical design calculations for 0.5 kW – 2.5 kW power PMLG.

Power	Bg	Vr	Ir	η	Poles	fe	w_s	h_s	MT	n_s	D
500	0.5	120	4.16	90	3	80	22	15.2	3	242	82.7
	0.6	120	4.16	90	3	80	22	12.6	4	200	56.5
	0.7	120	4.16	90	3	80	22	10.7	5	170	40.9
	0.8	120	4.16	90	3	80	22	9.4	6	149	30.88
	0.9	120	4.16	90	3	80	22	7.4	8	118	24
1000	0.5	120	8.3	90	4	80	22	17.4	3	138	132.7
	0.6	120	8.3	90	4	80	22	14.7	4	117	92.5
	0.7	120	8.3	90	4	80	22	13	5	103	66
	0.8	120	8.3	90	4	80	22	11.6	6	92	50.6
	0.9	120	8.3	90	4	80	22	9.4	8	74	39.6
1500	0.5	150	10	90	5	80	22	18.6	3	123	166.4
	0.6	150	10	90	5	80	22	15.9	4	105	114.9
	0.7	150	10	90	5	80	22	14.1	5	93	83.9
	0.8	150	10	90	5	80	22	12.7	6	84	63.8
	0.9	150	10	90	5	80	22	10.3	8	68	50

2000	0.5	175	11.4	90	5	80	22	19.2	3	111	22.5
	0.6	175	11.4	90	5	80	22	16.6	4	96	153.9
	0.7	175	11.4	90	5	80	22	14.87	5	86	112.5
	0.8	175	11.4	90	5	80	22	13.7	6	79	85.7
	0.9	175	11.4	90	5	80	22	11.1	8	64	67.3
2500	0.5	200	12.5	90	6	80	22	19.7	3	104	238.5
	0.6	200	12.5	90	6	80	22	17.2	4	91	165
	0.7	200	12.5	90	6	80	22	15.4	5	81	120.7
	0.8	200	12.5	90	6	80	22	14.2	6	75	91.9
	0.9	200	12.5	90	6	80	22	11.5	8	61	72.2

3.4 MATLAB GUI

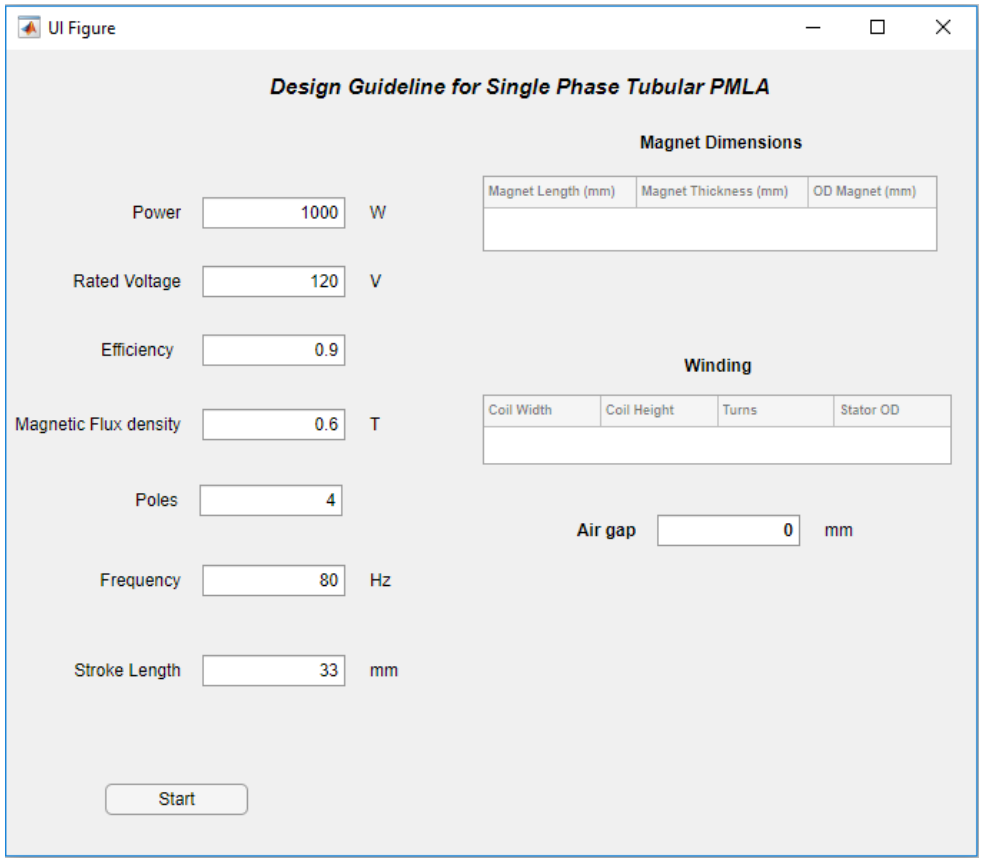

Figure 3-9 - Design guideline of the PMLG system.

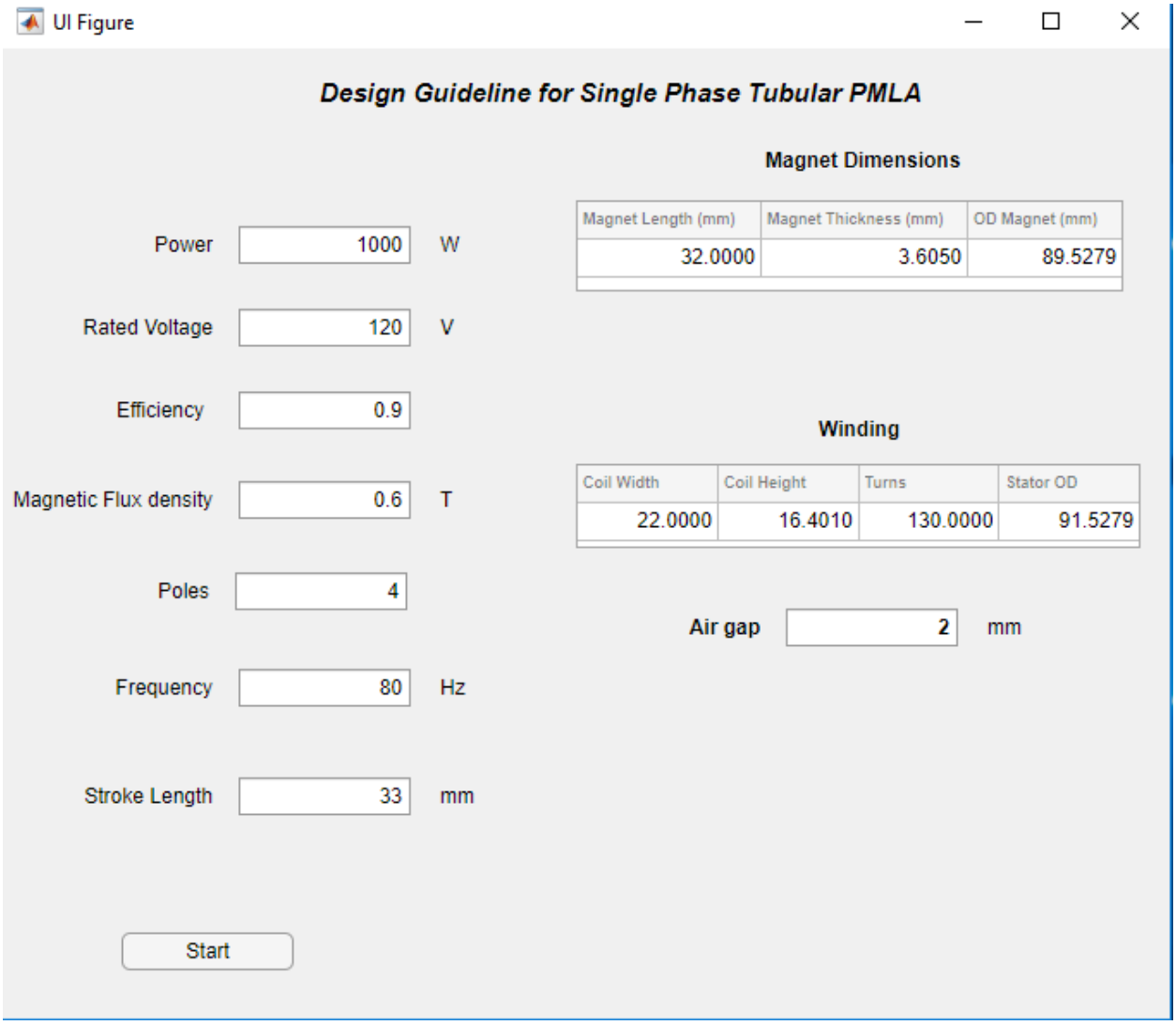

Figure 3-10 - Design guideline of the PMLG system with results.

3.5 Summary

In this chapter, a theoretical model and design guideline were developed for a single phase PMLG system. The design guideline utilizes the energy density and energy stored in the airgap as the starting point to calculate the electrical and geometric parameters of the PMLG system. The numerated steps below outline the basic guideline for design a PMLG system

1) Determine the input parameters of the PMLG system such as the output power, efficiency and rated voltage
2) Decide on the number of poles, airgap and flux density of the PMLG system
3) Calculate the magnet thickness of the PMLG using FEMM equations explained in (3-8), (3-9), (3-10), and (3-11) based on the airgap and flux density.
4) Calculate the energy density and energy stored in the airgap using (3-12) and (3-13).
5) Determine the outer diameter of the stator using (3-15).
6) Determine the geometric parameters of the magnet using (3-17) and (3-18)
7) Determine the stator parameter - slot height, slot width, number of turns per phase and number of turns per coil.
8) Choose the gauge of the wire using the current flowing through the windings and determine the resistance and inductance of the PMLG system using (3-27) and (3-28).

CHAPTER FOUR

4 Finite element modeling and validation of the PMLG system

Electromagnetic problems with complex geometry are difficult to solve directly through mathematical computations with closed-form solutions. This is because of the complicated geometries, different materials associated with the geometries and complex mathematical computations associated with determining the magnetic properties of the system. There are several techniques available to solve the electromagnetic problems as shown in Figure 4-1.

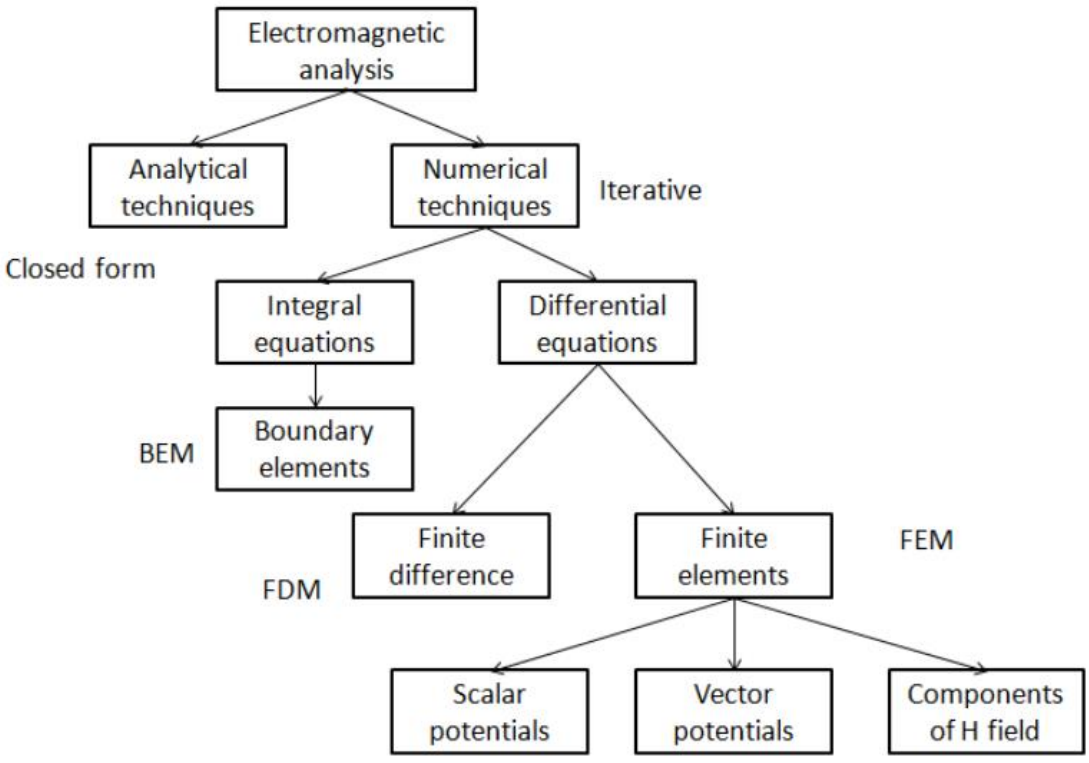

Figure 4-1 – Different types of electromagnetic analysis solutions [71].

Of these techniques, finite element method has emerged as one of the most robust methods for the analysis of electromagnetic problems.

This chapter reports the finite element modeling of the PMLG system using FEMM and MATLAB software. Specifically, FEMM was used to determine the magnetostatic properties of the PMLG system and MATLAB was used to process the results of magnetostatic parameters into electrical parameters. The FEMM model includes details on the geometry and material parameters specific to the PMLG system. Once the magnetostatic properties were captured from FEMM, different loading conditions were tested on the PMLG system using MATLAB. Finally, the FEMM model was compared with the theoretical model defined in Chapter 3 and the experimental PMLG system. The results obtained for all the test cases were discussed.

4.1 FEMM modeling of a PMLG system

The details on FEMM and the implementation of the PMLG system in FEMM is described in this section. FEMM is a finite element magnetics software which can calculate the magnetostatic parameters of electromagnetic systems. The advantage of FEMM is the flexibility and customization options in control and programming of the system. FEMM combined with MATLAB is a powerful tool to study electromagnetic systems. A simple graphical procedure used to control FEMM from MATLAB for the PMLG system is shown in Figure 4-2.

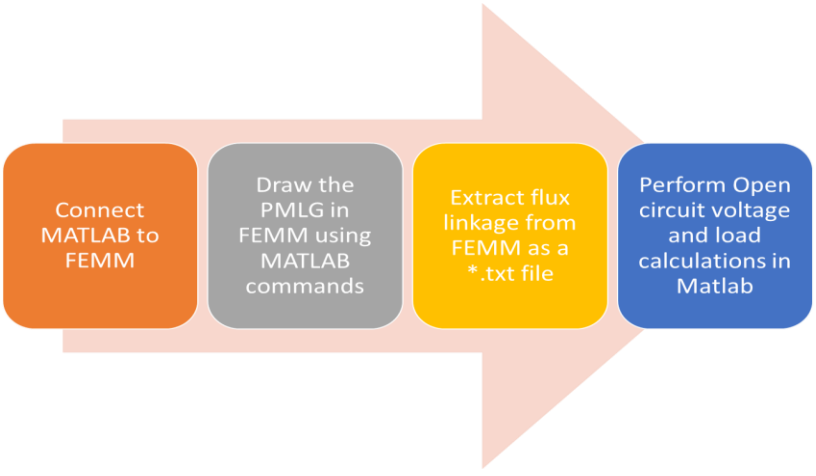

Figure 4-2 - FEMM / MATLAB process flow for modeling a PMLG system.

Each of the steps shown in Figure 4-2 is explained in detail below.

4.1.1 Step 1: Connect MATLAB to FEMM

The first step involved in modeling and analysis of a PMLG system using FEMM is to connect MATLAB and FEMM. While installing FEMM, files to connect MATLAB and FEMM is installed in the subdirectory of FEMM. This is usually in the directory C:\Program Files\femm42\mfiles. Therefore, the mfiles path of FEMM need to be added to the path of the MATLAB. The following lines need to be written in the command line of MATLAB.

addpath('C:\Program Files\femm42\mfiles');
savepath();

Once the path has been added, FEMM can be accessed from MATLAB using the command **"*openfemm*"**.

4.1.2 Step 2: Draw PMLG in FEMM using MATLAB

The second step involves drawing the PMLG system in FEMM using MATLAB commands. Since MATLAB can be used for drawing the PMLG system in FEMM, the ability to modify and control the PMLG geometry becomes very easy to implement. With this ability, sensitivity study, and optimizations can be done easily as shown in Chapter 5 and Chapter 6. Therefore, the control of the PMLG using MATLAB is a powerful tool to analyze the PMLG system. PMLG system consists of three main components - windings, laminations, and magnets. In addition, there is a back iron for the windings in the stator and an aluminum drum for the magnets. FEMM is a 2D modeling software and therefore the PMLG system was made as an axisymmetric model so that it is symmetric about its axis. Using the axisymmetric property and the symmetrical shapes of the PMLG system components, the model can be drawn in FEMM. The overall process flow to draw the PMLG system in FEMM is shown below in Figure 4-3.

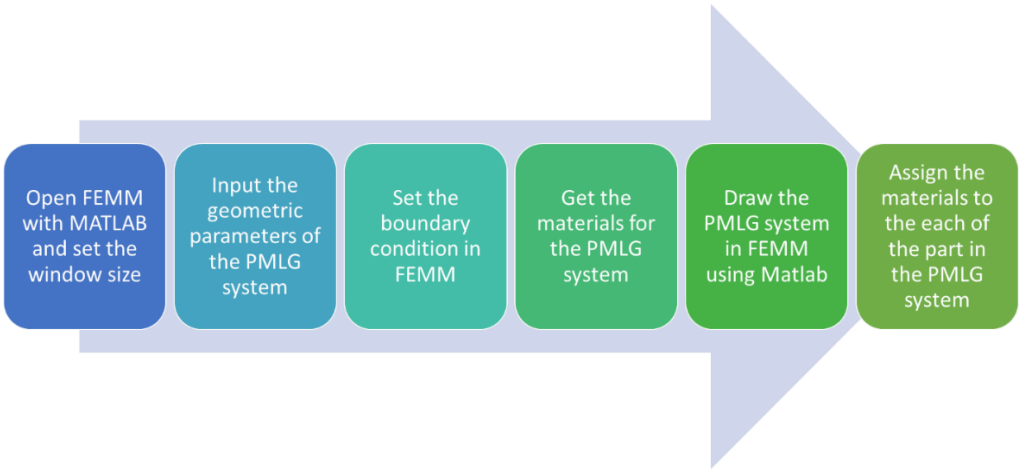

Figure 4-3 - Process flow for drawing PMLG system in FEMM using MATLAB.

4.1.3 Step 3: Flux linkage in FEMM

FEMM software can only perform magnetostatic calculations and cannot perform transient calculations. Therefore, the calculations of flux density and flux linkage are transformed from static to transient conditions using MATLAB. Another important aspect in this linear generator study is that the flux linkage is sinusoidal because of the sinusoidal motion of the translator. Therefore, magnetostatic calculations was sufficient for the determination of the linear generator characteristics. This technique will work for resistive loads and not for reactive loads as transient conditions cannot be determined using this method. To simulate the flux calculations, first, the stroke length of the PMLG is divided into discrete steps. Later, at each of these positions, the flux linkage of the PMLG system is determined. Based on the number of turns, the flux linkage for the windings is calculated.

Example: For a stroke length of 33 mm, the flux linkages are measured in steps of 0.5 mm. Therefore 67 different conditions (includes 0 mm position) of the flux linkages are calculated at each of the positions of the translator with respect to the stator in the PMLG system. Furthermore, to be more accurate, depending on the number of turns, flux linkage for each of the turns is calculated. Once the data for the flux linkages are calculated, they are saved as a text file.

Consider a 33 mm stroke length, 6 windings in the stator with 126 turns each. A total of 402 (6*67) files was created for the PMLG system. Each of the text file contains flux

linkages of the windings for each of the locations of the translator with respect to the stator of the PMLG system.

4.1.4 Step 4: Perform OC voltage and load calculations in MATLAB

Once the flux linkages of the PMLG system were known from FEMM, the following equation was used to convert flux linkage with respect to position to flux linkage with respect to time.

$$\frac{d\lambda}{dt} = \frac{d\lambda}{dx} * \frac{dx}{dt} \tag{4-1}$$

where,

λ – flux linkage,

x – position, and

t – time.

Induced emf in the PMLG system is given by the equation (4-2).

$$V = N * \frac{d\lambda}{dt} \tag{4-2}$$

where,

V – Induced emf, and

N – number of turns.

After the OC voltage (induced emf) was determined, the resistance and inductance of the PMLG system were calculated from FEMM. Later different loading resistances were used to load the PMLG system and the load voltage and currents were calculated. The power produced from the PMLG system is calculated based on the load voltages and currents. The equations to determine the impedance, load voltage, current and output power is shown below. First the impedances of the PMLG system are calculated based on the loads. Three different cases are chosen here. They are load resistance with 1) No capacitors 2) Capacitor in series 3) Capacitor in parallel.

Load resistance without capacitor:

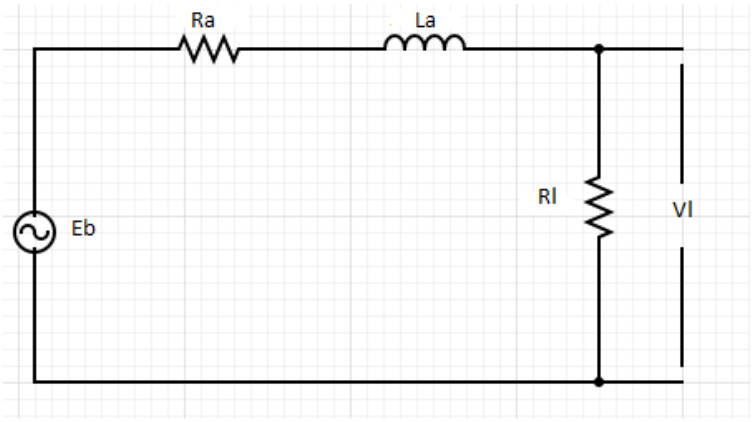

Figure 4-4 - PMLG equivalent circuit model without load capacitors.

The overall impedance of the system is calculated using the equation (4-3) and (4-4).

$$Z_{amp} = \sqrt{(R_a + R_l)^2 + (X_l)^2} \quad (4\text{-}3)$$

$$Z_{angle} = \tan^{-1}\left(\frac{X_l}{R_a + R_l}\right) \quad (4\text{-}4)$$

where,

$X_l = j\omega L_a$.

Load resistance with capacitor in series:

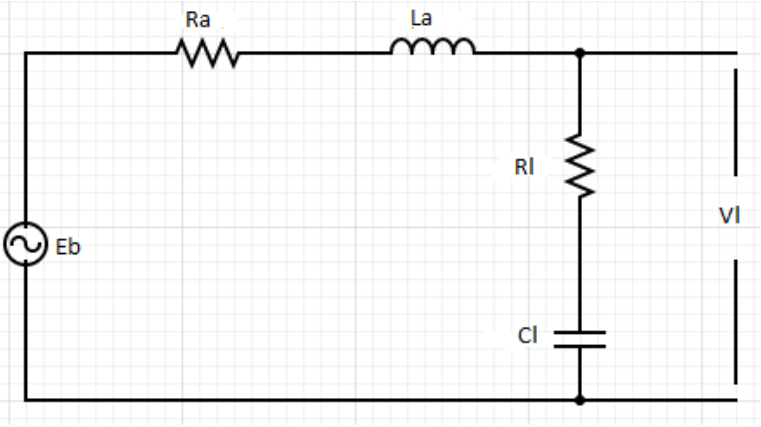

Figure 4-5 - PMLG equivalent circuit model with load capacitor in series.

The overall impedance of the system is calculated using the equation (4-5) and (4-6).

$$Z_{amp} = \sqrt{(R_a + R_l)^2 + (X_l - X_c)^2} \quad (4\text{-}5)$$

$$Z_{angle} = \tan^{-1}\left(\frac{X_l - X_c}{R_a + R_l}\right) \quad (4\text{-}6)$$

where,

$$X_c = \frac{1}{(2 * pi * f * C_l)} .$$

With capacitor in parallel

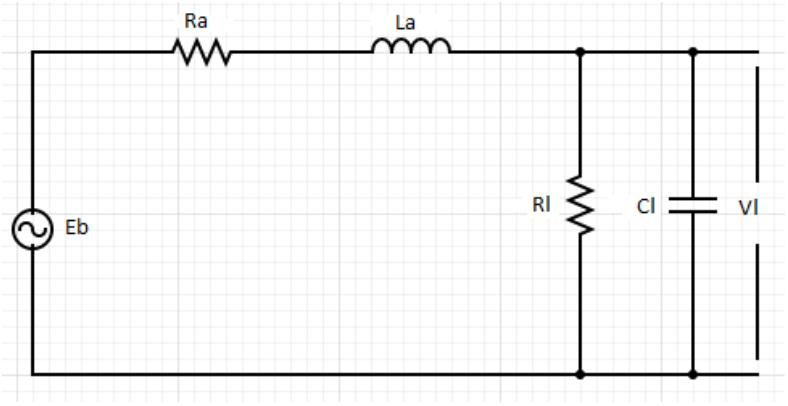

Figure 4-6 - PMLG equivalent circuit model with load capacitor in parallel

Impedance of this PMLG circuit is given by the equation (4-7) and (4-8).

$$Z_{amp} = \sqrt{(R_a + R_{rc})^2 + (X_l - X_{rc})^2} \quad (4\text{-}7)$$

$$Z_{angle} = \tan^{-1}\left(\frac{X_l - X_{rc}}{R_a + R_{rc}}\right) \quad (4\text{-}8)$$

where,

$$R_{rc} = \frac{R_l X_c^2}{R_l^2 + X_c^2} \quad (4\text{-}9)$$

$$X_{rc} = -\frac{R_l^2 X_c}{R_l^2 + X_c^2} \quad (4\text{-}10)$$

$$X_c = \frac{1}{(2 * pi * f * C_l)} \quad (4\text{-}11)$$

Once the impedance is known, the current flowing in the circuit is calculated using the equation (4-12) and (4-13).

$$Z = Z_{amp} \angle Z_{angle}$$

$$I_l = \frac{E_b}{Z} \tag{4-12}$$

$$V_l = I_l * R_l \tag{4-13}$$

From the loading conditions, the maximum power produced by the PMLG system is calculated based on the Thevenin's maximum power transfer equations given below.

$$P = \frac{E_b^2}{4 * R_a} \tag{4-14}$$

A model drawn in FEMM is shown below in Figure 4-7. Using this model and the calculations from the flux linkages, the electrical parameters of the PMLG system were calculated.

The complete MATLAB code to implement each of these steps in FEMM is attached in appendix.

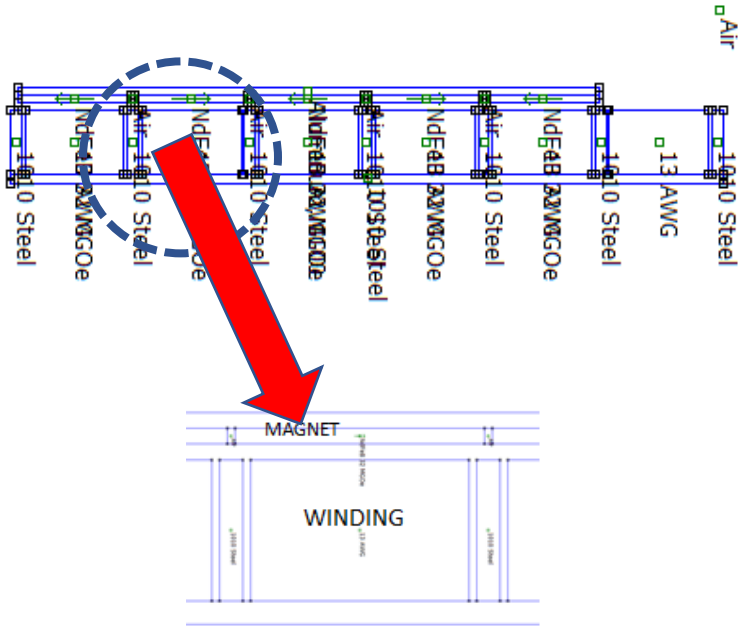

Figure 4-7 - FEMM model of the PMLG and the zoomed in version of a pole in the PMLG system

The basic calculations and procedure were set up to use FEMM and MATLAB to model and analyze a PMLG system. With the setup, three different PMLG configurations were compared with the FEMM model. The three different PMLG configurations were,

1) Theoretical model of a 1 kW machine from Chapter 3,
2) Alpha prototype of the PMLG system built at WVU, and
3) Beta prototype of the PMLG system built at WVU.

4.2 Theoretical model of a 1 kW machine from Chapter 3

In Chapter 3, several configurations of the PMLG system were provided based on flux density and rated output power in Table 3-2. From the table, one configuration for a 1 kW at 0.6T PMLG system was chosen.

The geometric parameters of the chosen configuration are shown in Figure 4-2.

Table 4-1 - Geometric parameters of the theoretical 1 kW PMLG system.

S.No	Part	Dimension
1	Coil height	14.7 mm
2	Coil width	22 mm
3	Back iron stator depth	3 mm
4	Lamination stack width	3 mm
5	Magnet radial thickness	3.6 mm
6	Airgap	2 mm
7	Oscillating frequency	80
8	Number of poles	4
9	Outer Diameter of Magnet	91.5 mm
10	Coil number of turns	130
11	Translator spacer width	1 mm
12	Wire gauge	13 AWG
13	Magnetic flux density	0.6 T
14	Phase	1
15	Magnet flux arrangement	Axial
16	Stroke length	33 mm

Based on the theoretical model parameters in Table 4-2, FEMM model was analyzed and the results were shown below in Figure 4-8, Figure 4-9, and Figure 4-10. To use AWG 13 wire, the slot height had to be modified from 14.7 mm to 22 mm. This results in a total number of turns to be 120. There was a 49% increase in slot height from the theoretical calculations. The change in slot height has an effect only on the geometric size of the PMLG system and not on the electrical parameters of the PMLG system. This was because all the other parameters, especially the number of turns was kept same as the theoretical model. The results from the FEMM model is shown in Figure 4-8. It was seen that the maximum power of 1.209 kW was produced for the theoretical model. The required rated power of 1 kW was produced at an efficiency of 91.7%. This was in line with the expected rated power of 1 kW at an efficiency of 90% in Table 3-2. The expected OC voltage from the theoretical calculations was 200 V whereas the OC voltage from FEMM was 186 V. There was a 7 % error in the OC voltage estimation from the theoretical calculations.

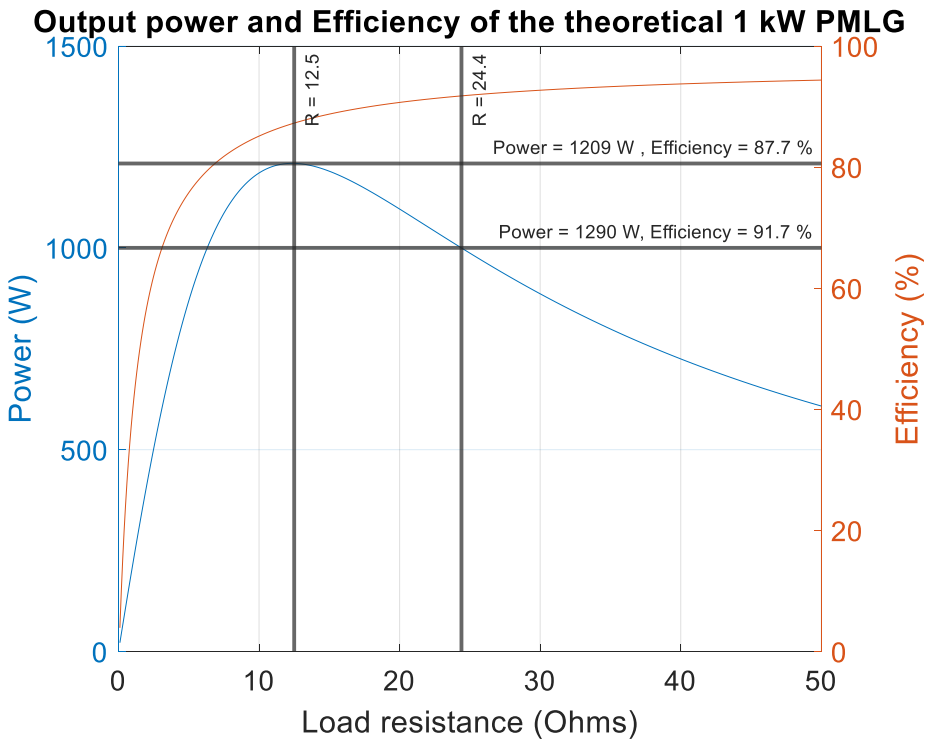

Figure 4-8 - Power and efficiency for the theoretical 1 kW PMLG system.

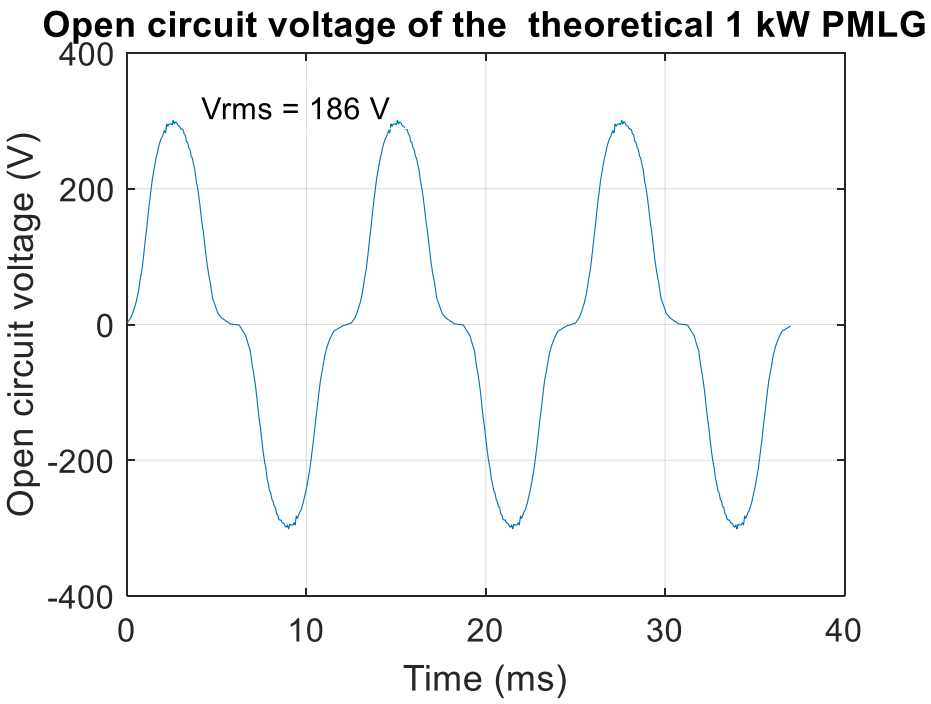

Figure 4-9 - OC voltage of the theoretical 1 kW PMLG system.

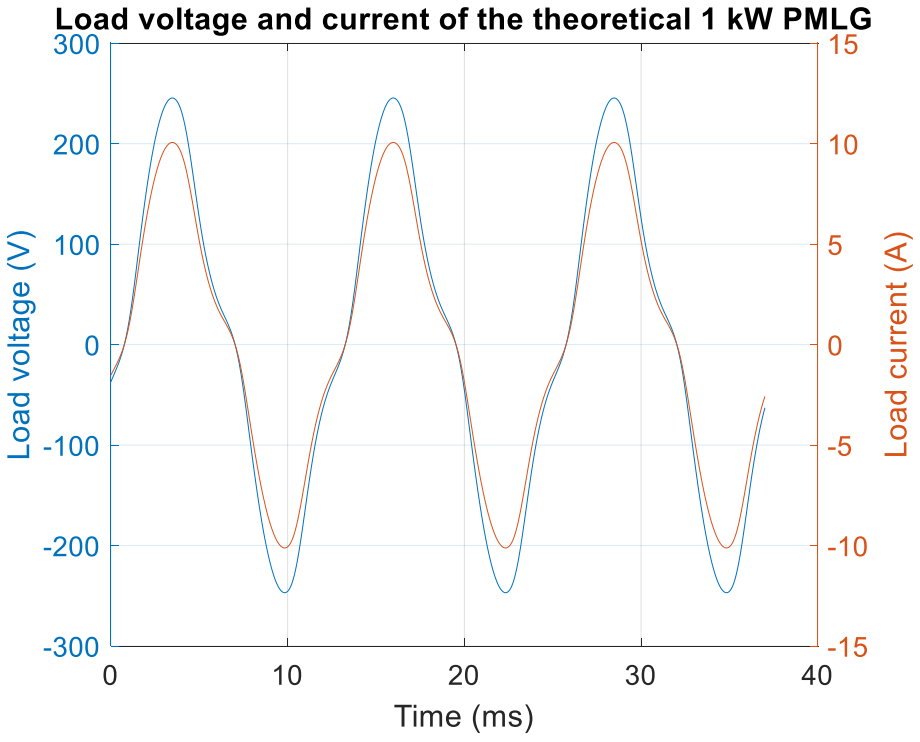

Figure 4-10 - Load voltage and load current of the theoretical 1 kW PMLG system.

Figure 4-10 shows the load current and load voltage of the theoretical 1 kW PMLG. From the FEMM model, the load voltage and current were 156 V and 6.4A. The expected load voltage and current from the theoretical calculations were 120V and 8.33A. So, there is a 23% error in the load voltage and a 15% error in the load current. Other parameters of the PMLG systems such as the voltage per coil and the harmonics in the OC voltage are shown in Figure 4-11.

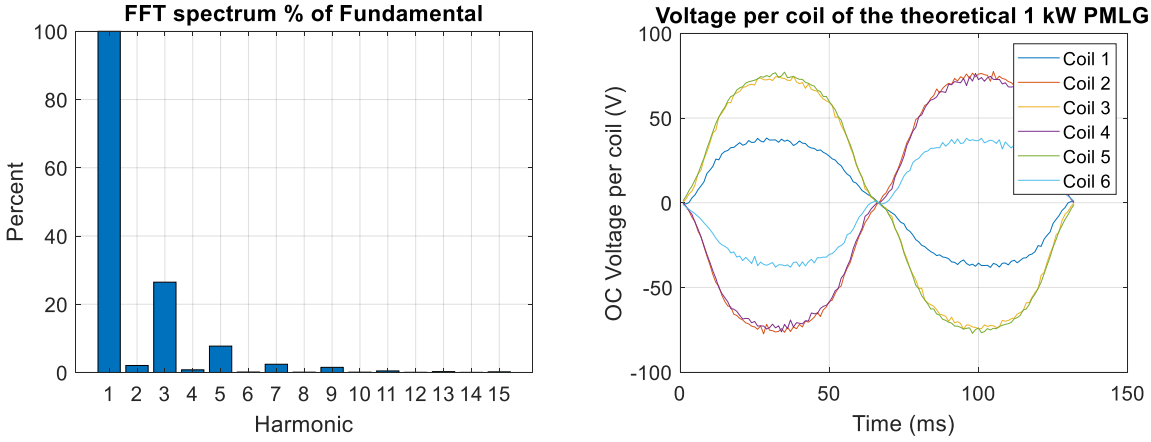

(a) (b)

Figure 4-11 - (a) Harmonic components of the OC voltage (b) voltage per coil of the theoretical 1 kW PMLG system.

From Figure 4-11 - a, the harmonics in the OC voltage were composed of mainly 3rd and 5th harmonics. For the theoretical model, 3rd harmonics were 26.5% and 5th harmonics were 7.7%. The detailed harmonics of the theoretical 1 kW PMLG are added in the appendix. Whenever there is a change in the direction of the translator, there is a dip seen in the OC voltage in Figure 4-9. A way to mitigate the harmonics in the system was to run the PMLG below its pole pitch or stroke length. But this results in a reduction in output power, efficiency or increase in the overall volume and the moving mass of the PMLG system. From Figure 4-11 – b, voltage per individual coils of the PMLG system was determined. It was seen that the Coils 2, 3, 4, and 5 have peak voltages of 75 V. Coils 1 and 6 have a peak voltage of 37 V. For a 4 pole PMLG system, there were 6 coils in the stator. Therefore, there is two coils are partially inactive in the system. The coils at the ends of the stator are active for only half of the cycle and therefore the voltage is

reduced by half in Coil 1 and Coil 6. In addition, because of the winding configuration, Coil voltages in 1, 3 and 5 were in phase with each other and Coil 2, 4, and 6 were in phase with each other. To combine them together, Coil 1, 3 and 5 were 180^0 out of phase with Coils 2, 4 and 6. This results in the OC voltage of 186 V as shown in Figure 4-9.

Comparison of FEMM with the theoretical PMLG system is shown in Table 4-2.

Table 4-2 - Comparison of FEMM and theoretical calculations from Chapter 3.

Parameter	Theory	FEMM	Error (%)
Output power (W)	1000	1000	0
Efficiency (%)	90	91.7	1.8
Load voltage (V)	120	156	23.1
Load current (A)	8.3	6.4	29.6
Slot height (mm)	14.7	22	33.1
Turns	130	130	2.5
Magnetic flux density (T)	0.6	0.66	9.1

The reasons for the error differences of more than 20% in the load voltage is attributed to the assumptions made in the design guidelines in Chapter 3. The two main factors which contribute to the error are the magnetic flux density, and the fringing effect in the PMLG system.

4.3 Description of the prototype free piston engine PMLG system built at West Virginia University

This section describes the construction of the experimental prototype of the 1 kW free piston engine PMLG system built at West Virginia University. Potential applications of this system are CHP and electrical generators for homes. The system is a single cylinder system with one engine cylinder and run by natural gas fuel. CAD model of the free piston engine PMLG system is shown below in Figure 4-12. There are three main components of the free piston engine PMLG system developed at West Virginia University. They are,

- Engine system,
- PMLG system, and

- Springs.

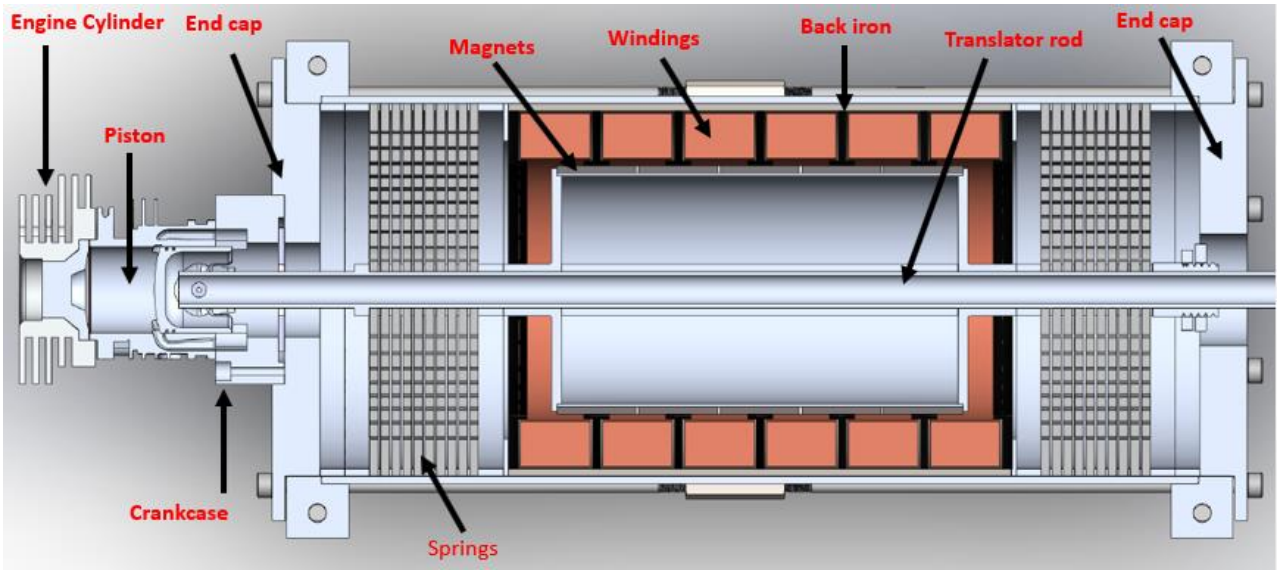

Figure 4-12 - CAD model of the free piston engine PMLG system.

4.3.1 Engine system

Components used in the engine system are 1) A cylinder where combustion happens 2) A piston and ring assembly located inside the cylinder 3) Crankcase 4) Intake system 5) Exhaust system 6) Spark plug in the cylinder head for ignition. Since it's a spark ignited system, the spark plug is located on the cylinder head. Intake and exhaust systems help in the exchange of the fuel + air gaseous mixture.

4.3.2 PMLG system

PMLG system consists of a stator and rotor. The stator is made of windings, laminations and back iron. Translator consists of magnets, aluminum drum and rod. PMLG system acts both as a motor and as a generator depending whether it is in the starting mode or generating mode.

4.3.3 Springs

The flexure spring used for the system as shown in Figure 4-13. The spring is made of Sandvik material 7C27Mo2. Springs are mounted on either side of the PMLG system. Springs in the PMLG system has two responsibilities.

1. They act as a bearing to maintain the airgap between the stator and translator in the PMLG system. To achieve this, springs were mounted on either side of the translator. The inner diameter of spring matches with the translator rod outer diameter. This outer diameter of the spring matches with the back iron of the stator. By matching the inner diameter and outer diameter with the translator and the stator of the PMLG system, springs maintain the airgap in the PMLG system.
2. They act as an energy storage system. If PMLG has to be started as a motor, a lot of force needs to be generated to start the overall free piston engine system to achieve the required stroke length for combustion to start. When PMLG is attached with springs, the overall system becomes a mass spring system. Therefore, as power is supplied to the PMLG system, the energy is stored in the springs in each cycle. As the number of cycles increases, the energy stored in the springs also increases, thereby able to provide the required stroke length for the PMLG system. The beta prototype has only one cylinder. Therefore, a return force is required for the piston to come back towards the top dead center of the cylinder. This is also provided by the springs.

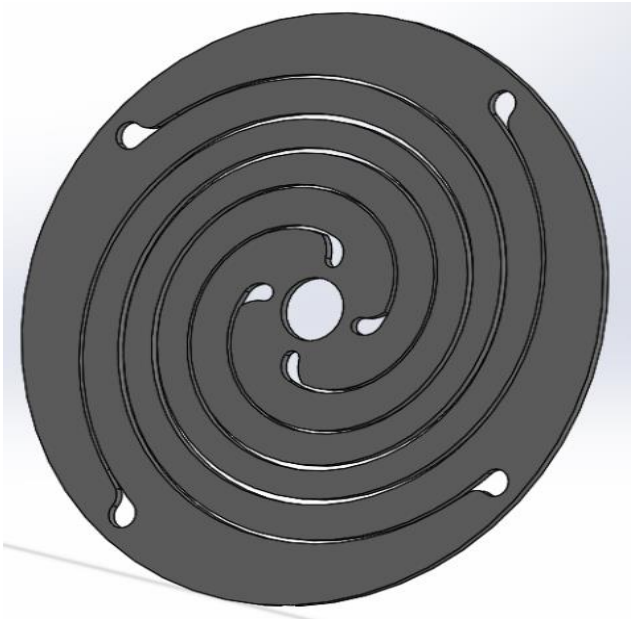

Figure 4-13 - Geometric design of flexure springs.

4.4 Operation of the experimental prototype PMLG system

Operation of the Beta prototype PMLG system involves two modes. They are,

- Motoring mode, and
- Generating mode.

4.4.1 Motoring mode

In a free piston engine PMLG system, PMLG system is started as a motor. This is done by using an H bridge inverter circuit, a Texas Instrument (TI) DSP 320f28335 controller and a DC power supply. The overview of the controller system for the PMLG system to act as a motor is shown in Figure 4-14. The TI DSP provides the necessary switching signals to the IGBTs in the H bridge circuit to start the PMLG system. From the controller circuit, the linear thrust force is provided by the PMLG system. With the aid of the springs, the energy in the PMLG system increases and thrust forces increase. This force creates the necessary compression force in the engine cylinder for the fuel mixture to ignite.

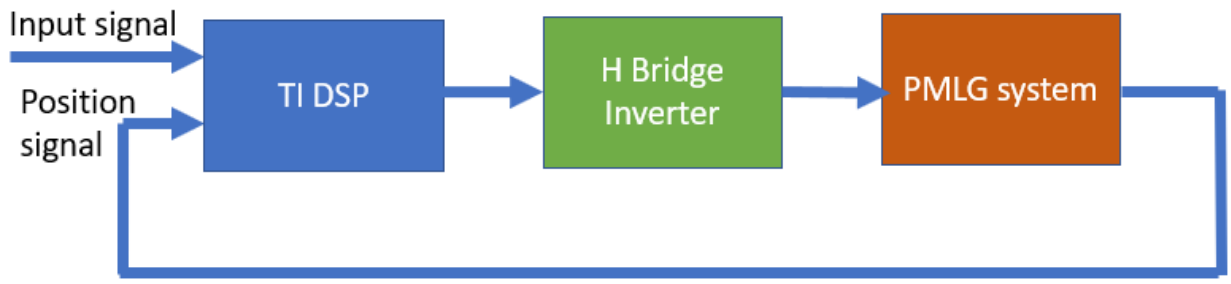

Figure 4-14 - Motoring mode of the PMLG system.

The DSP controller used in the system was a Texas instrument controller. A phase locked loop (PLL) technique was used to control the PMLG system as a motor. Details on the PLL technique used for the PMLG system is detailed in [98]. The H bridge inverter that is used for the PMLG system consists of four IGBTs to provide pulse signals to the PMLG system in both directions. For the PMLG system, signals were given to only two IGBTs and the springs provided the return force for the system. Figure 4-15 shows the TI DSP used in the PMLG system.

Figure 4-15 - Texas Instruments DSP 320f28335 used in the experimental PMLG system.

The H bridge circuit and the experiment board developed is shown below in Figure 4-16 and Figure 4-17.

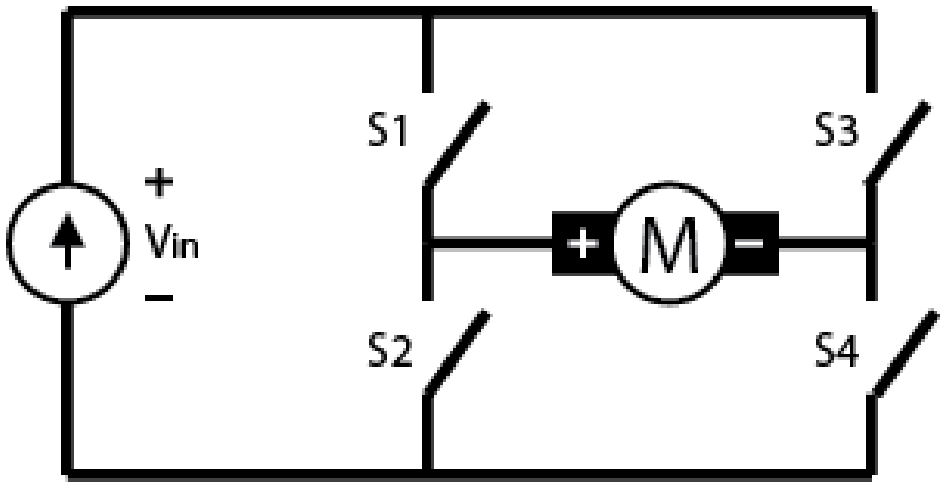

Figure 4-16 – Circuit diagram of a H bridge inverter

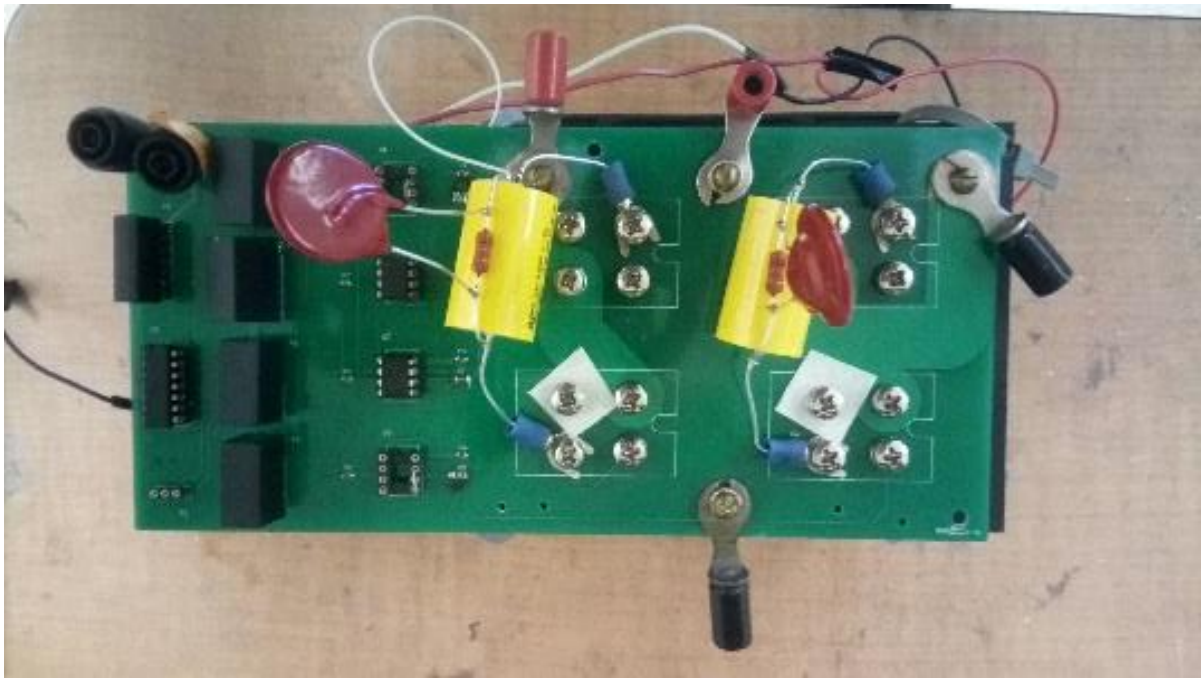

Figure 4-17 - Experimental H Bridge Inverter board built at WVU.

4.4.2 Generating mode

Generating mode starts once the engine starts combusting and produce power. For an engine to start, certain compression ratio and pressures need to be reached for the fuel mixture to ignite and produce engine power. In the experimental prototype of the PMLG system, the fuel used for the engine combustion is natural gas which contains 86% methane, 12% ethane, 1% propane, 0.5% nitrogen and 0.5% carbon dioxide.

Combustion starts once the PMLG system reaches a certain stroke length and the intake ports of the engine open. Once combustion starts and the engine starts producing power, the PMLG system was converted from a motoring phase to generating phase. This was done by switching off the inverter circuit and attaching a load to the windings of the PMLG system. Depending on the load resistance, the power delivered to the PMLG system can be controlled. System overview of the generating mode is shown in Figure 4-18.

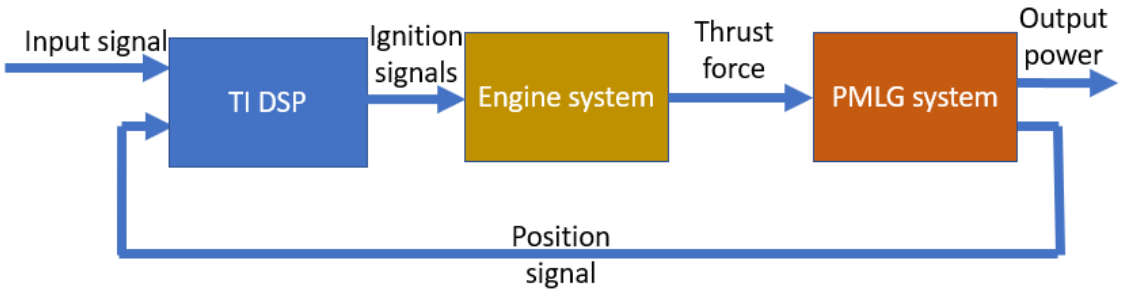

Figure 4-18 - Generating mode of the PMLG system.

4.5 Instrumentation in the experimental prototype of the PMLG system

This section describes the instrumentation used in measuring the different parameters in the beta prototype PMLG system. The TI DSP controller requires the position signal to determine the current location of the piston and provide ignition signals to combust the fuel in the engine cylinder. Measurement of the position is done in two ways – Analog potentiometer and a linear magnetic encoder. A softpot potentiometer from spectra symbol was used for the analog potentiometer. This was used to acquire the position data and perform engine and generator data analysis. Along with the soft pot potentiometer, a metal ball plunger was attached to the rod to track the rod's position. The potentiometer and ball plunger are shown in Figure 4-19.

Figure 4-19 - Potentiometer and ball plunger for measuring the position in the experimental PMLG system.

A linear magnetic encoder from RLS has the ability to measure the position accurately with a 5µm accuracy. But this accuracy cannot be translated to the measurement accuracy in the overall system because of the system is not perfectly rigid. This is because of the vibration of rod as well as the knuckle mechanism which attaches the rod to the piston. The RLS encoder is a quadrature encoder which provides three signals –

A, B and Z. The three signals are converted to position using a Quadrature encoder module in the TI DSP. Example of the three output signals from the encoder is shown below in Figure 4-20. A magnetic strip is mounted on the translator rod and the linear magnetic encoder is mounted on the end cap of the PMLG system. The encoder along with the magnet strip used for this purpose is shown in Figure 4-21.

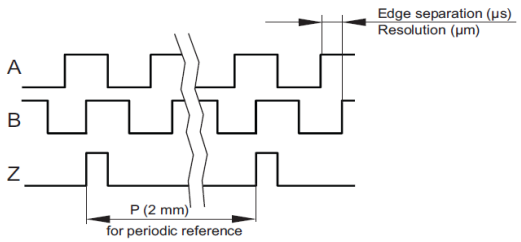

Figure 4-20 - A, B and Z signal from the linear encoder [99].

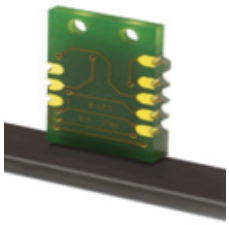

Figure 4-21 - RLS linear magnetic encoder used in the PMLG system.

The cylinder combustion pressure was measured using a Kistler piezoelectric pressure transducer of type 6054B with a 0 - 250 bar measuring range. Kistler pressure transducer converts the pressure into small voltage readings in the range of µV - mV. Therefore, amplifiers were used to amplify the pressure data into readings which are in the measurable range. Furthermore, Kistler data acquisition system was used to acquire and save the data for post-processing the results. This acquisition came with the necessary amplifiers to perform the amplification of the pressure transducer signals. There is a time delay in the pressure and other instrumentation measurements in Kistler but those delays have been assumed to be negligible. To measure and control the fuel flow, Alicat Scientific Mass flow controller (MFC) MC – 20 series was used. This had a measuring range of 0 – 20 SLPM. In addition, there was option in the MFC to measure different fuel mixtures and the natural gas mixture used in our study was setup in the MFC. To measure the intake airflow, the Meriam 50MW20 laminar flow element of 8 SCFM capacity was

used. A pressure gauge of 8 SCFM was used to measure the differential pressure in the intake air flow. The electrical current and voltage in the PMLG system were measured using DC current clamp meters (0 - 20A range) and voltage meters (0 - 500V range) respectively.

Two prototypes of the free piston engine PMLG were built at West Virginia University. They were named as,

- Alpha prototype (1st generation) and
- Beta prototype (2nd generation).

Details on the two prototypes, experimental results and the comparison with FEMM is discussed in the upcoming sections.

4.6 Alpha prototype

The first generation of the free piston engine PMLG system built at West Virginia University was called the alpha prototype. Figure 4-22 shows the alpha prototype built at WVU.

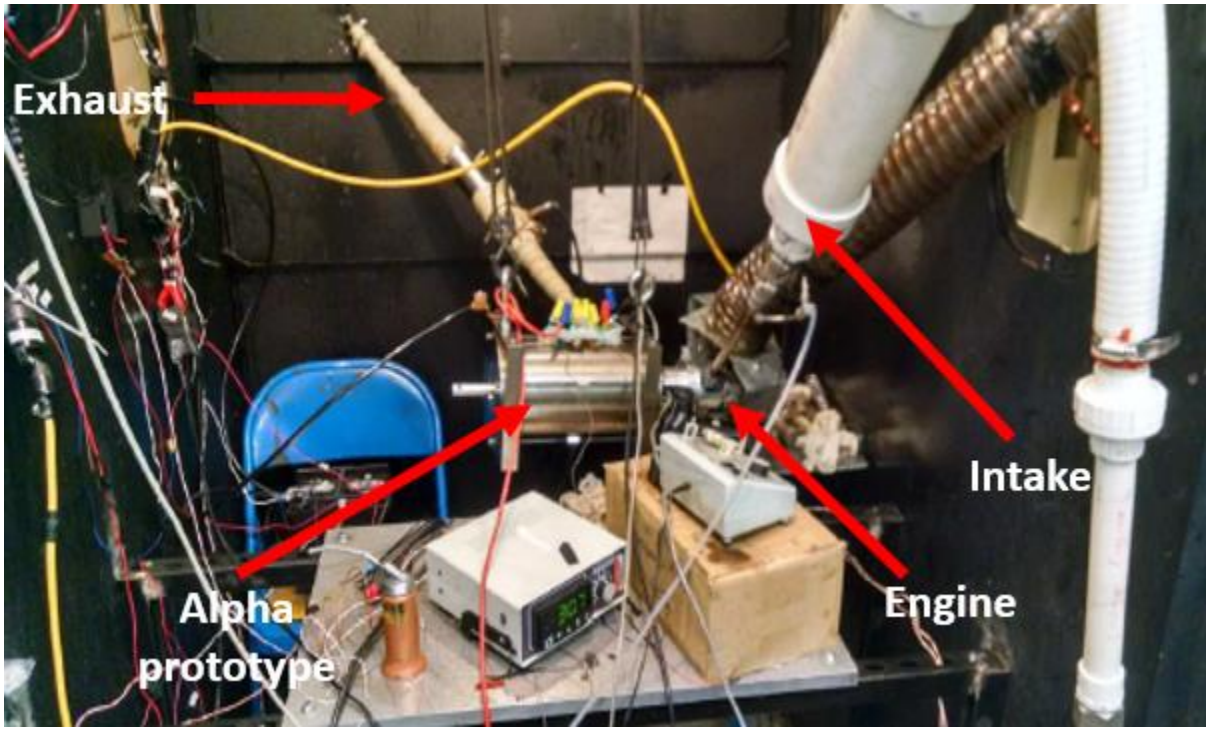

Figure 4-22 - Alpha prototype of the free piston engine PMLG system.

The prototype with the measuring instruments when the Alpha prototype was run as a motor is shown in Figure 4-23.

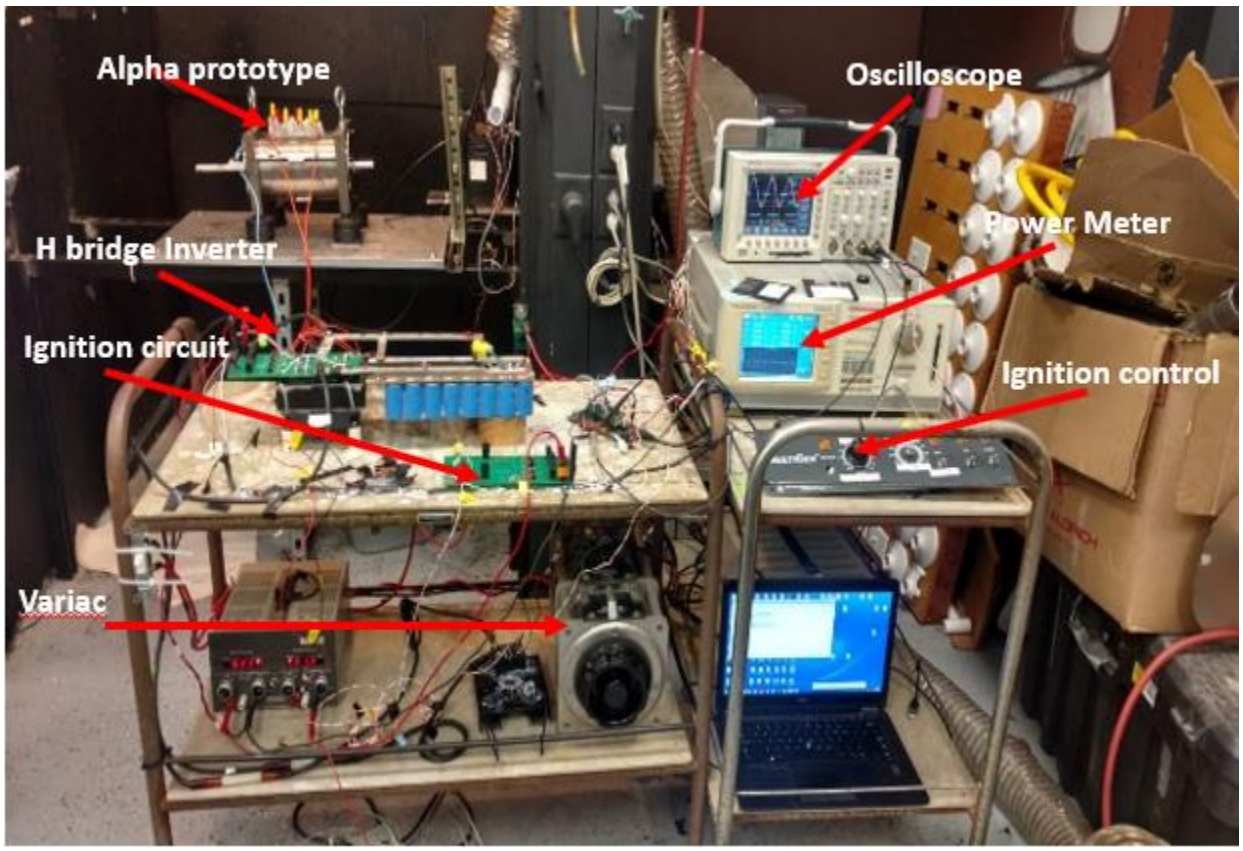

Figure 4-23 - Alpha prototype with measuring instruments as a motor.

The geometric parameters of the Alpha prototype PMLG system studied is shown in Table 4-3.

Table 4-3 - Geometric parameters of the alpha prototype.

S.No	Part	Dimension
1	Coil height	6 mm
2	Coil width	16 mm
3	Back iron stator width	3 mm
4	Lamination stack width	4 mm
5	Magnet radial thickness	2 mm

6	Airgap	2 mm
7	Oscillating frequency	74
8	Number of poles	4
9	Outer Diameter of Magnet	100 mm
10	Coil number of turns	24
11	Translator spacer width	1 mm
12	Wire gauge	13 AWG
13	Phase	1
14	Magnet flux arrangement	Axial
15	Stroke length	22 mm

Alpha prototype built at WVU had two different stator cores – Air core and Iron core. The results from the air core and iron core are discussed below.

4.6.1 Air core alpha prototype

The Air core alpha prototype had a resonant frequency of 74 Hz. The stator resistance and inductance of the Alpha prototype was 0.273 Ohms and 0.425 mH. The alpha prototype was tested at 5 different loads and the comparison of FEMM and experiment is shown in Table 4-4.

Table 4-4 - Comparison of the experimental tests with FEMM for Air core alpha prototype.

Load (Ohm)	Power (W) – Experiment	Power (W) – FEMM	Error (%)
1.125	49.5	53.05	7.2
0.844	58.6	60.81	3.8
0.563	65.1	69.1	6.1
0.281	74.9	70.2	6.3
0.094	63. 2	49	22.4

From the experiment, the stroke length of the alpha prototype was 26 mm as the engine's stroke length was 26 mm. Therefore, FEMM simulations were run at 26 mm and the output power obtained at different loads is shown in Figure 4-24.

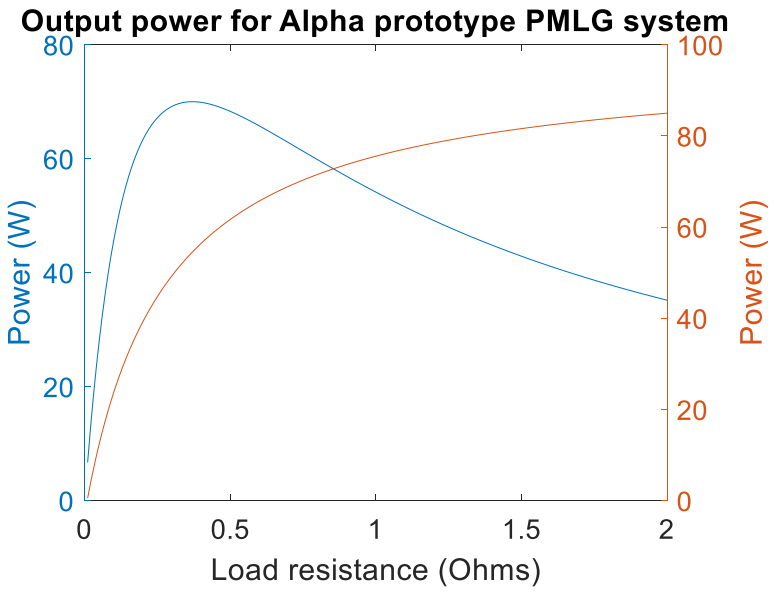

Figure 4-24 - Output power and efficiency for the Air core alpha prototype PMLG system – FEMM.

From Figure 4-24, maximum power of 68 W at 50 % efficiency is produced by the air core alpha prototype.

Based on the design parameters, the open circuit voltage of the Air core alpha prototype is shown in Figure 4-25. There is a hump at the end of each cycle, and this is because of the two reasons

1. The neutral position of the translator with respect to the stator was not aligned perfectly at 0mm. For a PMLG system, the center of the pole of the translator must lie directly underneath the center of the windings. In this condition, the PMLG system can move half of the stroke length on either side of the windings. If this is misaligned, harmonics and distortions in the waveforms occur. This is seen in the OC voltage waveform and is explained in detail in Chapter 5.
2. The pole pitch of the Alpha prototype was 22 mm. The stroke length of the engine in the Alpha prototype was 26 mm. Therefore, the engine operated the system at

26 mm. This caused the translator to move to a stroke length greater than the pole pitch. Therefore, humps occurred on either side of the OC voltage waveform.

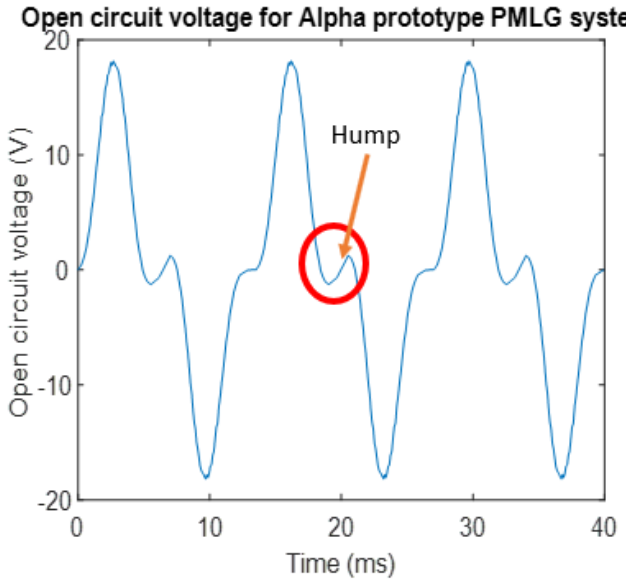

Figure 4-25 - OC voltage for the alpha prototype PMLG system – Experiment.

Voltage and current waveform for a load of 0.094Ω was captured and the comparison is shown in Figure 4-26 and Figure 4-27.

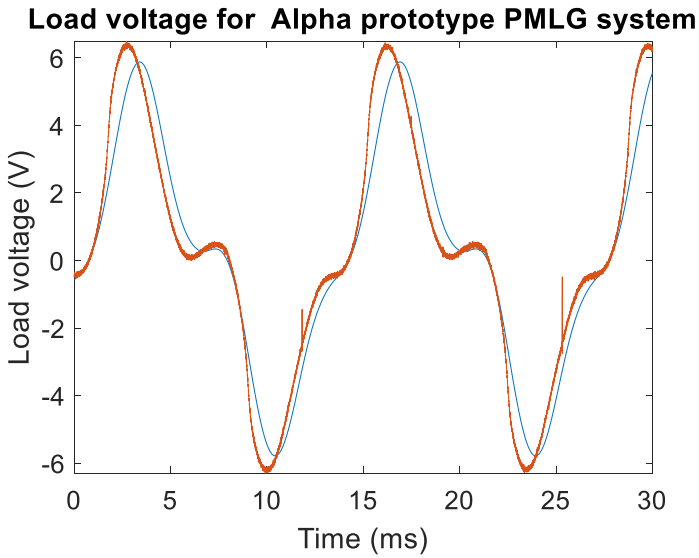

Figure 4-26 - Load voltage comparison between Experiment and FEMM.

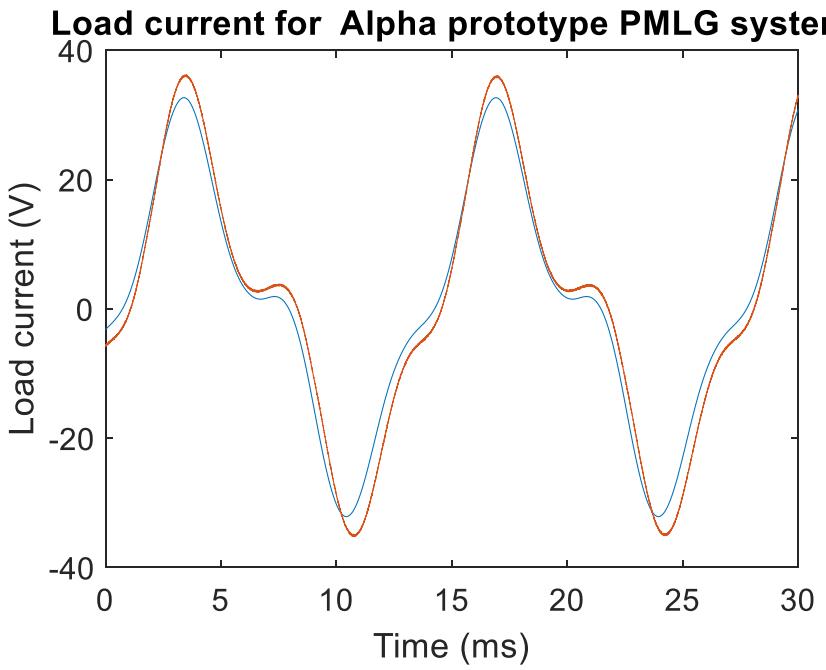

Figure 4-27 - Load current comparison between Experiment and FEMM.

From Figure 4-26 and Figure 4-27, the wave shapes of load current and load voltages are similar for the experiment and FEMM. But the peaks are different. This can be attributed to differences in the airgap, and slight changes in the neutral position between the experiment and FEMM. Overall a comparison of the alpha prototype with FEMM was modeled and studied. The output power was compared, and the error was less than 10 % for 4 different test conditions. This provides a confidence in the FEMM model to perform different parametric studies and optimization as discussed in Chapter 5 and Chapter 6.

4.6.2 Iron core alpha prototype

The Iron core Alpha prototype had a resonant frequency of 74 Hz. The stator resistance and inductance of the Alpha prototype was 0.273 Ohms and 0.75 mH. The alpha prototype was tested at 2 different loads and the comparison of FEMM and experiment is shown in Table 4-5.

Table 4-5 - Comparison of the experimental tests with FEMM for Iron core alpha prototype.

Load (Ohm)	Power (W) – Experiment	Power (W) – FEMM	Error (%)
1.125	127.3	128.6	1
0.844	158.9	145.3	8.5

For the two conditions, the error in the output power was 1% and 8.5%. Similar to the air core case, the error was less than 10%. Output power, efficiency, and OC voltage for the iron core alpha prototype is shown in Figure 4-28 and Figure 4-29. The asymmetry in the sinusoidal wave in Figure 4-29 can be attributed to the presence of spacer in between the magnets and neutral position of the translator with respect to the stator.

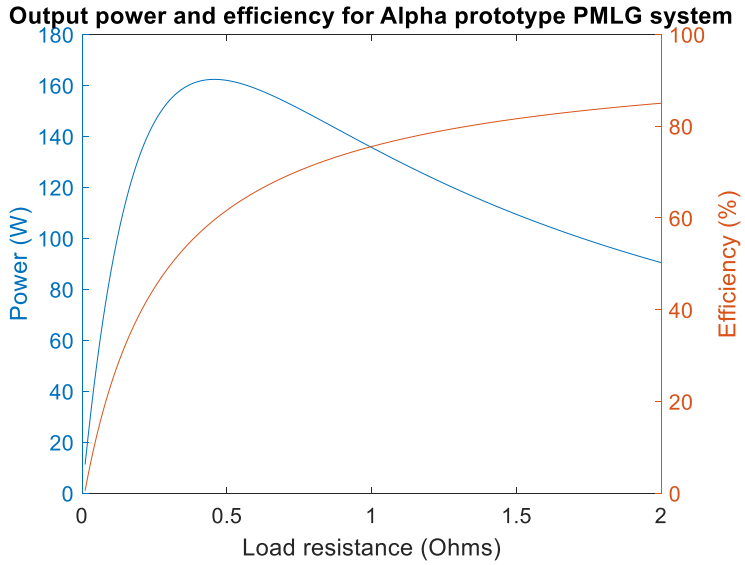

Figure 4-28 - Output power and efficiency for the Iron core Alpha prototype PMLG system – FEMM.

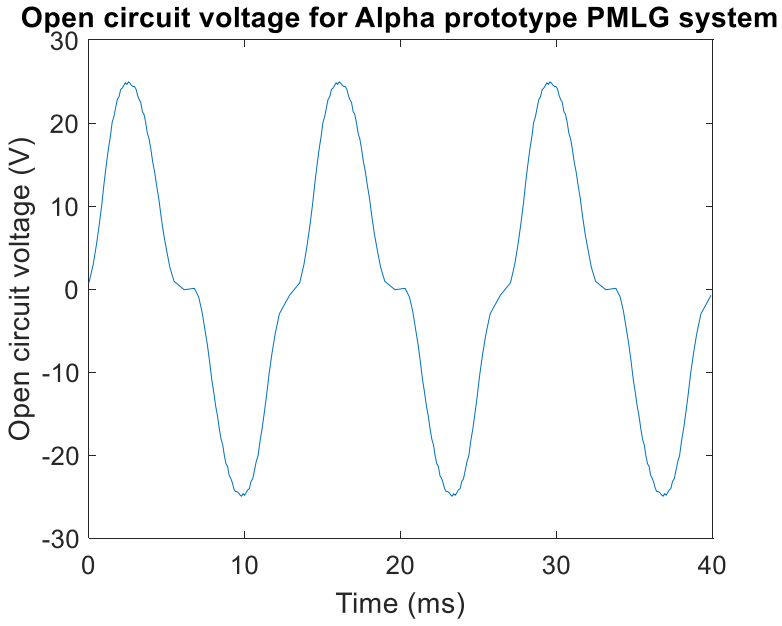

Figure 4-29 - OC voltage of the Iron core alpha prototype PMLG system – FEMM.

4.7 Beta prototype

Beta prototype of the free piston PMLG prototype built at WVU is shown in Figure 4-30.

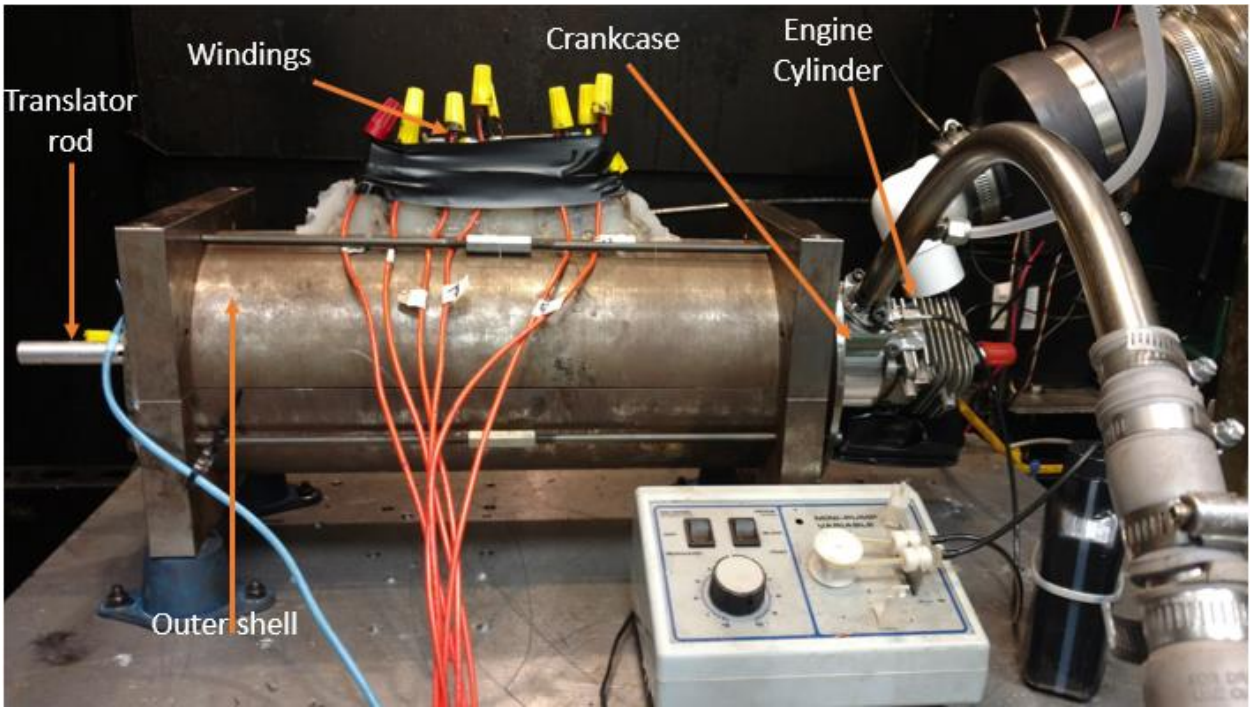

Figure 4-30 - Beta prototype PMLG system.

This section provides the comparison of the experimental results with the FEMM model of the Beta PMLG system. The stator resistance and inductance of the beta prototype was 1.65 Ohms and 21.5 mH.

Beta prototype built at WVU had two different stator cores – Air core and Iron core. The results from the air core and iron core are discussed below. The geometric parameters of the Beta prototype PMLG system studied is shown in Table 4-6.

Table 4-6 - Geometric parameter of the Beta prototype.

S.No	Part	Dimension
1	Coil Height	18 mm
2	Coil width	28 mm
3	Back iron stator width	3 mm

4	Lamination stack width	3 mm
5	Magnet radial thickness	2 mm
6	Airgap	2 mm
7	Oscillating frequency	80
8	Number of poles	4
9	Outer Diameter of Magnet	100 mm
10	Coil number of turns	126
11	Translator spacer width	1 mm
12	Wire gauge	13 AWG
13	Phase	1
14	Magnet flux arrangement	Axial
15	Stroke length	33 mm

4.7.1 Air core beta prototype

The air core alpha prototype had a resonant frequency of 75 Hz. The stator resistance and inductance of the Alpha prototype was 1.65 Ohms and 7.5 mH. Maximum power of 142 W was produced at 63 % efficiency. At a load of 2.25 Ohm, the output power from the experiment was 105 W with a load voltage of 16.6 V and 6.3 A. From the FEMM model, the output power was 112 W with a load voltage of 16.64 V and 6.85 A. The error difference between the output power was 6.7%, load voltage was 0.2 % and load current was 8.7 %. The output power and efficiency for the air core beta prototype from FEMM is shown in Figure 4-31. OC voltage comparison of the experiment and FEMM is shown in Figure 4-32. Comparison of load voltage and load current for the load of 2.25 Ohm is shown in Figure 4-33 and Figure 4-34.

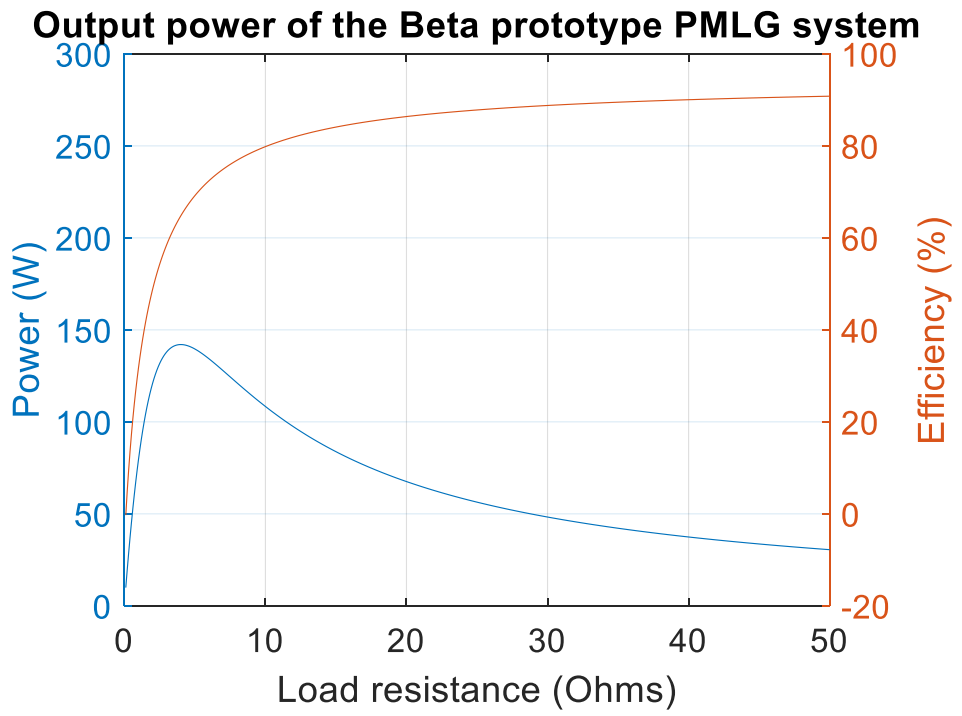

Figure 4-31 - Power and efficiency of the air core beta prototype PMLG system – FEMM.

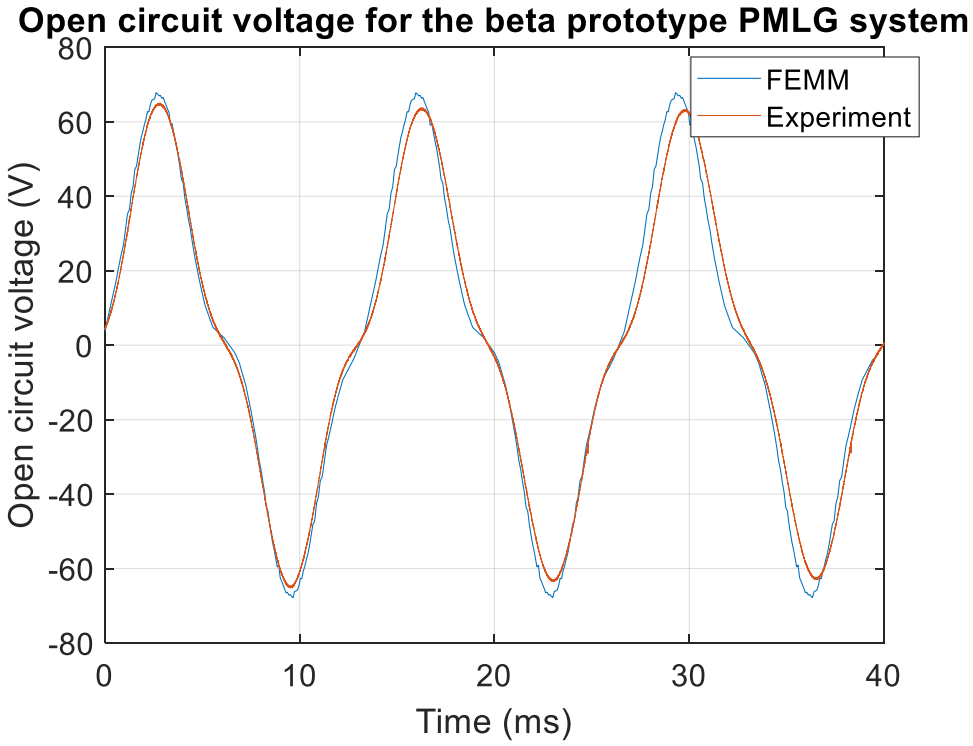

Figure 4-32 - OC voltage of the air core beta prototype PMLG system.

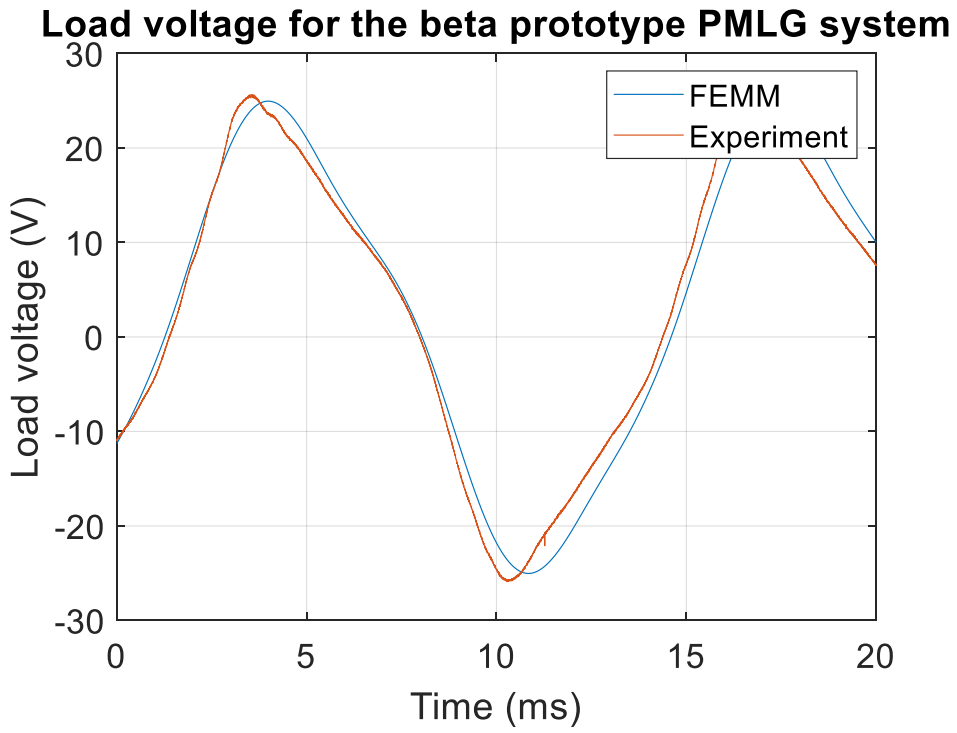

Figure 4-33 - Load voltage of the air core beta prototype PMLG system.

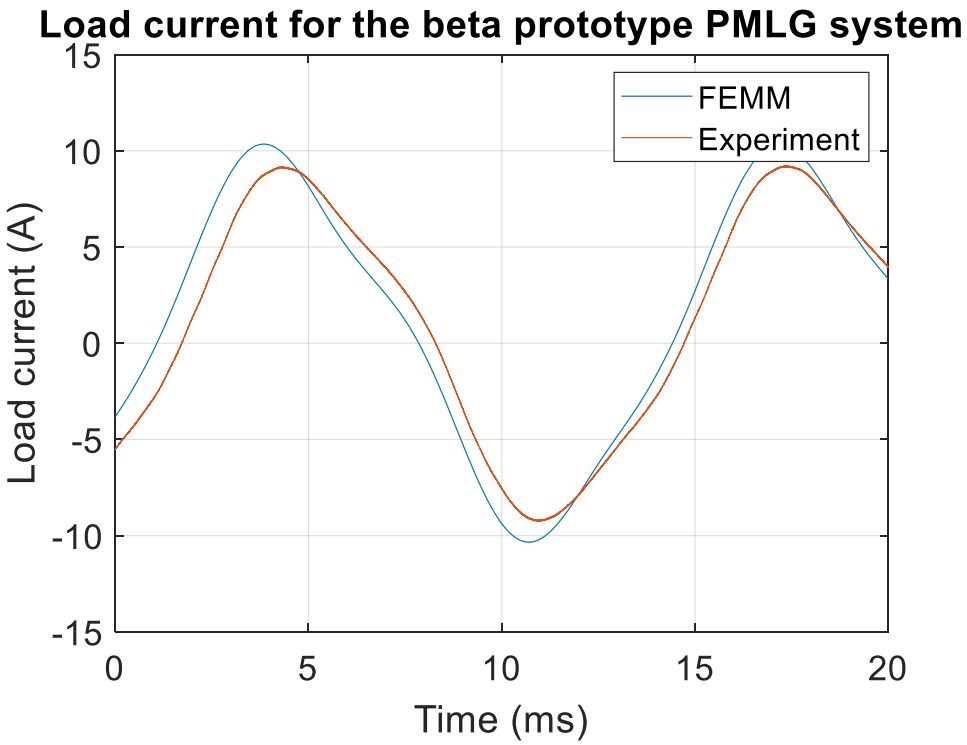

Figure 4-34 - Load current of the air core beta prototype PMLG system.

4.7.2 Iron core beta prototype

With these parameters, a FEMM model of the PMLG system was designed and studied. Based on the FEMM model, the flux linkage in the windings, open circuit voltage, load current, load voltage at maximum output power, Efficiency, maximum output power, flux density is calculated. The electrical parameters obtained from the FEMM study is shown below in Figure 4-35, Figure 4-36, Figure 4-37, and Figure 4-38. The results do not have capacitive compensation on the load side.

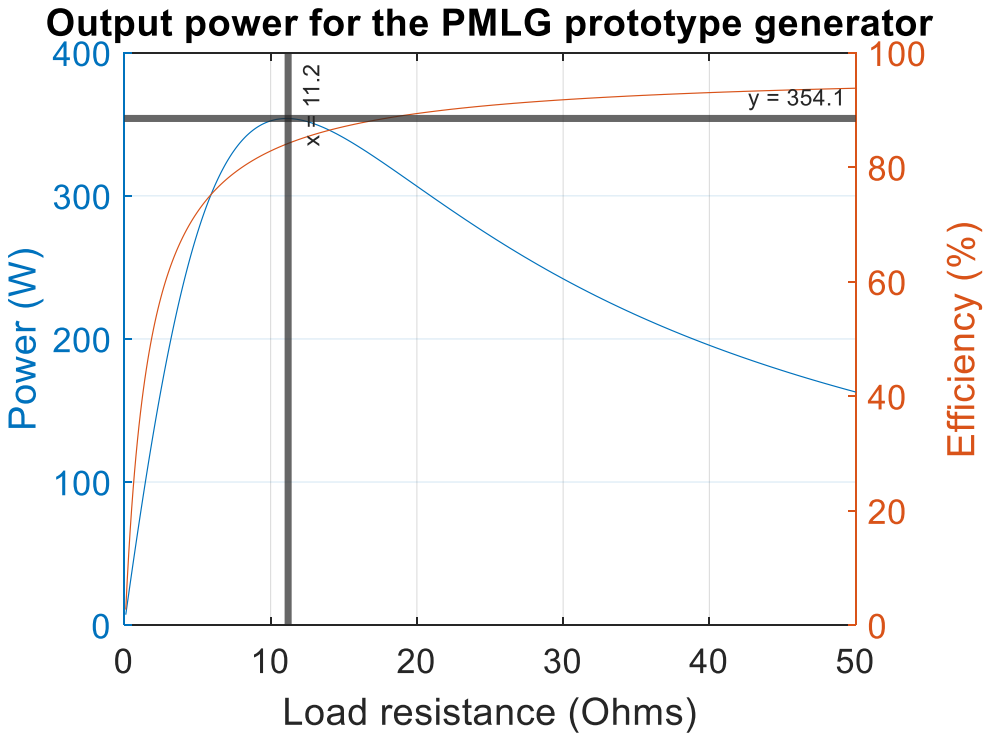

Figure 4-35 - Output power for the Beta prototype PMLG system – FEMM.

Table 4-7 shows the electrical parameters of the Beta prototype PMLG system with and without capacitive compensation. "With capacitors on the load" in Table 4-7 refers to the condition where capacitors are added to the load side to compensate the reactive power from the inductance in the windings of the PMLG system. The addition of capacitors helps in the improvement of output power of the PMLG system as seen in Table 4-7.

Table 4-7 - Output electrical parameters of the Beta prototype PMLG system without capacitive compensation.

Parameter	Without Capacitors on the load	With capacitors on the load
Maximum output power	354 W	1000
OC voltage	95.6 V	95.6
Load voltage	62.69 V	72.9
Load current	5.65 A	13.7
Efficiency	86 %	73 %

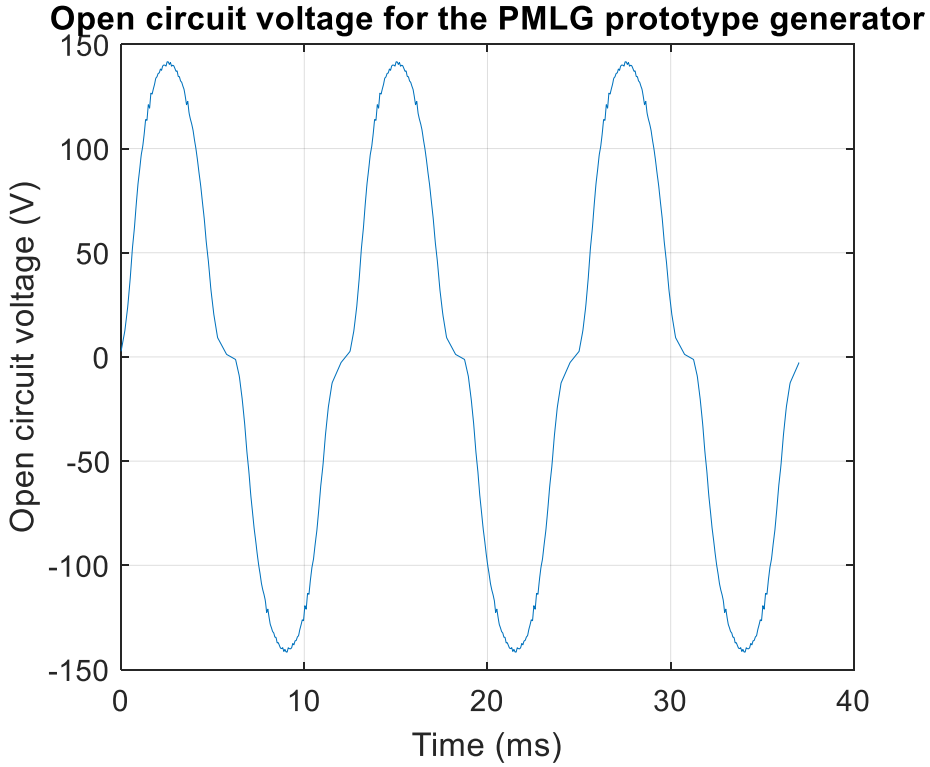

Figure 4-36 - OC voltage of the Beta prototype PMLG system – FEMM.

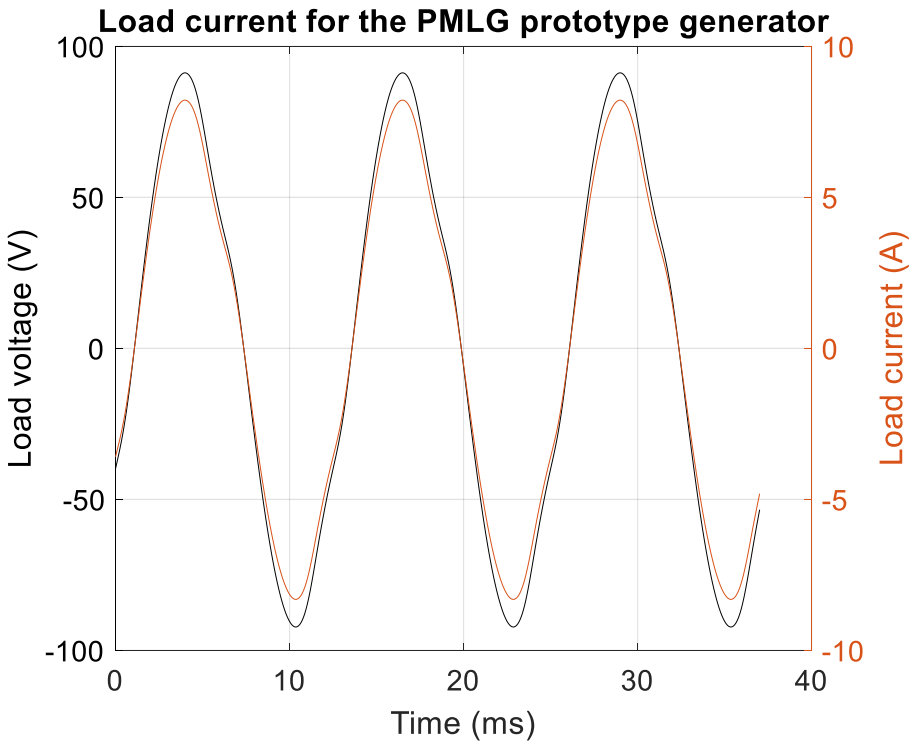

Figure 4-37 - Load voltage and load current of the Beta prototype PMLG system – FEMM.

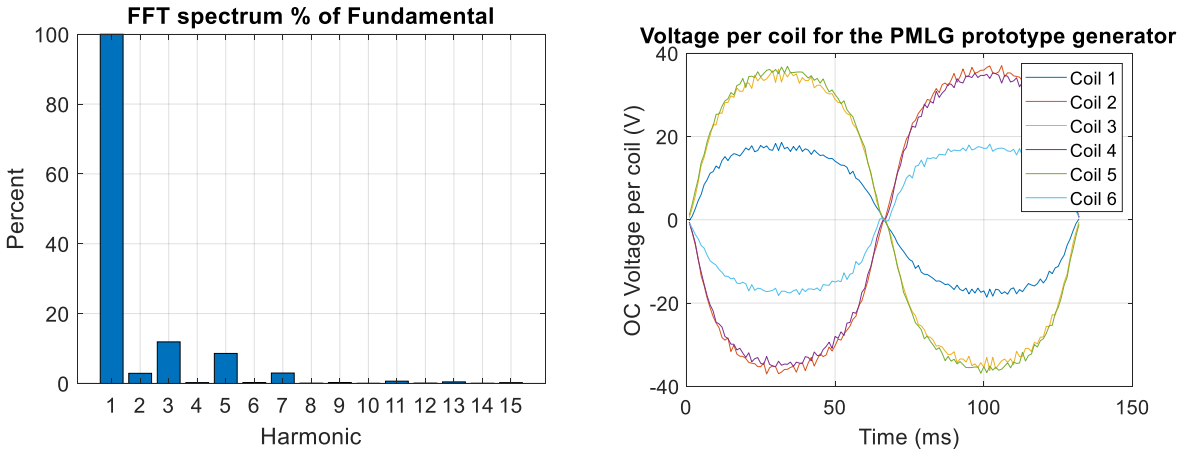

(a) (b)

Figure 4-38 - (a) Harmonic components of the OC voltage (b) voltage per coil of the Beta prototype PMLG – FEMM.

The experimental results and the comparison of the voltages and currents between FEMM and experiment is shown below.

The electrical power output from the beta prototype PMLG system was calculated for the experiment by measuring the instantaneous voltage and instantaneous current in the windings for 750 cycles. Later, using the equation $P = V_l * I_l$ and taking the average of P over 750 cycles, the power produced by the PMLG system was calculated. The resistance and the capacitance used for test case 1 was 12.3 Ohms and 25 µF in parallel. Frequency of operation was 75 Hz with 16 flexure springs and the stroke length was 29 mm. Based on the capacitance loading of 25 µF in parallel, using FEMM, the output power at different loading conditions and their efficiencies were calculated. This is shown in Figure 4-39.

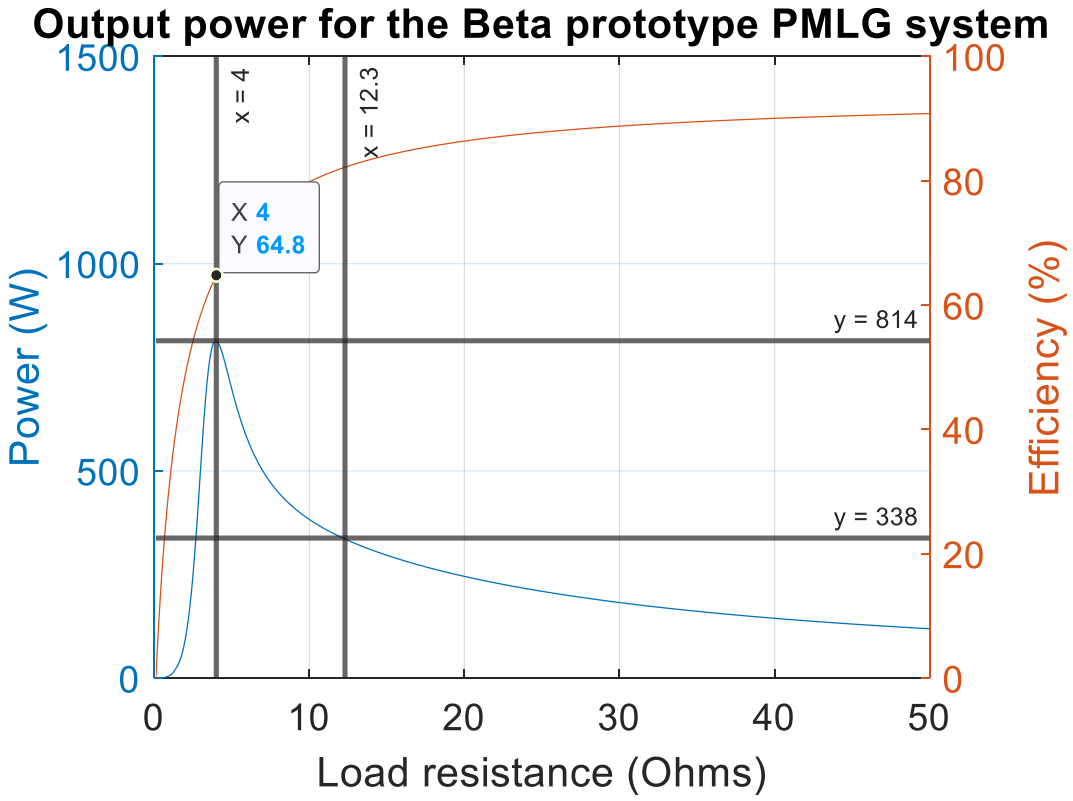

Figure 4-39 - Output power and efficiency for the beta prototype PMLG system with 25µF capacitor – FEMM.

For this condition, a maximum output power of 814 W can be produced with a load resistance of 4 ohms at an efficiency of 64.8 %. With the test condition, the efficiency was 82.8 % at 338 W.

The comparison of FEMM and the experimental voltage and current for 338 W is shown in Figure 4-40 and Figure 4-41.

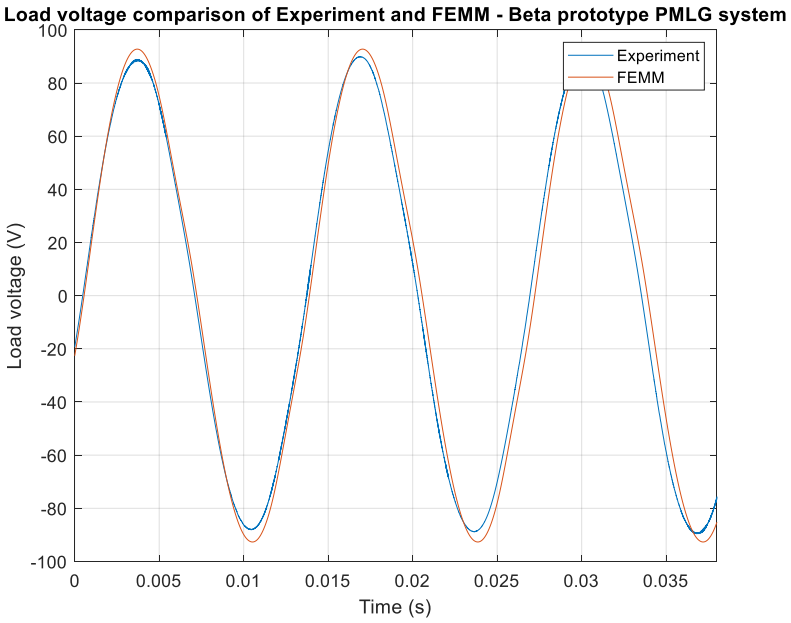

Figure 4-40 - Load voltage comparison between Experiment and FEMM.

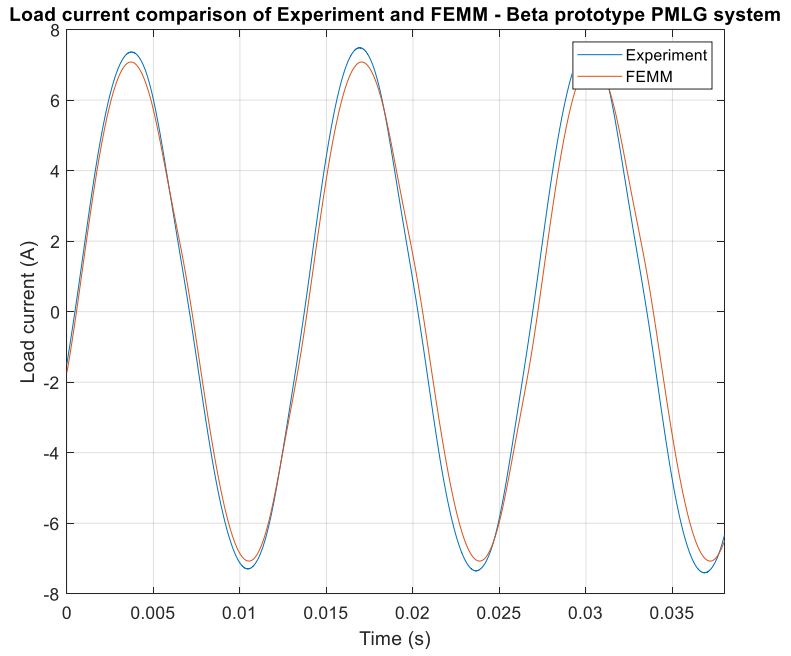

Figure 4-41 - Load current comparison between Experiment and FEMM.

From the above figures, it was seen that the results of FEMM was comparable with the experimental results. Table 2 shows the error percentage between FEMM and experiment for load voltage, current and output power. It was seen that the error for voltage was 3.4%,

current 5.2% and output power was 5.9%. The overall error was less than 6% for the voltage, current and power.

Table 4-8 - Error between FEMM and experiment for 338 W test condition.

Parameter	Experiment	FEMM	Error (%)
Output voltage (V)	62.85	65.01	3.44
Output current (A)	5.2	4.9	5.2
Output power (W)	338.5	318	5.9

Figure 4-42 shows the power distribution for 338 W test case. Engine produced a power of 565 W and electrical output power was 338 W. The copper losses were calculated, and it was 47 W. The other losses were 180 W. The other losses include iron losses in the PMLG system, losses from the spring material, piston ring friction losses, vibrational and windage losses.

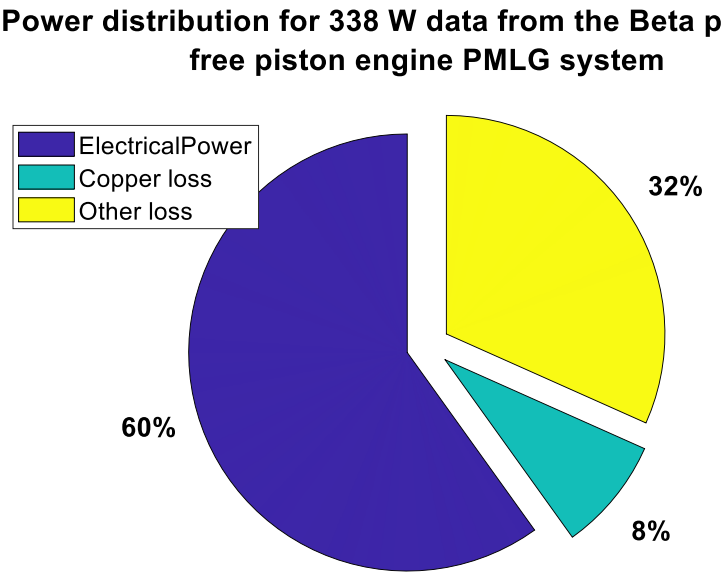

Figure 4-42 - Power distribution in the beta prototype PMLG system.

4.8 Summary

In this chapter, modeling, experimental setup and comparison of the experimental prototype of the PMLG system with FEMM was discussed in detail.

1) The steps involved in modeling a PMLG system using FEMM were provided. Later, controlling FEMM using MATLAB was detailed. Following that, the method to calculate the output power, load voltage and currents using flux linkages from FEMM and MATLAB was provided.
2) This was followed by a comparison of the model developed in the design guideline from Chapter 3 with FEMM was discussed. It was seen that error above 20% was seen in the output voltage and currents, whereas the output power matched well between the theoretical and FEMM model. Some of the reasons for the error were attributed to the neglection of the fringing effects in the theoretical model
3) The construction, and operation of the experimental prototype of the free piston engine PMLG system was discussed. Details on the sensors and data acquisition system was provided.
4) Alpha prototype built at WVU was modeled in FEMM and the results for air core and iron core stator were compared with the experimental prototype. Error less than 10 % was seen for different load conditions.
5) Beta prototype built at WVU was modeled in FEMM and the results for the 338 W data was compared with FEMM. Similar to the alpha prototype, the error between the experiments and FEMM was less than 10%
6) The reasons for some of the errors is attributed to the discrepancies in the exact airgap in the experimental prototype, and magnetic flux density in the air gap.
7) Overall, the FEMM was able to predict the experimental prototype within 10 % error and therefore, this model can be used as a starting point for further parametric and optimization studies.

CHAPTER FIVE

5 Parametric study of Tubular Permanent Magnet Linear Generators (PMLG)

Details on the design, modeling and the experimental prototype of the PMLG system was discussed in Chapter 3 and Chapter 4. This chapter discusses the parametric study of the PMLG system by varying its different geometric parameters. From this study, the effects of each of the parameters on the PMLG output power and moving mass of the translator were discussed. A One At a Time (OAT) and global sensitivity analysis was performed to determine the importance of the parameters based on the output power, open circuit voltage and moving mass of the PMLG system. The final outcomes from this study provides us an idea of how these parameters will affect the PMLG when optimization is performed. The optimization of the PMLG system is discussed in detail in Chapter 6.

Several geometric parameters affect the working and performance of the PMLG system. The parameters chosen to study the performance of the PMLG system were,

1. Magnetic flux arrangement,
2. Neutral position,
3. Magnet thickness,
4. Translator spacer width,
5. Outer diameter of the magnet,
6. Airgap,
7. Oscillating frequency,
8. Stroke length,
9. Number of poles, and
10. Coil windings/ number of turns.

All of these parameters have been studied individually in this chapter to understand their standalone effects on the PMLG system. Later combinations of these parameters were studied to understand their cumulative effects using global sensitivity analysis. Using these results, interesting details, effects and how PMLG can be built effectively have been provided at the end of the chapter.

5.1 Magnetic flux arrangement

Magnets are used in a variety of applications and one important application is in linear generators. In certain applications, the direction of magnet's pole doesn't matter as long as there is a force of attraction between the surfaces. In other applications, magnet's pole and orientation are an integral part of the system. In a permanent magnet linear generator (PMLG), magnet orientation plays an important role in determining its performance.

Magnets can be isotropic or anisotropic. Isotropic magnets have equal magnetic properties in all directions whereas anisotropic magnets have a preferred direction of magnetization. Since anisotropic magnets are magnetized in a specific direction, the magnet's performance potential is higher compared to isotropic magnets.

Common available magnet material types are,

1. Rare Earth magnets,
    a. Neodymium Iron Boron (NdFeB),
    b. Samarium Cobalt
2. Ceramic magnets,
3. Alnico, and
4. Magnetic Rubber.

Of these, NdFeB has the highest magnet power density and high temperature strength compared to other magnet materials. Therefore, for all the study in this chapter, NdFeB magnets have been used. NdFeB magnets come in different strengths such as N-27, N-30, N-32, N-33, N38, N-40, N-43, N-45, N-48, and N-50. They also come in different working temperature rating such as M, H, SH, UH, EH and AH. For all the studies in this section, N-32 magnets have been used. Details on their magnetism, coercive force,

maximum energy product, working temperature and Curie temperature have been provided in the appendix.

Conventional flux arrangement of magnets are,

1. Radial, and
2. Axial.

Figure 5-1 shows the two different field orientation of ring magnets.

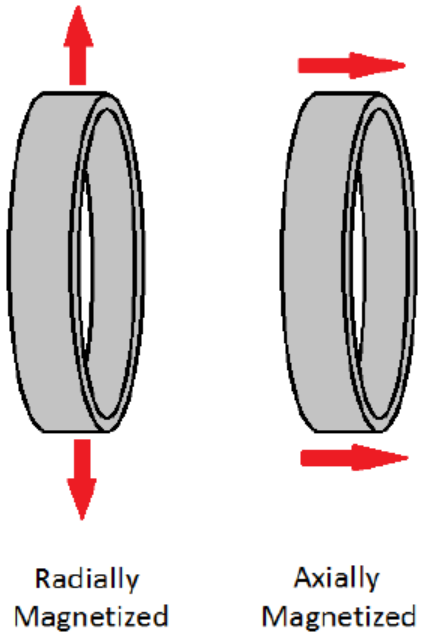

Figure 5-1 – Field orientation of ring magnets.

Using these magnets, three different translator arrangements can be made for the PMLG system. They are,

1. Axial arrangement,
2. Radial arrangement, and
3. Halbach arrangement.

Details on these arrangements have been discussed in Chapter 2 in Figure 2-14.

Design parameters used for the PMLG system is given below in Table 5-1.

Table 5-1 - Geometric parameters of the PMLG system used in the magnet orientation study.

S.No	Part	Dimension
1	Coil height	18mm
2	Coil width	28mm
3	Wire gauge	AWG13
4	Lamination stack width	3mm
5	Coil number of turns	126
6	Oscillating frequency	80 Hz
7	Phase	Single
8	Number of poles	4
9	Outer Diameter of Magnet	100mm
10	Stroke length	33 mm

A design study to test these three magnet arrangements for the PMLG system was done to understand their advantages and disadvantages. To perform the study, 6 different test cases were chosen to study these arrangements. This design study was aimed to compare the magnet arrangement under two different parameters of the PMLG system. The two different parameters are,

1. Output Power, and
2. Magnetic flux arrangement.

Test cases chosen for the magnetic flux arrangement study is shown in Table 5-2.

Table 5-2 - Test for magnetic flux arrangement in the PMLG system.

Test	Axial	Radial	Halbach
1	MT = 2mm, BI= 0mm	MT = 2mm, BI= 0mm	MT = 2mm, BI= 0mm
2	MT = 2mm, BI= 1mm	MT = 2mm, BI= 1mm	MT = 2mm, BI= 1mm
3	MT = 2mm, BI= 2mm	MT = 2mm, BI= 2mm	MT = 2mm, BI= 2mm
4	MT = 2mm, BI= 0mm	MT = 1mm, BI= 1mm	MT = 1mm, BI= 1mm
5	MT = 3mm, BI= 0mm	MT = 2mm, BI= 1mm	MT = 2mm, BI= 1mm MT = 3mm, BI= 0mm
6	MT = 4mm, BI= 0mm	MT = 2mm, BI= 2mm, MT = 3mm, BI= 1mm	MT = 2mm, BI= 2mm, MT = 3mm, BI= 1mm MT = 4mm, BI= 0mm

where,

MT – Magnet radial thickness, and

BI – Back Iron in the translator.

5.1.1 Test 1 – 2 mm Magnets and no back iron

First test in this study involves testing the magnet configurations with 2 mm thick magnets and no back iron in the translator below the magnets. It was seen from Figure 5-2 the power, electro-magnetic force and open circuit voltage were higher for Halbach compared to axial and radial magnet arrangement. This can be attributed to the unique arrangement of the halbach to concentrate all of its magnet flux lines through one direction as discussed in Chapter 2. Furthermore, axial magnet arrangement has higher power compared to radial arrangement. It can be attributed to the absence of back iron in the translator arrangement for the radial arrangement case. In radial arrangement design, flux lines pass through air on the outside and flux leakage happens. This leads to less power and force in radial compared to axial arrangement. It was seen that the flux lines flow through the magnets and the laminations in axial arrangement whereas in radial the flux lines pass through the air and then to the laminations as seen in Figure 5-3

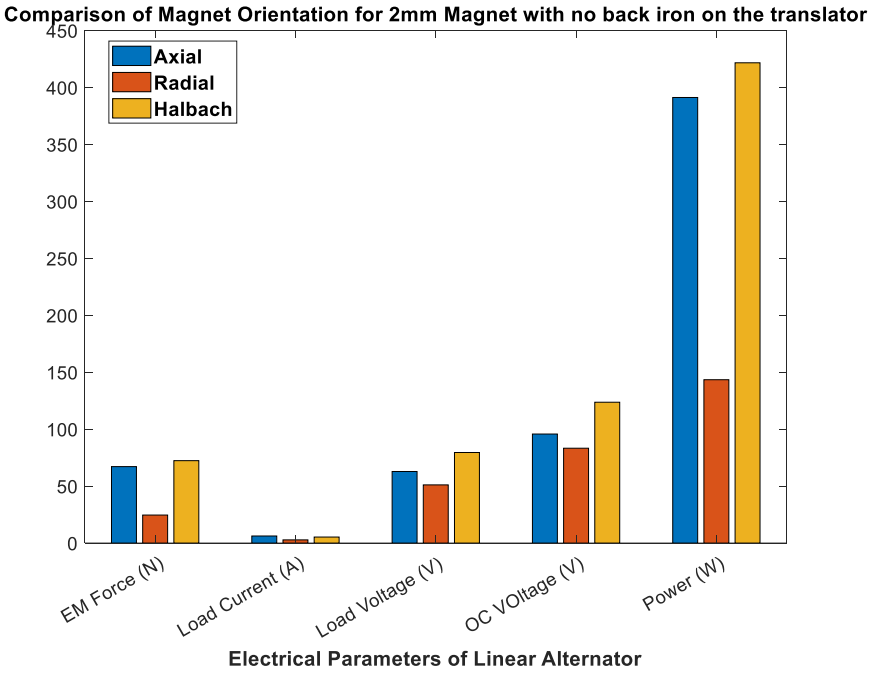

Figure 5-2 - Magnet Arrangement comparison for Test 1.

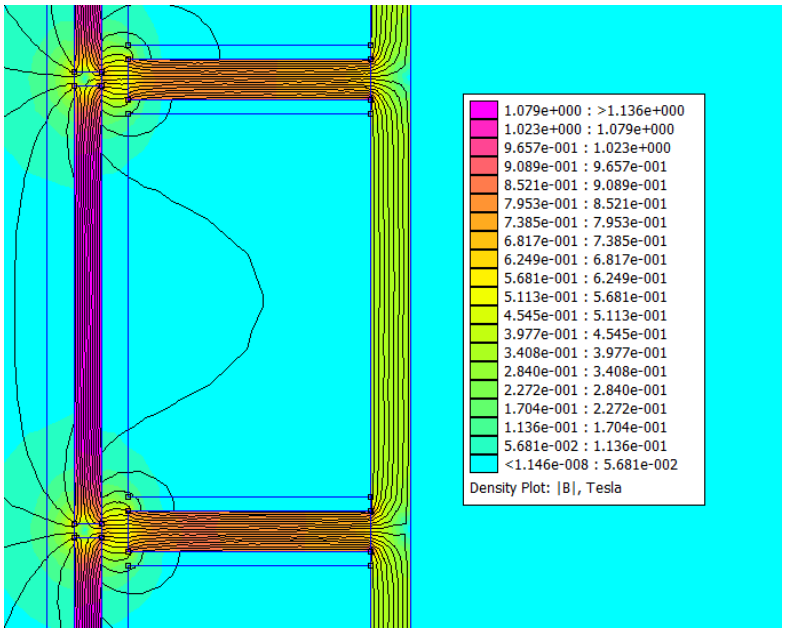

(a) Magnetic flux lines for Axial for Test 1.

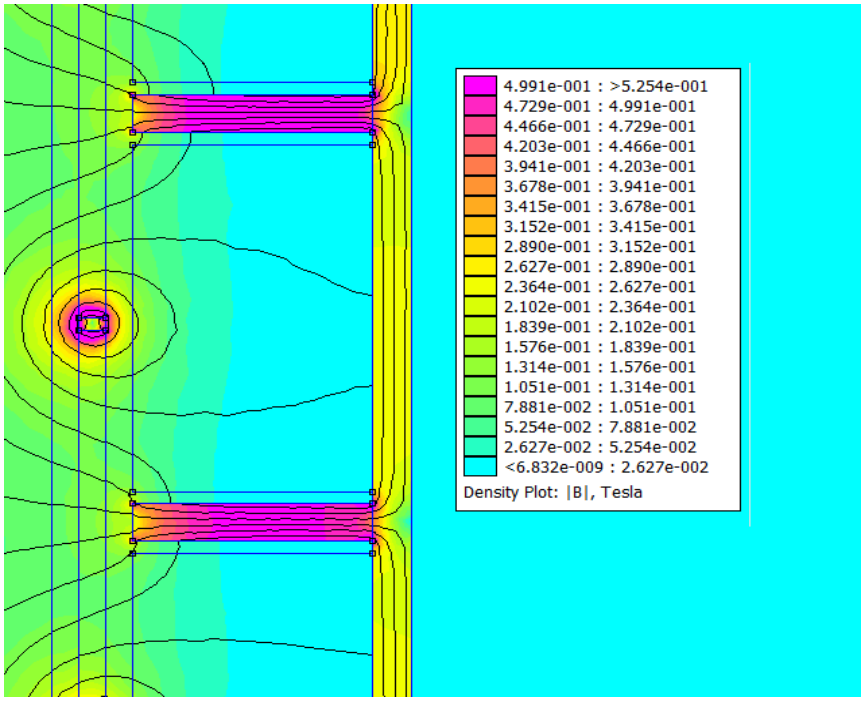

(b) Magnetic flux lines for Radial for Test 1.

Figure 5-3 - Magnetic flux lines for Test 1.

5.1.2 Test 2 – 2 mm magnets and 1 mm back iron

Second test in this study involves studying the magnet configurations with 2 mm magnet thickness and 1 mm back iron in the translator below the magnets. It was seen from Figure 5-4 that the power, electro-magnetic force and open circuit voltage were higher for Halbach compared to axial and radial magnet arrangement. In this case, radial magnet arrangement has higher power compared to axial arrangement. It can be attributed to the presence of back iron in the translator arrangement. In radial arrangement, flux lines pass through back iron on the outside and flux leakage is drastically reduced compared to Test 1. This leads to higher power and force in radial compared to axial arrangement. On the other hand, in the axial arrangement, the flux lines gets concentrated in the back iron of the translator and within the magnets as seen in Figure 5-5. Therefore, the flux lines do not pass through the laminations and the voltage is reduced. Hence the axial arrangement has way lesser power compared to radial and halbach arrangement.

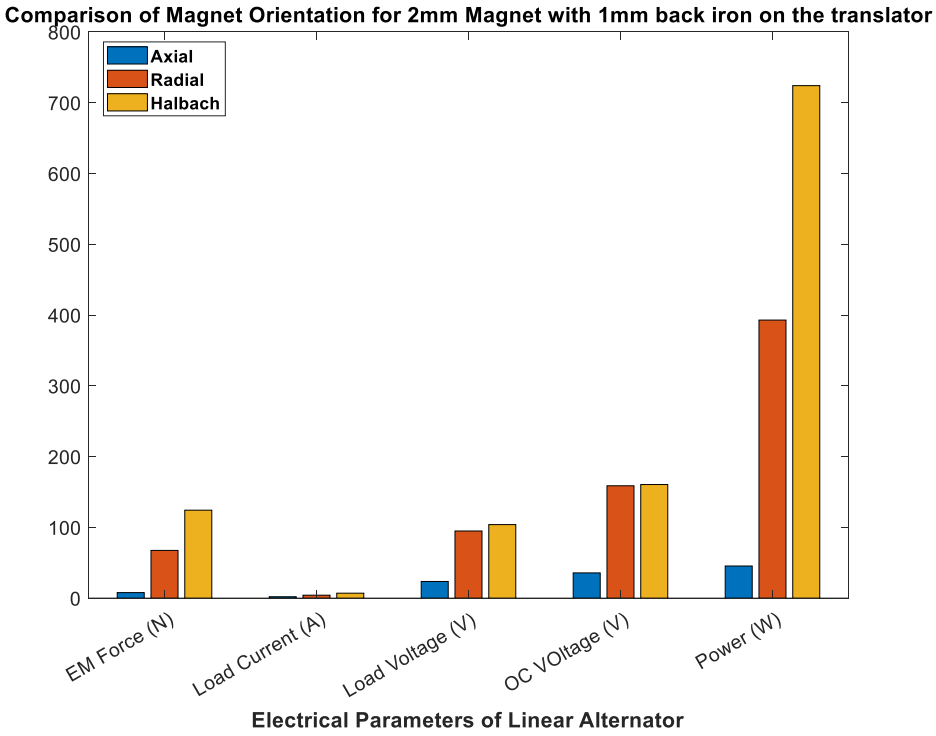

Figure 5-4 - Magnet Arrangement comparison for Test 2.

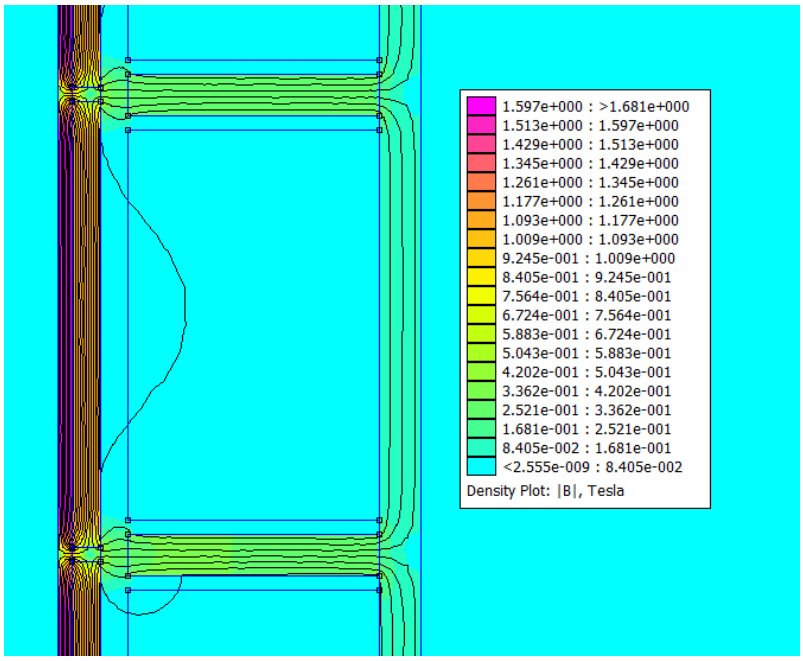

Figure 5-5 - Magnetic flux lines for Axial for Test 2.

5.1.3 Test 3 – 2 mm magnets and 2 mm back iron

Third test in this study involves testing the magnet configurations with 2mm thick magnets and 2mm back iron in the translator below the magnets. It was seen from Figure 5-6 that the power, electro-magnetic force and open circuit voltage are higher for Halbach compared to axial and radial magnet arrangement. Radial has higher power than the axial arrangement and the axial shows very low power compared to other two arrangements. This test provides similar results as Test 2 as seen in Figure 5-6.

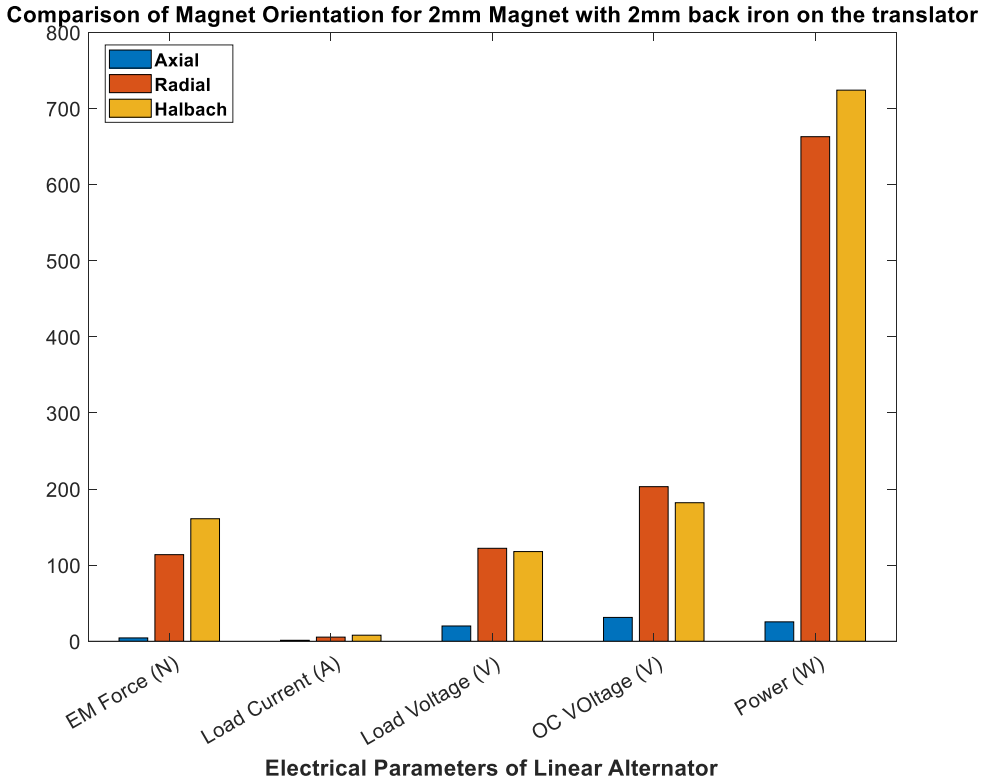

Figure 5-6 - Magnet Arrangement comparison for Test 3.

5.1.4 Test 4 – Axial (2 mm MT, no BI), Radial (1 mm MT, 1mm BI), Halbach (1 mm MT, 1mm BI)

Fourth test in this study involves testing the magnet configurations with different magnet thickness and back iron for axial, radial and halbach arrangement. Idea of this study is to compare the arrangements with same moving mass of the translator as well using the best possible condition for the magnet arrangement types. Therefore, the following conditions were chosen.

Axial – 2mm magnet thickness with no back iron

Radial – 1mm magnet thickness with 1mm back iron

Halbach – 1mm magnet thickness with 1mm back iron

It can be seen from Figure 5-7 that the power, electro-magnetic force and open circuit voltage were higher for Halbach is higher compared to axial and radial magnet arrangement. Radial has higher power than the axial arrangement machine.

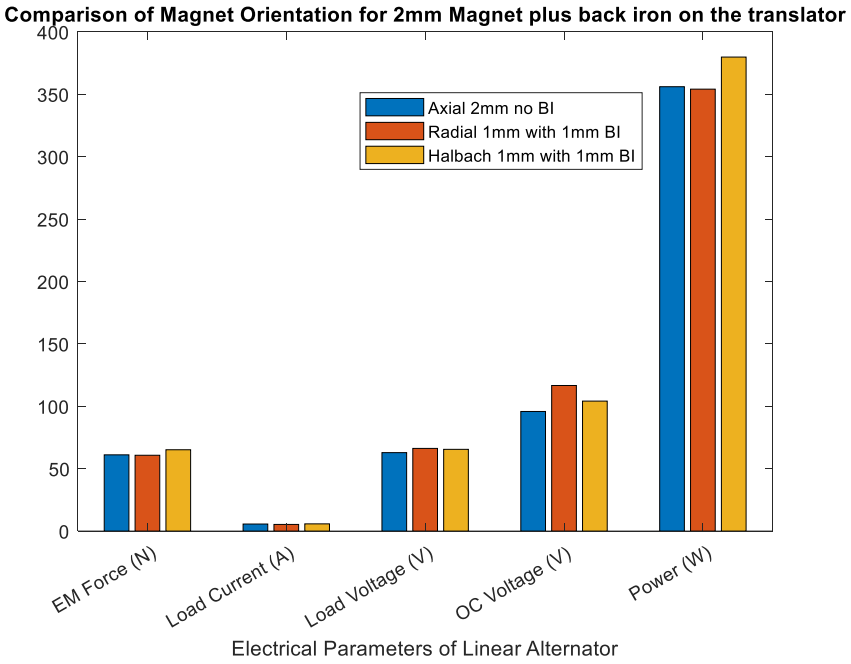

Figure 5-7 - Magnet Arrangement comparison for Test 4.

5.1.5 Test 5 - Axial (3 mm MT, no BI), Radial (2 mm MT, 1mm BI), Halbach (2 mm MT, 1mm BI)

Fifth test in this study involves testing the magnet configurations with different magnet thickness and back iron for axial, radial and halbach arrangement. Idea of this study is to compare the arrangements with same moving mass of the translator with a higher combined moving mass than Test 4. Therefore, the following conditions were chosen.

Axial – 3mm magnet thickness with no back iron

Radial – 2mm magnet thickness with 1mm back iron

Halbach – 2mm magnet thickness with 1mm back iron

It can be seen from Figure 5-8 that the power, electro-magnetic force and open circuit voltage are higher for Halbach compared to axial and radial magnet arrangement. Axial has higher power than the radial arrangement machine. The difference in Test 4 and Test 5 can be attributed the saturation in the back iron. Saturation of the laminations is shown by the pink region in the back iron of the translator where flux density goes to 2T as shown in Figure 5-9. Once the laminations reach the saturation region, large changes in current is required to have small changes in magnetic field. Therefore, lesser open circuit voltage and power is produced in radial arrangement in Test 5.

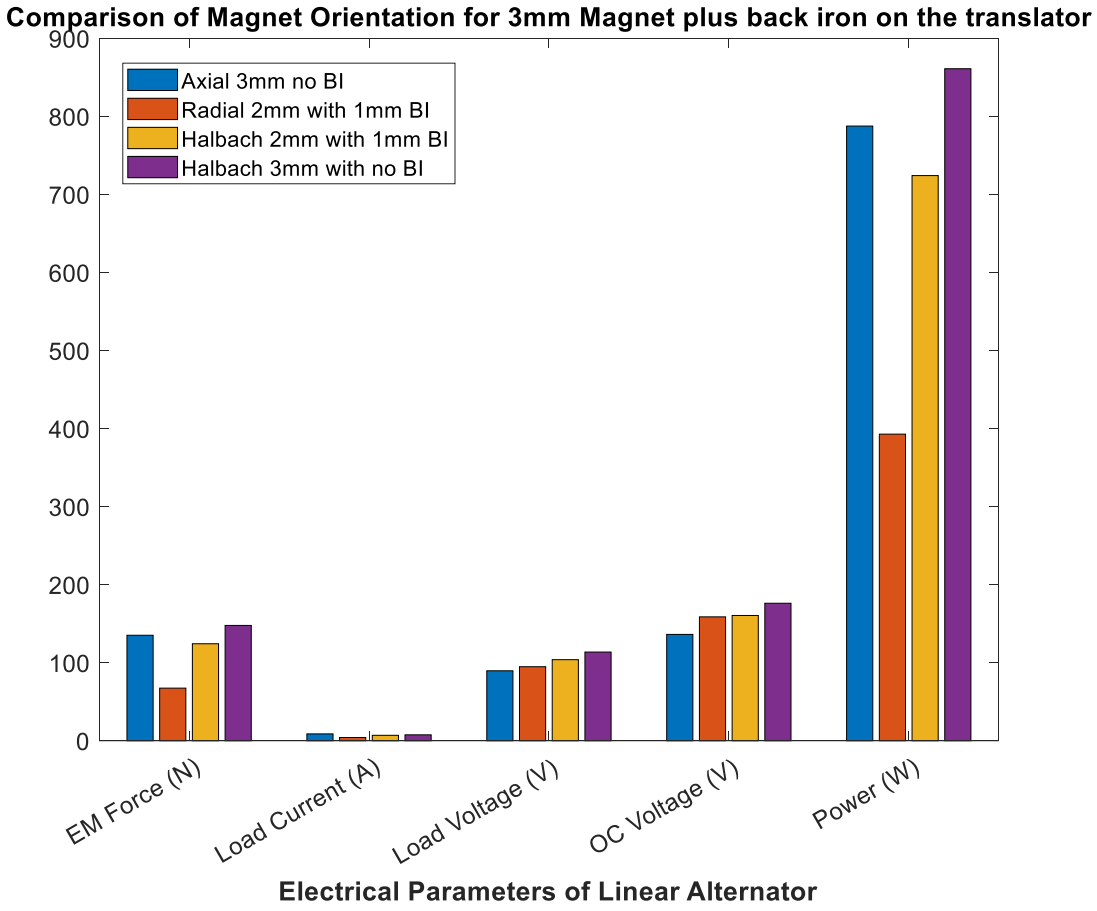

Figure 5-8 - Magnet Arrangement comparison for Test 5.

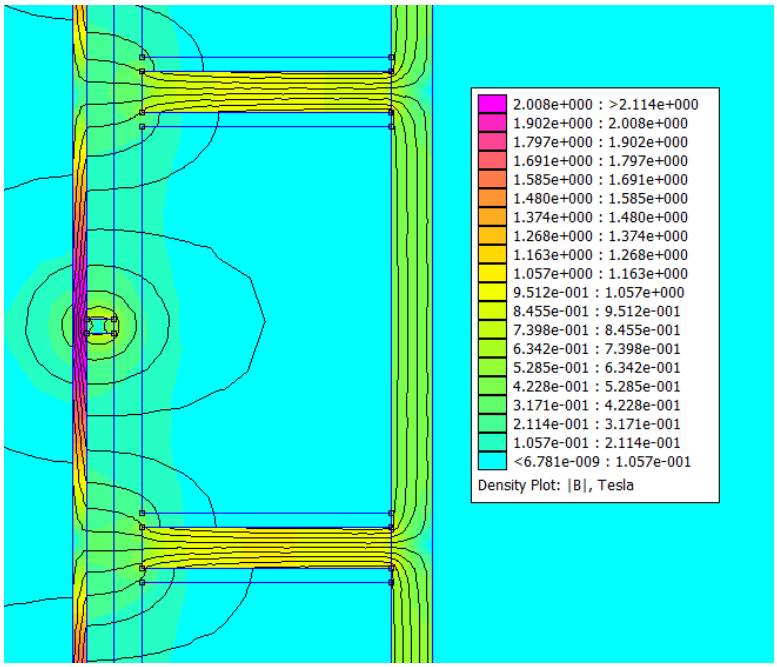

Figure 5-9 - Flux lines in radial arrangement for Test 5.

Test 6 – 5 different arrangements

Sixth test in this study involves studying the magnet configurations with different magnet thickness and back iron for axial, radial and halbach arrangement. Idea of this study is to compare the arrangements with same moving mass of the translator with a higher combined magnet plus back iron thickness compared to Test 4 and Test 5 and to reduce the saturation in Test 5 by increasing the back iron thickness. Also, this test helps to identify the saturation regions and which combination provides better results. Therefore, the following conditions were chosen.

Axial – 4mm magnet thickness with no back iron

Radial – 2mm magnet thickness with 2mm back iron

Halbach – 2mm magnet thickness with 2mm back iron

Radial – 3mm magnet thickness with 1mm back iron

Halbach – 3mm magnet thickness with 1mm back iron

It can be seen from Figure 5-10 that the power, electro-magnetic force and open circuit voltage are higher for Halbach compared to axial and radial magnet arrangement. Axial with 4mm was higher than radial with 3mm but lesser than radial with 2mm because

saturation effect was reduced in 2mm case. Halbach with 3mm magnet is higher than halbach with 2mm magnet.

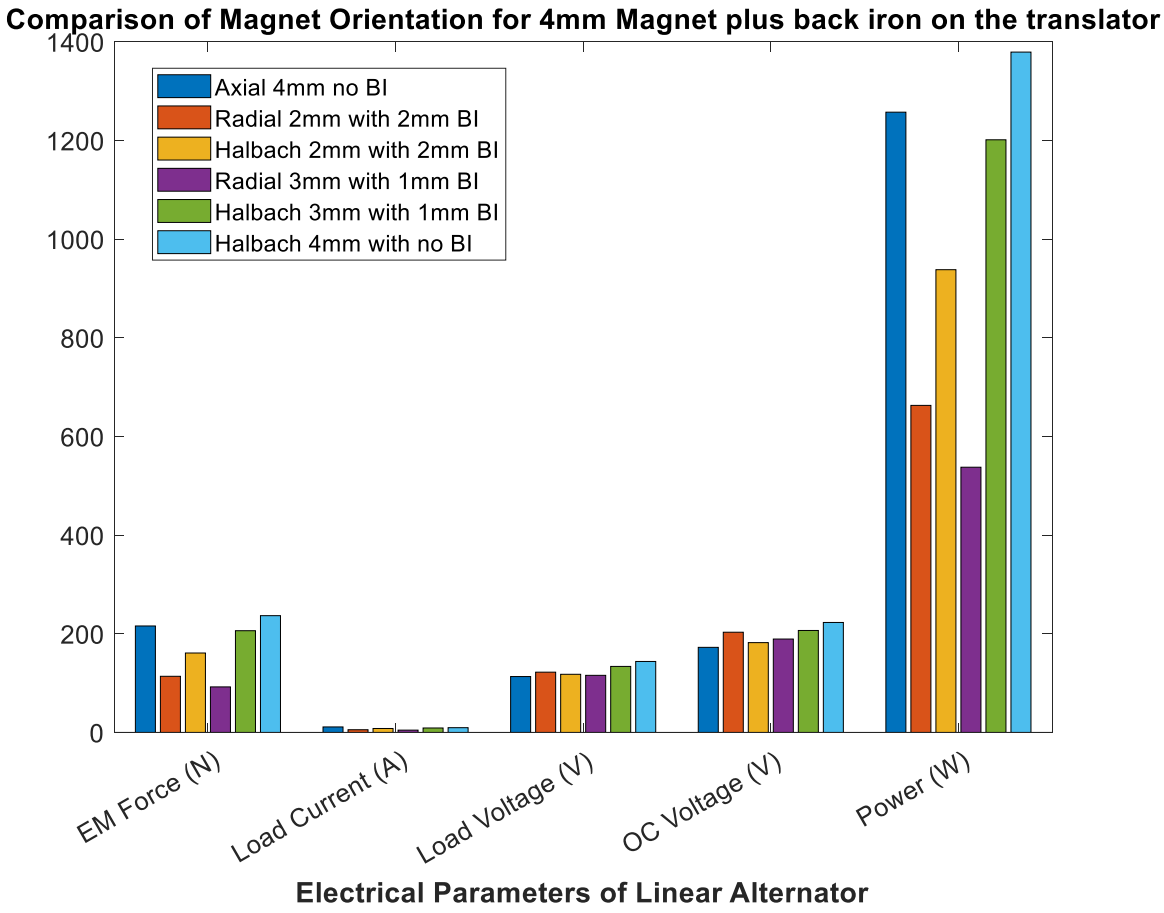

Figure 5-10 - Magnet Arrangement comparison for Test 6.

Inferences from magnet orientation study:

Inferences from the 6 tests are shown below

1. **Output Power**

In terms of output power, halbach arrangement outperforms both axial and radial arrangement in all the six conditions. Therefore, it is very clear that, halbach is the best possible arrangement in terms of output power. In axial arrangement, back iron is detrimental for its operation. Therefore, back iron below the magnets should not be used in axial arrangement. In the halbach arrangement, back iron is not useful compared to going with a thicker magnet as seen in Test 6. For radial arrangement,

back iron is essential for its operation. Amount of back iron to magnet thickness is determined by the saturation limits which can be quickly decided by performing some simple finite element models.

2. Cost of the magnets

Keeping the cost of the magnet/volume same for all the types of magnets, it can be seen that, halbach is the ideal choice of arrangement for linear electric generators. This is followed by radial and then axial magnets. Radial arrangement requires lesser magnets but requires a back iron. Therefore, depending on the application cost, specific magnet arrangement has to be decided.

3. **Ease of magnet arrangement**

Halbach arrangement requires three different types of magnets, radial requires two different types of magnet and axial requires only one type of magnet to build the translator. Therefore, axial magnet arrangement is easier of the three whereas halbach is the most complicated.

5.2 Neutral Position of the Translator

The parameter of PMLG studied here was the neutral position of the translator with respect to the stator. Neutral position refers to the position of the magnet pole of the translator from where it moves to a displacement of stroke length. The linear machine could be started either with magnet pole under the center of the coil or under the center of the laminations or in between the coil/laminations. Discussions have been provided for the three different magnet arrangements – Axial, Radial and Halbach to determine the best neutral position of the PMLG system.

5.2.1 Axial Arrangement

Study of axial arrangement neutral position was done by moving the magnet from 0 mm neutral position to 16.5 mm neutral position. Neutral position refers to the initial location of the magnet arrangement. In axial arrangement, 0 mm refers to the location where the magnet end is under the center of the laminations (It can be either on the left side or right side – Right side has been chosen in this case) as shown in Figure 5-11 - a and 16.5 mm

refers to the location where the magnet end is under the center of the coil as shown in Figure 5-11 – b.

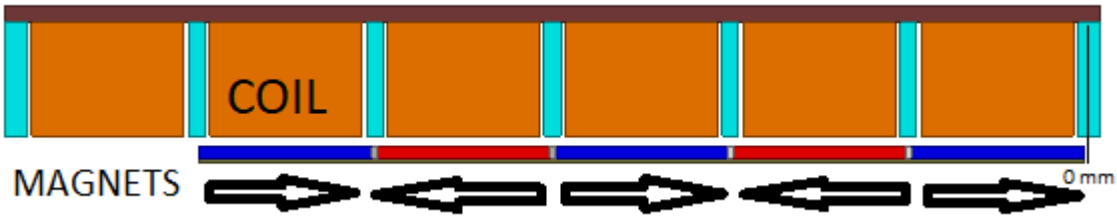

(a) Axial Arrangement at 0mm neutral position.

(b) Axial Arrangement at 16.5mm neutral position.

Figure 5-11 - Axial Arrangement for neutral position study.

Analysis was done to see which location produces best output power, and open circuit voltage. It was seen that, 0 mm neutral position provided best output power and open circuit voltage as shown in Figure 5-12. A closer look at the open circuit voltage waveform shows that the voltage waveform for 16.5 mm neutral position is distorted and oscillated at twice the operating frequency. The reason can be attributed to the 2^{nd} and 4^{th} harmonics developed in the system. This is shown in Figure 5-13. From these results, it was seen that the machine needs to start at the center of the laminations and move the complete stroke length compared to the center of the coil to achieve a sinusoidal voltage waveform with less distortion. It can be understood that, the magnet pole of the translator of the PMLG system is in between the two magnets. Therefore from Figure 5-12 and Figure 5-13 , it can be seen that it is better to start the PMLG system with its magnet pole under the center of the laminations and not under the center of the winding coil. Completed details on the harmonics of 0 mm and 16.5 mm neutral position is added in the appendix.

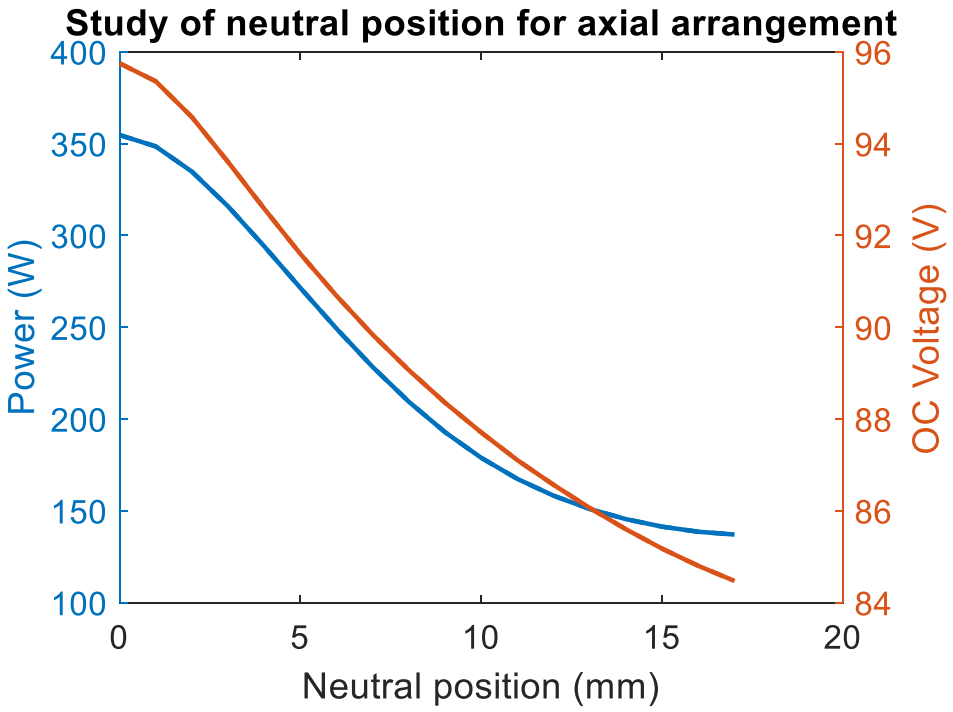

Figure 5-12 - Power and OC Voltage for the axial neutral position study.

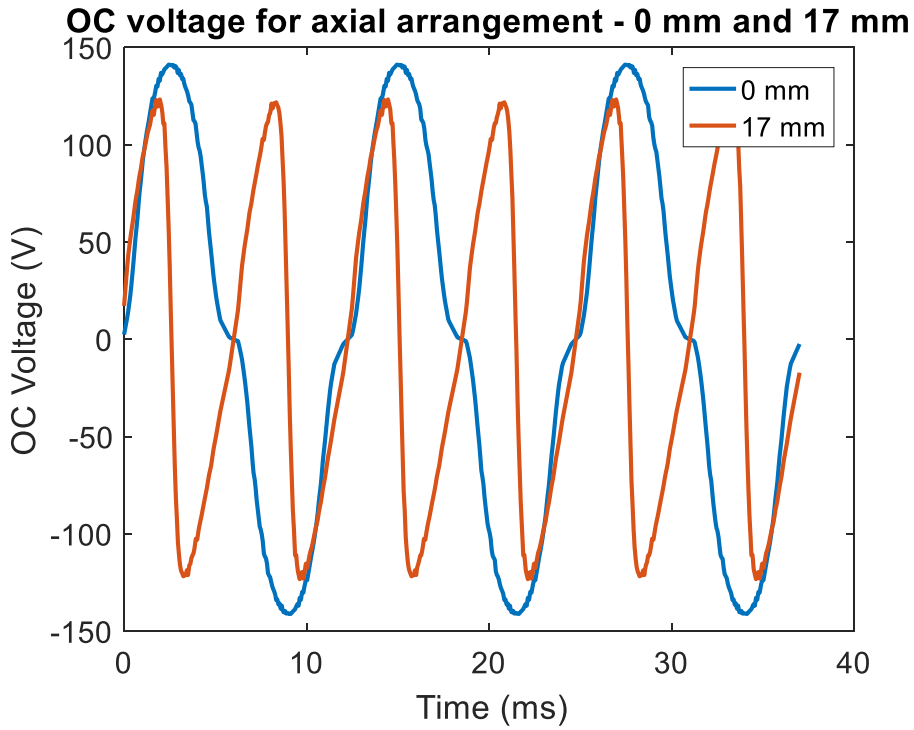

Figure 5-13 - OC Voltage waveform for the axial neutral position study -.

5.2.2 Radial Arrangement

Similar to axial arrangement, radial arrangement study was done for the neutral position. Neutral position referred in radial is similar to axial arrangement as shown in Figure 5-11. Power and open circuit voltage was studied for neutral positions from 0 mm to 17 mm. It was seen that, for radial arrangement, 16.5 mm neutral position provides higher power and voltage compared to 0mm as seen in Figure 5-14. This is different from axial arrangement in terms of neutral position. But it can be seen that, the magnet pole of the radial arrangement magnet is at the center of each magnets. Therefore, it can be seen that for the radial arrangement, it is better to start the PMLG system with its magnet pole under the center of the laminations and not under the center of the winding coils. From Figure 5-15, it can be seen that the 2nd and 4th harmonics are higher for 16.5 mm compared to 0mm which further leads to reduction in the OC voltage and power for 16.5 mm neutral position arrangement. The complete harmonics of all the frequencies are attached in the appendix.

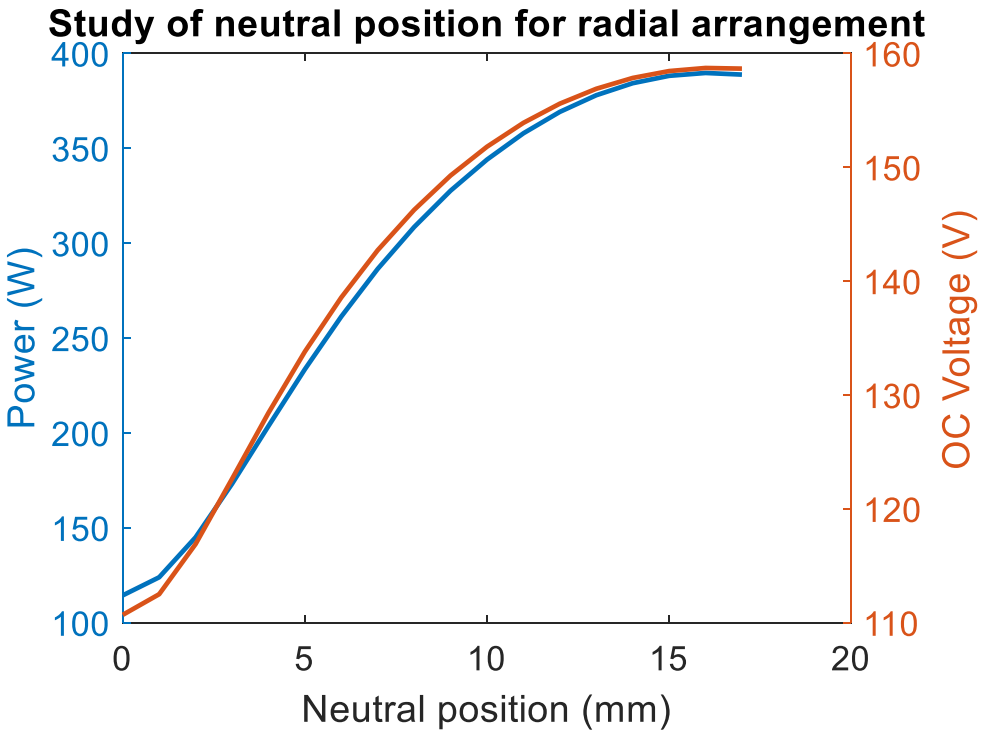

Figure 5-14 - Power and OC Voltage for the radial neutral position study -.

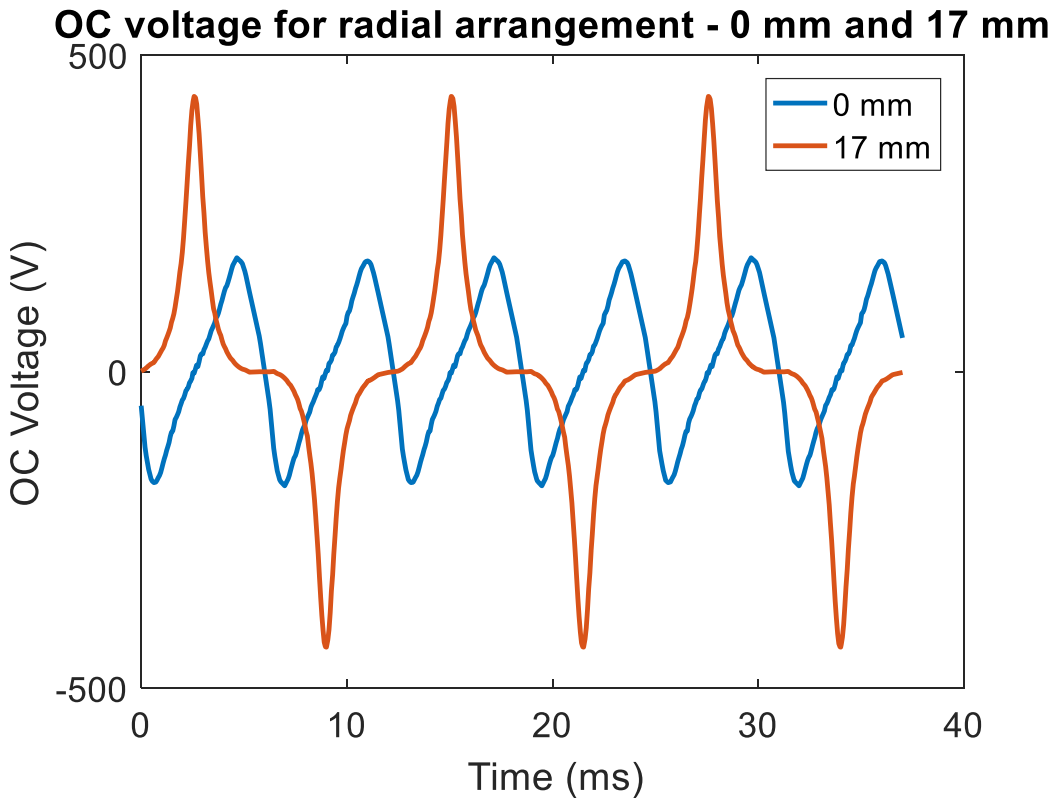

Figure 5-15 - OC Voltage waveform Radial Neutral position study.

5.2.3 Halbach Arrangement

Similar to axial and radial arrangement, halbach arrangement study was done for the neutral position. Neutral position referred in radial is similar to axial arrangement as shown in Figure 5-11. Halbach arrangement of magnets is shown in Figure 5-16.

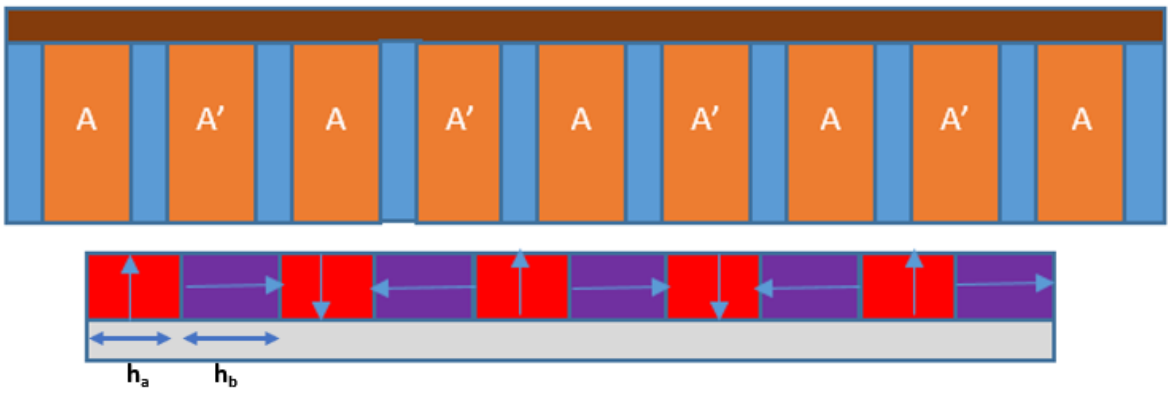

Figure 5-16 - Halbach arrangement.

In Figure 5-16, h_a and h_b refers to the length of the axial and radial magnets used in the arrangement. It can be seen that the length of h_a and h_b can be varied to have a total length of the pole pitch given by the equation below.

$$h_a + h_b = \tau \quad (5\text{-}1)$$

where τ – pole pitch.

Length of h_a was chosen to be in steps of pole pitch (0.1 – 0.9 times of pole pitch). Accordingly, h_b was calculated based on equation (5-1).

Power and open circuit voltage was studied for neutral positions from 0 mm to 17 mm for 9 test condition of h_a and h_b. The results are shown in Figure 5-17. The neutral position for the best output power varied according to the lengths of h_a and h_b. The best neutral position and best combination of h_a and h_b is 6 mm and h_a of 0.6 times pole pitch and h_b of 0.4 times pole pitch. Furthermore, it was seen that as the length of h_a is varied, the neutral position also varied. Table 5-3 shows the best neutral position for multiples of pole pitch for h_a.

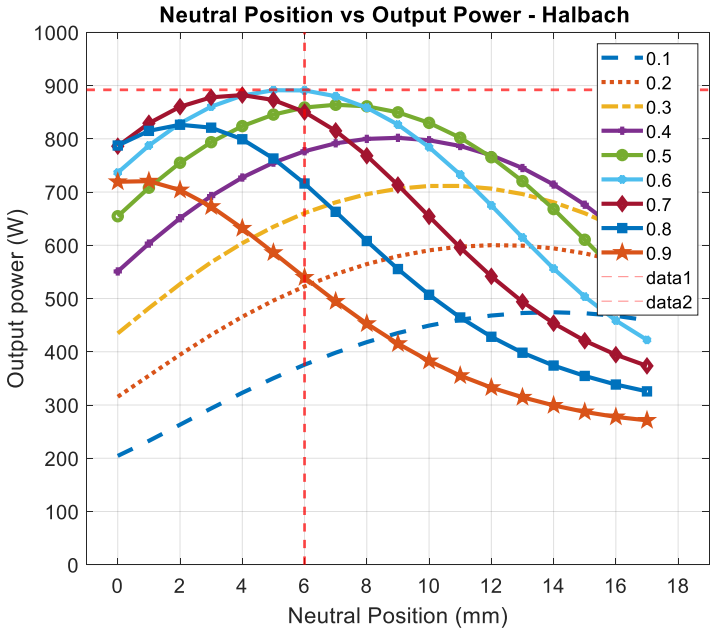

Figure 5-17 – Output power for the halbach neutral position study.

Table 5-3 - Neutral position in Halbach arrangement.

h_a as multiples of pole pitch	Neutral position (mm)
0.1	16
0.2	13.5
0.3	11.5
0.4	8.5
0.5	7.5
0.6	6
0.7	4
0.8	2
0.9	0

From Table 5-3, it was seen that as the multiple of h_a increased, the neutral position changed from 16 mm to 0 mm. When h_a was 0.1 times the pole pitch, it was almost similar to an axial arrangement and therefore, the maximum power was at 16 mm similar to the axial arrangement study. When h_a was 0.9 times the pole pitch, it was almost similar to an axial arrangement and therefore, the maximum power was at 0 mm similar to the axial arrangement study. When h_a was 0.5 times the pole pitch, the neutral position was in between the results obtained from the axial and radial arrangement studies. Therefore, in general, if PMLG system is modeled in halbach arrangement, it is better to start the machine at 6 mm neutral position with h_a as 0.6 times the pole pitch.

5.3 One At a Time (OAT) method

Simplest method to understand the effect of the PMLG parameters is to use an OAT method. In an OAT method, one input parameter is varied, and the rest of the other parameters fixed. With that condition, the PMLG parameters were studied, and the individual effect of the input parameters are studied. The advantage of this method is the simplicity of the method in determining the effect of the input parameter on the output. The disadvantage of this scheme is the absence of knowledge on the interdependence of the input parameters on the output. In addition, this scheme requires all the input parameters to have a linear or a generic relationship with the output. In this method,

sensitivity of the parameter was obtained by calculating the slope of the relationship between the input and the output. The following equation was used to determine the sensitivity of the input parameters of the PMLG system.

$$S_i = \frac{dx/dy}{B_i} \tag{5-2}$$

where,

x – output parameter,

y – input parameter, and

B_i– Base index.

Output parameters for this study were the output power, open circuit voltage and power / moving mass (P/M) ratio. Input parameters for the OAT study were MT, spacer length, poles, OD, airgap, frequency, stroke length, and turns. Base index for the output parameter was based on the beta prototype PMLG system.

This study involved varying each of these parameters individually keeping the other parameters constant. Initial parameters of this study are same as in Table 5-1.

5.3.1 Magnet radial thickness (MT)

In the magnet thickness study, magnet thickness of the PMLG system was varied from 0.5 mm to 10 mm and 100 values were chosen in between this range. The upper and lower bounds were chosen in such a way that the PMLG system was analyzed over a wide power range up to 3 kW. Figure 5-18 shows the output power and OC voltage for the magnet thickness study.

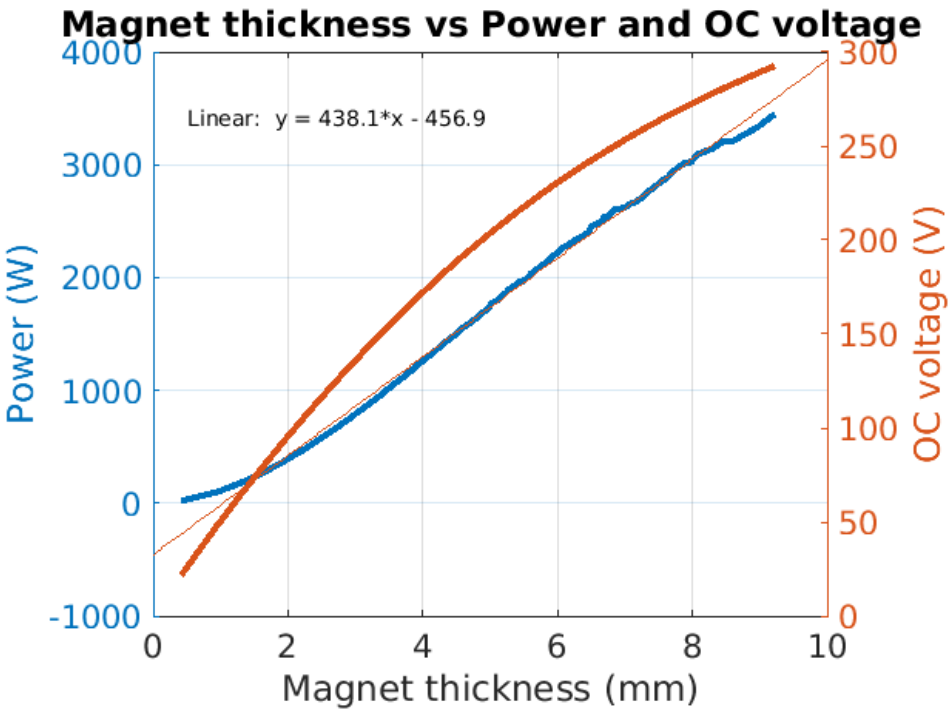

Figure 5-18 - Power and OC voltage for the magnet thickness study.

It was seen that there is a linear relationship between MT and power. The equation of the fit was given by the equation (5-3).

$$Power = 438 * MT - 456.9 \quad (5\text{-}3)$$

From 2 mm to 8 mm, there is a linear fit with a slope of 438 whereas beyond 8 mm, the slope reduces. This can be attributed to the saturation in the laminations as the MT increases. As MT increases, the flux density increases and when the flux density in the laminations go beyond 1.2 T, the laminations saturate and the rate of change of flux decreases. Therefore, the slope decreases beyond 8 mm.

Another important aspect that needs to be studied for a free piston engine PMLG system is to understand the effect of magnet thickness on the moving mass of the PMLG system. This is shown in Figure 5-19.

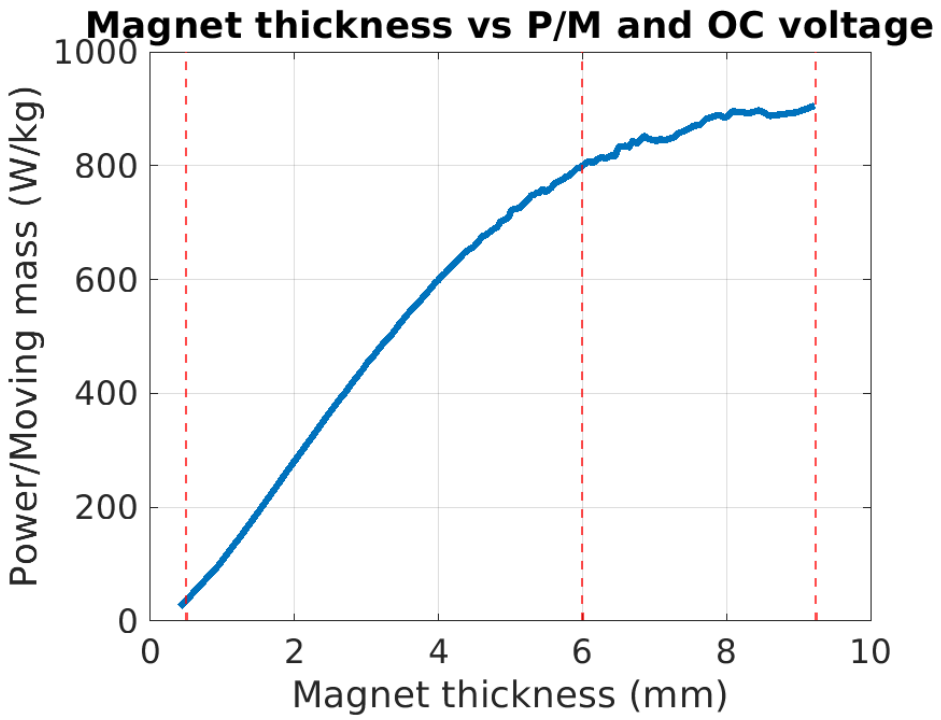

Figure 5-19 - P/M for the magnet thickness study.

It was seen that the as the magnet thickness increases, the P/M of the PMLG system increases up to 6 mm magnet in a linear manner and then starts to saturate slowly as it reaches 9.4 mm. Maximum P/M ratio of up to 900 W can be achieved by varying the MT. From Figure 5-18, the output power keeps increasing with increasing magnet thickness up to 8 mm and almost remains constant after that. Two factors play a role for this condition.

1. Saturation of the laminations because of the high flux density
2. As the magnet thickness increases by 2 times, the mass of the magnet increases almost 4 times. Therefore, with saturation of laminations at higher MT and the rate of increase of the moving mass, the P/M ratio starts becoming constant.

Therefore, magnet thickness and its saturation effects need to be taken into consideration while designing a PMLG system.

5.3.2 Translator spacer width

In the spacer study, the spacer width was varied between 0 mm and 33 mm and 100 different points were chosen between these limits. Stroke length for this study was 33 mm

and therefore, the lower and upper limits of 0 mm and 33 mm was chosen respectively. Figure 5-20 shows the output power and open circuit voltage for the spacer study.

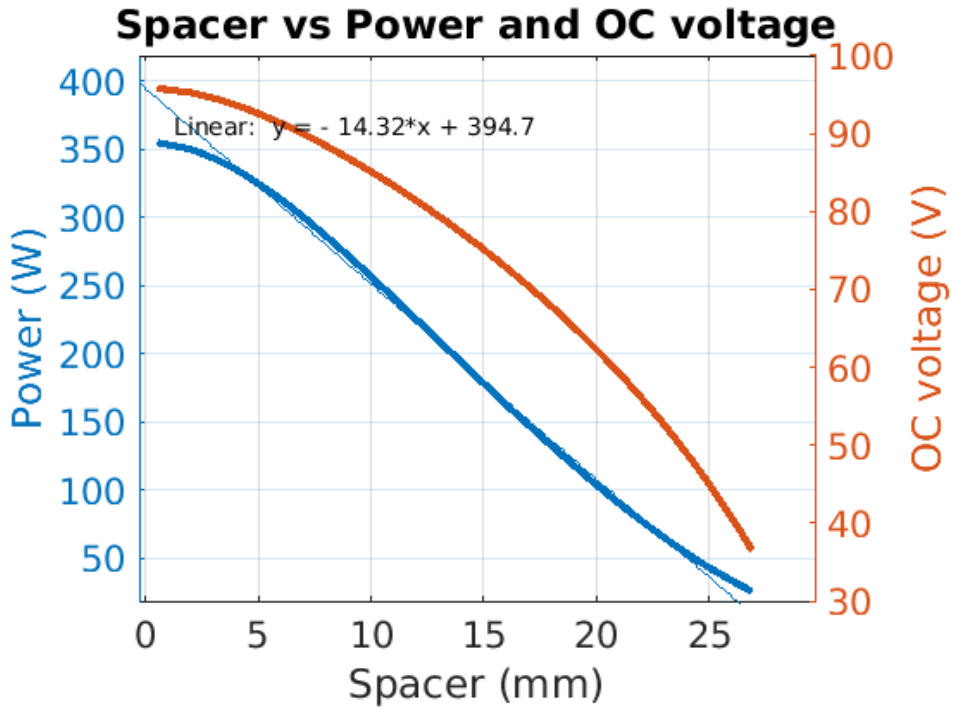

Figure 5-20 – Translator spacer width study.

The linear fit relationship is given by the equation (5-4).

$$Power = -14.32 * Spacer + 394.7 \quad (5\text{-}4)$$

As the spacer width increases, the output power of the PMLG system decreases. This is expected as the spacer width increases, the length of the length of the magnet decreases. Therefore, the output power decreases. P/M ratio for the spacer study is shown in Figure 5-21.

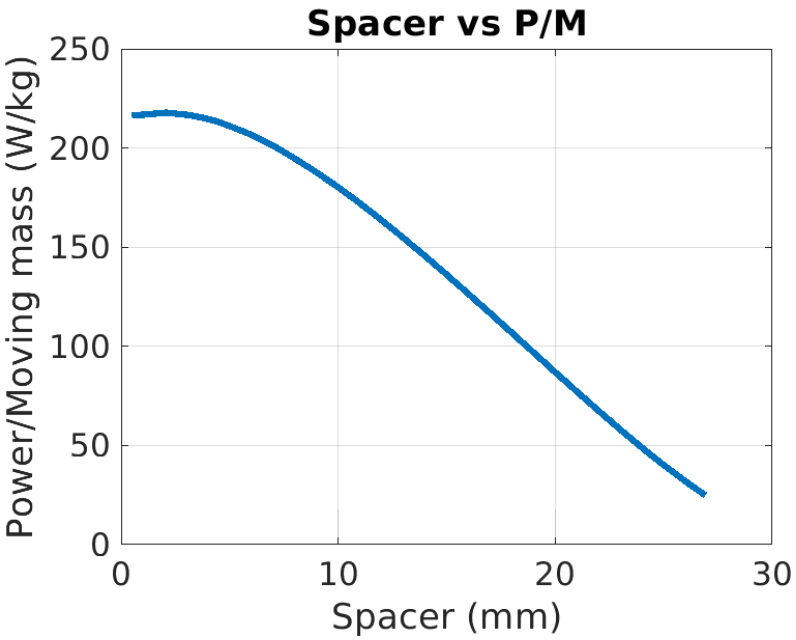

Figure 5-21 - P/M ratio for the translator spacer width study.

From Figure 5-21, the P/M ratio decreases from 220 W and decreases close to 18 W. The reason for the decrease in the P/M ratio was because of the harmonics as the spacer width increases. This is shown in Figure 5-22 and Figure 5-23.

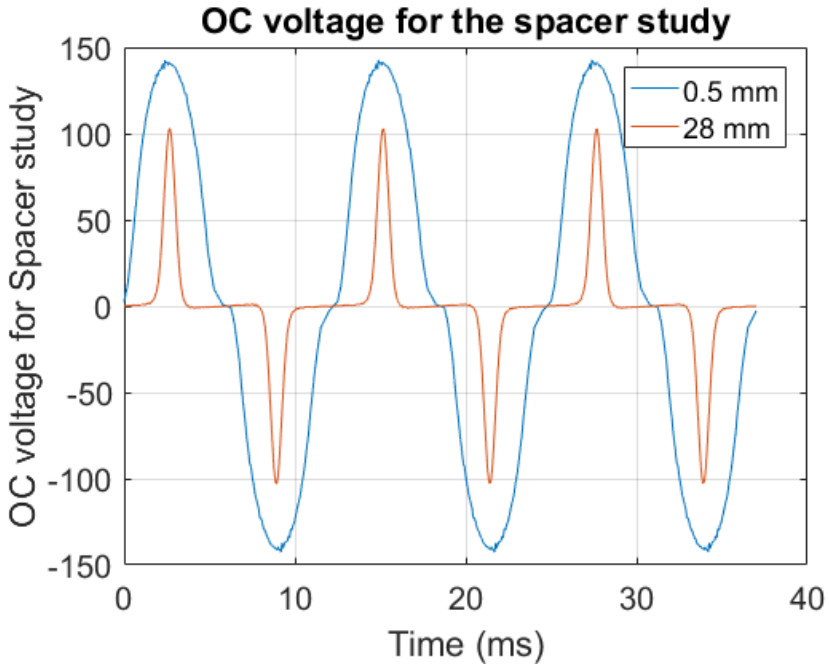

Figure 5-22 - OC voltage waveform for two spacer width cases.

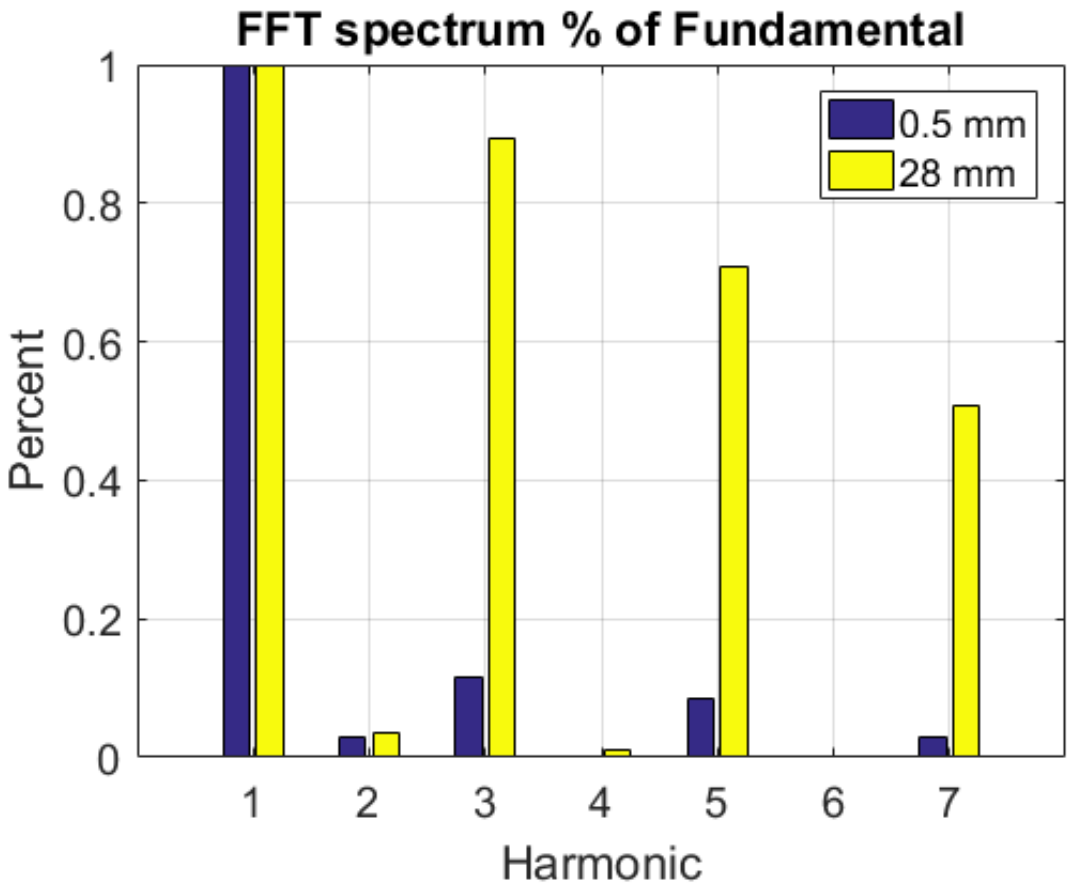

Figure 5-23 - Harmonics of the OC voltage waveform.

From Figure 5-23, 3rd, 5th and 7th harmonics were higher for spacer of 28 mm compared to spacer of 0.5 mm. Therefore, as the spacer increases, harmonics increases and the power decreases.

5.3.3 Airgap

Airgap of the PMLG system was varied from 0.5 mm to 10 mm for this study. Figure 5-24 shows the output power and OC voltage for the OD study. From Figure 5-24, it was seen that as the airgap increases, the output power decreases. When airgap in the PMLG system increases, the flux density in the airgap decreases. As the flux density decreases, the rate of change of flux in the windings decreases. Rate of change of flux density is proportional to the OC voltage as shown in equation (5-5).

$$V = N * \frac{d\lambda}{dt} \quad (5\text{-}5)$$

Therefore, as the OC voltage decreases, the output power decreases. With respect to a PMLG system smaller the airgap, better the performance in terms of OC voltage and output power.

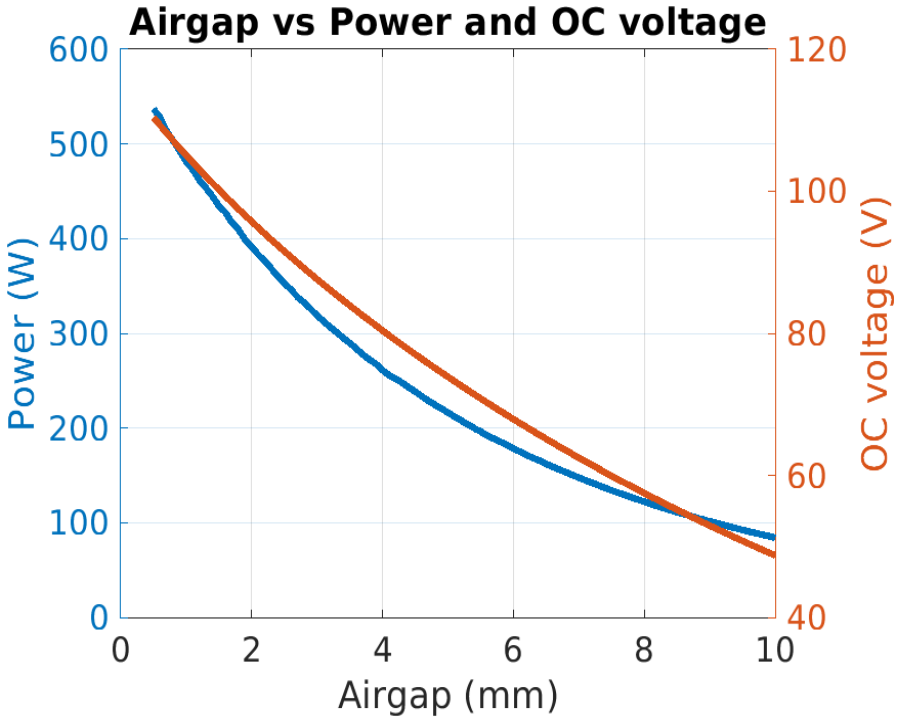

Figure 5-24 – Airgap study for output power and open circuit voltage.

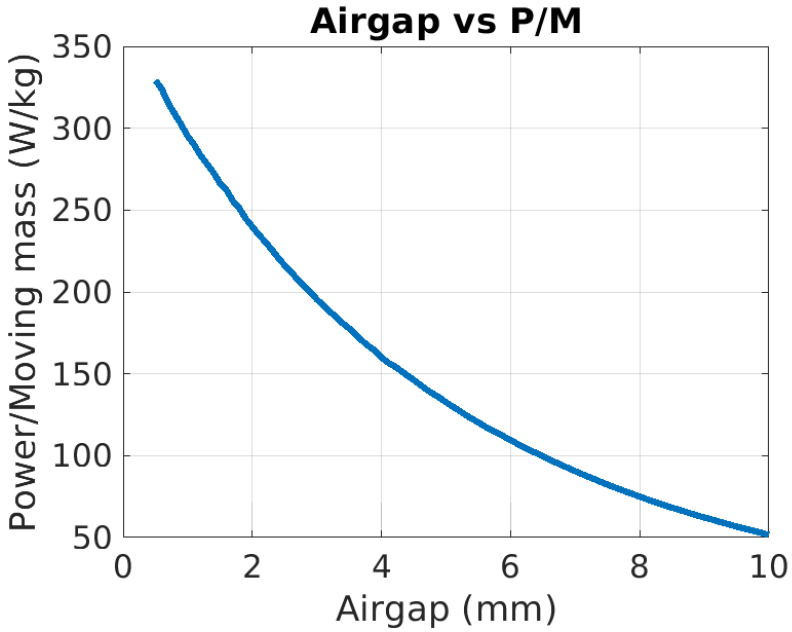

Figure 5-25 - P/M ratio for the airgap study.

From Figure 5-25, airgap does not affect the moving mass of the translator and therefore, the trend of the P/M is similar to the output power of the PMLG system. Furthermore, two things need to be kept in mind in terms of airgap.

1. Airgap is decided based on the designer's requirement.
2. Airgap depends on the manufacturing capability of the company building it.
3. Airgap needs to be large enough to prevent saturation in the laminations of the PMLG system

5.3.4 Stroke length

In the stroke length study for the PMLG system, stroke length was varied from 10 mm to 100 mm. Figure 5-26 shows the power and OC voltage for the stroke length study. The equation of the linear fit for the output power is shown in (5-6).

$$Power = 14.25 * stroke - 107.8 \quad (5\text{-}6)$$

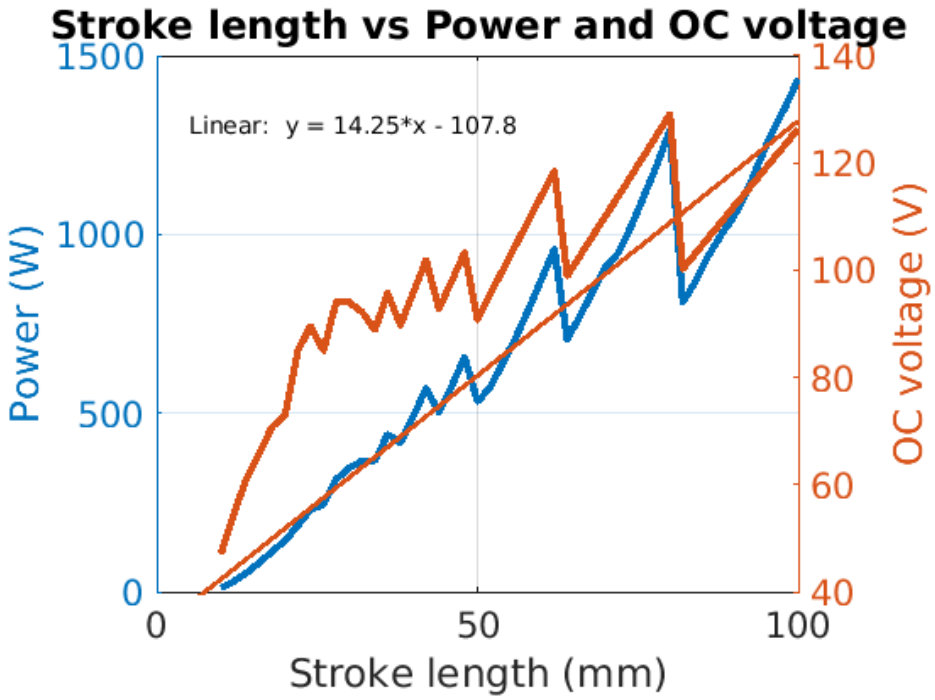

Figure 5-26 - Power and OC voltage for the stroke length study.

Some adjustments needed to be made to the FEMM model to account for the stroke length. When the stroke length changes, the slot width and slot height need to be changed to keep the turns constant at 126 with AWG 13 wire gauge. This modification caused

some of the cases to not match the turns to be exactly at 126. This caused some of the spikes and jagged lines in the output power and OC voltage as seen in Figure 5-26.

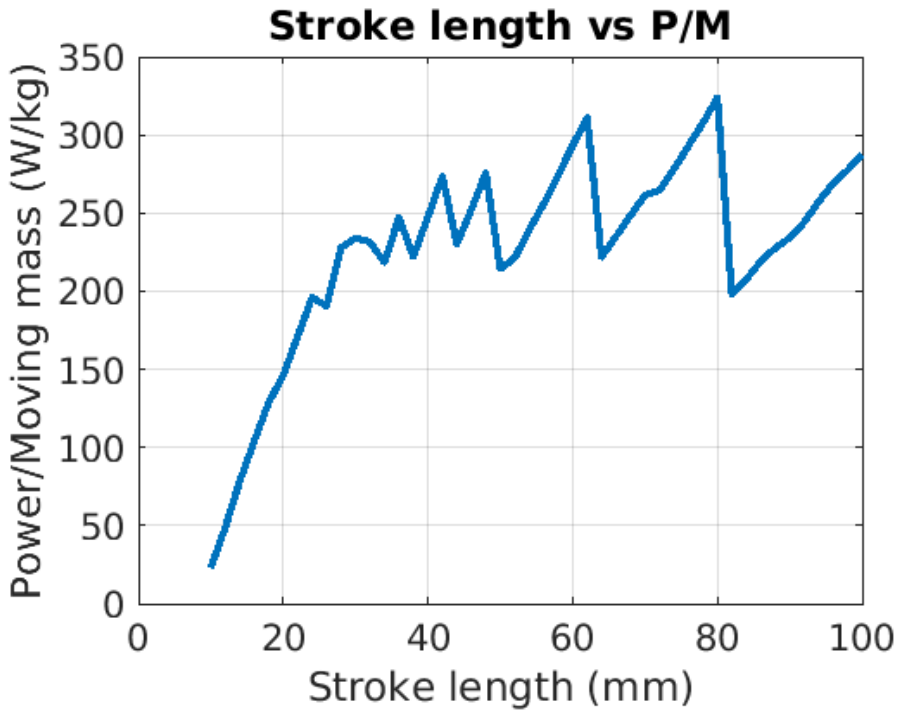

Figure 5-27 - P/M for the stroke length study.

5.3.5 Number of poles

In the poles study, number of poles was varied from 2 to 10. Figure 5-28 shows the output power and open circuit voltage for the spacer study. Figure 5-29 shows the P/M ratio for the poles study. P/M ratio was in the range between 228 W and 255 W.

There is a linear relationship between output power and the number of poles and was given by the equation (5-7).

$$Power = 93.61 * poles + 18.54 \quad (5\text{-}7)$$

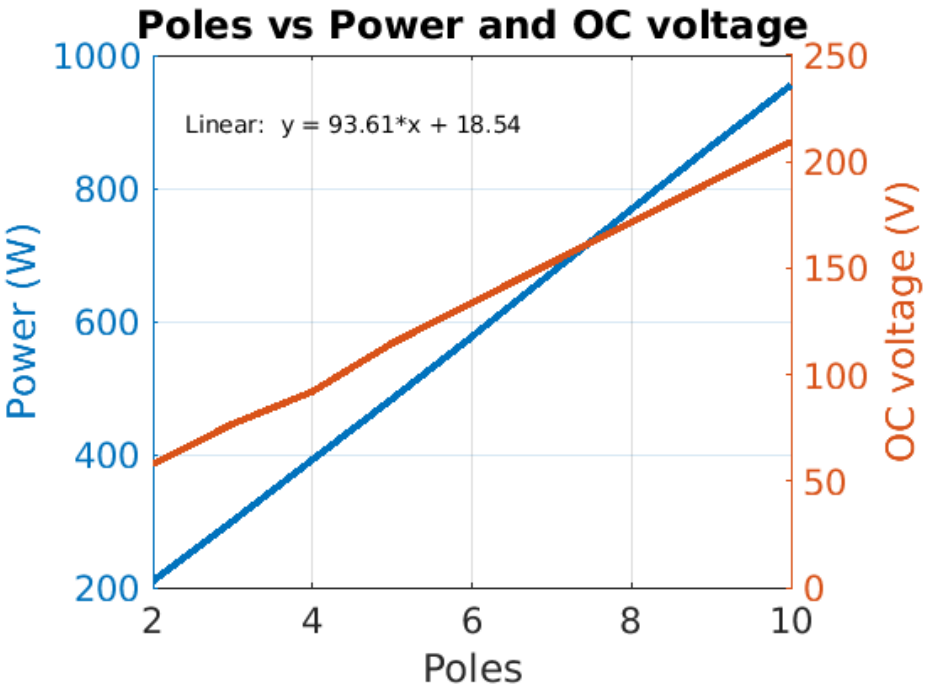

Figure 5-28 - Power and OC voltage for the poles study.

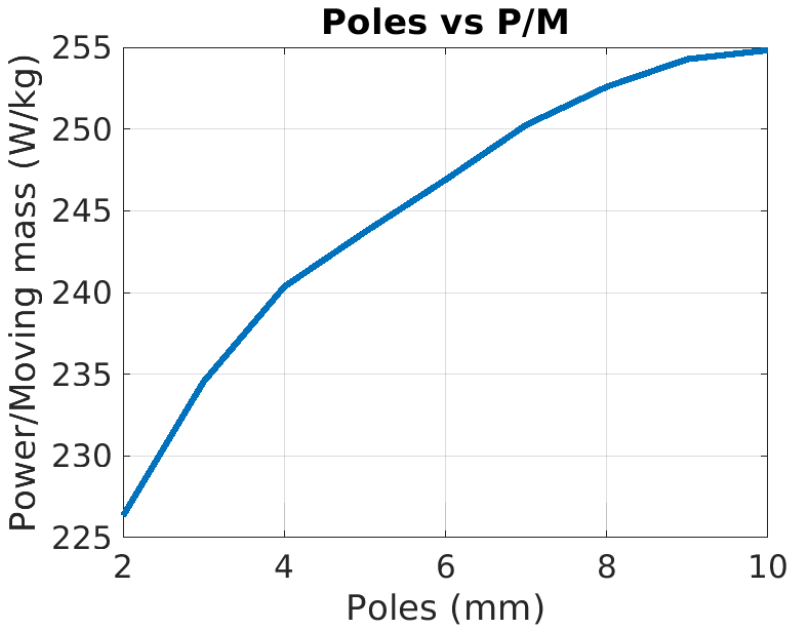

Figure 5-29 - P/M for the poles study.

5.3.6 Outer diameter of the magnet (OD)

Outer diameter of the magnet was varied from 25 mm to 500 mm for this study. Figure 5-30 shows the output power and open circuit voltage for the OD study. Figure 5-30 shows the P/M ratio for the OD study.

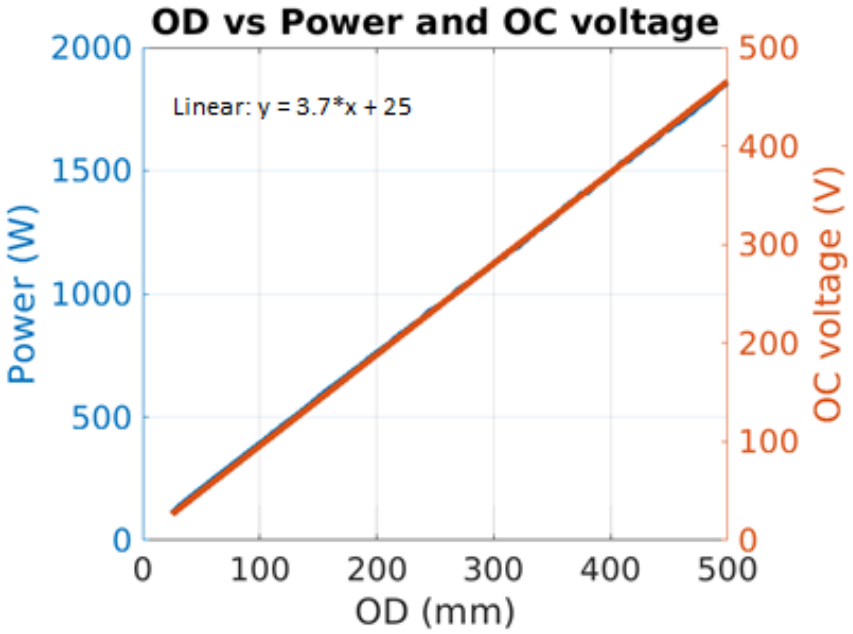

Figure 5-30 –Outer Diameter of the magnet study for output power.

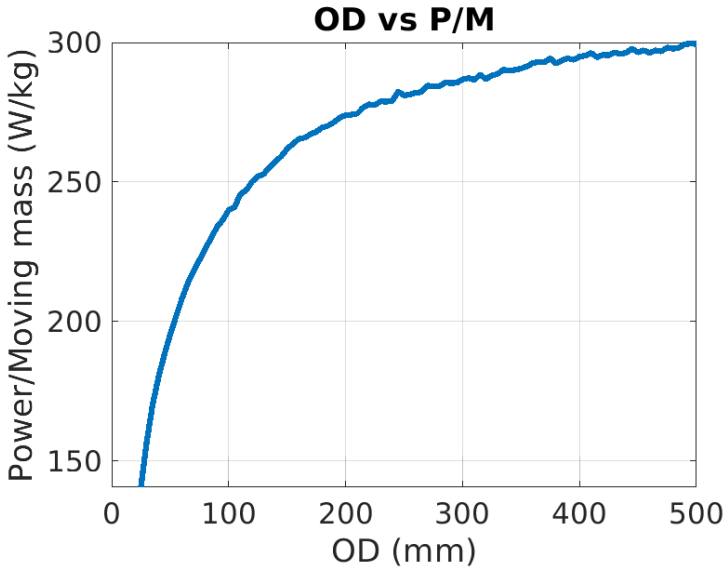

Figure 5-31 - P/M for the OD study.

There is a linear relationship between output power and the number of poles and was given by the equation (5-8).

$$Power = 3.7 * OD + 25 \quad (5\text{-}8)$$

From Figure 5-31, it was seen that the P/M ratio for the OD study was in the range of 150 W – 300 W. Furthermore, as OD increases the volume of the overall system increases and that needs to be remembered when designing the PMLG system. If the volume of the overall needs to be small, OD plays a major role in determining the volume of the PMLG system.

5.3.7 Oscillating frequency

Oscillating frequency of the PMLG system was varied from 25 Hz to 150 Hz. Based on equation 5-5, OC voltage is proportional to rate of change of flux linkage. Therefore, as the frequency increases, the OC voltage and output power increases. Change in frequency does not affect the moving mass of the translator. This was shown in Figure 5-32.

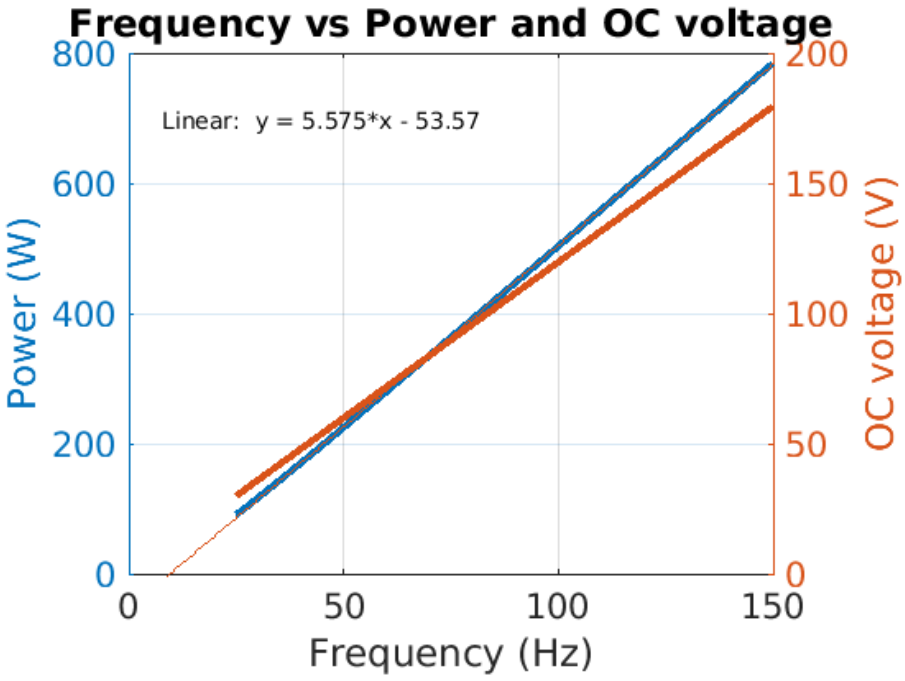

Figure 5-32 – Oscillating frequency study for output power.

There is a linear relationship between output power and the number of poles and was given by the equation (5-9).

$$Power = 5.575 * frequency - 53.57 \quad (5\text{-}9)$$

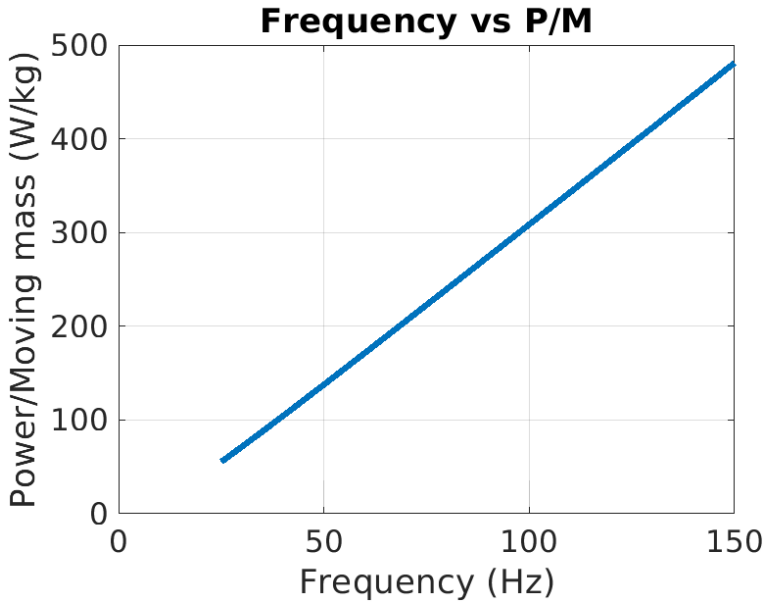

Figure 5-33 - P/M for the oscillating frequency study.

P/M ratio followed the same trend as the output power in Figure 5-33. This is because the moving mass is affected by only changing the frequency of operation of the PMLG system.

5.3.8 Number of turns

In the turns study, number of turns in the windings of the PMLG system were varied from 14 to 1372 for 96 cases keeping all the other parameters the same including the wire gauge. This was done by changing only the slot height with increasing turns. All the other parameters were kept the same as in Table 5-1.

Figure 5-32 and Figure 5-33 shows the output power and OC voltage for the turns study. It is seen from Figure 5-32, that as the number of turns increases, output power increases up to 70 turns but beyond that the output power starts to decrease. On the other hand, open circuit voltage continues to increase, and this can be attributed to equation (5-6) shown in the airgap study.

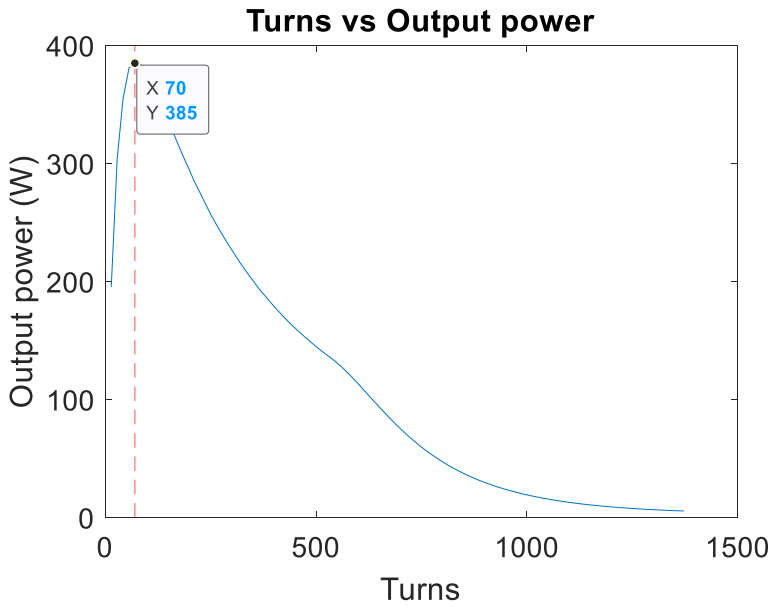

Figure 5-34 – Output power for the turns study.

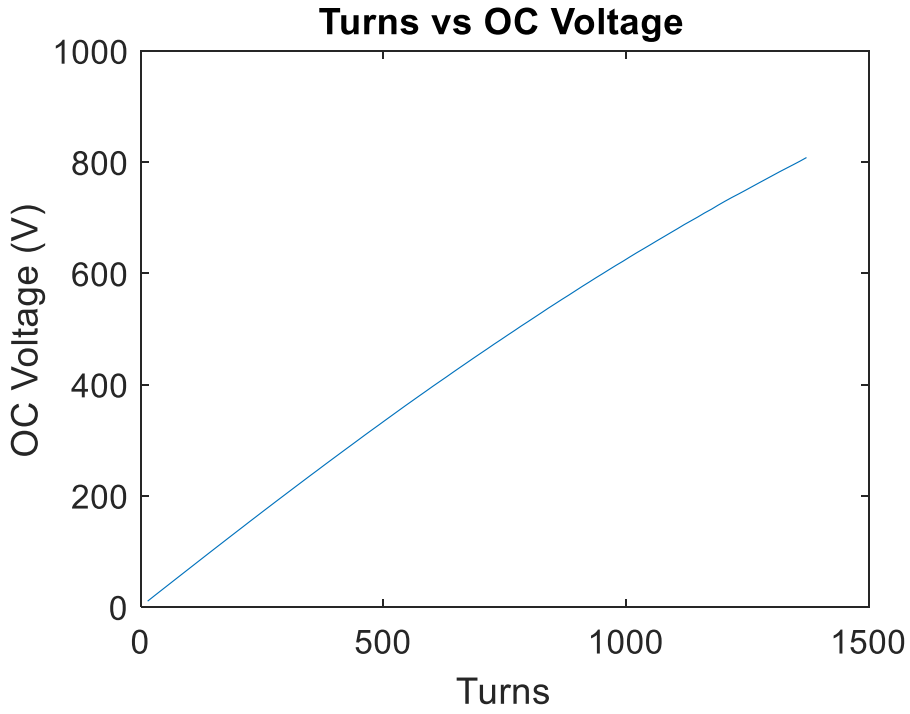

Figure 5-35 - OC Voltage for the turns study.

The reason for the decrease of the input power after 70 turns was because as the number of turns increase, the resistance and inductance of the PMLG system increases. As they

increase, the output power decreases. The maximum output power was given by the equation (4-14) where the output is inversely proportional to the square of the impedance of the system. Therefore, it was found that beyond 70 turns, for the PMLG system considered in Table 5-1, the increase in number of turns works against the output power. The increase in the R and L is shown in Figure 5-36.

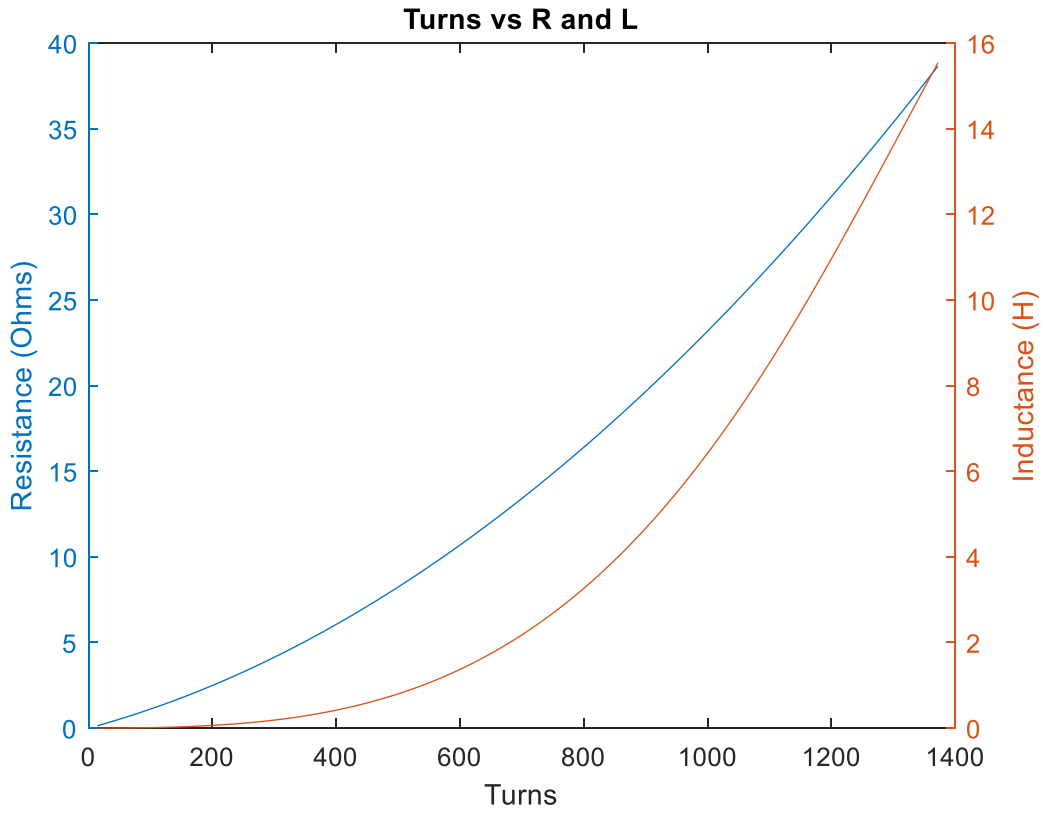

Figure 5-36 - Resistance and inductance for the turns study.

5.3.9 Comparison of all the input parameters

This section shows the comparison of the input parameters for the OAT study. Based on the equation in (5-1), the Jacobian values were calculated. All the values were calculated and normalized so that the sum of all the values obtained for the input parameters equal 1. This shows the importance of each of the parameters. Table 5-1 shows the baseline values used for the comparison. The baseline values of the output variables are,

1. Power – 354 W,
2. OC voltage – 92 V, and

3. P/M – 239 W/kg.

Figure 5-37 shows the comparison of the input parameters for the OAT study for the output variable - Output power. It was seen that the magnet thickness has the highest importance followed by poles, airgap, stroke, spacer, frequency and OD respectively. MT has sensitivity index of 0.7 compared to OD which has a sensitivity index of 0.009. Therefore, the most important parameter to modify when we need to improve the output power is to increase the magnet thickness whereas the outer diameter has to be given the least importance.

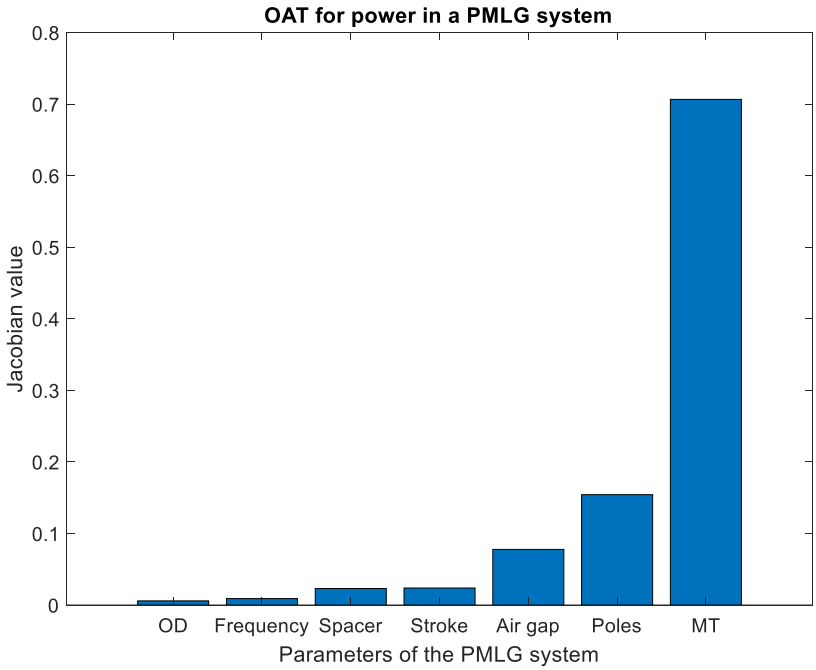

Figure 5-37 – Comparison of different parameters for the Power – OAT study.

Based on Figure 5-38, MT is the most important parameter whereas stroke is the least important parameter that affects the OC voltage of the PMLG system.

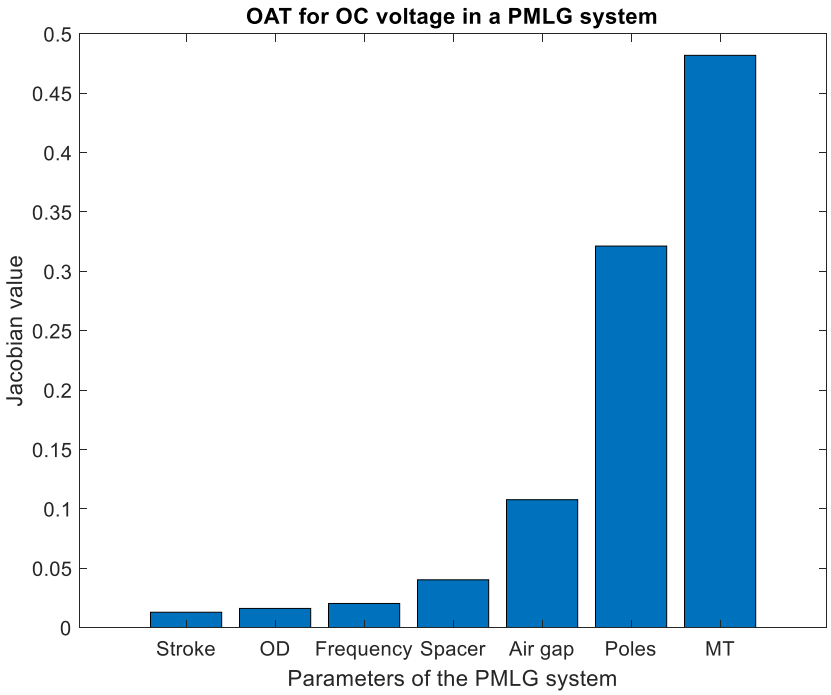

Figure 5-38 – Comparison of parameters for the OC voltage – OAT study..

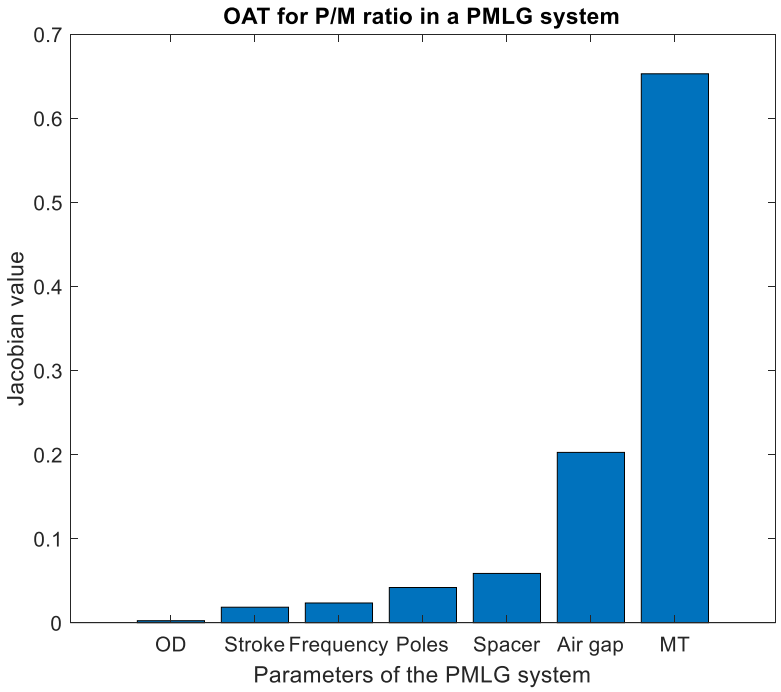

Figure 5-39 - Comparison of parameters for the P/M – OAT study.

P/M ratio is an important characteristic when designing a PMLG system. It tells us which parameter to focus on when there is a need to reduce the moving mass and improve the output power. Based on Figure 5-38, MT was the most important parameter and OD was the least important parameter that affects the P/M ratio.

The inferences from the OAT study are tabulated below.

1. MT is the important parameter and OD is the least parameter for both output power and P/M.
2. A small change in magnet thickness produces a greater effect on the flux density compared to other parameters. Furthermore, the small change in MT results in an increase in moving mass which is substantially lesser than the increase in the output power. In this case, a 3.7% change in magnet thickness produces a 7.8% change in output power and 5.4% improvement in P/M.
3. Increase in OD produces an increase in power but at the same time, there is increase in the moving mass. In this case, a 3.2% change in OD produces a 3.1% change in output power and 0.008% improvement in P/M.
4. Turns was not included in the OAT comparison because it does not have a linear effect on the output power, OC voltage and P/M.
5. Poles is the second important factor for the output power but fourth important factor for P/M. This is because power was calculated on a base of 4 poles where when the poles increases, output power increases and moving mass increases as well. This causes a decrease in the P/M ratio.

5.4 Global Sensitivity Analysis

An OAT study was performed in the previous section. It was seen that only one parameter was varied at a time. Through this procedure, the interdependence of the parameters cannot be found. Furthermore, they give a preliminary result to understand the effects of each of the parameters. To understand the overall effects of all the parameters, a global sensitivity analysis (GSA) of the PMLG was performed. One of the common methods of GSA is a variance based decomposition method or sobol method. The procedure and equations to determine the sobol method is explained below.

Step 1:

First step in GSA is to generate random datapoints for the variables. This was done by using sobol sequence command in SIMULINK. Eight input parameters were used, and 125 different data points were generated for the sobol sequence. Once the data points were generated, a complementary data set for the 125 data points were also generated based on sobol sequence using MATLAB SIMULINK. A uniform probability distribution was used for all the input parameters with upper and lower bounds as shown in Table 5-4.

Table 5-4 - Lower and upper bounds for the GSA input parameters.

Parameter	Lower bound	Upper bound
MT (mm)	2	10
Translator spacer width (mm)	1	10
Airgap (mm)	0.5	5
Number of poles	2	10
OD (mm)	25	500
Oscillating frequency (Hz)	25	150
Stroke length (mm)	20	50
Coil number of turns	40	200

Step 2:

Once 250 data points were generated for the GSA, they were modified to generate another 1000 different data points from these 250 data points.

The generated data points were 125 * 8 matrix. This was added to complementary data point to form 125 * 16 matrix. With this matrix, the data points were modified to generate another 1000 different data points. The procedure for 3 variables is shown in Figure 5-41. Similar procedure for followed for the eight variables to generate the sobol sequences. The code used to generate this matrix is added in the appendix.

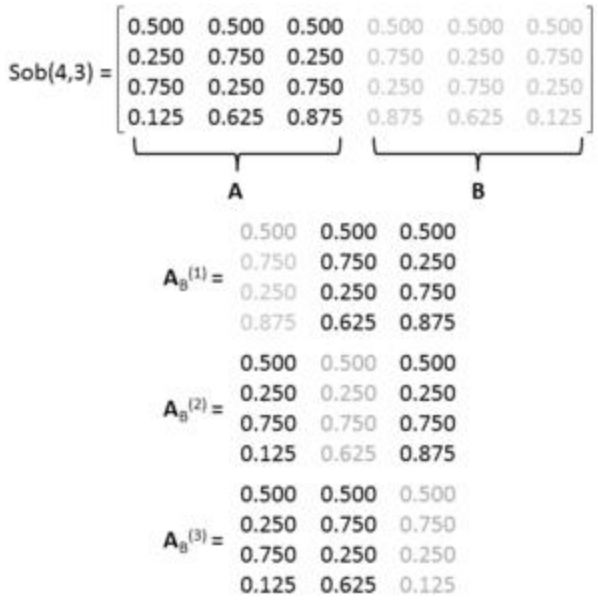

Figure 5-40 - Step to generate the input data points for the GSA (3 variables) [100].

The generated sobol sequence for MT and spacer is shown below in Figure 5-41.

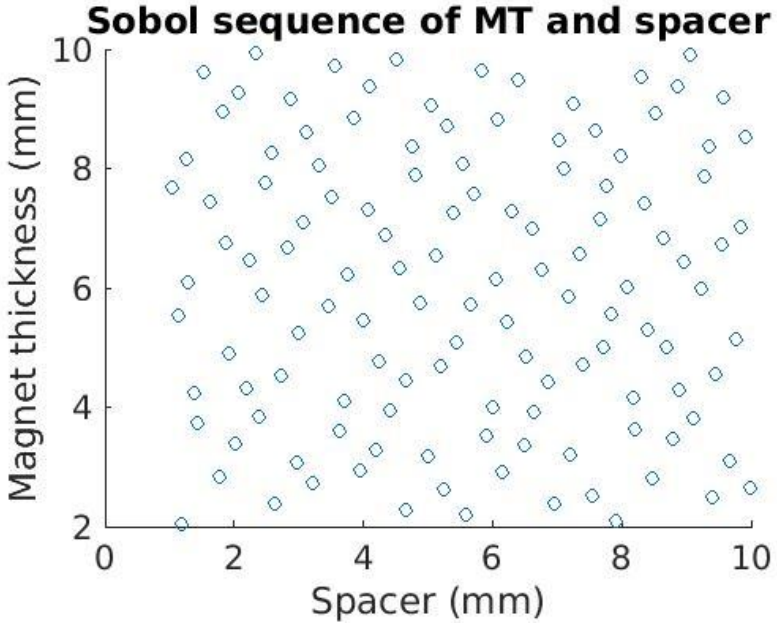

Figure 5-41 - Generated sobol sequence in MATLAB SIMULINK for MT and spacer.

Once the data points were generated, all the data points were evaluated in FEMM and the results were obtained for the output power, OC voltage and P/M.

Step 3:

GSA using sobol method is a variance based decomposition method. Therefore, the variances for the output variables were calculated. The equations to calculate the variances and the sobol indices are shown below.

First order Sobol indices:

$$S_i = \frac{V_i}{Var(Y)} \tag{5-10}$$

where,

S_i – first order sobol indices, and

$Var(Y)$ – Variance of Y (output).

$$Var_{Xi}(E_{Xi}(Y|Xi) = \frac{1}{N}\sum_{j=1}^{N} f(B)_j(f\left(A_B^j\right)_j - f(A)_j) \tag{5-11}$$

$$V_i = Var_{Xi}(E_{Xi}(Y|Xi) \tag{5-12}$$

where,

N refers to number of data points chosen (125 in this case), and

A & B matrices refers to the matrices in Figure 5-40.

A refers to the output from the first set of 125 points and B refer to the output from the second of 125 data points obtained from the sobol sequence.

First order indices help to determine the variance in output due to contribution of only the input variance as shown by the equation (5-10). Higher order interactions are not considered in the first order sobol indices.

Total Sobol index:

To include the interactions from other input parameters on a given input parameter, total sobol index is used. This measures the output variance by including all the interactions a given input parameter has with other input parameters.

The equations to calculate the total sobol index is shown below.

$$S_{Ti} = \frac{E_{Xi}(Var_{Xi}(Y|Xi))}{Var(Y)} \tag{5-13}$$

where,

$$E_{Xi}\left(Var_{Xi}(Y|Xi)\right) = \frac{1}{2N}\sum_{j=1}^{N}(f(A)_j - f\left(A_B^j\right)_j)^2 \tag{5-14}$$

Using these equations, the first order and total sobol indices were found for the input parameters. The results from the sobol method for the GSA is shown below in Figure 5-42, and Figure 5-43.

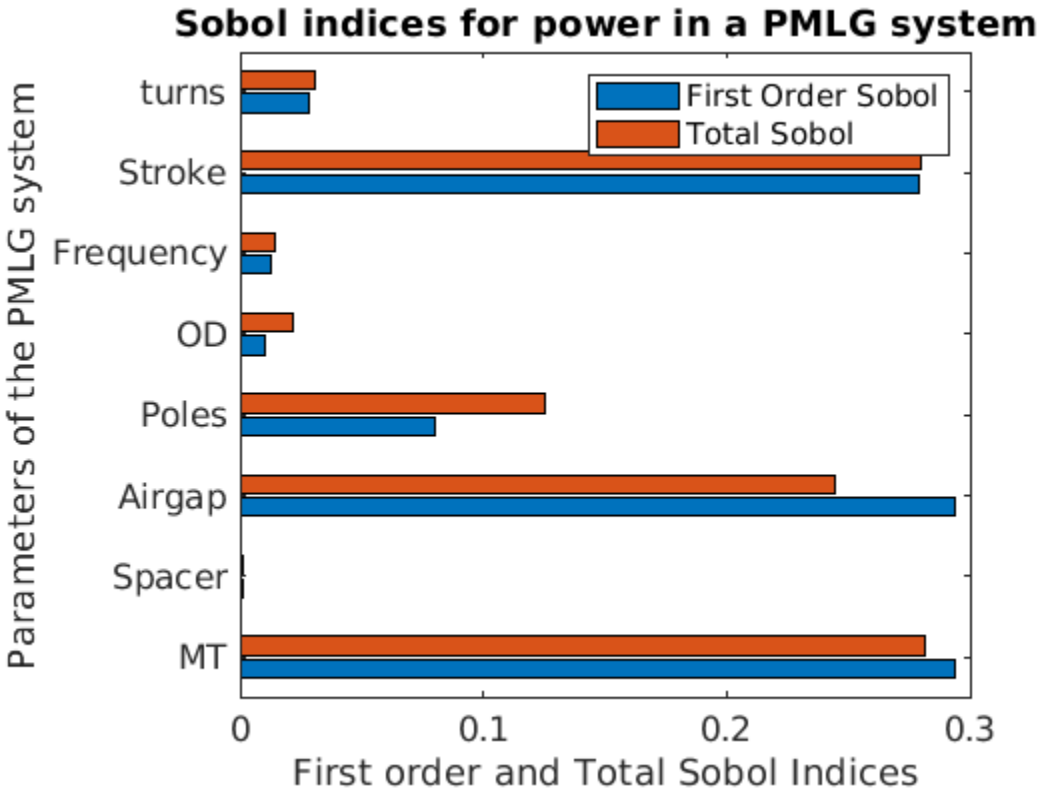

Figure 5-42 - Sobol index – First order and Total index for Power.

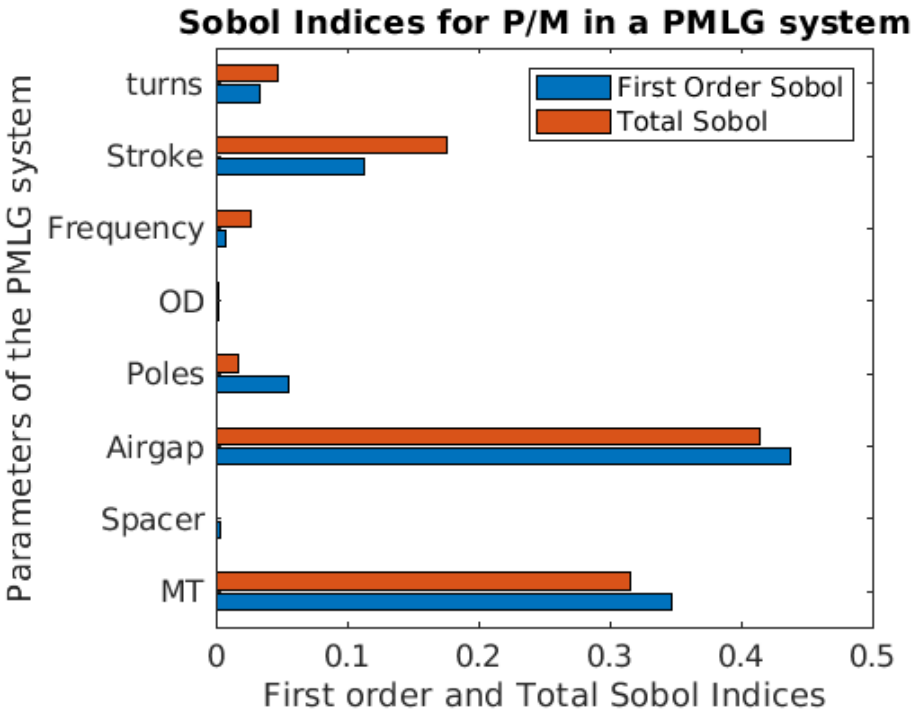

Figure 5-43 - Sobol index – First order and Total Sobol indices for P/M.

From the figures, it can be seen that the important parameters that affect the PMLG system are given by the highest indices in first order and total sobol index. Total sobol index helps to include the interdependency between the parameters. Therefore, total sobol index gives a better picture on the importance of the parameters in the PMLG system. It is seen that for the output power, MT plays the major factor and spacer is the least important factor. The order of importance is MT, stroke length, airgap, pole, turns, OD, frequency and spacer. For P/M ratio, airgap is the important factor and OD is the least important factor. The order of importance is airgap, MT, stroke length, turn, poles, frequency, spacer and OD. Airgap is the important parameter that affects the PMLG system for the P/M ratio. This is because airgap does not affect the moving mass of the PMLG system. But airgap depends on the manufacturability of the system. Therefore usually, it will be difficult to modify the airgap of the system. The second important factor is MT and this result is similar to OAT results. Therefore, importance must be given MT compared to the other parameters. OD and spacer were the least important parameters and therefore, they must be chosen to be small as possible. Depending on the weight, importance must be stroke length, turns and poles in the given order. Although turns have

the ability to provide higher OC voltage, care must be taken while deciding on the number of turns as with the increase in turns, the resistance and inductances increase as explained in the turns study.

Overall, a GSA study was done and the important parameters that affect the PMLG were found.

5.5 Summary

In this chapter, parametric study of the PMLG system with FEMM was discussed in detail.

1) Comparison of three different magnet arrangements (axial, radial and halbach) was performed. Six different cases were compared for these three arrangements. It was found that the axial magnets should not have back iron, radial magnets need to have back iron to provide a better path for the flux to pass through the laminations. Furthermore, out of the three arrangements, halbach produced the best output power. This was because of the flux concentration on one side of magnets because of their arrangement. But one of the disadvantages of this arrangement is the need of magnets.
2) Neutral position location for the three different magnet arrangements were studied and their locations were determined. For all three conditions, it was seen that the poles of the arrangement need to lie under the center of the laminations and move the distance equal to pole pitch (stroke length) from that location.
3) An OAT study was performed by studying different input parameters of the PMLG system. It was found that the magnet thickness plays an important factor and OD plays the least important factor in affecting the output power and P/M of the PMLG system.
4) A global sensitivity analysis using variance based decomposition method was performed for input parameters of the PMLG system. The results were closer to the OAT analysis. Magnet thickness was the most important factor and spacer was the least important factor for the power of the PMLG system. Airgap was the most important factor the P/M ratio followed by the magnet thickness of the PMLG system and OD was the least important parameter of the PMLG system.

CHAPTER SIX

6 Optimization of tubular permanent magnet linear generators

Techniques to design and model PMLG was discussed in Chapter 3, and 4. Later, the important parameters that affect the PMLG were discussed in Chapter 5. The natural progression from understanding a system is to move towards developing an optimized system. Therefore, the optimization of PMLG system is discussed in detail in Chapter 6. Research has been conducted in developing PMLG with high power density, low moving mass, and low cost. This chapter focusses on the optimization of PMLG based on two criteria 1) low moving mass of the translator and 2) low volume of the overall PMLG system.

The optimization routines were evaluated for different power ranges (500 W, 1000 W, 1500 W, and 2000 W) for the PMLG system. Following the optimization, the results were compared with FEMM to validate the optimized system. The optimized PMLG system provides details on the electrical and geometric parameters for the different test cases.

The following sections describe the procedure used to determine the optimization routine in detail.

6.1 Optimization routine

There are several electrical and geometric parameters which affect the performance of the PMLG system. Therefore, it is important to decide on the input variables which affect the electrical parameters of the PMLG system. The input variables chosen for the optimization were,

1. Magnet radial thickness (MT),
2. Outer diameter of the magnet (OD),
3. Translator spacer width,
4. Number of poles,

5. Stroke length, and
6. Number of turns.

Each of these parameters were studied in detail in Chapter 5 and sufficient knowledge has been gained to understand their effects on the performance of the PMLG system. Using this knowledge and optimization functions available in MATLAB, a Genetic algorithm (GA) optimization procedure was employed to design an optimized PMLG system.

The flowchart for the optimization procedure of the PMLG system using GA is shown in Figure 6-1. The procedure involved in each of the steps is described below. A MATLAB GUI was developed to perform the optimization. Images of the MATLAB GUI are shown at the end of the chapter.

Step 1:

The first step is to send the input parameters to the MATLAB code from MATLAB GUI. The developed MATLAB GUI requires the following initial parameters.

1. Output power (W) and
2. Moving mass of the linear generator (kg).

Once the initial two parameters are provided, lower bounds (LB) and upper bounds (UB) of the input variables need to be specified. The parameters that need to be specified are,

1. Magnet radial thickness – LB and UB,
2. Outer Diameter – LB and UB,
3. Spacer width – LB and UB,
4. Number of poles – LB and UB,
5. Stroke length – LB and UB, and
6. Number of turns – LB and UB.

All the geometric dimensions are provided in mm.

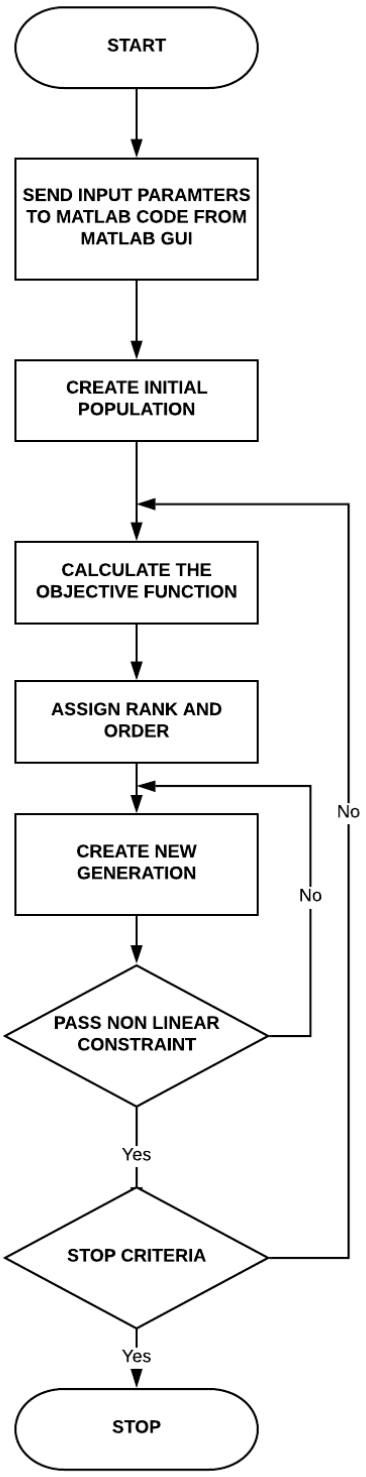

Figure 6-1 - Genetic algorithm procedure for optimization of a PMLG system.

Step 2: Create an initial population

A genetic algorithm (GA) procedure available in MATLAB was used for this process. Therefore, in the MATLAB code, the number of initial population that needs to be generated was specified. There are two options available in MATLAB GA procedure. Create our own initial population or to allow MATLAB to create its own initial population based on the input parameters. There are different techniques to determine the population size as shown in [101]. But all of these suggest running the simulation for different population sizes to determine an appropriate number for the population. This procedure was done to set the population size to be 50.

The results for different population with respect to minimizing the objective function for one condition (varying 3 input variables) is shown below in Figure 6-2.

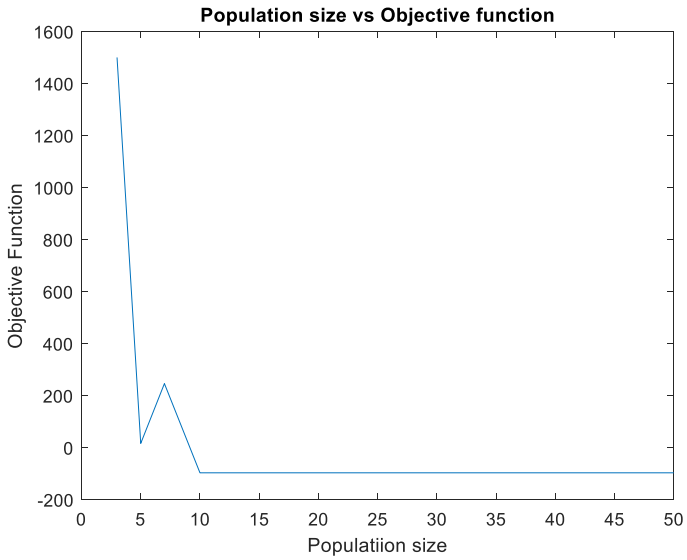

Figure 6-2 - Initial population size for minimizing the objective function.

Based on the results in Figure 6-2, a minimum population size of at least 10 is needed to make the objective function reach its optimized value. An initial population of 50 was chosen for the system because, in addition to 3 variables, the MATLAB application was used for more than three variables (5, 6 variables) when chosen as the input variables in other test cases. All of the initial population is passed through the non-linear constraint function and run until the constraint function is satisfied.

Step 3: Calculate the objective function

The objective function for a genetic algorithm is the function that determines the output value for the given input variables. The output of the objective function is usually a single value or a vector that needs to be optimized to be either a maximum or a minimum. In the case of optimizing the PMLG, the objective function of the PMLG system is to produce the maximum output power.

The usual procedure to calculate the output power of the PMLG system is to draw the finite element model, calculate the flux linkages, load the PMLG with different resistances and calculate the output power. This procedure was detailed in Chapter 4. The time required to determine the final output power of the given design of the PMLG system is 15 minutes in FEMM. The computer setup used for this test was a 128 GB RAM, Intel Xeon E5 core system. In the case of a genetic algorithm optimization,

- Total number of initial population was 50 and
- Number of generations was 50 or more.

Therefore, 2500 evaluations will be required to come with an optimized solution for a genetic algorithm problem. This will take about 625 hours of simulation. If parallel processing is done with several cores, it could be reduced to a lesser time depending on the number of cores. But still, the time required to perform the simulation is not feasible. Therefore, a different methodology needs to be designed to calculate the objective function, i.e. the output power of the PMLG.

One of the techniques that is used in such situations is to model the function using a neural network (NN) technique. To develop the neural network model, input and target datasets are required. In Chapter 5, several parametric studies were performed, and these data sets were used to train and develop the neural network model. The detailed procedure developed to calculate the objective function through the neural network model is described in the next section.

Step 4: Assign rank and order

The initial population data set was chosen, and the results of the objective functions were evaluated. Later based on the results, the population was ordered according to its fitness value. The raw fitness values were then scaled into values suitable for the selection function of the algorithm. The selection function uses scaled fitness function values to select the parents for the next generation. The ones with the lowest objective function were considered as an elite and these individuals was passed on to the next population set.

Step 5: Create a new set of population

Based on the parent population, children were produced which includes mutation and crossover. Thus, the next set of population was generated. The procedure requires looking at the assigned rank and utilize crossover and mutation to develop a new population for the next generation. Like the initial population, the new population was passed through the constraint function. Figure 6-3 shows the cross over and mutation procedure for a genetic algorithm.

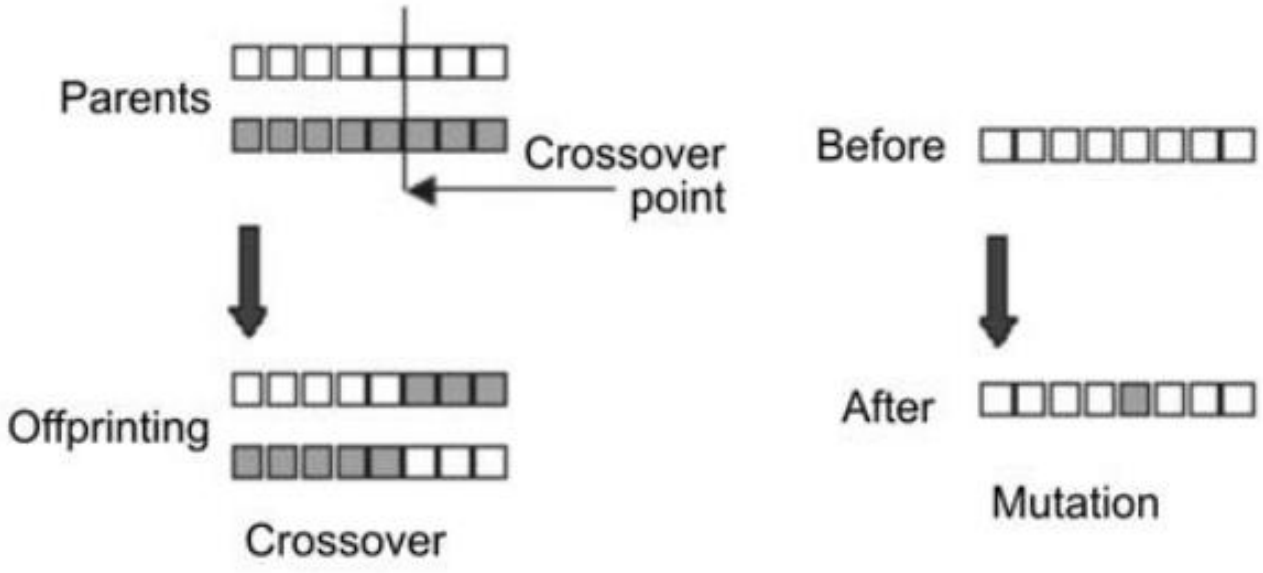

Figure 6-3 - Genetic crossover and mutation operation [102].

Step 6: Nonlinear constraint

Constraints are necessary for the GA problem if we need to restrict the input parameters from exceeding a certain limit. But it is different from the upper and lower bounds. Bounds are used to prevent the individual parameter of the population to go beyond a certain limit. Constraints define a function which the population needs to satisfy. Genetic algorithm (GA) in MATLAB has two options to implement a constraint function. One is a linear constraint function, and another is a nonlinear constraint function. Linear constraints involve a simple and direct calculation of the input parameters which the population set needs to satisfy. Further, the population sets always satisfies the criteria throughout the optimization. In the case of a nonlinear constraint, a function computes the values of all the inequality and equality constraints and returns two vectors. Besides, GA may not satisfy all the nonlinear constraints at every generation. When the GA converges to a solution, the nonlinear constraints are satisfied. When crossover and mutation are used to produce the new population, nonlinear constraints are checked and non-feasible children from the population are discarded.

In case of a PMLG system, the nonlinear constraint for the PMLG system was the moving mass of the translator. Therefore, all the input variables used for the optimization were considered. Later equations to determine the moving mass of the translator were used to calculate the mass of the translator. Basic equations to calculate the moving mass of the translator is shown below.

$$M_{magnet} = \left(\pi * \left(\tau - h_{spacer}\right) * Density_{magnet} * \frac{OD^2 - ID^2}{4}\right) * (m_r + 1) \quad (6\text{-}1)$$

$$M_{spacer} = (\pi * \left(h_{spacer}\right) * Density_{spacer} * \frac{OD^2 - ID^2}{4}) * m_r \quad (6\text{-}2)$$

$$M_{alumdrum} = \pi * \left((m_r * \tau) + (\tau - h_{spacer}\right) * Density_{alum} * (OD_{alumdrum}{}^2 - ID_{alumdrum}{}^2)/4 \quad (6\text{-}3)$$

$$M_{shaft} = \pi * \left(h_{alumshaft}\right) * Density_{alum} * (OD_{alumdshaft}{}^2)4 \quad (6\text{-}4)$$

Detailed equations and calculations of the constraint function are shown in the appendix.

Step 7: Stop criteria

Stopping criteria need to be given to the algorithm to stop the process when a certain condition is reached. Some of the stopping criteria given for this procedure are,

1. Number of generations,
2. Time limit,
3. Objective function limit,
4. Number of generations having the same best point, and
5. Function tolerance – Relative change between the objective functions is within a certain limit.

These procedures are directly implemented in MATLAB and the values to implement these need to be given.

The condition given for the stopping criteria in this procedure is a) maximum number of generations – 50, b) Stall generations – 5, c) Function tolerance of 1e-6.

6.2 Neural network modeling of the objective function

As previously mentioned, the time taken to run the FEMM model is 15 minutes. This makes it difficult to perform the optimization fast and efficient. Therefore, a NN model was used to predict the output of the objective function i.e. Output power of the PMLG system.

Modeling of a neural network was based on Bayesian algorithm for the PMLG system. One of the usual problems with classical neural network modeling is over fitting. Therefore, a regularization technique needs to be used to prevent overfitting. Bayesian regularization is a technique that works better against overfitting. It also allows the usage of a higher number of neurons without overfitting. The detailed procedure of Bayesian regularization is shown in [103].

The main objective of any neural network model is to reduce the sum of squared errors for the target. This is given by the equation (6-5).

$$E = \sum_{i=1}^{n} (t_i - nn_i)^2 \qquad (6\text{-}5)$$

where,

t – Target, and

nn – Neural network response.

Neural network modeling can be done based on supervised and unsupervised learning methods. In the PMLG system, a supervised learning scheme was used. One of the important parameters for having a good neural network model is a good data set. It was seen in chapter 5 that several different parametric studies were performed to analyze different geometric parameters of the PMLG system. The results from this study were used as the training set for the current neural network model. The results from the neural network model are shown below.

The initial parameters for the study are shown below in Table 6-1.

Table 6-1 - Geometric parameters of the PMLG system.

S.No	Part	Dimension
1	Coil Height	18 mm
2	Coil width	28 mm
3	Back Iron Stator	3 mm
4	Lamination stack width	5 mm
5	Magnet radial thickness	2 mm
6	Airgap	2 mm
7	Oscillating frequency	80
8	Number of poles	4
9	Outer Diameter of Magnet	100 mm
10	Number of turns	126
11	Translator spacer width	1 mm
12	Wire gauge	13 AWG
13	Phase	1

14	Stroke length	33 mm
15	Magnetic flux arrangement	Axial

6.2.1 Test Case 1: Neural network for MT and OD

1000 different data points for magnet thickness and outer diameter of the magnet was used as the input data set for NN modeling. The rest of the parameters were kept constant as shown in Table 6-1. The range of the values used are shown below.

- Magnet radial thickness – 0.5 – 10 mm, and
- Outer diameter of the magnet – 25 – 500 mm.

A uniform distribution scheme was used to determine the 1000 data points. These 1000 data points were run in FEMM and the output power produced for the PMLG system for the 1000 data points were saved as the target. The neural network model consists of 10 neurons and a Bayesian regularization algorithm was used to train the neural network. The algorithm was implemented using a MATLAB neural network toolbox. Total dataset was divided into three sets. They are,

1. Training,
2. Validation, and
3. Test.

A training set was given to the neural network and the model was trained to minimize the error. Validation set was used to measure the network generalization and to stop the training when the error reduces below the tolerance. Finally, the testing set was used to look at the performance of the neural network and this testing set was unknown to the neural network model. For this model, 70% of the input dataset was used as the training set, 15% as validation set and 15% as testing set. A neural network model with 10 neurons is shown below in Figure 6-4.

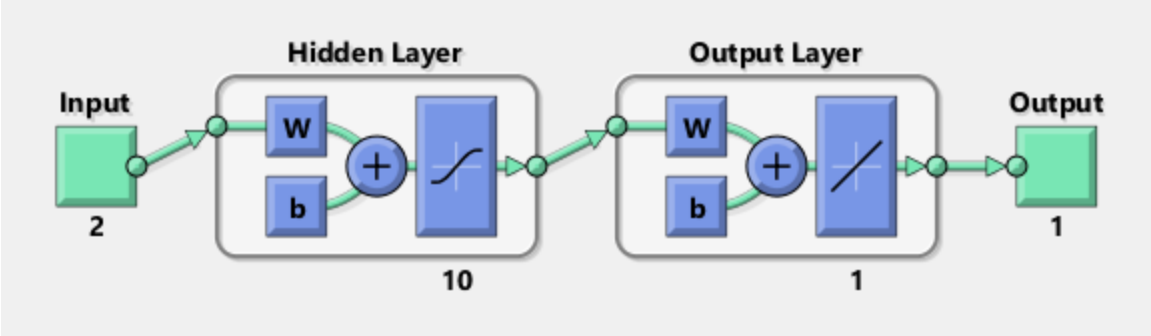

Figure 6-4 – Block diagram of a neural network model.

An error histogram for the model is shown below in Figure 6-5. Figure 6-6 shows the error percentage of each of the data points. It was seen from Figure 6-6 that the error for about 800 data points is about 40 Watts. It was also seen that the error of 10% or more between target and output is about 2% of total 1000 data points and 98% of the data points have an error less than 5%.

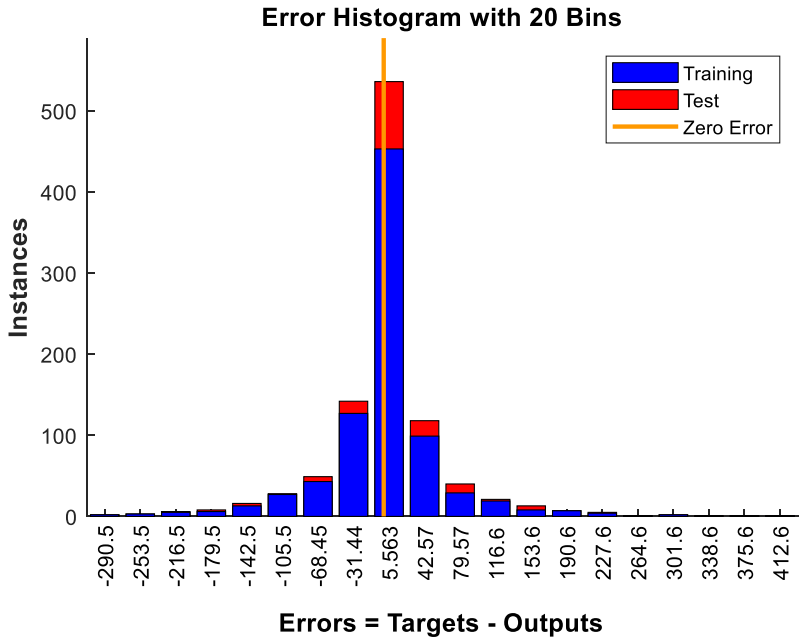

Figure 6-5 - Error histogram for the neural network model.

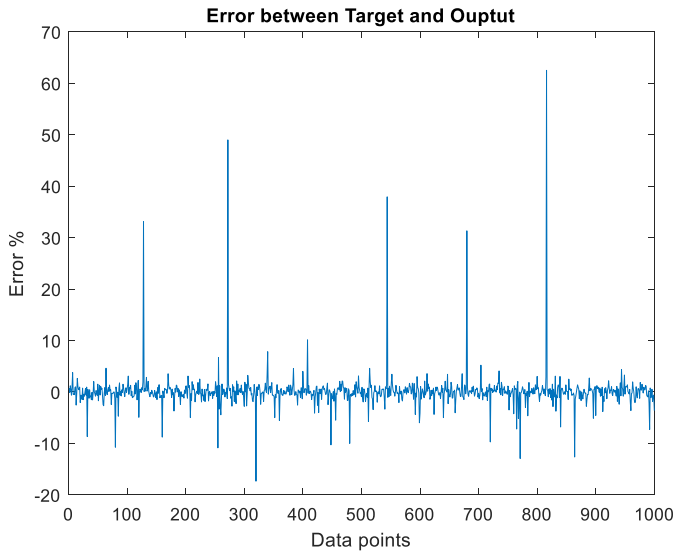

Figure 6-6 - Error percentage between the target and the output for the neural network model.

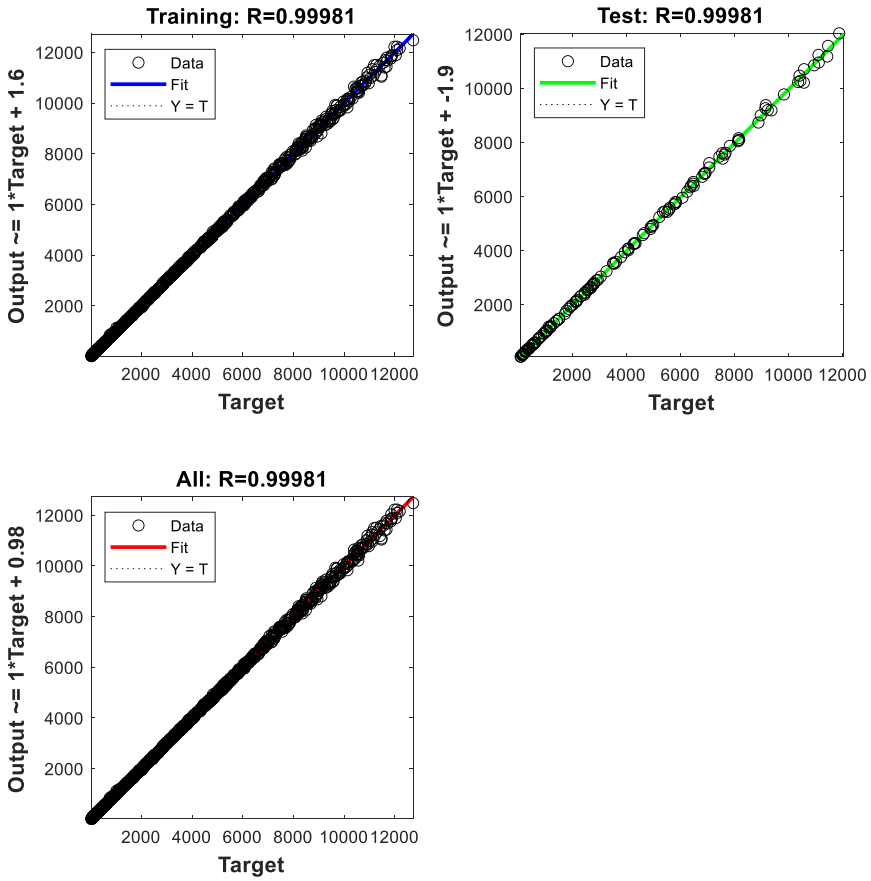

Figure 6-7 - Regression plot of the dataset for the neural network model.

Figure 6-7 shows the linear regression fit between the target and the output. Both for the training and the test data set, the regression fit has an R (correlation) value of 0.999. This shows that the fit is good and neural network can be used for predicting the output power of the PMLG system.

6.2.2 Test Case 2: Neural network for MT, OD and Spacer

Progression to Case 1 was made by adding more input parameters from the parametric study to the neural network. When more input parameters are added to the neural network care must be taken while training the data set. Case 2 consists of 1000 data points for MT, OD and spacer keeping the rest of the parameters the same as in Table 6-1.

While training the neural network, the number of neurons plays an important role in determining the accuracy of the neural network. This was shown in Figure 6-8, Figure 6-9, Figure 6-10, and Figure 6-11. As the number of neurons increases, the error percentage between the target and the output decreases. This will increase the prediction accuracy of the model. Comparison of Figure 6-8, Figure 6-9, Figure 6-10 and Figure 6-11 shows that with an increase in neurons, the errors decrease for the PMLG system.

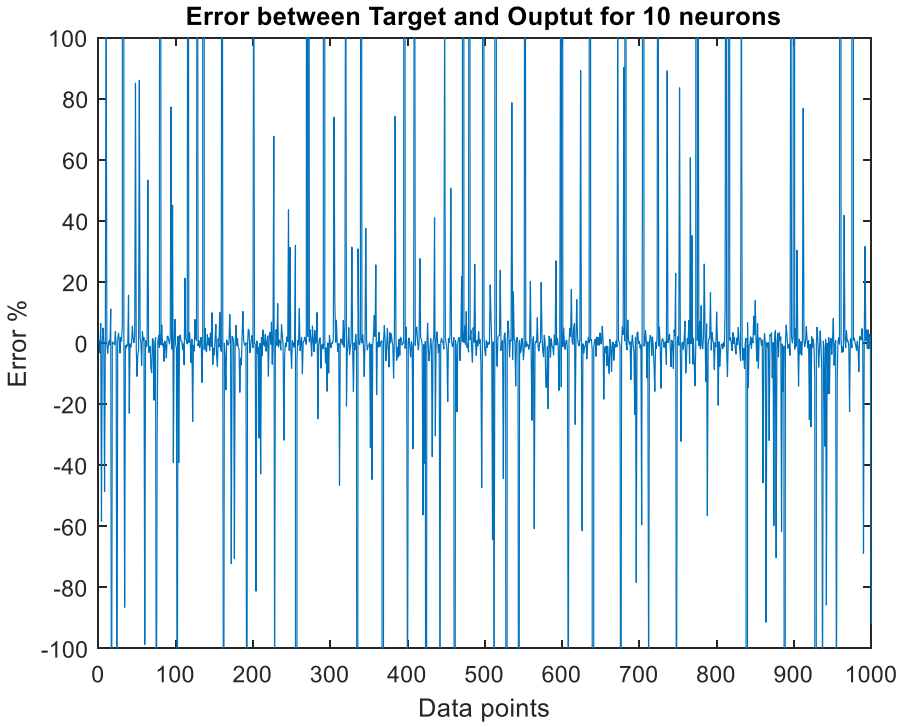

Figure 6-8 - Error percentage for 10 neurons in the neural network model.

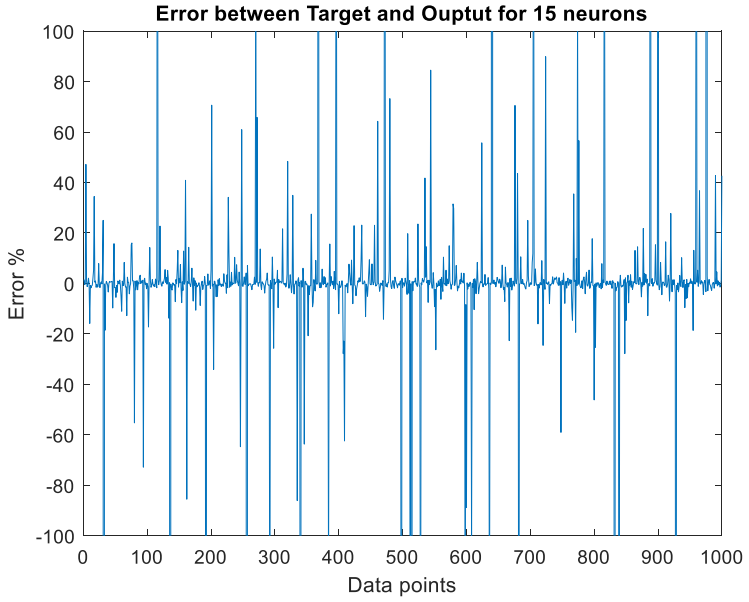

Figure 6-9 - Error percentage for 15 neurons in the neural network model.

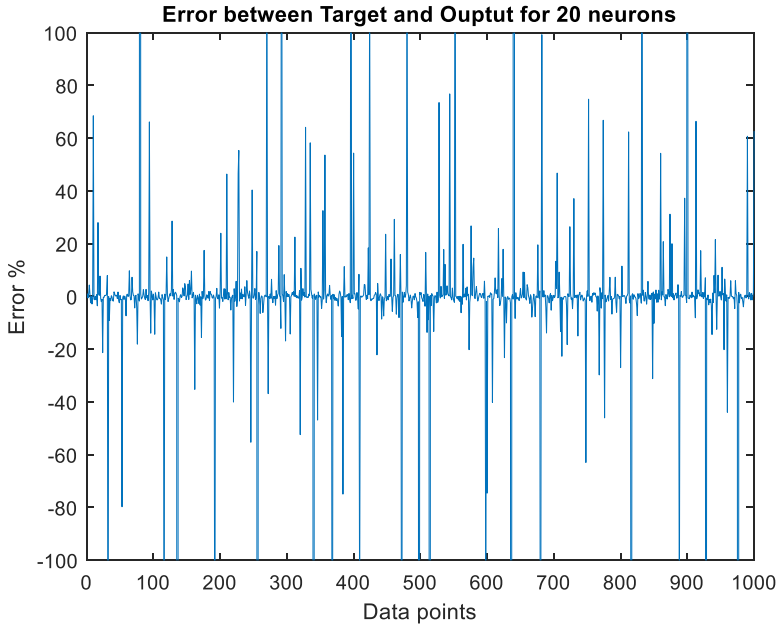

Figure 6-10 - Error percentage for 20 neurons in the neural network model.

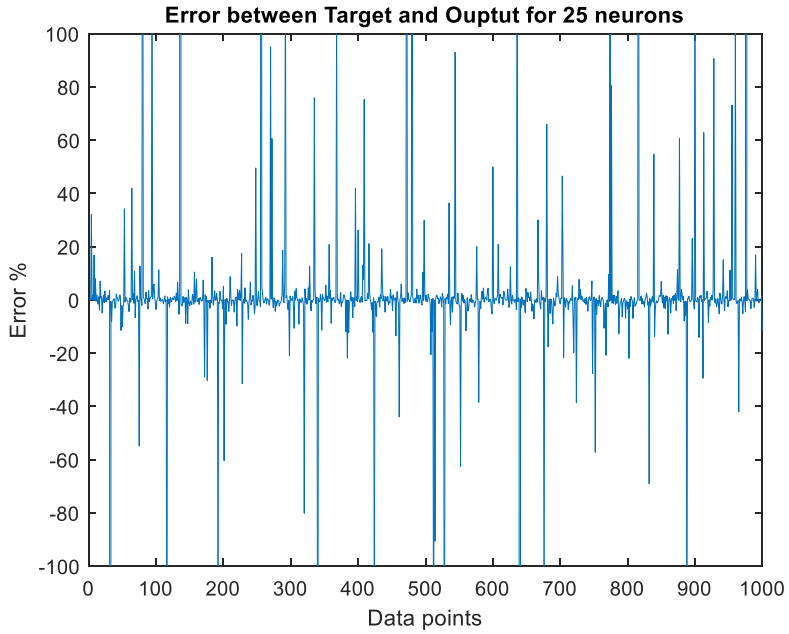

Figure 6-11 - Error percentage for 25 neurons in the neural network model.

When 10 neurons were used, there were 208 data points (20.8%) which had an error percentage greater than 10 as shown in Figure 6-8. When 15 neurons were used, there were 122 data points (12.2%) which had an error percentage greater than 10 shown in Figure 6-9. When 20 neurons were used, there were 118 data points (11.8%) which have an error percentage greater than 10 as shown in Figure 6-10 and when 25 neurons were used, there was 98 data points (9.8%) which have an error percentage greater than 10 in Figure 6-11.

Table 6-2 - Neurons vs error percentages for the data points.

Neurons	Error > 10%	Error > 20%	Error > 30%	Error > 40%	Error > 50%
10	20.8	14.4	11.5	10	8.7
15	12.2	9.2	6.9	5.9	4.9
20	11.8	7.9	5.6	4.2	3.7
25	9.8	5.9	4.8	4.1	2.8

To determine the number of neurons for the NN model, a genetic algorithm was run to minimize the error percentages function. The results from the minimized error function are shown below in Figure 6-12. The number of neurons required to reduce the error was 97. Although this number of neurons might seem huge, since the time to train the neural network model was less than 5 minutes. Therefore, this parameter was used to train the PMLG neural network model. The final prediction accuracy of the neural network model was 92% for errors less than 10%. The actual error percentage of the neural network model is shown in Figure 6-13. It was seen that 80 data points have an error greater than 10% error.

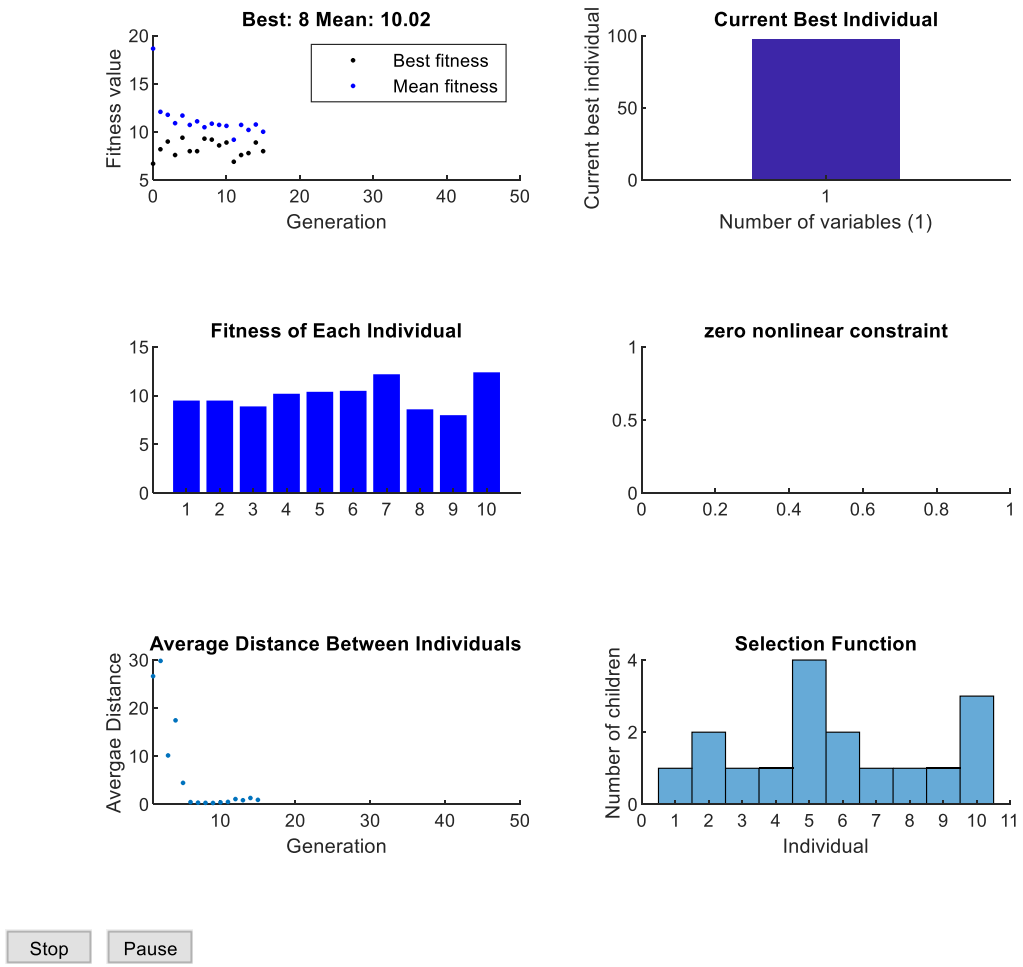

Figure 6-12 - Genetic algorithm to determine the neuron for the PMLG NN – Case 2.

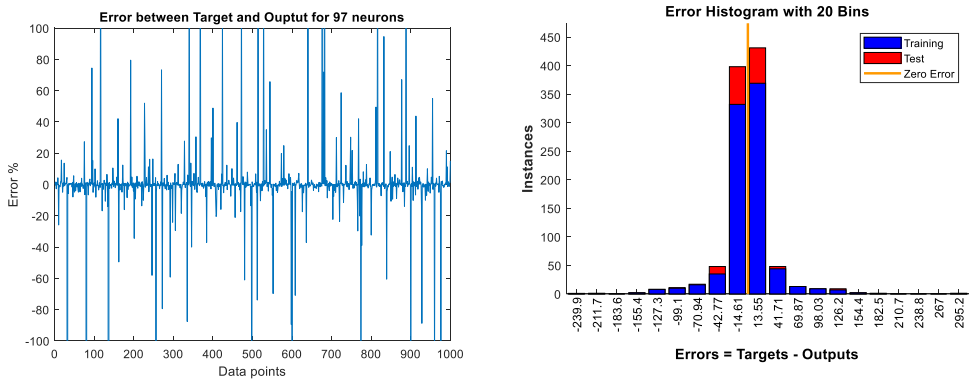

Figure 6-13 - Error percentage and Error histogram for the PMLG NN – Case 2.

6.2.3 Test Case 3: Neural network for MT, OD, Spacer, Poles, Turns and Stroke

Test case 3 consists of 6 parameters - MT, OD, Spacer, Poles, Turns, and Stroke. 1000 data points were chosen and the parameters which produced output power greater than 250W were finally used for the NN training. Finally, 653 data points were sent to the neural network model.

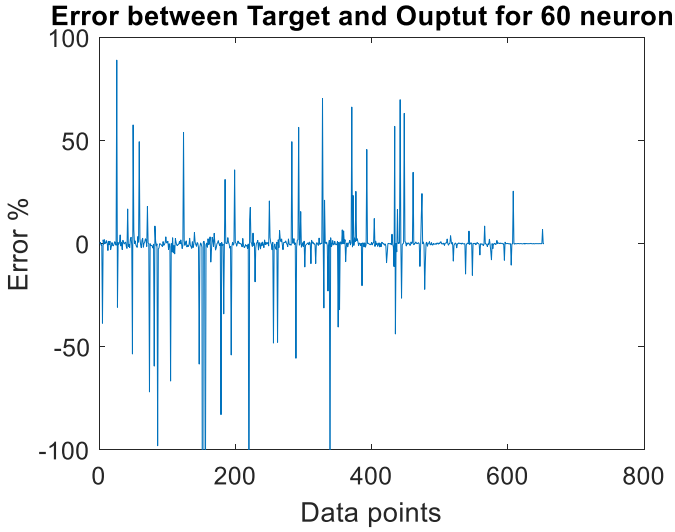

Figure 6-14 - Error percentage for the PMLG NN – Case 3.

It was seen that about 90% of the data points have less than 10% error, whereas 3.4% of the data points have more than 50% error. This objective function acts as a black box

to predict the output power given different values of input parameters (MT, OD, spacer, poles, turns and stroke length).

To implement an objective function for the main Genetic algorithm in MATLAB, the following steps were performed.

1. Load the developed PMLG NN model to MATLAB workspace
2. Use the biases for the parameters such as poles, frequency and stroke length into the model to predict the output power for the 6 variables.
3. Use the SIM function in MATLAB to run the NN model and predict the output

Detailed code on the NN model and implementation is added to the appendix.

6.3 Single objective Optimization of the PMLG system

With the PMLG NN model available, the next step was to perform optimization as shown in the flowchart in Figure 6-1. The initial input parameters chosen for the optimization are shown in Table 6-1.

Three cases of the study were performed for optimizing the moving mass of the translator. The first case involves three input variables to optimize the moving mass of the translator. The second case involves five input variables to optimize the moving mass of the translator. The third case involves six input variables to optimize the moving mass of the translator. Airgap and frequency of operation were not chosen as input variables for optimization. The airgap of the PMLG system depends on the manufacturing capability of the PMLG. Therefore, two different airgap conditions were chosen for optimization – 1 mm and 1.5 mm. If airgap was chosen as an optimization variable, the optimization routine will go towards the lower bound of the airgap as this would provide the least reluctance path and therefore higher flux density in the system. Similarly, higher the frequency, the higher will be the rate of change of flux and higher open circuit voltage. Therefore, frequency was not chosen as an optimization variable.

6.3.1 Case 1: MT, OD and Spacer

Input variables used for Case 1 were Magnet thickness, Outer diameter of the magnet and spacer (3 variables). Airgap of the system was chosen to be 1 mm. The bounds chosen for the optimization variables were shown in Table 6-3.

Table 6-3 - Bounds for the optimization input variables – Case 1.

Parameter	Lower bound	Upper bound
Magnet radial thickness (MT)	2 mm	10 mm
OD	25 mm	500 mm
Translator spacer width	1 mm	10 mm

The result of the optimization for Case 1 is shown below in Table 6-4.

Table 6-4 - Optimization results for Case 1 – 1 mm Airgap.

Rated Power (W)	Mass (kg)	W / kg	Magnet thickness (mm)	Diameter (mm)	Spacer (mm)
500	0.6	833.3	10	25.4	1.6
1000	0.8	1250	10	30	4.2
1500	1.5	1071	10	45.1	5.9
2000	2.1	1111	10	62.2	6.2

The results from Table 6-4 provide us information on the design parameters (MT, OD and spacer) that needs to be used for achieving 0.5 – 2 kW PMLG system. It was seen that the upper bound chosen for the magnet thickness was 10 mm and the optimization routine moved the MT towards its upper bound for all the power conditions. The reason for this can be deduced from the parametric analysis done in Chapter 5. It was seen that the magnet thickness has a higher effect on the moving mass compared to the outer diameter and spacer. This is validated through the optimization results where MT moves towards its maximum followed by OD and spacer. To validate the results obtained from the optimization, FEMM was used to compute the results. The electrical parameters of the linear generator obtained from the optimized PMLG system are shown in Table 6-5.

Table 6-5 - FEMM results for the optimized input variables in Table 6-4.

Rated Power (W)	Max Power (W)	OC voltage	Load voltage	Current	Efficiency
500	1178	87	81.9	6.1	93
1000	1510	105.6	93.2	10.8	90.4
1500	2325	162	144	10.3	91.7
2000	3190	223.7	201	9.9	92.3

The optimization results produce results comparable to FEMM for an efficiency of 90% or more. Therefore, the optimized input variables can be used for designing the PMLG system.

Results for 1 kW machine optimized for an airgap of 1 mm is shown below in Figure 6-15 and Figure 6-16.

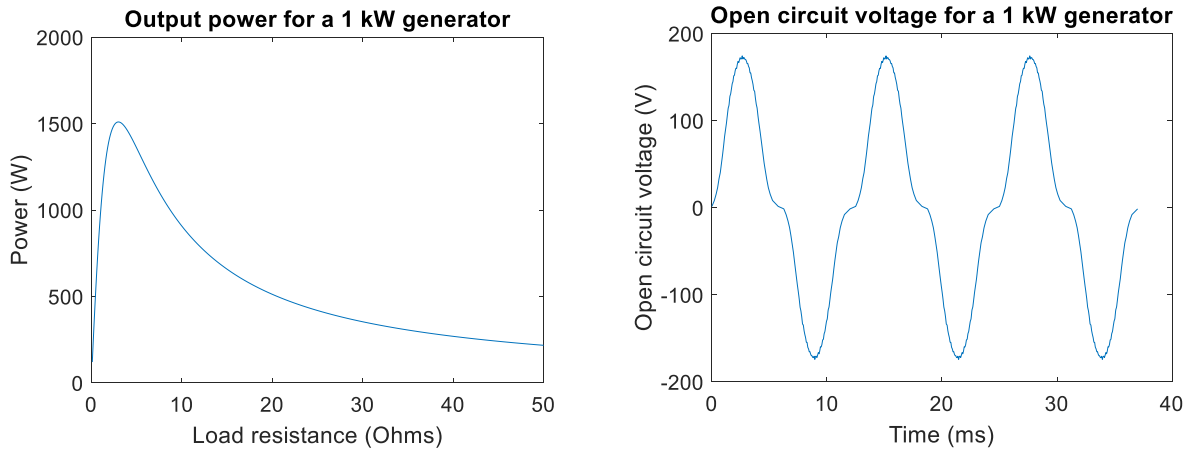

Figure 6-15 - Output power and Open circuit voltage for Case 1 – 1000W.

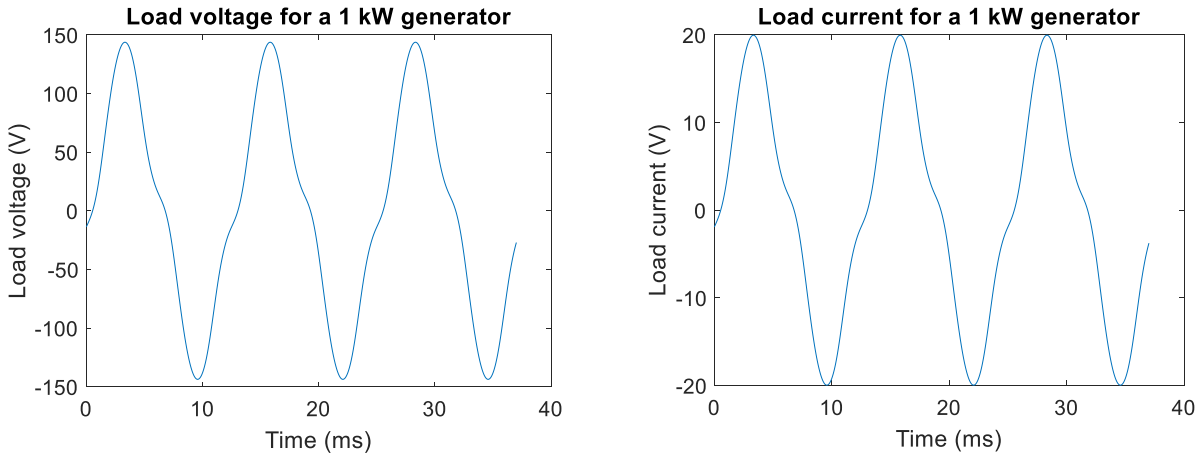

Figure 6-16 - Load voltage and load current for Case 1 – 1000W.

Similarly, optimization was done for an airgap of 1.5 mm and the results of the optimization are shown below in Table 6-6.

Table 6-6 - Optimization results for Case 1 – 1.5 mm Airgap.

Power (W)	Mass (kg)	W / kg	Magnet thickness (mm)	Diameter (mm)	Spacer (mm)
500	0.8	625	10	30	4.2
1000	1.8	555	10	57	8.3
1500	2.6	578	10	79.7	8
2000	3.3	689	10	98.5	7.3

Figure 6-17 shows the optimization results obtained over five generations for an airgap of 1 mm at 1 kW.

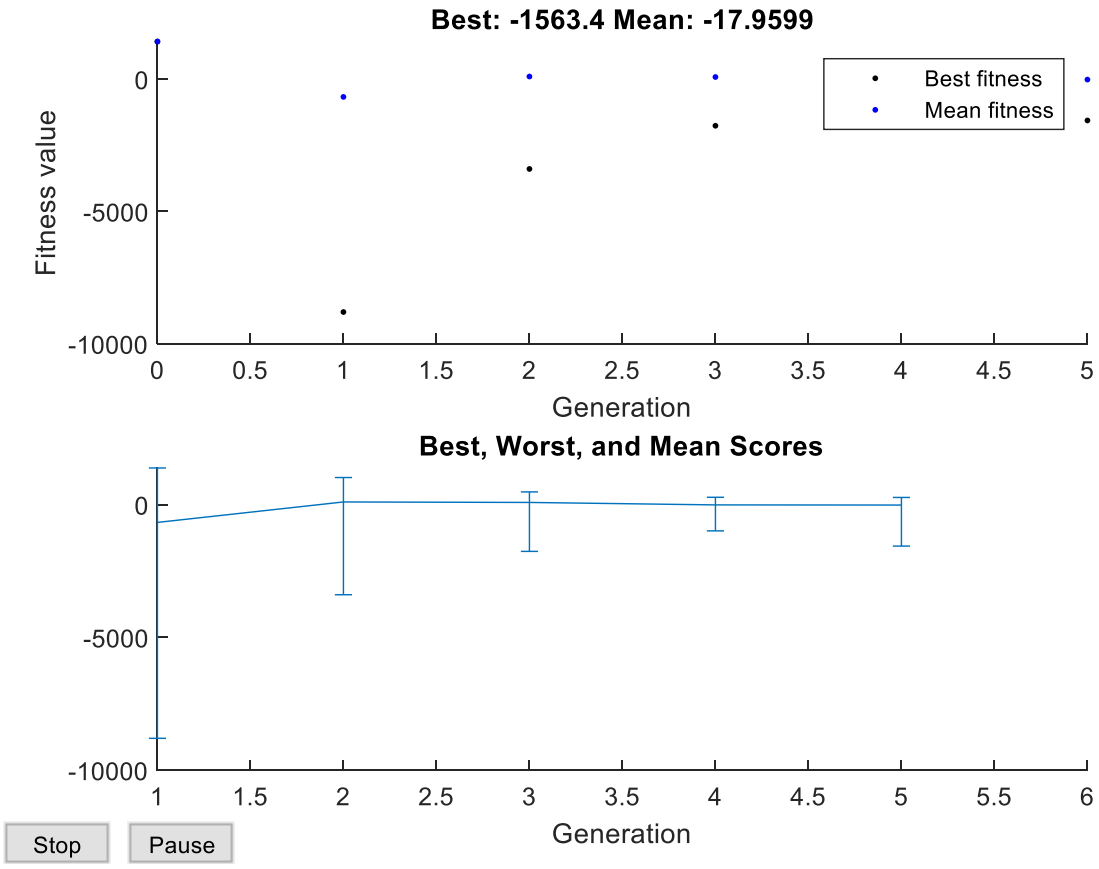

Figure 6-17 - Optimization results from MATLAB GA for best fitness value and scores in for each generation for a mass of 0.8 kg and 1 kW PMLG system at 1 mm air-gap.

Table 6-7 - Genetic algorithm generation results for Case 1 – 1 mm Airgap.

Generation	Func-count	Best f(x)	Max Constraint	Stall Generations
1	338	846.6	0	0
2	626	472.18	0	0
3	914	56.52	0	0
4	1202	-10.9	0.000079	0
5	1490	-16.85	0.0008135	0

From Table 6-7, the constraint tolerances increase beyond the maximum tolerance limit in the GA and therefore, the optimization routine stopped. Furthermore, 1490 functions

were evaluated with constraints on the moving mass of the translator. Of these 1490 functions, most of the functions which weren't following the constraints were removed from the actual results by MATLAB. Some of the functions were evaluated even though the constraints were not satisfied. This is shown by the max constraint column in Table 6-7. In Figure 6-17, the best function shows a value of -1563.4 and this value translates to 2563 W of output power from the PMLG system. From Table 6-4, the maximum output power / moving mass was 1000 W at 0.8 kg whereas Figure 6-17 shows the best output power of 2.563 kW at 0.8 kg. The reason for that is because, the best output power shown in Figure 6-17 corresponds to a condition when the constraints were not satisfied and therefore the best output cannot be used.

The FEMM results of the optimization for 1.5 mm airgap are shown below in Table 5.

Table 6-8 - FEMM results for the optimized parameters in Table 6-6.

Power (W)	Max Power (W)	OC voltage	Load voltage	Current	Efficiency
500	1351	102.6	97.7	5.2	93.9
1000	2440	190	180.7	5.6	94
1500	3351	267	243.2	8.3	91.4
2000	4388	334	315	6.4	94

The optimization routine was able to come up with options for different power outputs of 500 W, 1000 W, 1500 W and 2000W. Power / moving mass (P/M) ratio of about 800 – 1100W/kg was achieved with a 1 mm airgap and about 500 – 690 W/kg was achieved with a 1.5 mm airgap. Once a base value of the input variables is known, further modifications to the design can be done to tailor it according to the designer's requirements. Furthermore, it was seen that there is no compensation added to reduce the effect of the inductance in the PMLG system. To further improve the output power, efficiency and W/kg, capacitors can be added to compensate the reactive power of the inductances for the PMLG. Details on the compensation of the inductance using capacitors have been discussed in Chapter 4. FEMM results obtained in Table 6-8 agrees with the input variables optimized for 1.5 mm. The efficiency of the system was also above 90%.

Furthermore, with the optimized results, off the shelf magnets can be chosen with parameters closer to the optimized value to reduce the manufacturing costs. If further improvement is required in the model to reduce the moving mass of the translator, additional variables need to be added to the optimization routine. This is discussed in Case 2 and Case 3.

6.3.2 Case 2: MT, OD, Spacer, Poles and Stroke

Optimization was done for 5 variables – Magnet thickness, Outer diameter of the magnet, spacer, poles, and stroke. Airgap of the system was chosen to be 1 mm. The upper and lower bounds of the optimization parameters are shown in Table 6-9. The results of the optimization are shown below in Table 6-10.

Table 6-9 - Bounds for the optimization parameters – Case 2.

Parameter	Lower bound	Upper bound
Magnet radial thickness	1 mm	10 mm
OD	25 mm	500 mm
Translator spacer width	1 mm	10 mm
Number of poles	2	10
Stroke length	20 mm	50 mm

Table 6-10 - Optimization results for Case 2 – 1 mm Airgap.

Power (W)	Mass (kg)	W / kg	Magnet thickness (mm)	Diameter (mm)	Spacer (mm)	Poles	Stroke (mm)
500	0.55	833	10	25.2	9	10	21.3
1000	0.8	1250	10	25	9	10	25.7
1500	1.15	1363	10	26	7	10	33
2000	1.4	1333	10	25	4	10	40

The results from Table 6-10 are similar to the results in Table 6-4 in Case 1. From Table 6-10, magnet thickness moves towards its upper bound of 10 mm. Furthermore, in comparison with Case 1, the P/M ratio was higher in Case 2. This can be attributed to the additional flexibility in the number of optimization input variables. The ability to vary the poles and stroke aided in the improvement of the P/M ratio. Furthermore, the poles have

a major effect in the improvement of the P/M ratio as can be seen in the output power as it reached its upper bound of 10. Results obtained from FEMM for the input variables in Table 6-10 is shown below in Table 6-11.

Table 6-11 - FEMM results for the optimized parameters in Table 6-10.

Power (W)	Max Power (W)	OC voltage	Load voltage	Current	Efficiency
500	620	114	94.3	5.3	90
1000	1070	130	117	10.3	87
1500	2637	186	168	9	91
2000	3950	187.8	171	11.6	90.9

From Table 6-11, it was seen that the results are agreeable with the expected output power from Table 6-10 for the optimized power output. Furthermore, the efficiencies are also close to or above 90%.

Electrical parameters for a 1 kW machine optimized for an airgap of 1 mm is shown below in Figure 6-18 and Figure 6-19.

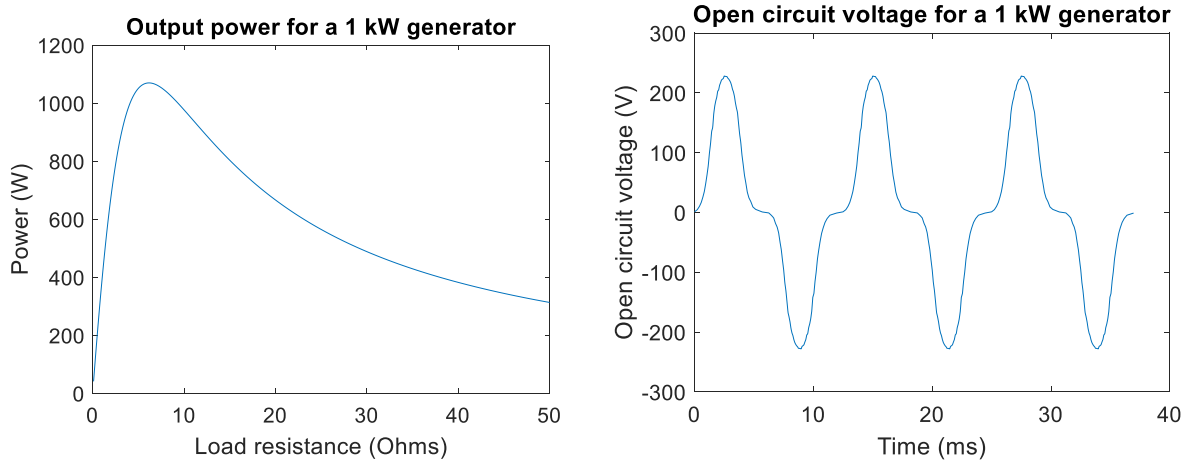

Figure 6-18 - Output power and Open circuit voltage for Case 2 – 1000W.

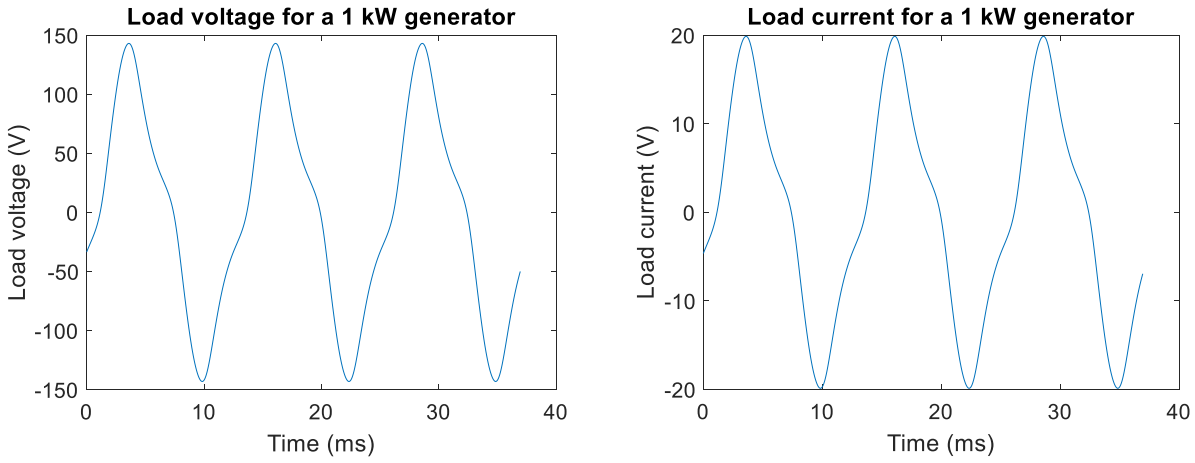

Figure 6-19 - Load voltage and load current for Case 2 – 1000W.

Like Table 6-10, optimization was done with an airgap of 1.5 mm and the results are shown below.

Table 6-12 - Optimization results for Case 2 – 1.5 mm Airgap.

Power (W)	Mass (kg)	W / kg	Magnet radial thickness (mm)	Diameter (mm)	Translator spacer width (mm)	Poles	Stroke (mm)
500	0.8	625	10	25	3.4	5	39
1000	1.2	833	10	25	5.1	10	33
1500	1.6	937	10	26	3.8	10	42
2000	2.5	800	10	29	3	10	45

The results obtained from FEMM from Table 6-12 are shown below.

Table 6-13 - FEMM results for the optimized parameters in Table 6-12.

Power (W)	Max Power (W)	OC voltage	Load voltage	Current	Efficiency
500	1670	97.1	93.1	5.4	93
1000	2385	176	165	6	93
1500	3526	178	166	9	91.8
2000	5500	227.8	215.1	9.1	92.6

The results obtained from Case 2 are better in terms of P/M ratio compared to Case 1. Power density above 1200 W/kg can be obtained by modifying five variables instead of only three as in Case 1 for an airgap of 1 mm.

6.3.3 Case 3: MT, OD, Spacer, Poles, Stroke, and Turns

The NN model created in the earlier section for the optimization variables – Magnet thickness, Outer diameter of the magnet, spacer, poles, turns and stroke was used to perform the optimization of the PLMG system. Airgap of the system was chosen to be 1 mm. The upper and lower bounds of the optimization parameters are shown in Table 6-14. The results of the optimization are shown below in Table 6-15.

Table 6-14 - Bounds for the optimization parameters – Case 3.

Parameter	Lower bound	Upper bound
Magnet radial thickness	1 mm	10 mm
OD	25 mm	500 mm
Translator spacer width	1 mm	10 mm
Number of poles	2	10
Stroke length	20 mm	50 mm
Number of turns	20	500

Table 6-15 - Optimization results for Case 3 – 1 mm Airgap.

Power (W)	Mass (kg)	W / kg	Magnet radial thickness (mm)	Diameter (mm)	Translator spacer width (mm)	Poles	Stroke (mm)	Turns
500	0.4	1250	10	25	2	2	38	222
1000	0.7	1428	10	25	4	5	35	200
1500	0.9	1666	10	25	5	7	34	176
2000	1.2	1666	10	25	2.5	6	48	186

The results from Table 6-15 were similar to the results in Table 6-4 and Table 6-10 in Case 1 and Case 2. From Table 6-15, magnet thickness moves towards its upper bound

of 10 mm. Furthermore, in comparison with Case 1 and Case 2, the P/M ratio is higher in Case 3 compared to Case 1 and Case 2. This can be attributed to the additional flexibility in the number of input variables with the addition of turns which does not increase the moving mass of the translator. The ability to vary the poles and stroke also aided in the improvement of the P/M ratio with respect to Case 1 & 2. Results obtained from FEMM for the parameters in Table 6-15 is shown below in Table 6-16.

Table 6-16 - FEMM results for the optimized parameters in Table 6-15.

Power (W)	Max Power (W)	OC voltage	Load voltage	Current	Efficiency
500	611	90.2	76.1	6.6	91
1000	1186	145	120	8.35	90
1500	1650	186	146.5	10.2	89
2000	3002	175	153.3	13	89

Similar to Table 6-15 and Table 6-16, the results for an airgap of 1.5 mm are shown below in Table 6-17 and Table 6-18.

Table 6-17 - Optimization results for Case 3 – 1.5 mm Airgap.

Power (W)	**Mass (kg)**	**W / kg**	**Magnet radial thickness (mm)**	**Diameter (mm)**	**Translator spacer width (mm)**	**Poles**	**Stroke (mm)**	**Turns**
500	0.5	1000	10	25	4	4	31	211
1000	0.7	1428	10	25	5	6	32	192
1500	1	1500	10	25	5	6	42	192
2000	1.3	1538	10	25	4	7	48	180

Table 6-18 - FEMM results for the optimized parameters in Table 6-17.

Power (W)	**Max Power (W)**	**OC voltage**	**Load voltage**	**Current**	**Efficiency**
500	600	123	103.2	4.9	91.7
1000	1043	167.2	125.6	8	89
1500	2000	177	152.2	9.9	90
2000	3299	195	174.6	11.35	90.7

Of the three cases, Case 3 provides a solution with high power density and lower moving mass. Maximum Power / moving mass ratio of 1666 was achieved with Case 3 compared to 1110 and 1300 for Case 1 and Case 2 respectively. Therefore, once a design with the moving mass or Power / moving mass requirement is known, optimization can be done to determine the maximum output power.

6.4 Multi-objective optimization (MOO)

In the previous section, optimization was done to only lower the moving mass of the translator. In this study, a multi-objective optimization with 3, 5 and 6 variables were performed to design a suitable PMLG system given a moving mass or power output. Besides, another optimization routine was performed to understand the effect of the volume of the system with respect to the output power of the PMLG system.

Multi-objective optimization is also known as Pareto optimization or multi-criteria optimization. The multi-objective optimization involves optimization with more than one objective function. For non-trivial optimization problems, only one solution will not exist for the problem. In that case, several Pareto solutions will be available for a multi-objective optimization problem. A trade-off has to be made between the competing objective functions. A generic MOO problem follows the equations shown below.

$$min/\max\ f_m(x),\quad m = 1, 2, \dots, M \tag{6-6}$$

$$subject\ to\ g_j(x) \trianglerighteq 0, j = 1, 2, \dots, J \tag{6-7}$$

$$x_{lb} \trianglelefteq x_i \trianglelefteq x_{ub}, i = 1, 2, \dots, n \tag{6-8}$$

In a single objective optimization problem, the superiority of a solution over another solution is determined by comparing the objective function values, whereas in a MOO problem, dominance of one objective function over the other could be found. This is called as dominance. If there is a non- dominated solution, it leads to a decision space called as Pareto optimal set. A general goal in MOO problem is to determine the sets of solution close to a pareto-optimal set. Also, the set needs to cover a wide space as possible to provide different options of solution for the problem.

There are different algorithms to solve this optimization problem. The classical method to solve the MOO problem is the weighted sum method [104]. This algorithm combines the multiple objective functions by pre-multiplying a user-defined weight to the result of the individual objective function. The weight of an objective function is determined based on the importance of the objective. The advantage of this method is the simplicity. The problems with this method are the user-supplied weights for the objective functions. Depending on the mass, the optimal solution might cover our desired space. Also, it might be difficult to obtain a Pareto-optimal solution. Another method to solve the problem is to use a genetic algorithm similar to the single objective function problem. Classical optimization algorithms operate on a single candidate solution. Genetic algorithm operated on a set of candidate solutions. A detailed algorithm of the multi objective genetic algorithm is shown in [105]. To implement the algorithm, MATLAB's inbuilt multi objective genetic algorithm has been used for this study. The algorithm implemented in MATLAB is a controlled elitist genetic algorithm which is a variant of NSGA – II [106]. An elitist GA favors only the individuals with the highest rank. But a controlled elitist algorithm gives importance to the diversity of the individuals in addition to the individual with the highest rank. To achieve an optimal Pareto solution, the diversity of the individuals is important. The appendix section gives details on the functions and implementation of the code for this study.

The goal of the MOO study is as follows:

- Test the MOO problem with different number of input variables, and
- Validate the MOO problem results with FEMM.

Three cases were studied for the MOO problem set. They are,

1. MOO with 3 variables – MT, OD, and Spacer,
2. MOO with 5 variables – MT, OD, Spacer, Poles and Stroke length, and
3. MOO with 6 variables – MT, OD, Spacer, Poles, Stroke length and Turns.

6.4.1 Case 1 - 3 Variables – MT, OD and Spacer

The initial parameters for the PMLG were same as in Table 6-1. The three variables used for optimization were magnet thickness, outer diameter of the magnet and spacer. The goal of this optimization was to determine the values of the three parameters which will solve the multi-objective problem with the two objective functions – Output power and moving mass of the translator. Two airgap - 1 and 1.5 mm were chosen. Optimization was done to determine the Pareto optimal solution in the moving mass range below 2 kg. A constraint was used so that to keep the moving mass below 2 kg so that the best possible solutions within this range can be found. Figure 6-21 shows the Pareto optimal objective function results for the output power and moving mass.

From Figure 6-20 and Figure 6-21, the Pareto optimal set for the output power and the moving mass was determined for the PMLG system. This helps us in deciding the parameters of the PMLG for a wide range of power output from 500 W to 2000 W. Figure 6-22 shows the Power /Moving mass ratio of the Pareto optimal set. It was seen that the power /moving mass (P/M) ratio greater than 1 kW/kg was achieved for 1 mm airgap and about 0.5 – 0.6 kW/kg for 1.5 mm airgap system.

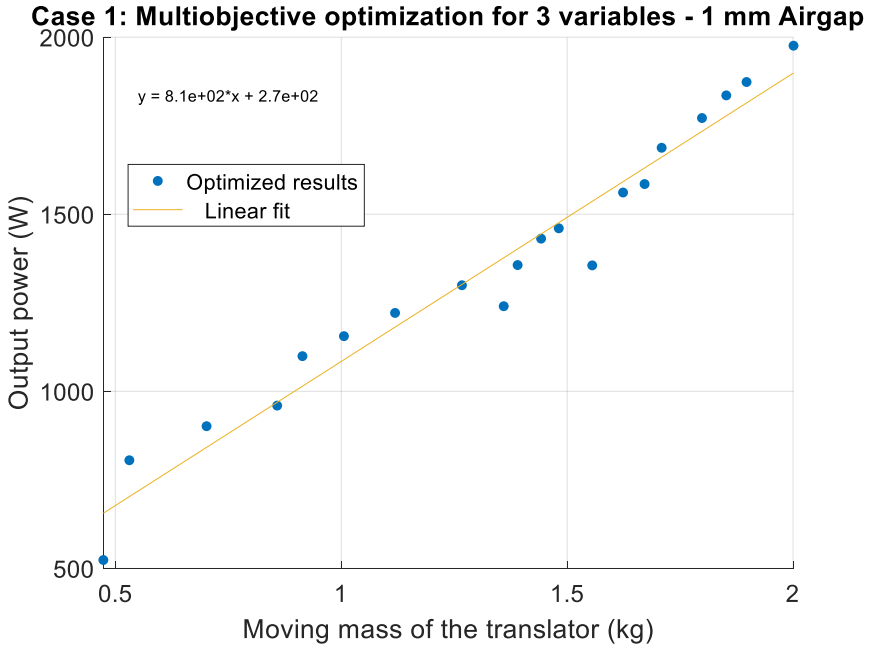

Figure 6-20 - Case 1 - Pareto optimal set for 1 mm airgap.

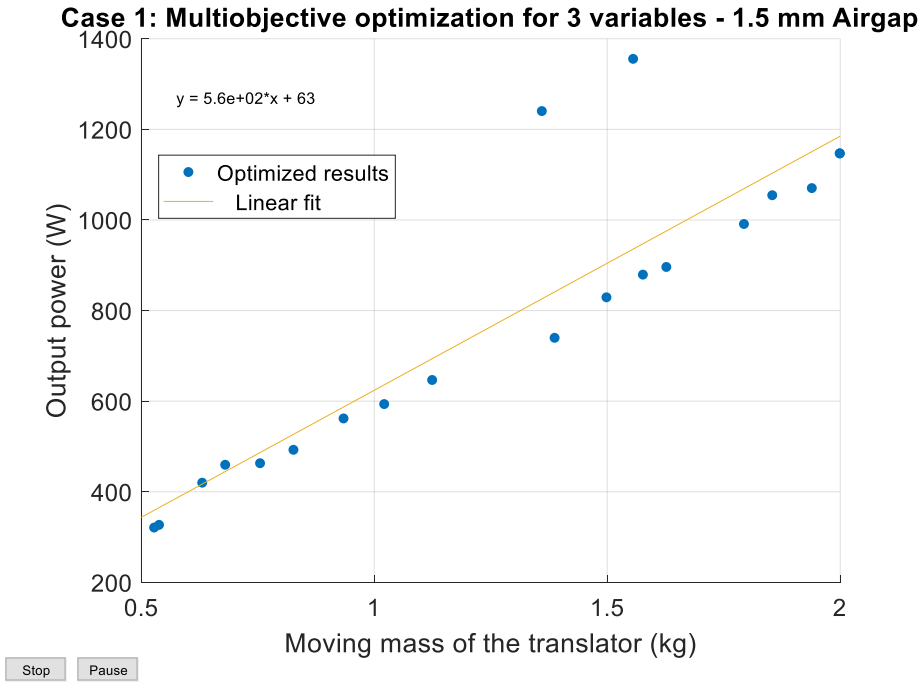

Figure 6-21 - Case 1 - Pareto optimal set for 1.5 mm airgap.

Pareto optimal set equations for 1 mm and 1.5 mm airgap are shown below.

$P = 810 * M + 270$ for 1 mm airgap (6-9)

$P = 560 * M + 63$ for 1.5 mm airgap (6-10)

where

P – Output power and

M – Moving mass of the translator.

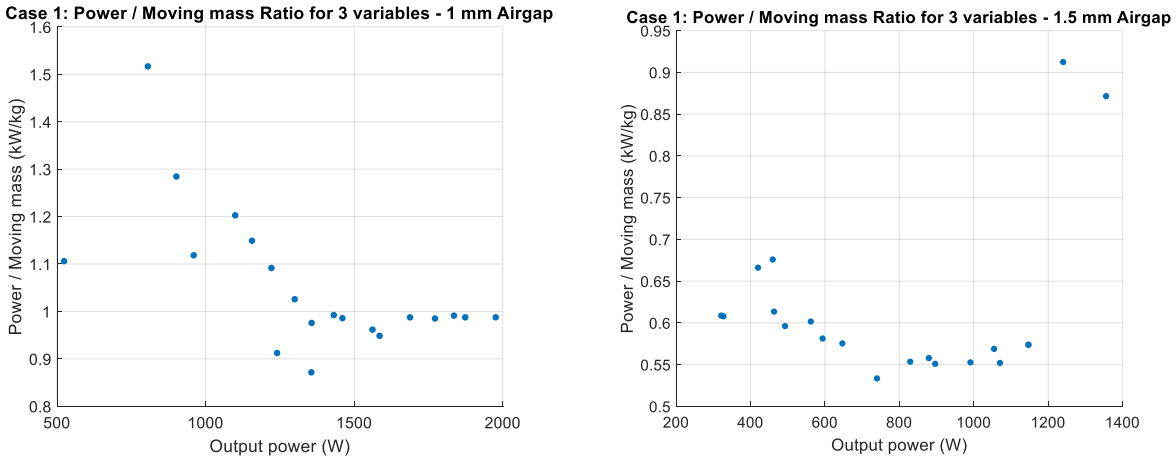

Figure 6-22 - Case 1 - Power/Moving mass ratio for 1 mm and 1.5 mm airgap.

From Table 6-19, it was seen that as the moving mass increases, the output power increases. Interesting to note that, the magnet thickness variable was close to 10 mm. From the previous study in Chapter 5 and the optimizations done for single objective function in the previous section, it was seen that magnet thickness has a major effect on the output power of the PMLG system. Therefore, the optimization algorithm was moving the magnet towards the upper bound but keeping the mass constraints below 2 kg. This resulted in the magnet thickness of all the values being close to 10 mm. OD was increased as OD is directly proportional to the output power and spacer is inversely proportional to the output power. Therefore, the optimization algorithm worked in varying the OD and the spacer to achieve the maximum output power because the rest of the variables were kept constant. The input variables of the optimized Pareto set are shown in Table 6-19.

Table 6-19 - Case 1 - Input variable from the optimization for 1 mm airgap.

S.No	MT (mm)	OD (mm)	Spacer (mm)	Power (W)	Mass
1	9.80	25.25	9.26	523.68	0.47
2	10.00	25.19	5.46	805.37	0.53
3	9.84	28.67	5.39	901.57	0.70
4	9.45	30.73	3.65	959.72	0.86
5	9.99	31.52	3.00	1099.33	0.91
6	9.99	32.79	2.51	1155.79	1.01
7	10.00	34.26	1.93	1221.39	1.12
8	10.00	36.07	1.26	1299.61	1.27

9	9.90	39.43	3.54	1240.37	1.36
10	9.77	42.33	5.66	1356.57	1.39
11	9.91	43.14	5.29	1431.21	1.44
12	9.89	44.92	5.96	1460.30	1.48
13	9.59	48.26	6.47	1355.63	1.56
14	9.62	49.21	5.66	1561.38	1.62
15	9.54	51.85	6.54	1585.29	1.67
16	9.90	50.33	5.21	1687.77	1.71
17	9.95	54.43	6.61	1771.70	1.80
18	9.98	54.32	5.47	1835.66	1.85
19	9.94	56.24	5.91	1873.42	1.90
20	10.00	60.42	6.92	1976.02	2.00

6.4.2 Case 2 - 5 Variables – MT, OD, Spacer, Poles, and Stroke

Five variables chosen for the optimization are magnet thickness, outer diameter of the magnet, spacer, poles, and stroke. The goal of this optimization was to determine the values of the five input variables which will solve the multi-objective problem with the two objective functions – Output power and moving mass of the translator. Two airgap - 1 and 1.5 mm were chosen similar to Case 1. Optimization was done to determine the Pareto optimal solution in the moving mass range below 2 kg. Similar to Case 1, Pareto optimal set for the optimization as well as the optimized input parameters are shown below in Figure 6-23, Figure 6-24 , and Figure 6-25.

Pareto optimal set equations for 1 mm and 1.5 mm airgap are shown below.

$P = 2000 * M - 900$ – 1 mm airgap (6-11)

$P = 1300 * M - 650$ – 1.5 mm airgap (6-12)

For M > 0.5

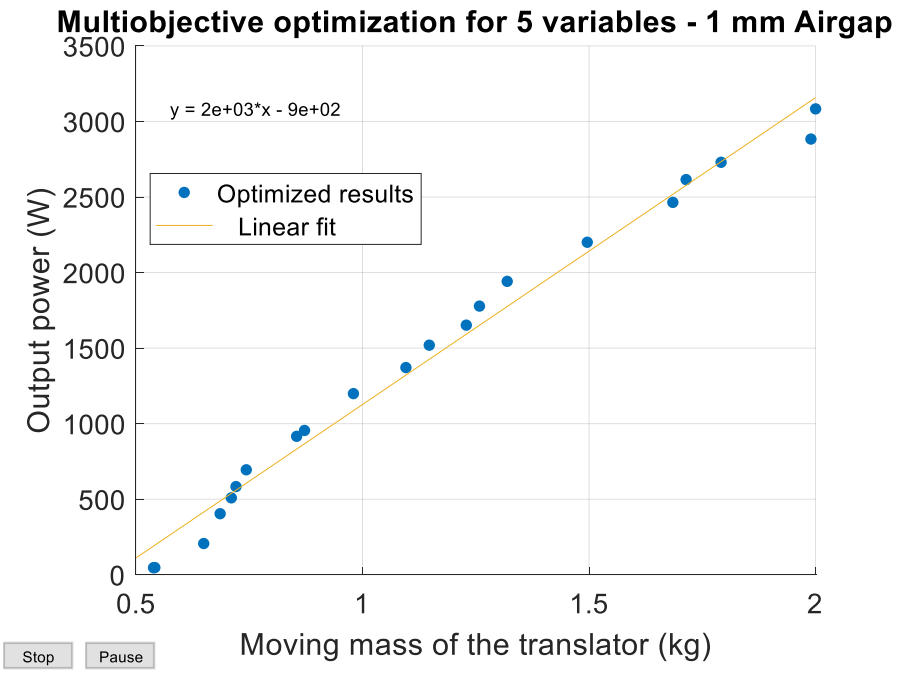

Figure 6-23 - Case 2 - Pareto optimal set for 1 mm airgap.

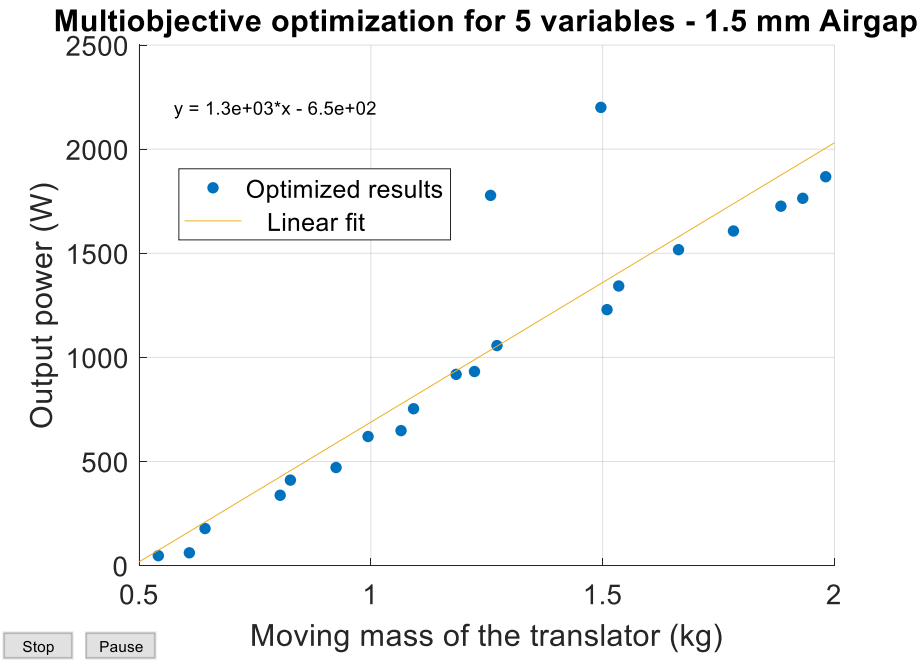

Figure 6-24 - Case 2 - Pareto optimal set for 1.5 mm airgap.

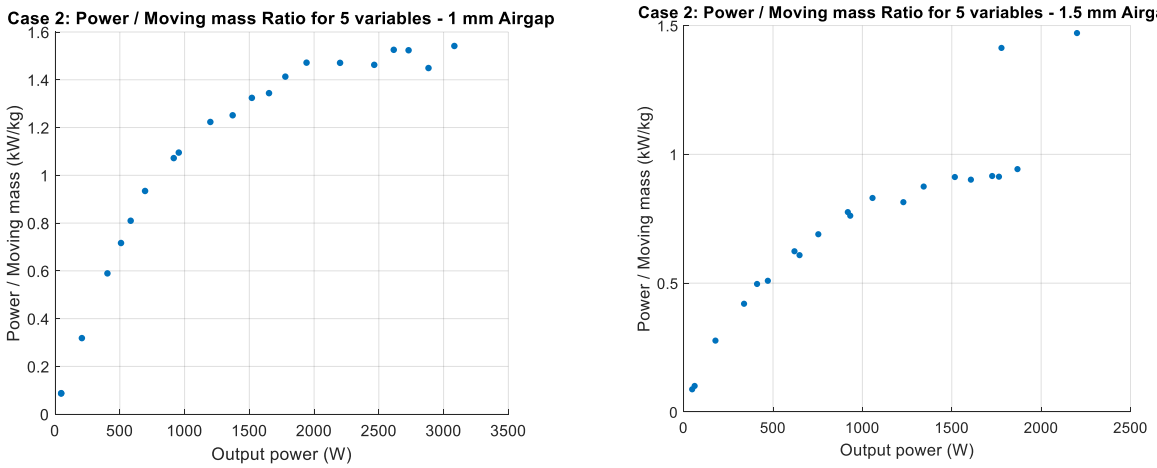

Figure 6-25 - Case 2 - Power/Moving mass ratio for 1 mm and 1.5 mm airgap.

Power/Moving mass (P/M) was as high as 1.5 kW/kg when five variables were used for the multi-objective optimization. Case 2 provides better results than Case 1 with the addition of two variables – poles and stroke. With the additional flexibility, the poles and stroke were increased as needed in comparison to the OD to achieve higher output power. The optimized input parameters for 1 mm airgap for Case 2 is shown below in Table 6-20. The parameters obtained for 1.5 mm airgap has been attached in the appendix.

Table 6-20 - Case 2 - Input variable from the optimization for 1 mm airgap.

S.No	MT (mm)	OD (mm)	Spacer (mm)	Pole	Stroke (mm)	Power (W)	Mass (kg)
1	7.24	25.46	2.48	4.00	29.50	47.65	0.54
2	7.39	25.32	2.75	5.00	29.89	206.84	0.65
3	8.44	25.39	2.78	5.00	31.79	404.23	0.69
4	8.89	25.49	2.64	5.00	32.68	509.15	0.71
5	9.23	25.48	2.68	5.00	33.32	583.76	0.72
6	9.75	25.55	2.68	5.00	34.26	694.80	0.74
7	9.72	25.47	2.86	6.00	34.12	916.23	0.85
8	9.84	25.56	2.70	6.00	34.42	955.04	0.87
9	9.87	25.37	3.31	7.00	34.88	1198.88	0.98
10	9.83	25.37	2.77	7.00	38.22	1371.26	1.10
11	9.88	25.33	3.25	8.00	36.22	1519.51	1.15
12	9.87	25.30	2.99	8.00	38.49	1651.95	1.23
13	9.91	25.16	3.84	9.00	36.77	1778.01	1.26

14	9.91	25.04	4.34	10.00	35.92	1941.71	1.32
15	9.83	25.07	3.47	10.00	39.40	2200.56	1.50
16	9.71	25.09	2.90	10.00	43.40	2464.39	1.69
17	9.99	25.10	2.89	10.00	44.19	2615.07	1.71
18	9.97	25.13	2.55	10.00	45.67	2729.58	1.79
19	9.55	25.21	1.34	10.00	48.99	2883.43	1.99
20	10.00	25.15	1.73	10.00	49.99	3083.14	2.00

It was seen from Table 6-20 that the MT moves towards its upper bound of 10 mm as expected because it has the most effect on the output power. After MT, poles, and stroke start changing compared to OD because their changes have a higher effect of Power /Moving mass ratio compared to OD. Therefore, poles start moving towards 10 and stroke starts moving towards 50 mm, whereas OD stays close to 25 mm. Therefore, higher output power can be achieved with Case 2.

6.4.3 Case 3: 6 Variables – MT, OD and Spacer, Poles, Stroke and Turns

Six variables were used for the optimization of the PMLG system. They are MT, OD, Spacer, Poles, Stroke and Turns. In this case, three objective functions were given to the multi objective optimization routine. The three objectives were,

$Objective\ 1 - maximize\ P$,

$Objective\ 2 - minimize\ M$, and

$Objective\ 3 - minimize\ V$.

The objective function for P was found using the NN model created in the earlier section of this chapter. M (Moving mass) was calculated based on the function parameters as explained in the earlier section and detailed calculation of the moving mass is shown in the appendix. V – Volume of the PMLG system was calculated using the formula for a volume of the cylinder.

$$V = \pi * r^2 * h \tag{6-13}$$

Where, r and h represent the overall radius and length of the PMLG system. The constraints used for the optimizations were

$M < 2\,kg$, and

$V < 0.01\,m^3$.

The bounds used for the optimization is shown in Table 6-14.

This optimization routine was done for 2 different airgap – 1 mm and 1.5 mm.

Figure 6-26 shows Power, Power / Moving mass and Power / Volume results from the optimization routine for six variables with an airgap of 1mm.

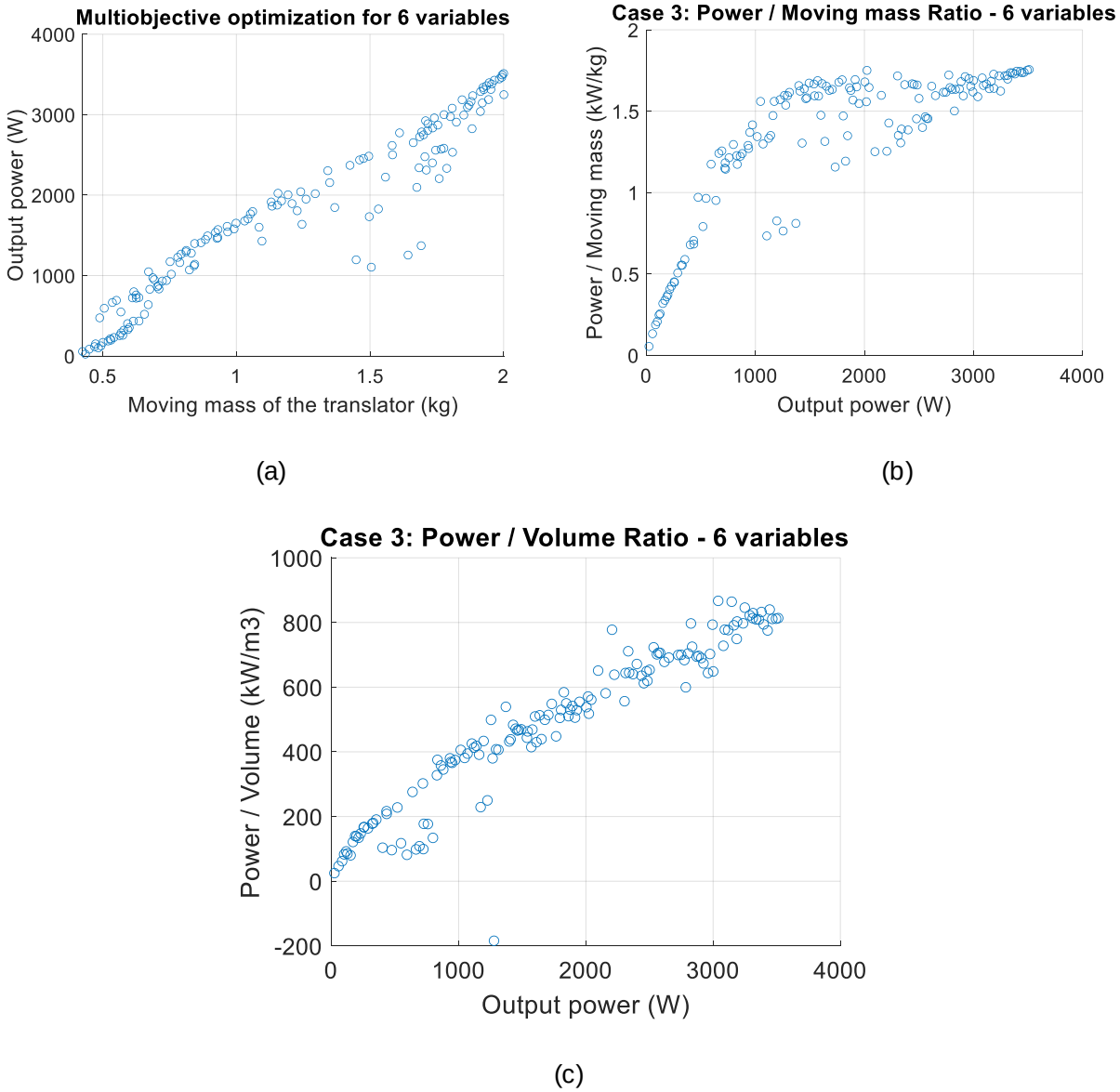

(a) (b)

(c)

Figure 6-26 - Case 3 - Power vs Moving mass for an Airgap of 1mm (b) - Case 3 – P/M vs power for an Airgap of 1mm (c) - Case 3 – P/V vs power for an Airgap of 1mm..

It was seen that the output power increases almost linearly with an increase in moving mass of the translator. Stroke length, Pole and MT are directly proportional to the output power as well as the moving mass of the PMLG system. Therefore, it was seen that as the moving mass increases, power increases.

With respect to the Power / Moving mass ratio, it was seen that as power increases, Power / Moving (P/M) mass ratio increases up to 1 kW but beyond that, the P/M ratio starts tapering close to 1.5 kW / kg. This can be attributed to the reason that poles, stroke length and MT are linearly proportional to the output power of the PMLG system and not proportional to the square or cube of the power. Therefore, P/M ratio starts saturating beyond 1 kW.

From Figure 6-26 – c, it is seen that as the volume increases, the P/V increases with an increase in power output of the PMLG system. This can be attributed to the quadratic relation of volume and radius of the PMLG system. The rate of change of increase in MT causes a greater increase in power compared to the increase in volume of the PMLG system. Therefore, P/V ratio increases almost linearly with an increase in output power.

Similar to 1 mm Airgap, optimization was done for 1.5 mm Airgap and results are shown below.

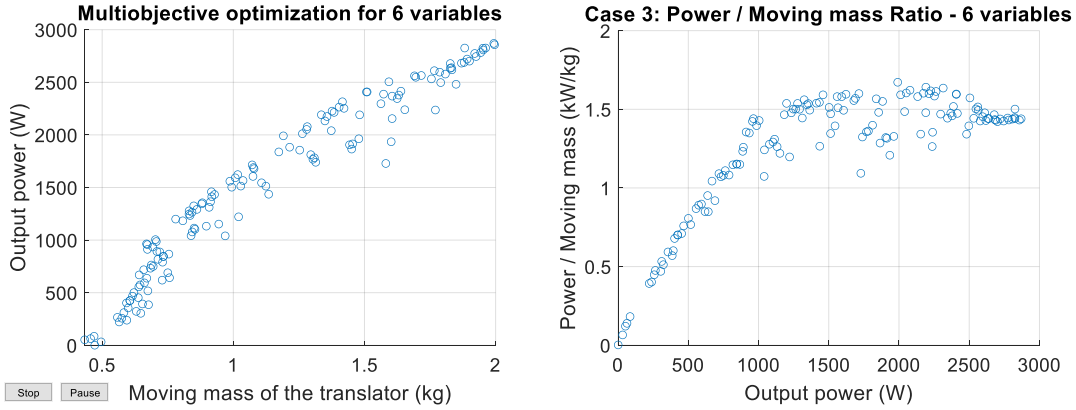

(a) (b)

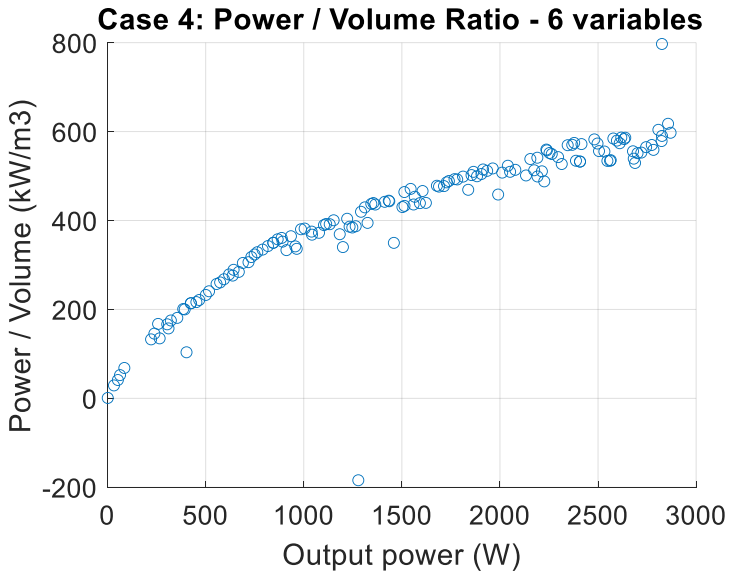

(c)

Figure 6-27 - (a) Case 3 - Power vs Moving mass for an Airgap of 1.5 mm (b) - Case 3 – P/M vs power for an Airgap of 1.5 mm (c) - Case 3 – P/V vs power for an Airgap of 1.5 mm.

The results for 1.5 mm airgap are similar to the results of 1 mm airgap. From Figure 6-27, it is seen that the P/M ratio and P/V ratio are smaller for 1.5 mm airgap as the flux density is lower for a larger airgap.

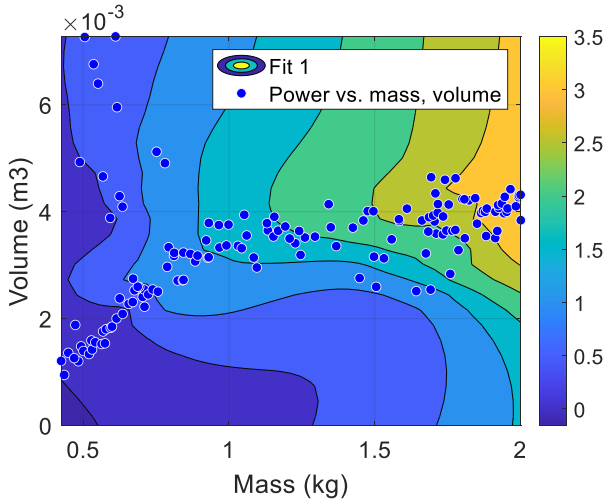

Figure 6-28 - Case 3 - Contour plot of Power (kW) vs moving mass vs Volume for an airgap of 1 mm.

Figure 6-28 shows the parameter space of operation of the PMLG system for different power ranges. Based on this figure, a PMLG can be designed for a given volume and the

moving mass of the system. The comparison of optimization parameters obtained for Case 3 is shown in Figure 6-29.

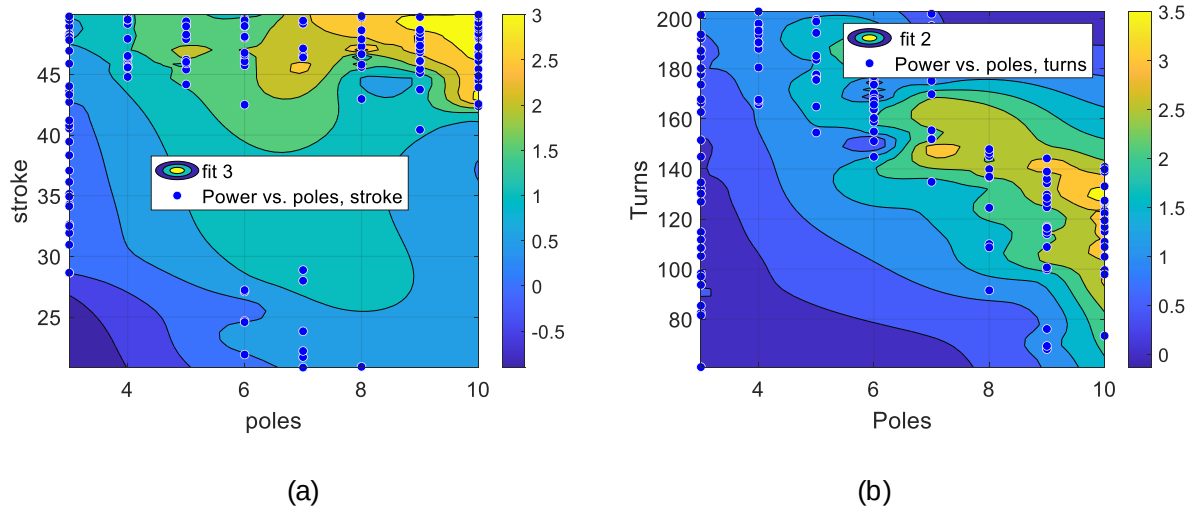

(a) (b)

Figure 6-29 - (a) Case 3 - Contour plot of Power (kW) vs poles vs stroke for an airgap of 1 mm (b) Case 4 – Contour plot of Power (kW) vs poles vs turns for an airgap of 1 mm.

From Figure 6-29 - a, it was seen that as the poles increases, power increases and as the stroke increase, power increases. Therefore, more power output was seen on the top right hand corner of the design. In Figure 6-29 - b, it was seen that as the turns increase, the power does not increase linearly. There is actually a region in the center of the plot where there is higher power output. This can be explained on the basis that as the turns increase, the resistance and inductance increase. There comes a point where the increase in inductance and resistance overcome the effect of the increase in output power. This condition was shown in Figure 6-29 – b. Some of the optimized parameters for the input variables were shown in Table 6-21. Complete optimized parameters for 1 mm airgap and 1.5 mm airgap is attached in the appendix.

Table 6-21 - Optimized parameters for Case 3 – 1 mm airgap.

S.No	OD	AG	Frequency	MT	Poles	Spacer	Turns	Stroke	Power	Mass	Volume
1	25.34	1	80	7.14	3	2.09	98	34.13	169.26	0.50	0.0014
2	25.09	1	80	8.44	3	2.25	130	40.54	320.42	0.58	0.0018
3	25.23	1	80	8.75	6	4.09	176	24.58	547.43	0.57	0.0047

4	25.11	1	80	9.28	6	4.13	174	27.22	758.47	0.62	0.0043
5	25.28	1	80	9.65	3	2.66	192	48.15	948.74	0.69	0.0026
6	25.14	1	80	9.88	4	3.05	181	44.79	1161.08	0.79	0.0030
7	25.28	1	80	9.94	4	3.01	196	45.57	1312.54	0.81	0.0032
8	25.29	1	80	9.97	4	2.71	195	49.52	1492.70	0.89	0.0032
9	25.33	1	80	9.84	5	2.62	199	46.03	1651.03	1.00	0.0038
10	25.15	1	80	9.70	7	1.23	135	46.61	1845.84	1.37	0.0034
11	25.56	1	80	9.93	6	1.98	160	49.47	2017.67	1.30	0.0035
12	25.27	1	80	9.42	9	1.27	116	46.05	2311.33	1.71	0.0036
13	25.03	1	80	9.83	8	2.26	146	46.67	2483.79	1.50	0.0040
14	25.04	1	80	9.94	9	1.68	127	46.83	2725.73	1.69	0.0039
15	25.11	1	80	9.98	9	2.89	136	48.41	2886.47	1.72	0.0041
16	25.13	1	80	9.98	9	1.66	139	49.73	3080.47	1.81	0.0042
17	25.35	1	80	9.91	10	1.35	109	48.86	3248.78	2.00	0.0038
18	25.03	1	80	9.99	10	1.34	133	49.27	3428.48	1.97	0.0044

6.5 Comparison of MOO test cases

Three different cases of MOO problem were evaluated for the PMLG system. The individual effects of the parameters as well as the totality were studied through this MOO study. The first step in comparison was to validate some of the points obtained from the MOO study through FEMM. Three points were chosen for three power outputs – 1 kW, 1.5 kW and 2 kW for Case 1, Case 2 and Case 3 respectively.

Table 6-22 - FEMM results for MOO study.

Case	Design Point	Max output power (W)	Rated Power (W)	OC voltage (V)	Load voltage (V)	Load current (A)	Efficiency
1	6	1565	1000	111	98	10.2	91
2	14	3600	1500	154	142	11.4	90.75
3	11	3142	2000	107	91.6	18	85

Comparison of the output power for the three cases is shown in Table 6-23.

Table 6-23 - Comparison of P/M ratio for MOO cases.

MOO Case	Max Power output (kW)	Moving mass at 1 kW	Moving mass at 2 kW	Max P/M (kW/kg)
Case 1	1.976	1.27	2.1	1.1
Case 2	3.083	0.79	1.3	1.54
Case 3	3.428	0.66	1.17	1.76

From the three cases, it was seen that Case 3 is better than Case 2 and Case 1. This can be attributed to the addition of turns to the optimum input variable. Furthermore, Case 2 is better than Case 1 since there is the addition of poles and stroke as optimization input variables. Therefore, depending on the available optimization variables, PMLG can be designed based on the designer's requirement.

6.6 MATLAB GUI

To perform all the optimization routines with the given input parameters, a MATLAB GUI was designed. MATLAB App Designer was used for the User Interface design and functions were written to include call backs for the button and optimization routines. Detailed functional implementation is added in the appendix.

The GUI developed in MATLAB for the optimization routine is shown below in Figure 6-30 and Figure 6-31.

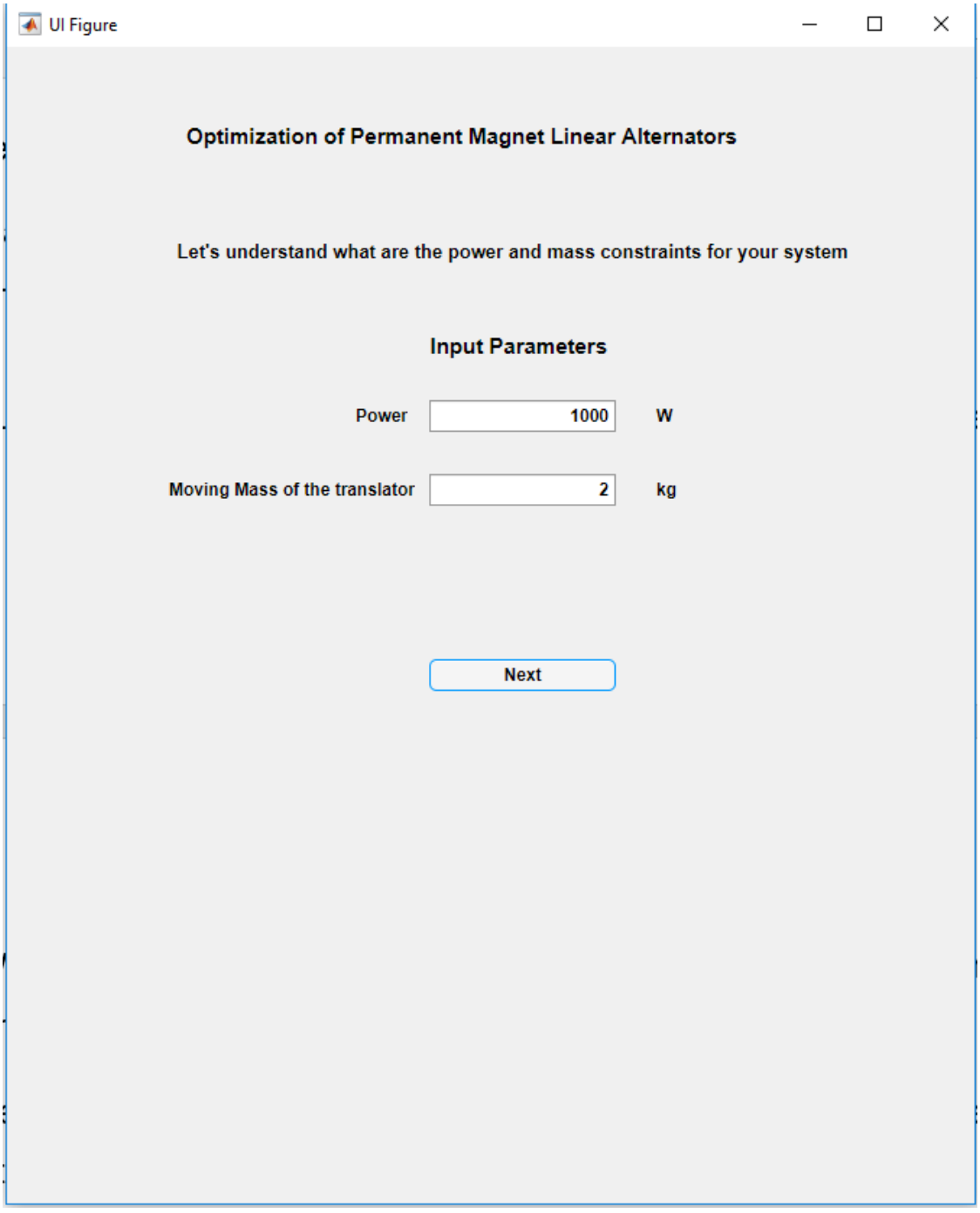

Figure 6-30 - MATLAB GUI - First page of the Optimization.

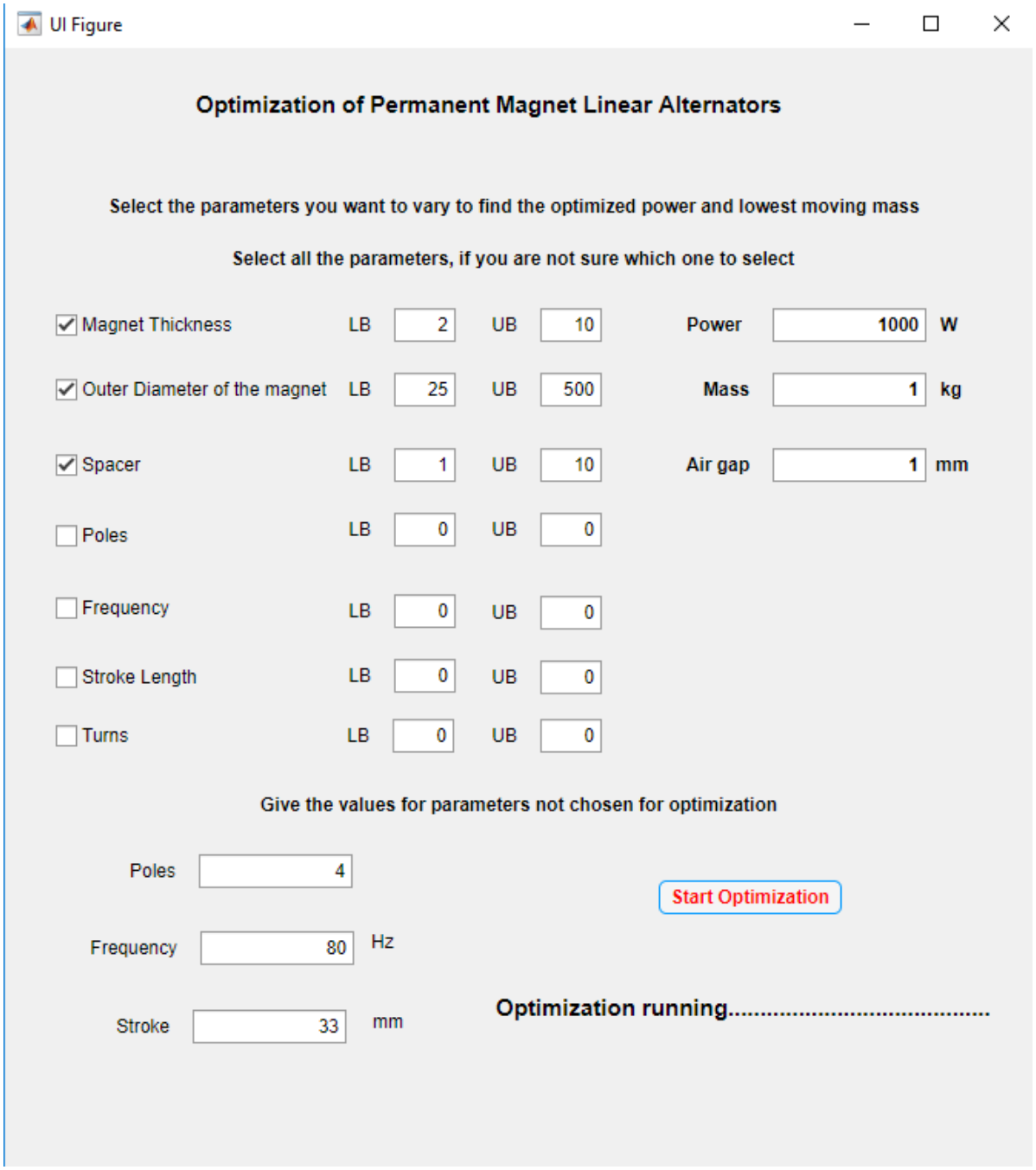

Figure 6-31 - MATLAB GUI - Second page of the Optimization.

6.7 Summary

In this chapter, the optimization of PMLG using different parameters was performed. Two different optimizations – Single objective and multi objective optimization schemes were implemented to understand and explore the design space as well as provide designs for 1 kW and 2 kW machine based on the user requirements.

The steps used for the single objective optimization were,

- Choose 3, 5 and 6 parameters and optimize the design variable at different power levels to determine the power density of the linear generator.
- Understand the important parameters affecting the output power of the linear generator.

The steps used for the multi-objective optimization were,

- Develop a model to study the effect of the output power, moving mass and volume of the linear generator keeping all three as the objective functions.
- Provide design choices for the linear generator designer to choose based on the designer's requirements.

From the single and multi-objective optimization, it was clear that to achieve high power density and lower moving mass of the translator, MT has to increase, and OD has to decrease. The other parameters were varied based on the moving mass requirements to achieve the required output power. In addition, if we start with certain fixed input variables, using the MATLAB GUI, optimization can be done to design a PMLG system. Overall, it was seen that the MT is the most important factor, followed by poles and then comes spacer, stroke length, and OD of the magnet. Using this knowledge, the designer can design PMLG efficiently with high power density.

CHAPTER SEVEN

7 Conclusions and future work

7.1 Discussion of research results

The main objective of the thesis was to design and optimize a tubular permanent magnet linear generator for free piston engine applications. Further the goal was to provide an easy to use method to design a PMLG system. This was implemented through the following four steps.

- **Develop a design guideline for a single phase PMLG system**

Nassar and Boldea had developed a design guideline for 3 phase PMLG system for Stirling engine and high power (> 10 kW) applications in [96, 97]. These papers did not account for small scale applications in the order of 1 kW. Furthermore, it didn't have equations to calculate all the geometric dimensions of the PMLG system. Therefore, a design guideline was developed for the PMLG system for low power systems (0.5 - 2 kW). This research focused specifically on developing a design guideline for a single phase PMLG system. Furthermore, a table of designs choices was provided based on the developed design guideline for 0.5 kW, 1 kW, 1.5 kW and 2 kW. Finally, a MATLAB GUI was developed to simplify the design process of the PMLG system.

- **Develop a finite element model and validate it with the experimental prototype built at West Virginia University**

The second step was to understand the characteristics of the PMLG system by developing finite element model and analysis tools. This was done by combining Finite Element Method Magnetics (FEMM) and MATLAB software. Later, two experimental prototypes of the free piston engine PMLG system were built. The results from the prototypes were used to refine the FEMM model to predict the experiments with better accuracy. Finally, comparison of the open circuit voltage, load voltage, load current and output power was made to determine the accuracy of the FEMM model.

- **Sensitivity study of the geometric parameters of the PMLG system**

The third step was to perform a sensitivity analysis of the PMLG system parameters. This focused on understanding the design space of the PMLG system. Therefore, two types of studies were performed on the PMLG system with the developed finite element model - One At a Time (OAT) study and Global sensitivity analysis. OAT study helped in understanding the individual effects of the geometric parameters of the PMLG system. Parameters such as magnet thickness, outer diameter of the magnet, spacer, airgap, frequency, stroke length and turns were chosen as input parameters for the study. Using this, the output parameters such as output power, open circuit voltage, and Power / Moving mass of the translator ratio of the PMLG system were investigated for changes in the input. Global Sensitivity analysis was done to understand the interdependence of the input parameters with respect to the output parameter. Finally, sensitivity analysis helped in understanding the effects of the input parameters on the output and the important parameters that affect the behavior of the PMLG system.

- **Optimization of the PMLG system for low moving mass of the translator and low volume of the overall system**

The fourth step was to develop a PMLG with low moving mass of the translator. Understanding from the sensitivity study was used to design an efficient optimization routine for the PMLG system. Initially a framework of the optimization was developed where a neural network model was used to predict the output power of the PMLG system. Later, Single and Multi-objective optimizations were performed to design PMLG with high power density and low moving mass of the translator. Different input parameters and constraints were chosen for the optimization and the PMLG system was designed with different Power/Moving mass ratios and Power/Volume ratios.

7.2 Findings from the research

- Easy to use methods were not available in the literature to design a complete PMLG system from start to end for reciprocating engine applications. This thesis provides equations and calculations to design a preliminary design of the PMLG

system. This was done by combining the experience obtained from running the experiments and matching them with the finite element model.

- During the study of the orientation of the magnets, it is seen that the halbach arrangement provides the best output power and performance compared to radial and axial orientation. This can be attributed to the concentration of the magnetic flux in the halbach arrangement.
- In comparison to axial and radial arrangements, axial arrangement should not have a back iron in the translator whereas the radial arrangement must have a back iron for better performance.
- In terms of the neutral position, for a PMLG system, poles of the translator must lie under the lamination and move a distance equal to the pole pitch from that location or the pole of the translator must lie under the center of the windings and move half the pole pitch on either side of that location.
- One at a Time study helped to understand the effect of individual parameters of the PMLG system and it was found that the magnet thickness has the major role in affecting the output power and performance of the PMLG system. This can be attributed to the improvement in the air gap magnetic flux density of the PMLG system.
- Global sensitivity analysis helped to determine the importance of the PMLG parameters with respect to one another. It was seen that the magnet thickness was the most important factor and spacer was the least important factor for the output power of the PMLG system. Airgap was the most important factor the P/M ratio followed by the magnet thickness of the PMLG system and OD was the least important parameter of the PMLG system.
- Single and multi-objective optimizations helped to develop different PMLG systems according the designer's requirements.

7.3 Future work

The results of this research can be used as a starting point for different research projects as described below.

- **Complete modeling of free piston engine PMLG system:**

In this research, the modeling of the PMLG system for free piston engine has taken the force from the free piston engine as a sinusoidal force directly applied to the PMLG system. Therefore, there is an opportunity to develop a complete system model for free piston engine PMLG system.

Detailed modeling of the free piston engine using MATLAB has been performed in [107]. This model can be combined with the FEMM model developed in this research to work towards building a detailed and a complete system for the PMLG system.

Another research route for the modeling is to use Ansys Simplorer and MATLAB to develop a complete model for the free piston engine PMLG system. Model of the PMLG system using Ansys is discussed in [32]. This model combined with the power electronics (in Ansys Simplorer), control design (MATLAB) and engine system (Ansys Simplorer / Ansys Fluent /Forte) could make a more robust model.

The preliminary workflow for the Ansys model is shown below in Figure 7-1.

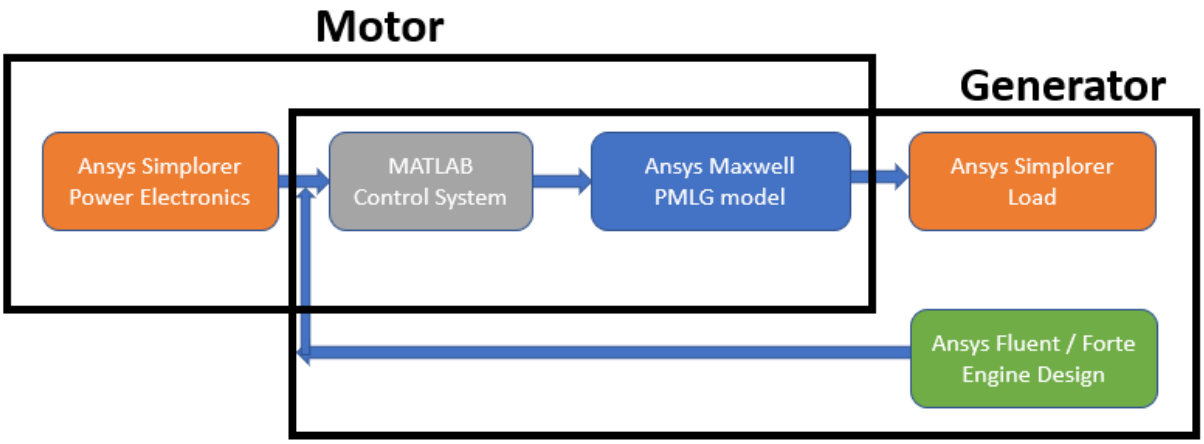

Figure 7-1 - Ansys Simulation workflow for the PMLG system model.

- **Design Guideline**

The design guideline provided in this research has been modeled and test for systems in the range of 0.5 kW to 5kW systems. This can be modified further to design high power applications for hybrid vehicles and wave energy applications. The design guideline has equations for the single phase PMLG system. This can be modified to design three phase PMLG systems.

- **Three phase PMLG system**

Whole research in this thesis has focused on the single phase PMLG system. The detailed FEMM model has been developed to understand the performance and characteristics of the single phase PMLG systems. To design, high power applications, three phase PMLG systems would be better. Therefore, detailed analysis of the three phase PMLG system can be done. The developed PMLG system and the codes provided for the finite element model are flexible to modify and convert to three phase systems. Therefore, studying three phase PMLG systems would provide a useful understanding for high power applications. Three phase PMLG systems have some characteristics of unbalanced phase voltages as shown in [26]. Therefore, studies can be done to mitigate the unbalanced phase voltages.

- **Experimental comparison of different magnet arrangements**

A finite element modeling comparison of the magnet arrangements was provided in this research. Experiments in this research were performed in an axial magnet arrangement. Radial and Halbach arrangements can be tested using the same setup by swapping the translator and keeping the rest of the experimental system setup the same. This will provide validation of the results obtained from FEMM in Chapter 5.

CHAPTER EIGHT

8 Bibliography

[1] British Petroleum Company, "BP Statistical Review of World Energy," 2019.

[2] Enerdata Inc., "Global Energy Statistical Yearbook," 2019.

[3] "ourworldindata.org," 2019. [Online].

[4] S.A.Nassar and I.Boldea, Linear motion electric machines, Michigan: Wiley, 1976.

[5] I. Boldea and S.A.Nassar, Linear Electric Actuators and Generators, Cambridge University Press, 2005.

[6] V.I.Goncharov, Y.V.Yezhov, V.G.Chirkin and S.V.Shirinskii, "Linear Reciprocating Generator-Sizing Equations and Mathematical Model," 2016.

[7] K.Thorburn and M. Leijon, "Farm size comparison with analytical model of linear generator wave energy converters," *Ocean Engineering,* vol. 34, no. 5, pp. 908 - 916, 2007.

[8] L.Li, W.Li, D.Li, J.Li and Y.Fan, "Research on Strategies and Methods Suppressing Permanent Magnet Demagnetization in Permanent Magnet Synchronous Motors based on a Multi -Physical Field and Rotor Multi-Topology Structure," *Energies,* vol. 11, no. 40, 2018.

[9] D. Li, B. Bai, Q. Yu and D. Chen, "Cogging Force Minimization in a Permanent Magnet Linear Generator for Sea Wave Energy Extraction Applications," in

International Conference on Energy and Environment Technology, Guilin, Guangxi, 2009.

[10] X. Fan, G. H. Liu, L. Xu, W. X. Zhao, Y. Zeng and X. X. Du, "Influence of magnet materials on performances of fault-tolerant permanent-magnet vernier machines," in *015 IEEE International Conference on Applied Superconductivity and Electromagnetic Devices (ASEMD)*, Shanghai, 2015.

[11] G. Becherini, "Gyroscopic stabilization of launch package in induction type coilgun," *IEEE Transaction of Magnetics,* vol. 37, no. 1, pp. 116-122, 2001.

[12] T. G. Engel, J. M. Neri and M. J. Veracka, "Solid-projectile helical electromagnetic launcher," *IEEE Transactions on Plasma Science,* vol. 37, no. 4, pp. 603-607, 2009.

[13] I.Boldea, Linear Electric Machines, Drives and MAGLEVs Handbook, Boca Raton, FL: Taylor and Francis Group, 2013.

[14] M.Hosseini, S.H.Hosseinian, S.J.Moghani and M.Abedi, "Multisided linear induction generator, analytical modeling, 3-D finite elemen analysis and experiment test," *Elektronika ir Elektrotechnika,* vol. 19, no. 8, p. 8, 2013.

[15] D. Hall, J. Kapinsk, M. Krefta and O. Christianson, "Transient Electromechanical Modeling for Short Secondary Linear Induction Machines," *IEEE Transactions on Energy Conversion,* vol. 23, no. 3, pp. 789 - 795, 2008.

[16] A.Ghaempanah, M.Mirsalim and M.Mirzayee, "Simulation of Linear Induction Generators in Hybrid Electric Vehicle Applications," in *3rd IET International Conference on Power Electronics, Machines and Drives (PEMD)*, Dublin, Ireland, 2006.

[17] R. Cao, M. Lu, N. Jiang and M. Cheng, "Comparison Between Linear Induction Motor and Linear Flux-Switching Permanent-Magnet Motor for Railway

Transportation," *IEEE Transactions on Industrial Electronics,* vol. 66, no. 12, pp. 9394 - 9405, 2019.

[18] P.Francois, I.G.Burrel, H.B.Ahmed, L.Prevond and B.Multon, "3D Analytical Model for a Tubular Linear Induction Generator in a Stirling cogeneration system," in *IEEE International Electric Machines & Drives Conference*, Antalya, 2007.

[19] J.Faiz, B.Rezaeealam and S.Yamada, "Reciprocating flux-concentrated induction generator for free-piston generator," *IEEE transactions on Magnetics,* vol. 42, pp. 2172-2178, 2006.

[20] T.T.Dang, M.Ruellan, L.Prevond, H.Ben and B.Multon, "Sizing Optmization of Tubular Linear Induction Generator and Its Possible Application in High Acceleration Free-Piston Stirling Microcogeneration," *IEEE Transactions on Industry Applications,* vol. 51, no. 5, pp. 3716-3733, 2015.

[21] G.Brady, C.Loghlin, J.Massey, D.Griffiths and C.Villegas, "Design and test of a linear switched reluctance generator for use in wave-energy applications," in *4th International Conference on Ocean Energy*, Dublin, 2012.

[22] R.P.G.Mendes, M.R.A.Calado and S.J.P>SMariano, "Identification of some tubular topologies of linear witched reluctance generator for direct drive applications in ocean wave energy conversion," in *Proceedings of the World Congress on Engineering*, London, 2014.

[23] H. Chen, X. Wang and J. J. G. a. S. Lu, "Design of bilateral Switched Reluctance linear generator," in *2010 IEEE Electrical Power & Energy Conference*, Halifax, NS, 2010.

[24] H.Chen and X.Ju, "Fuzzy logic control for switched reluctance variable speed linear generator system," in *IEEE/PES Transmission and Distribution Conference and Exhibition:Asia and Pacific*, 2005.

[25] J.L.Torralba and M.P.Martin, "Switched reluctance linear motor/generator". US Patent 12467092, 2010.

[26] A.Pirisi, G.Gruosso and R.E.Zich, "Novel modeling design of three phase tubular permanent magnet linear generator for marine applications," in *2009 International Conference on Power Engineering, Energy and Electrical Drives*, Lisbon, 2009.

[27] L.Cappelli, F.Marignetti, E.Santis, Y.Coia and R.Stefano, "Design of a Moving-Coil Linear Generator for Marine Energy Conversion," *Applied Mechanics and Materials,* Vols. 416-417, pp. 311-316, 2013.

[28] M.Fazal, S.A.Zulkifli, T.Ibrahim and K.S.Rao, "Modeling and simulation of a moving coil-generator," in *2010 International Conference on Intelligent and Advanced Systems*, Manila, 2010.

[29] I.Fazal, K.S.RamaRao and M.N.Karsiti, "Modeling and Simulation of Moving Iron Linear Generator," *Applied Mechanics and Materials,* Vols. 110-116, pp. 2464-2468, 2012.

[30] P. R. Upadhyay and K. R. Rajagopal, "Comparison of performance of the axial-field and radial-field permanent magnet brushless direct current motors using computer aided design and finite element methods," *Journal of Applied Physics,* vol. 97, no. 10, 2005.

[31] V.A.Neumann and R. Homrich, "Comparison between radial and axial permanent magnet generators for low speed application," in *2014 IEEE International Instrumentation and Measurement Technology Conference (I2MTC) Proceedings pp. 251-256*, Montevideo, Uruguay, 2014.

[32] J.Subramanian, G.Heiskell, F.Mahmudzadeh and P.Famouri, "Study of radial and axial magnets for linear alternator — Free piston engine system," in *2017 North American Power Symposium (NAPS)*, Morgantown, 2017.

[33] R. Krishnan and K. Sitapati, "Performance Comparisons of Radial and Axial Field, Permanent-Magnet, Brushless Machines," *IEEE Transactions on Industry Applications,* vol. 37, no. 5, pp. 1219-1226, 2001.

[34] Q. L. Peng, S. M. McMurry and J. M. D. Coey, "Axial magnetic field produced by axially and radially magnetized permanent rings," *Journal of Magnetism and Magnetic Materials,* vol. 268, no. 1-2, p. 165 –169, 2004.

[35] M. K.El-Nemr and A. E. ElGebaly, "Design and performance evaluation of halbach array linear generator for wave energy converters," in *IEEE 8th GCC Conference & Exhibition*, Muscat, 2015.

[36] B. Sugiyantoro, S. A. R. Susilo and W. Yusuf, "Slot-less Tubular Linear Permanent Magnet Generator Using Halbach-Array Excitation," in *10th International Conference on Information Technology and Electrical Engineering*, Kuta, 2018.

[37] T.Yang, L.Zhou and L.Li, "Influence of Design Parameters on End Effect in Long Primary Double Sided Linear Induction Motor," *IEEE Transactions on Plasma Science,* vol. 39, no. 1, pp. 192-197, 2011.

[38] H.W.Lee, C.Park, B.S.Lee and H.J.Park, "Exit end effect reduction of a linear induction motor for the deep-underground GTX," in *The XIX International Conference on Electrical Machines - ICEM*, 2010.

[39] A.H.Selcuk and H.Kurum, "Investigation of End Effects in Linear induction motors using the Finite Element Method," *IEEE Transactions on Magnetics,* vol. 44, pp. 1791-1795, 2008.

[40] J.Liu, F.Lin, Z.Yang and T.Q.Zheng, "FIeld Oriented Control of Linear Induction Motor considering Attraction Force and End Effects," in *CES/IEEE 5th International Power Electronics and Motion Control Conference*, Shangai, 2006.

[41] H.Zhang, B.Kou, Y.Jin and H.Zhang, "Investigation of auxiliary poles optimal design on reduction of end effect detent force for PMLSM with typical slot-pole combinations," *IEEE Transactions on Magnetics,* vol. 51, no. 11, pp. 1-4, 2015.

[42] H.Arof, A.M.Eid and K.M.Nor, "Cogging force reduction using special magnet design for tubular permanent magnet linear generators," in *39th International Universities Power Engineering Conference*, Bristol, 2004.

[43] A.M.Eid, H.Lee and M.Nakaoka, "Cogging force minimization of linear engine-coupled tubular permanent magnet linear AC synchronous generator," in *3rd IET Conference on Power Electronics, Machines and Drives PEMD*, Dublin, 2006.

[44] D.Li, B.Bai, Q.Yu and D.Chen, "Cogging force minimization in a permanent magnet linear generator for sea wave energy extraction applications," in *2009 International Conference on Energy and Environmental Technology*, Guilin, 2009.

[45] The International Agency, "iea.org," [Online]. Available: iea.org/data-and-statistics/data-tables.

[46] US Energy Information Administration, "eia.gov," [Online]. Available: https://www.eia.gov/todayinenergy.

[47] B.Czech and P.Bauer, "Wave energy converter concepts: Design challenges and classifications," *IEEE Industrial Electronics Magazine,* vol. 6, no. 2, pp. 4-16, 2012.

[48] A.Muetze and J.G.Vining, "Ocean Wave Energy Conversion - A Survey," in *Conference Record of the 2006 IEEE Industry Applications Conference Forty - First IAS Annual Meeting*, Tampa, 2006.

[49] M.Scuotto and H.Polinder, "Wave energy converters and their impact on power systems," in *International Conference on Future Power Systems*, Amsterdam, 2005.

[50] Electric Power Research Institute, "Mapping and Assessment of the US ocean wave energy resource," Palo Alto, USA, 2011.

[51] B.Meinhold, "https://inhabitat.com/," March 2016. [Online]. Available: https://inhabitat.com/portugal-wavepower-plant-goes-live/. [Accessed 2016].

[52] M. J. Witt, E. V. Sheehan, S. Bearhop, A. C. Broderick and e. all, "Assessing wave energy effects on biodiversity: the Wave Hub experience," *Philosophical transactions of the Royal Society - Mathematical, Physical and Engineering Sciences,* vol. 370, pp. 502-529, 2012.

[53] S.Ryan, C.Algie and G.Mcfarlane, "The Bombora wave energy converter: A novel multi-purpose device for electricity, coastal protection and surf breaks. In: Proceedings of the Australian coasts and ports," in *22nd Australasian coastal and ocean engineering conference and the 15th Australasian port and harbour conference*, Auckland, 2015.

[54] Carnegie Clean Energy, "https://www.carnegiece.com/," 2017. [Online]. Available: https://www.carnegiece.com/projects/wave/.

[55] Oceanlinx technology, "http://www.oceanlinx.com/(last," [Online].

[56] Ocean Wave Energy Trust, "Offshore ocean wave energy: A summer 2009 technology and market assessment update," Oregon, 2009.

[57] M.P.kazmierkowski and M.Jasinski, "Ocean waves energy converter - Wave Dragon MW," *Przeglad Elektrotechniczny,* vol. 84, no. 2, pp. 8-14, 2008.

[58] J.Vining, "A double fed linear generator for ocean wave energy conversion," Wisconsin, 2011.

[59] A. H. Memon, T. B. Ibrahim and P. Nallagowden, "Design analysis, optimization and identification of optimum single-phase linear PM generator using different magnet shape for wave energy conversion," in *2016 6th International Conference*

on Intelligent and Advanced Systems (ICIAS) pp. 1-6, Kuala Lumpur, Malaysia, 2016.

[60] A.H.Memom, T.B.Ibrahim and N.Perumal, "Portable and pico-scale linear generator for wave energy conversion," in *5ht International Conference on Intelligent and Advanced System*, Kuala Lumpur, 2014.

[61] L.Huang, H.Yu, M.Hu, C.Liu and B.Yuan, "Research on a Tubular Primary Permanent Magnet Linear Generator for Wave Energy Conversion," *IEEE Transactions on Magnetics,* vol. 49, no. 5, pp. 1917-1920, 2013.

[62] R.Vermaak and M.J.Kamper, "Design Aspects of a Novel Topology Air-Core Permanent Magnet Linear Generator for Direct Drive Wave Energy Converters," *IEEE Transactions on Industrial Electronics,* vol. 59, no. 5, pp. 2104-2115, 2012.

[63] F.Bizzozero, M.Giassi, G.Gruosso, S.Bozzi and G.Passoni, "Dynamic model, parameter extraction and analysis of two topologies of a tubular linear generator for seawave energy production," in *International Symposium on Power ELectronics Electrical Drives, Automation and Motion*, Ischia, 2014.

[64] L.Huang, J.Liu, H.Yu, R.Qu, H.Fang and H.Chen, "Winding Configuration and Performance Investigations of a Tubular Superconducting Flux-Switching Linear Generator," *IEEE Transactions on Applied Superconductivity,* vol. 25, no. 3, pp. 1-5, 2015.

[65] O.Farrok and M.M.Ali, "A new technique to improve the linear generator designed foroceanic wave energy conversion," in *8th International Conference on Electrical and Computer Engineering*, Dhaka, 2014.

[66] N.Hodging, O.Keysan, A.S.McDonald and M.A.Mueller, "Design and Testing of a linear generator for Wave-Energy Applications," *IEEE Transactiosn on Industrial Electronics,* vol. 59, no. 5, pp. 2094-2103, 2012.

[67] Z.Xu and S.Chang, "Prototype testing and analysis of a novel internal combustion linear generator integrated power system," *Applied Energy,* vol. 87, no. 4, pp. 1342-1348, 2010.

[68] A. Eid, K.Kwon, S.Lee and M.Nakaoka, "Linear Engine Coupled Linear Generator starting for Hybrid Electric Behicle Applications," in *International Conference on Electrical Engineering*, 2006.

[69] F. Rinderknecht and F. Kock, "A high efficient converter for hybrid vehicle concept," *World electric vehicle journal,* vol. 5, pp. 475 - 481, 2012.

[70] H. Feng, Y. Song, Z. Zuo, J. Shang, Y. Wang and A. P. Roskilly, "Stable Operation and Electricity Generating Characteristics of a Single-Cylinder Free Piston Engine Linear Generator: Simulation and Experiments," *Energies,* vol. 8, no. 2, pp. 765-785, 2015.

[71] M.Andriollo and A.Tortella, "Dynamic model of a free piston tubular linear generator for vehicle auxiliary power supply," in *IEEE International Electric Vehicle Conference*, Florence, 2014.

[72] P.Zheng, A.Chen, P.Thelin, W.M.Arshad and C.Sadarangani, "Research ona Tubular Longitudinal Flux PM Linear Generator Used for Free-Piston Energy Converter," *IEEE Transactions on Magnetics,* vol. 43, no. 1, pp. 447-449, 2007.

[73] M.R.Hanipah, R.Mikalsen and A.P.Roskilly, "Recent commerical free-piston engine developments for automotive applications," *Applied Thermal Engineering,* vol. 75, pp. 493-503, 2015.

[74] P.M.Najt, R.P.Durrett and V.Gopalakrishnan, "Opposed Free Piston Linear Alternator". USA Patent 112468A1, 2012.

[75] K.Hidemasa, O.Yuichi, H.Yoshihiro, N.Kiyomi and A.Kosuke, "Free-piston Type Generator". Japan Patent JP2012202385A, 2012.

[76] O.Lindgarde, "Method and System for Controlling a Free-Piston Energy Converter". USA Patent US20130298874A1, 14 11 2013.

[77] T.Osamu, S.Kohei, T.Kenichi and K.Kohei, "The Control Apparatus of an Internal Combustion Engine". Japan Patent JP2011202621A, 2011.

[78] M. Gräf, S.-E. Pohl, F. Rinderknecht and C. Ferrari, "Free Piston Linear Generator with high partload efficency," in *Proceedings in SAE Conference 2007*.

[79] S. Goto, K. Morita, H. Kosaka, T. Akita, Y. Hotta, T. Umeno and K. Nakakita, "Development of free piston engine linear generator system part 2 - investigation of control system for generator," in *SAE Technical Paper*, 2014.

[80] M. T. L. Terry A. Johnson, "Experimental Evaluation of the Free Piston Engine - Linear Alternator," Sandia National Laboratories, Albuquerque, 2015.

[81] W. Cawthorne, P. Famouri and N. Clark, "Integrated design of linear alternator/engine system for HEV auxiliary power unit," in *IEEE International Electric Machines and Drives Conference pp. 267-274*, Cambridge, MA, USA, 2001.

[82] P. Famouri, W. Cawthorne, N. Clark, S. Nandkumar, C. Atkinson, R. Atkinson, T. McDaniel and S. Petreanu, "Design and testing of a novel linear alternator and engine system for remote electrical power generation," in *IEEE Power Engineering Society. 1999 Winter Meeting (Cat. No.99CH36233) vol. 1 pp. 108-112*, New York, NY, USA, 1999.

[83] P. Famouri, J. Chen, N. Clark, T. McDaniel, R. Atkinson, S. Nandkumar, C. Atkinson and S. Petreanu, "Development of a linear alternator-engine for hybrid electric vehicle applications," *IEEE Transactions on Vehicular Technology,* vol. 48, no. 6, pp. 1797 - 1802, 1999.

[84] S.Nandkumar, "Two-Stroke Linear Engine," West Virginia University, Morgantown, 1998.

[85] P. Pillay and H. Li, "A Linear Generator Powered from Bridge Vibrations for Wireless Sensors," in *IEEE Industry Applications Annual Meeting*, New Orleans, LA, 2007.

[86] D.Isarakorn and T. Sudhawiyangkul, "Design and optimization of a small-scale linear electromagnetic energy harvester," in *12th International Conference on Electrical Engineering/Electronics, Computer, Telecommunications and Information Technology (ECTI-CON)*, Hua Hin, 2015.

[87] P. Zeng, H. Chen and Z. Y. a. A. Khaligh, "Unconventional wearable energy harvesting from human horizontal foot motion," in *Twenty-Sixth Annual IEEE Applied Power Electronics Conference and Exposition (APEC)*, Fort Worth, TX, 2011.

[88] A.Nasiri, S.A.Zabalawi and D.C.Jeutter, "A Linear Permanent Magnet Generator for Power Implanted Electronic Devices," *IEEE Transactions on Power Electronics,* vol. 26, no. 1, pp. 192-199, 2011.

[89] R. G. Hauser, D. L. Hayes, L. M. Kallinen, D. S. Cannom, A. E. Epstein, A. Almquist, S. L. Song, G. F. Tyers, S. C. Vlay and M. Irwin, "Clinical experience with pacemaker pulse generators and transvenous leads: an 8-year prospective multicenter study," *J. Heart Rhythm,* vol. 4, no. 2, pp. 154 - 160, 2007.

[90] M. G. R. Peters, "Implantable cardiac defibrillators," *Med. Clin. North Amer,* vol. 85, no. 2, pp. 342 - 367, 2001.

[91] T. Mussivand, K. S. Holmes, A. Hum and W. J. Keon, "Transcutaneous energy transfer with voltage regulation for rotary blood pumps," *Journal of Artificial Organs,* vol. 20, no. 6, pp. 621 - 624, 1996.

[92] K.Ishida, J.Muranishi, S.Ohashi and T.Aoki, "The generation characteristics of the improved configuration of the stator and mover in the linear generator using vibration energy," in *IEEE Region 10 Conference (TENCON)*, Singapore, 2016.

[93] Z.Zhang, X.Zhang, Y.Rasim, C.Wang, B.Du and Y.Yuan, "Design and modeling and practical tests on a high voltage kinetic energy harvesting system for a renewable road tunnerl based on linear alternators," *Applied Energy,* vol. 164, pp. 152-161, 2016.

[94] Z. Zhang, Y. Ma, M. Li and L. Zhao, "Recent advances of energy recovery expanders in the transcritical CO2 refrigeration cycle," *HVAC&R Research,* vol. 19, no. 4, pp. 376 - 384, 2013.

[95] P.Heyl and H.Quack, "Free piston expander -compressor for CO2 - design, application and results," in *International Congress of Refrigeration*, Sydney, 1999.

[96] S.A.Nasar and I.Boldea, "Permanent-magnet linear alternators part 1: Fundamental equations," *IEEE Transactions on Aerospace and Electronic Systems,* vol. 23, no. 1, pp. 73-78, 1987.

[97] S.A.Nasar and I.Boldea, "Permanent-Magnet Linear Alternators Part II: Design Guidelines," *IEEE Transactions on Aerospace and Electronic Systems,* vol. 23, no. 1, pp. 79-82, 1987.

[98] F. Mahmudzadeh, "Development of Resonating Oscillating Linear Engine Alternator - Instrumentation and Control," West Virginia University, Morgantown, 2018.

[99] Texas Instruments, "TMS320x2833x, TMS320x2823x Technical Reference Manual SPRUI07," TI, 2020.

[100] I.M.Sobol, "Global sensitivity indices for nonlinear mathematical models and their Monte Carlo estimates," *Mathematics and Computers in Sumulation,* vol. 55, no. 3, pp. 271-280, 2001.

[101] A.Alajmi and J.Wright, "Selecting the most efficient genetic algorithm sets in solving unconstrained building optimization problem," *International Journal of Sustainable Built Environment,* vol. 3, no. 1, pp. 18-26, 2014.

[102] A.El.Garhy, F.Amer, M.Awadulla, S.Rashid and A.Abdien, "A real-valued genetic algorithm to optimize the parameters of support vector machine for classification of multiple faults in NPP," *NUKLEONIKA,* vol. 56, no. 4, pp. 323-332, 2001.

[103] F.Burden and D.Winkler, "Bayesian Regularization of Neural Networks.," *Artificial Neural Networks. Methods in Molecular Biology,* vol. 458, 2008.

[104] R.T.Marler and J.S.Arora, "The weighted sum method for multi-objective optimization: new insights," *Structural and Multidisciplinary Optimization,* vol. 41, pp. 853-862, 2009.

[105] D.Kalyanmoy, Multi-Objective Optimization using Evolutionary Algorithms, John Wiley & Sons, 2001.

[106] T.Deb, K. Pratap, A. Meyarivan and S. Agarwal, "A fast and elitist multiobjective genetic algorithm: NSGA-II," *IEEE Transactions on Evolutionary Computation,* vol. 6, no. 2, pp. 182-197, 2002.

[107] M. R. Bade, "Measured and Modeled Performance of a Spring Dominant Free Piston Engine Generator," West Virginia University, Morgantown, 2019.

CHAPTER NINE

9 Appendix

Magnet properties - NdFeB – Chapter 2

Sintered NdFeB	Residual Induction Br (KGs)		Coercive Force bHc (KOE)		Intrinsic Coercive Force iHc(KOE)	Maximum Energy Product (BH)max (MGOE)		Curie Temperature Tc	Vickers Hardness Hv	Working Temperature Tw	Temperature Coefficient (0-100 °C) (%/	
	Nom.	Min.	Nom.	Min.		Nom.	Min.				Br	iHc
N-27	10.6	10.2	9.8	9.3	≥12.0	27	25	320-330	500-600	<80	-0.11	-0.55
N-30	11.2	10.8	10.5	9.8	≥12.0	30	28	320-330	500-600	<80	-0.11	-0.55
N-33	11.7	11.4	11.0	10.3	≥12.0	33	31	320-330	500-600	<80	-0.11	-0.55
N-35	12.1	11.7	11.5	10.8	≥12.0	35	33	320-330	500-600	<80	-0.11	-0.55
N-38	12.6	12.2	11.5	10.8	≥12.0	38	36	320-330	500-600	<80	-0.11	-0.55
N-40	12.9	12.6	11.0	10.5	≥12.0	40	38	320-330	500-600	<80	-0.11	-0.55
N-43	13.3	13.0	11.0	10.5	≥12.0	43	41	320-330	500-600	<80	-0.11	-0.55
N-45	13.7	13.3	11.0	10.5	≥12.0	45	43	320-330	500-600	<80	-0.11	-0.55
N-48	14.0	13.6	11.0	10.5	≥12.0	48	45	320-330	500-600	<80	-0.11	-0.55
N-27H	10.6	10.2	10.0	9.3	≥17.0	27	25	330-340	600-700	<120	-0.10	-0.51
N-30H	11.2	10.8	10.7	10.0	≥17.0	30	28	330-340	600-700	<120	-0.10	-0.51
N-33H	11.7	11.4	11.0	10.3	≥17.0	33	31	330-340	600-700	<120	-0.10	-0.51
N-35H	12.1	11.7	11.5	10.8	≥17.0	35	33	330-340	600-700	<120	-0.10	-0.51
N-38H	12.6	12.2	12.0	11.5	≥17.0	38	36	330-340	600-700	<120	-0.10	-0.51
N-40H	12.9	12.6	12.0	11.5	≥17.0	40	38	330-340	600-700	<120	-0.10	-0.51
N-42H	13.5	12.9	12.9	11.5	≥17.0	42	40	330-340	600-700	<120	-0.10	-0.51
N-27SH	10.6	10.2	10.2	9.6	≥20.0	27	25	340-350	600-700	<150	-0.10	-0.47
N-30SH	11.2	10.8	11.0	10.2	≥20.0	30	28	340-350	600-700	<150	-0.10	-0.47
N-33SH	11.7	11.4	11.0	10.3	≥20.0	33	31	340-350	600-700	<150	-0.10	-0.47

N-35SH	12.1	11.7	11.5	10.8	≥20.0	35	33	340-350	600-700	≤150	-0.10	-0.47
N-38SH	12.8	12.2	12.1	11.4	≥20.0	38	36	340-350	600-700	≤150	-0.10	-0.47
N-27UH	10.7	10.4	10.4	10.0	≥26.0	27	25	350-360	600-700	≤180	-0.09	-0.43
N-30UH	11.2	10.8	10.6	10.1	≥26.0	30	28	350-360	600-700	≤180	-0.09	-0.43
N-33UH	11.7	11.5	11.0	10.3	≥26.0	33	31	350-360	600-700	≤180	-0.09	-0.43
N-28EH	10.8	10.4	10.2	9.8	≥30.0	28	26	360-370	600-700	≤200	-0.09	-0.43
N-30EH	11.5	10.9	11.2	10.0	≥30.0	32	29	360-370	600-700	≤200	-0.09	-0.43

FEMM code in MATLAB – Chapter 4

Main function

```
clear all
clc
tic
global counterAG HandleToFEMM
% Load the test parameters
sobolParameters = xlsread('Sobol.xlsx'); %Read the Sobol variables
counterAG = 1;


% Run 1000 different test conditions
parfor x = 1:1000

    openfemm(0); % Open FEMM software
    hand = HandleToFEMM; % Create handle to run multiple instances of FEMM model
    designGuideline(sobolParameters(x,:)); %Initialise the input parameters
    RLcalc(a); %Calculate the resistance and inductance of the machine
    getMaterials() %Get the materials such as Cu, Fe, NdFeB from the library
    boundaryCondition() %Set the boundary conditions for the model
    setWindowsize() %Set the window size within the screen
    drawLinearAlternator() %Draw the alternator using the design parameters
    blockProperties() %Assign the materials to the FEMM model
    a = strcat('betaTranslator',num2str(x),'.fem'); %Assign a name to the model
    b = strcat('betaTranslator',num2str(x),'.ans'); %Assign a name to the solution
    mi_saveas(a); %Save the model
    mi_refreshview();
    generateFluxfiles(a,x) %Generate and save the flux linkage for the machine
    loadFluxfiles(magnetParfor(x)); %Load the flux linkage files from the text file
    fluxLinkagecalculations(); %Calculate flux linkage for each windings
    voltageCalculations(); %Calculate the voltage in each winding from the flux linkage
    EgenFFT(); %Calculate the open circuit voltage from the voltage in the windings
```

```
    voltageLoadcalculationsAG(); %Perform load calculations and the power
    counterAG = counterAG + 1;
    movefile(a, 'myfiles')
    movefile(b, 'myfiles')

end
toc
```

Design function

```
function designGuideline = designGuideline(sobolParameters)
clc
%Set the global variables
global spacer magnetThickness magnetHeight alumDrumthickness backIron turns OutermagnetDia
InnermagnetDia coilWidth coilHeight poles airGap strokeLength coilInnergap coilOutergap lamination Gap
lamination Width Aslot freq
global wireGauge lr

%Set all the machine parameters
strokeLength = 33; %Stroke length
OutermagnetDia = sobolParameters(1); %Outer diameter of the magnet
airGap  = sobolParameters(2);  %Air gap
freq = round(sobolParameters(3)); %Frequency
magnetThickness = sobolParameters(4); %magnet thickness in mm
poles = sobolParameters(5); %Number of poles
spacer = sobolParameters(6); %Spacer
turns = sobolParameters(7); %turns

magnetHeight = (33 - spacer);
alumDrumthickness = 2; %Alum drum thickness in mm
backIron = 3; %Back iron thickness in mm

coilWidth = 28; %Width of the winding /coil
coilHeight = turns*4/coilWidth; %Height of the winding/Coil

wireGauge = 2; %Wire size

InnermagnetDia = OutermagnetDia - 2*magnetThickness;

coilInnergap = 0.0;
coilOutergap = 0.0;
laminationGap = 1.0;
laminationWidth = strokeLength -coilWidth - 2*laminationGap ; %Lamination width

end
```

Resistance and inductance calculation function

```
function RLcalc = RLCalc(a)
%Calculate the resistance and inductance of the machine
global strokeLength RL RL1 counterAG turns
openfemm(1) % Open FEMM software
getMaterials() % Get the materials required for the model
boundaryCondition() % Define the boundary condition for the model
setWindowsize() % Set the window size for the model
drawLinearAlternator() % Draw the linear alternator
blockProperties() %Define the materials in the model
mi_saveas(a); %Save the model
mi_refreshview();


mi_addcircprop('Coil circuit', 1, 1) ;% Coil circuit properties
mi_seteditmode('group') ; %Select the edit group - WIndings
mi_selectgroup(1);
mi_movetranslate(0,strokeLength/2); %Shifts Translator in group 1 up 16.5mm
mi_analyze(1);      %run analysis
mi_loadsolution();  %Loads solution

RL = mo_getcircuitproperties('Coil circuit'); %Obtain the resistance and inductance
RL1(counterAG,:) = RL;
closefemm;
end
```

Get materials function

```
function getMaterials = getMaterials()
global magnetType copper lamSteel alum
newdocument(0) % the 0 specifies a magnetics problem
mi_hidegrid();
units ='millimeters'; % Set dimension units
mi_probdef(0, units, 'axi', 1.e-8, 0, 30);
%New material
mi_addmaterial('13 AWG', 1, 1, 0, 0, 58, 0, 0, 1, 6, 0, 0, 1, 1.86);
copper = '13 AWG'; %Winding AWG
magnetType = 'NdFeB 32 MGOe' %Magnet type
lamSteel = '1010 Steel'; %Lamination steel
alum = 'Aluminum, 1100';

% adds these materials from the Material Library to the project
mi_getmaterial(magnetType); %Magnet material NdFeB
mi_getmaterial('Air'); %Air for the outer space in the model
mi_getmaterial(lamSteel);
mi_getmaterial(alum);
end
```

Boundary condition

```
function boundaryCondition = boundaryCondition()
global OutermagnetDia radius c0

radius = 15*OutermagnetDia; %Decides the radius of the boundary
c0_scale=10000.0;
c1=0;
uo = 1.0;
c0= c0_scale/(radius); %Scale the overall boundary to match the machine size
%
mi_addboundprop('Asymptotic',0,0,0,0,0,0,c0,c1,2); % create the Asymptotic Boundary Condition for the
problem
% % draw the r=0 axis and the outer boundary
mi_addnode(0,-radius);
mi_addnode(0, radius);
mi_addsegment(0,-radius,0,radius);
mi_addarc(0,-radius,0,radius,180,1);
mi_selectarcsegment(0,radius);
mi_setarcsegmentprop(1,'Asymptotic',0,0); % make sure we set the Asymptotic boundary condition for
the problem
mi_refreshview();

end
```

Set window size

```
function setWindowsize = setWindowsize()

global radius
mi_refreshview();

mi_zoom(-radius*0.1, -radius*1.05, radius*1.5, radius*1.05); % set the window to a nice size for the problem
end
```

Draw the PMLG system

```
function drawLinearAlternator = drawLinearAlternator()
global spacer magnetHeight alumDrumthickness backIron OutermagnetDia InnermagnetDia coilWidth
coilHeight poles airGap strokeLength coilInnergap coilOutergap laminationGap laminationWidth
phase = 1;
%%%%%%%%%%%%%%%%%%%%%%%%%%%%%% ROTOR / TRANSLATOR
%%%%%%%%%%%%%%%%%%%%%%%%%%%%
% draw the magnets %%%%%%%%%%%%%%%%%%%%%%%%%%%%%
magnetCount = 0;
for n=1: poles+1
mx1 = InnermagnetDia/2.0; %% Set the inner radius
mx2 = OutermagnetDia/2.0; %% Set the outer radius of the magnets
mz1 = strokeLength*magnetCount;
mz2 = magnetHeight + strokeLength*magnetCount;
mi_addnode(mx1, mz1); % bottom left
mi_addnode(mx1, mz2); % top left
mi_addsegment(mx1, mz1, mx1, mz2);
mi_addnode(mx2, mz2); % top right
mi_addsegment(mx1, mz2, mx2, mz2);
mi_addnode(mx2, mz1); % bottom right
mi_addsegment(mx2, mz2, mx2, mz1);
mi_addsegment(mx2, mz1, mx1, mz1);
mi_refreshview();
magnetCount = magnetCount+1;
end
% draw spacers %%%%%%%%%%%%%%%%%%%%%%%%%%%%%%%%
spacerCount = 0;
for n=1:poles
sx1 = InnermagnetDia/2.0;
sx2 = OutermagnetDia/2.0;
sz1 = strokeLength*spacerCount + magnetHeight;
sz2 = strokeLength*(spacerCount+1);
mi_addnode(sx1, sz1); % bottom left
mi_addnode(sx1, sz2); % top left
mi_addsegment(sx1, sz1, sx1, sz2);
mi_addnode(sx2, sz2); % top right
mi_addsegment(sx1, sz2, sx2, sz2);
mi_addnode(sx2, sz1); % bottom right
mi_addsegment(sx2, sz2, sx2, sz1);
mi_addsegment(sx2, sz1, sx1, sz1);
spacerCount = spacerCount + 1;
end
%
% draw the AlumDrum %%%%%%%%%%%%%%%%%%%%%%%%%%%%%
alx1 = InnermagnetDia/2.0 - alumDrumthickness;
alx2 = InnermagnetDia/2.0;
alz1 = 0;
alz2 = strokeLength*(poles+1)-spacer;
mi_addnode(alx1, alz1); % bottom left
mi_addnode(alx1, alz2); % top left
mi_addsegment(alx1, alz1, alx1, alz2);
mi_addnode(alx2, alz2); % top right
mi_addsegment(alx1, alz2, alx2, alz2);
mi_addnode(alx2, alz1); % bottom right
```

```
mi_addsegment(alx2, alz2, alx2, alz1);
mi_addsegment(alx2, alz1, alx1, alz1);
%%%%%%%%%%%%%% END OF ROTOR / TRANSLATOR
%%%%%%%%%%%%%%%%%%%%%%%%%%%%%%%%
%%%%%%%%%% STATOR MODEL
%%%%%%%%%%%%%%%%%%%%%%%%%%%%%%%%%%%%%%%%%%%%%%%%%%%%%%%%%%%%%%%%%%%%
% draw the coils %%%%%%%%%%%%%%%%%%%%%%%%%%%%%%%%%%%
coilCount = 0;
for n=1:(poles+2)*phase
c_x1 = OutermagnetDia/2.0 + airGap + coilInnergap;
c_z1 = strokeLength/phase*coilCount - (laminationWidth + spacer)/2.0 + laminationWidth +
laminationGap;
c_x2 = OutermagnetDia/2.0 + airGap + coilInnergap + coilHeight;
c_z2 = strokeLength/phase*coilCount - ( laminationWidth + spacer)/2.0 + laminationWidth +
laminationGap + coilWidth;
mi_addnode(c_x1, c_z1) % bottom left
mi_addnode(c_x1, c_z2) % top left
mi_addsegment(c_x1, c_z1, c_x1, c_z2)
mi_addnode(c_x2, c_z2); % top right
mi_addsegment(c_x1, c_z2, c_x2, c_z2);
mi_addnode(c_x2, c_z1) % bottom right
mi_addsegment(c_x2, c_z2, c_x2, c_z1);
mi_addsegment(c_x2, c_z1, c_x1, c_z1);
mi_refreshview();
coilCount = coilCount+1;
end

% draw laminations %%%%%%%%%%%%%%%%%%%%%%%%%%%%%%%%%%%%-
lamCount = 0;
for n=1:(poles+2)*phase +1
l_x1 = OutermagnetDia/2.0 + airGap;
l_z1 = strokeLength/phase*lamCount - (laminationWidth + spacer)/2.0;
l_x2 = OutermagnetDia/2.0 + airGap + coilInnergap + coilHeight + coilOutergap;
l_z2 = strokeLength/phase*lamCount - (laminationWidth + spacer)/2.0 + laminationWidth;
mi_addnode(l_x1, l_z1) % bottom left
mi_addnode(l_x1, l_z2) % top left
mi_addsegment(l_x1, l_z1, l_x1, l_z2)

mi_addnode(l_x2, l_z2); % top right
mi_addsegment(l_x1, l_z2, l_x2, l_z2);

mi_addnode(l_x2, l_z1) % bottom right
mi_addsegment(l_x2, l_z2, l_x2, l_z1);
mi_addsegment(l_x2, l_z1, l_x1, l_z1);

mi_refreshview();
lamCount = lamCount + 1;
end

% draw BackIron %%%%%%%%%%%%%%%%%%%%%%%%%%%%%%%%%%%%-
bi_x1 = OutermagnetDia/2.0 + airGap + coilInnergap + coilHeight + coilOutergap;
bi_z1 = -(laminationWidth + spacer)/2.0;

bi_x2 = OutermagnetDia/2.0 + airGap + coilInnergap + coilHeight + coilOutergap + backIron;
```

```
bi_z2 = strokeLength*(poles+2) + (laminationWidth - spacer)/2.0 ;

mi_addnode(bi_x1, bi_z1) % bottom left
mi_addnode(bi_x1, bi_z2) % top left
mi_addsegment(bi_x1, bi_z1, bi_x1, bi_z2)

mi_addnode(bi_x2, bi_z2); % top right
mi_addsegment(bi_x1, bi_z2, bi_x2, bi_z2);

mi_addnode(bi_x2, bi_z1) % bottom right
mi_addsegment(bi_x2, bi_z2, bi_x2, bi_z1);
mi_addsegment(bi_x2, bi_z1, bi_x1, bi_z1);
mi_refreshview();

end
```

Block properties function

```
function blockProperties = blockProperties()
global spacer magnetHeight alumDrumthickness backIron turns OutermagnetDia InnermagnetDia
coilWidth coilHeight poles airGap strokeLength magnetType copper lamSteel alum coilInnergap
coilOutergap laminationGap laminationWidth
phase = 1;
%set block properties for boundary
mi_clearselected();
boundary_x1 = InnermagnetDia/4.0;
boundary_z1 = (poles+2)*strokeLength;
mi_addblocklabel(boundary_x1, boundary_z1) ;% Find the boundary region
mi_selectlabel (boundary_x1, boundary_z1); %select the magnet center label
mi_setblockprop('Air', 1, 'triangle', '', 0, 0 , 0); %Set boundary dimension as air
mi_clearselected();
%set block properties for magnet
direction = 90;
magnetCount = 0;
for n=1:poles+1 %Number of poles loop
direction = -direction;
mi_clearselected();
magnet_x1 = (InnermagnetDia + OutermagnetDia)/4.0; %Find the x axis location of the magnet center
magnet_z1 = strokeLength*magnetCount + magnetHeight/2.0; %Find the z axis location of the magnet
center
mi_addblocklabel(magnet_x1 , magnet_z1) ;% Magnet center
mi_selectlabel (magnet_x1 , magnet_z1); %select the magnet center label
mi_setblockprop(magnetType, 1, 'triangle', '', direction, 1 , 0); %Set magnet material
mi_clearselected();
magnetCount = magnetCount + 1;
end
%set block properties for magnet rectangle
magnetCount = 0;
for n=1:poles+1
magnetrect_x1 = InnermagnetDia/2.0;
magnetrect_x2 = OutermagnetDia/2.0;
magnetrect_z1 = strokeLength*magnetCount;
```

```
magnetrect_z2 = magnetHeight + strokeLength*magnetCount;
mi_selectrectangle(magnetrect_x1, magnetrect_z1,magnetrect_x2, magnetrect_z2, 1); % Magnet
rectangle
magnetCount = magnetCount + 1;
end
mi_setgroup(1); %Set the group of magnets to 1
%set block properties for spacers
spacerCount = 0;
for n=1:poles
mi_clearselected();
spacercenter_x1 = (InnermagnetDia + OutermagnetDia)/4.0; %Find x axis space center
spacercenter_z1 = strokeLength*spacerCount + magnetHeight + spacer/2.0;%Find z axis space center
mi_addblocklabel(spacercenter_x1 , spacercenter_z1) ;% Spacer center
mi_selectlabel (spacercenter_x1, spacercenter_z1); %select the spacer center label
mi_setblockprop('Air', 1, 'triangle', '', 0, 1 , 0); %Set spacer material as air
mi_clearselected();
spacerCount = spacerCount + 1;%Set the group of spacers to 1
end
%set block properties for spacer rectangle
spacerCount = 0;
for n=1:poles
spacerrect_x1 = InnermagnetDia/2.0;
spacerrect_x2 = OutermagnetDia/2.0;
spacerrect_z1 = strokeLength*spacerCount + magnetHeight;
spacerrect_z2 = strokeLength*(spacerCount+1);
mi_selectrectangle(spacerrect_x1, spacerrect_z1, spacerrect_x1 , spacerrect_z2, 1); % Magnet rectangle
spacerCount = spacerCount + 1;
end
mi_setgroup(1);
% Set alum drum properties
mi_clearselected();
alumcenter_x1 = InnermagnetDia/2.0 - alumDrumthickness/2;
alumcenter_z1 = (strokeLength*(poles+1)-spacer)/2;
mi_addblocklabel(alumcenter_x1,alumcenter_z1) ;% Alum drum center
mi_selectlabel (alumcenter_x1, alumcenter_z1); %select the Alum drum center label
mi_setblockprop(alum, 1, 'triangle', '', 0, 0 , 0);
mi_clearselected();
%set block properties for alum rectangle
alumCount = 0;
alumrect_x1 = InnermagnetDia/2.0 - alumDrumthickness;
alumrect_x2 = InnermagnetDia/2.0;
alumrect_z1 = 0;
alumrect_z2 = strokeLength*(poles+1)-spacer;
mi_selectrectangle(InnermagnetDia/2.0 - alumDrumthickness, 0,InnermagnetDia/2.0,
strokeLength*(poles+1)-spacer, 1 ); % Magnet rectangle
alumCount = alumCount + 1;
mi_setgroup(1); %Set the aluminium drum  to 1
% Set Coil properties
%mi_addcircprop('Coil circuit', 0, 1) ;% Coil circuit properties
coilCount = 0;
for n=1: (poles+2)*phase
turns = -turns;
mi_clearselected();
coilcenter_x1 = OutermagnetDia/2.0 + airGap + coilInnergap + coilHeight/2.0; %Coil x axis center
```

```
coilcenter_z1 = strokeLength/phase*coilCount+ - (laminationWidth + spacer)/2.0 + laminationWidth +
laminationGap + coilWidth/2.0; %Coil z axis center
mi_addblocklabel(coilcenter_x1 , coilcenter_z1); % coil center
mi_selectlabel (coilcenter_x1, coilcenter_z1); %select the coil center label
mi_setblockprop(copper, 1, 'triangle', 'Coil circuit', 0, 0 , turns); %Set number of turns
coilCount = coilCount+1;
end

%-Set Lamination properties
lamCount = 0;
for n=1: (poles+2)*phase+1
mi_clearselected();

lamcenter_x1 = OutermagnetDia/2.0 + airGap + coilInnergap + coilHeight/2.0; %Lamination x axis center
lamcenter_z1 = strokeLength/phase*lamCount - (laminationWidth + spacer)/2.0 + laminationWidth/2.0;
%Lamination z axis center

mi_addblocklabel(lamcenter_x1, lamcenter_z1); % lam center
mi_selectlabel (lamcenter_x1 , lamcenter_z1 ); %select the lam center label
mi_setblockprop(lamSteel, 1, 'triangle', '', 0, 0 , 0); %Set lamination material as air
lamCount = lamCount+1;
end

% Set backiron properties
mi_clearselected();

bicenter_x1 = OutermagnetDia/2.0 + airGap + coilInnergap + coilHeight + coilOutergap + backIron/2.0;
bicenter_z1 = (poles+2)/2*strokeLength;

mi_addblocklabel(bicenter_x1, bicenter_z1) ;% backIroncenter
mi_selectlabel (bicenter_x1, bicenter_z1 ); %select the backIron center label
mi_setblockprop(lamSteel, 1, 'triangle', '', 0, 0 , 0);%Set backIron material as air

mi_clearselected();
end
```

Generate flux files

```
function generateFluxfiles = generateFluxfiles(a,x)
global spacer OutermagnetDia coilWidth coilHeight poles airGap strokeLength coilInnergap
laminationWidth
global wireGauge;
phase = 1;
wireGauge = 2;
mi_setfocus(a); % Iron core Model
number = 1; %Create Loop for moving translator 0.5mm increments for total of 33mm
while (number <= strokeLength*2+1) %%CHANGE THIS
    mi_analyze(1); %run analysis
    mi_loadsolution(); %Loads the solution
    coilCount = 0;
    for k=1: (poles+2)*phase %Single or three phase
        fileName = fullfile(GSA1000SobolSet\', sprintf('Coil%dN%dAxial%dRow.txt',k,number, x));
        handle=fopen(fileName,'w'); %Creates Txt file of Normal Flux Values at coil ij
```

```
        mt = []; % create the matrix
        mt_col=[];
        for i=1:1:coilWidth/wireGauge
            %Go through each turn in the windings
            mo_clearcontour();
            %Set the line for which flux linkage needs to be calculated
            line_x1 = 0;
            line_x2 = OutermagnetDia/2.0 + airGap + coilInnergap + wireGauge/2.0;
            line_z1 = strokeLength/phase*coilCount + (lamination Width -spacer )/2.0 + wireGauge/2.0 +
wireGauge*(i-1);
            line_z2 = strokeLength/phase*coilCount + (lamination Width - spacer)/2.0 + wireGauge/2.0 +
wireGauge*(i-1);
            mo_addcontour(line_x1 ,line_z1);
            mo_addcontour(line_x2, line_z2);

            for j=1:1:coilHeight/wireGauge
                mo_addcontour(OutermagnetDia/2.0 + airGap + coilInnergap + wireGauge/2.0 + wireGauge*(j-
1), strokeLength/phase*coilCount  + (lamination Width - spacer)/2.0 + wireGauge/2.0 + wireGauge*(i-1));
                flux_linkage =  mo_lineintegral(0); %Determine the flux linkage at the line

                mt(i,j)=[flux_linkage(1)];
                fprintf(handle,num2str(flux_linkage(1)));  %Write it in the text file
                %write(handle,mt[i][j])
                if j ~= coilHeight/wireGauge
                    %write(handle,'','')
                    fprintf(handle,','); %Write the flux values in the text file
                end
            end

            fprintf(handle,'\n');
        end


        coilCount = coilCount + 1;
        fclose(handle);
    end
    number = number + 1 ;   %Increment Counter

    mi_seteditmode('group') ;
    mi_selectgroup(1);
    mi_movetranslate(0,0.5) ;   %Shifts Translator in group 1 up 0.5mm
end

mi_selectgroup(1);


end
```

Load flux files

```
function loadFluxfiles = loadFluxfiles(x)
% Load all the generated flux files as a 4D matrix (Winding/Stroke/Turn x, y
```

```
global fluxdatacoil poles coil_number strokeLength ;
coil_number = (poles+2)*1;
row = x;
%Go through the coils and stroke length
for coil = 1:coil_number
    for i=1: strokeLength*2+1
    fileName = fullfile('GSA1000SobolSet\', sprintf('Coil%dN%dAxial%dRow.txt',coil,i, row));
    matFileName = fileName;
    fluxdatacoil(coil, i,:,:) = csvread(matFileName); %Loads Data into 3D matrix
    end
end
clear i;
clear matFileName
end
```

Flux linkage calculations

```
function fluxLinkagecalculations = fluxLinkagecalculations()
global fluxdatacoil position strokeLength freq coil_number coilWidth coilHeight
fluxlinkagesumcoil_fwdbwd fluxlinkagesumcoil

global tn wireGauge
phase = 1;
position = [-strokeLength/2:.5:strokeLength/2]; %Stroke is in steps of 0.5mm
xn = [position,fliplr(position(1:length(position)-1))] ; %Position converted to reciprocating motion

t=1/(2*pi*freq)*acos(position/(strokeLength/2)); %Sinusoidal position referred back to find time
t = fliplr(t);%time in Secs
 tn = [t,t+1/freq/2];  % One full cycle time
tn(strokeLength*2+1) = [];
%Go through the flux files and separate it according to each winding
fluxlinkagesumcoil = [zeros(coil_number,strokeLength*2+1)];
for coil = 1: 1 :coil_number
    for k = 1:strokeLength*2+1
      for i=1:coilWidth/wireGauge
       for j=1:coilHeight/wireGauge
           fluxlinkagesumcoil(coil, k) = fluxdatacoil(coil,k,i,j) + fluxlinkagesumcoil(coil, k); %Sum the values of
the flux according to the windings
       end
      end
    end
end
fluxlinkagessumcoil_fwdbwd = [zeros(coil_number, strokeLength*4+1)]; %Make the flux sinusoidal by
adding for both directions of motion
%Make the flux files into complete cycle by adding forward and return
%stroke
for coil = 1: coil_number
    fluxlinkagesumcoil_fwdbwd(coil,:) = [fluxlinkagesumcoil(coil,:),fliplr(fluxlinkagesumcoil(coil,
1:length(fluxlinkagesumcoil(coil,:))-1))] ;
end


end
```

Voltage calculations

```
function voltageCalculations = voltageCalculations()

%Set the global variables to be used for this function
global voltagecoil strokeLength fluxlinkagesumcoil_fwdbwd coil_number Egen Totalvoltagenn
Totalvoltageeven
global freq tnn teven tn counterAG rmsOCVoltage

voltagecoil = [zeros(coil_number, strokeLength*4)];
%Use faradays law of electromagnetism
for coil = 1: coil_number
    voltagecoil(coil,:) = diff(fluxlinkagesumcoil_fwdbwd(coil,:))./diff(tn);
end

dir = -1;
Egen = [zeros(1, 4*strokeLength)];
%Sum of coil voltages is used to determine the OC voltage
for coil = 1:coil_number
    dir = -dir;
    Egen = voltagecoil(coil,:)*dir + Egen;
end

tnn=[tn(2:length(tn)), tn(2:length(tn))+1/freq, tn(2:length(tn))+2/freq]; % Make three cycles
Totalvoltagenn = [Egen, Egen, Egen]; %Three cycles

teven = [0:1/1.25e6:3*1/freq]; %1.25MHz sample rate
%Interolation to achieve better resolution
Totalvoltageeven = interp1(tnn,Totalvoltagenn,teven);
Totalvoltageeven = Totalvoltageeven(~isnan(Totalvoltageeven))';
%Added to incorporate the difference between FEMM and Experiment
Totalvoltageeven = Totalvoltageeven*0.8;
%RMS calculation of the OC voltage
rmsOCVoltage(counterAG) = rms(Totalvoltageeven);
end
```

Generate FFT from open circuit voltage

```
function EgenFFT = EgenFFT()
global Fs tfft teven xfft x1fft x2fft X2FFT f2 freq FFTtable THD iFFT Totalvoltageeven iFFT1 counterAG
FFTtable1
Fs = 1.25e6;
tfft=teven(1:size(Totalvoltageeven));

xfft = Totalvoltageeven'; %input data

%Perform FFT on the voltage to find the harmonics
x1fft = xfft.*hanning(length(xfft))';
x2fft=[x1fft zeros(1,Fs*4-length(x1fft))];
X2FFT = fft(x2fft);
f2 = ((1:length(x2fft)) - 1)/length(x2fft)*Fs;

%FFT of upto 15 harmonics are determined
```

```
FFTtable = [1:15];
FFTtable(2,:) = FFTtable(1,:) * freq;
FFTtable(3,:) = abs(X2FFT(freq*FFTtable(1,:)*length(x2fft)/Fs+1))/(length(xfft)/4);
FFTtable(4,:) = angle(X2FFT(freq*FFTtable(1,:)*length(x2fft)/Fs+1));
FFTtable(5,:) = FFTtable(3,:) / FFTtable(3,1); % Percent of Fundamental Distortion
THD = FFTtable(3,:);
THD(1) = [];
THD = rssq(THD)/FFTtable(3,1); %root sum of squares / fundamental
FFTtable = FFTtable';
FFTtable1(counterAG,:) = FFTtable(:,5);


iFFT = 0;
%Reverse of FFT is done to cross check the EMF voltage
for k=1:size(FFTtable,1)
    iFFT = iFFT + FFTtable(k,3)*cos(2*pi*FFTtable(k,2)*tfft+FFTtable(k,4));
end

end
```

Load the PMLG system

```
function voltageLoadcalculationsAG = voltageLoadcalculationsAG()
global r_mac L_mac FFTtable omega Z Z_angle Xl I_harmonic I_harmonic_angle Vl_harmonic
Vl_harmonic_angle Vl tfft freq
global Vl_waveform Il Pl  Pl_max RL counterAG  indice Vl_max_waveform Il_max_waveform Il_waveform
global EM_Power EM_force position velocity OCVoltage LoadvoltageMax LoadcurrentMax
Totalvoltageeven
resistances = RL(2);
inductances = RL(3);
r_mac = resistances(1); %Ohm
L_mac = inductances(1); %H

i=1;
Vl_waveform = [];
for Rl = 0.1:0.1:50 %resistance from 0.1Ohm to 50Ohm - Load

omega = 2*pi*FFTtable(:,2);
Xl = omega*L_mac; %Inductive reactance
Z = sqrt((Rl+r_mac)^2+Xl.^2); %Impedance
Z_angle = atan(Xl/(Rl+r_mac)); %Impadance angle

%Current calculation from the harmonics of OC voltage and load
for q=1:size(FFTtable,1)
    I_harmonic(q) = FFTtable(q,3)/Z(q); %Current in A
    I_harmonic_angle(q) = FFTtable(q,4)-Z_angle(q); %Current angle
end


Vl_harmonic = I_harmonic.*Rl; %Harmonics of the voltage load
Vl_harmonic_angle = I_harmonic_angle; %Angle of voltage harmonics same as current harmonics

Vl=0;
```

```
%Load voltage from the FFT harmonics
for q=1:size(FFTtable,1)
    Vl = Vl + Vl_harmonic(q)*cos(2*pi*FFTtable(q,2)*tfft+Vl_harmonic_angle(q)); %Calculate the voltage
load from the harmonics
end

Il = 0;
for q=1:size(FFTtable,1)
    Il = Il + I_harmonic(q)*cos(2*pi*FFTtable(q,2)*tfft+I_harmonic_angle(q)); %Calculate the current load
from the harmonics
end

Vl_waveform(i,:)=Vl(1,:)';
Il_waveform(i,:) = Il(1,:)';
Pl(i) = rms(Vl)^2/Rl; %Power calculation
[Pl_max12, Pl_max_indice] = max(Pl); %Determine the maximum from the array
indice = Pl_max_indice;
Pl_max(counterAG) = max(Pl);
i = i+1;
end
rload = [0.1:0.1:25];

%Calculate the position, velocity, force, OC voltage, load voltage and currents
Vl_max_waveform = Vl_waveform(indice,:);
Il_max_waveform = Il_waveform(indice,:);
EM_Power = (Vl_waveform(indice,:).*Il_waveform(indice,:));
position = 16.5e-3*sin(2*pi*freq*tfft);
velocity = rms(gradient(position)./gradient(tfft));
EM_force(counterAG) = mean(EM_Power)/velocity;
OCVoltage(counterAG) = rms(Totalvoltageeven);
LoadvoltageMax(counterAG) = rms(Vl_max_waveform);
LoadcurrentMax(counterAG) = rms(Il_max_waveform);
end
```

Theoretical modeling harmonics – Chapter 4

S.No	Freq	Value	Angle	Percentage
1	80	251.7994	-1.35152	1
2	160	5.161742	-1.14064	0.020499
3	240	66.64833	2.268371	0.264688
4	320	1.94945	2.510945	0.007742
5	400	19.45342	2.674786	0.077258
6	480	0.300602	2.907454	0.001194
7	560	6.070302	0.093075	0.024108
8	640	0.202541	0.258746	0.000804

9	720	3.780298	0.475137	0.015013
10	800	0.202855	-2.33676	0.000806
11	880	1.140036	-2.23084	0.004528
12	960	0.114151	-1.64747	0.000453
13	1040	0.603316	-2.07959	0.002396
14	1120	0.079361	0.191521	0.000315
15	1200	0.446171	2.326465	0.001772

Neutral position – Chapter 5

Axial arrangement

Harmonics of the OC voltage for a neutral position of 0 mm

Harmonic	Frequency	Harmonic Value	Harmonic Angle	Percentage of Fundamental
1	80	132.9355	-1.359	1
2	160	3.823618	-1.16659	0.028763
3	240	15.74523	2.327476	0.118443
4	320	0.316713	2.929776	0.002382
5	400	11.48258	2.69804	0.086377
6	480	0.365859	3.117936	0.002752
7	560	3.892909	3.039579	0.029284
8	640	0.080234	-2.45692	0.000604
9	720	0.404173	1.638287	0.00304
10	800	0.034289	-0.07644	0.000258
11	880	0.830058	1.166372	0.006244
12	960	0.024413	-0.83323	0.000184
13	1040	0.538508	1.618931	0.004051
14	1120	0.055248	1.311599	0.000416
15	1200	0.233657	2.416854	0.001758

Harmonics of the OC voltage for axial arrangement for a neutral position of 17 mm

Harmonic	Frequency	Harmonic Value	Harmonic Angle	Percentage of Fundamental
1	**80**	**2.81354**	**1.890249**	1
2	160	109.0378	-1.15168	38.75468
3	240	7.158695	-0.91232	2.544373
4	320	38.93989	2.578818	13.84018
5	400	4.741963	2.758221	1.685408
6	480	19.00331	-0.28133	6.754236
7	560	3.365967	0.02282	1.196346
8	640	11.81538	-2.767	4.199472
9	720	2.467072	-2.61072	0.876857
10	800	5.665462	0.668102	2.013642
11	880	1.667945	0.968766	0.592828
12	960	3.941247	-1.91409	1.400814
13	1040	1.115934	-1.70794	0.39663
14	1120	1.836223	1.76383	0.652638
15	1200	0.679536	1.942321	0.241524

Radial arrangement

Harmonics of the OC voltage for a neutral position of 0 mm

Harmonic	Frequency	Harmonic Value	Harmonic Angle	Percentage of Fundamental
1	80	4.985642	-1.34943	1
2	160	147.5777	1.93515	29.60054
3	240	1.337368	2.221085	0.268244
4	320	46.07953	2.23173	9.242448

5	400	0.55893	2.57404	0.112108
6	480	7.550562	1.376645	1.514461
7	560	0.066287	1.997945	0.013296
8	640	8.85806	0.696284	1.776714
9	720	0.059043	3.057323	0.011843
10	800	4.859258	0.989071	0.97465
11	880	0.038686	1.235335	0.007759
12	960	1.658285	1.217251	0.332612
13	1040	0.117437	1.435538	0.023555
14	1120	0.48158	0.311141	0.096593
15	1200	0.026648	-1.53298	0.005345

Harmonics of the OC voltage for a neutral position of 17 mm

Harmonic	Frequency	Harmonic Value	Harmonic Angle	Percentage of Fundamental
1	80	177.5818	-1.34428	1
2	160	13.21917	-1.13093	0.07444
3	240	110.7305	2.26388	0.623546
4	320	11.37235	2.508275	0.06404
5	400	59.09642	-0.41119	0.332784
6	480	9.313281	-0.19305	0.052445
7	560	34.96147	-3.09211	0.196875
8	640	7.127137	-2.85844	0.040134
9	720	20.60189	0.518703	0.116014
10	800	5.061755	0.75236	0.028504
11	880	12.11553	-2.16647	0.068225
12	960	3.665402	-1.95472	0.020641
13	1040	6.699707	1.451795	0.037727
14	1120	2.211332	1.715771	0.012452
15	1200	3.72046	-1.22958	0.020951

MATLAB code to create the sobol sequence – Chapter 6

```
clear all
PS= xlsread('Sobol1.xlsx'); %Load the sobol sequence
comp_PS = xlsread('Sobol2.xlsx'); %Load the complementary sobol sequence
a = [PS1; comp_PS];
N = 1000; %total number of test points
kp = [1 1 1 1 1 1 1 1];
n_base = floor(1000/8); %For 125 test points
n_p = 8;
outputVariables=[];
%Use the sobol and complementary sobol to create 1000 different data
%points
kp1 = [comp_PS(1:125,1) PS(1:125, 2:8)];
kp2 = [PS(1:125,1), comp_PS(1:125,2) PS(1:125, 3:8)];
kp3 = [PS(1:125,1:2), comp_PS(1:125,3) PS(1:125, 4:8)];
kp4 = [PS(1:125,1:3), comp_PS(1:125,4) PS(1:125, 5:8)] ;
kp5 = [PS(1:125,1:4), comp_PS(1:125,5) PS(1:125, 6:8)] ;
kp6 = [PS(1:125,1:5), comp_PS(1:125,6) PS(1:125, 7:8)];
kp7 = [PS(1:125,1:6), comp_PS(1:125,7) PS(1:125, 8)];
kp8 = [PS(1:125,1:7), comp_PS(1:125,8)];

%Final output Sobol sequence used for the study
outputVariables = [kp1; kp2; kp3; kp4; kp5; kp6; kp7; kp8];
```

GA code for Neural Network model

```
clc
rng default % For reproducibility
FitnessFunction = @objfun; %Fitness function is the objective function
ConstraintFunction = []; %No constraints
numberOfVariables = 1;
lb = [1];
ub = [100];

%Optimization routine implementation using optimization options and genetic algorithm
opts = optimoptions(@ga, 'UseParallel', true, 'UseVectorized', false,
'PopulationSize',10,'MaxGenerations',50,'MaxStallGenerations',10, 'Display','iter','PlotFcn', {@gaplotbestf,
@gaplotbestindiv, @gaplotscores, @gaplotselection, @gaplotmaxconstr, @gaplotdistance,
@gaplotselection });
[x,fval,exitflag, output] = ga(FitnessFunction,numberOfVariables,[],[],[],[],lb,ub,ConstraintFunction,opts);
```

Objective function (NN code)

```
%%%%%%%%%%%%%%%%%%%%%%%%%%%%%%%%%%%%%%%%%%%%%%%%%%%%%%%%%%%%%%%%
%%%% OVERALL NEURAL NETWORK MODEL %%%%%%%%%%
%%%%%%%%%%%%%%%%%%%%%%%%%%%%%%%%%%%%%%%%%%%%%%%%%%%%%%%%%%%%%%%%
function error10Percentage = objfun(x)

    load('ODMagnetSpacerSobol.mat') %Load the dataset
    input2 = [ODMagnetSpacer]';
```

```
    output2 = PlmaxODMagnetSpacer';
    neurons = round(x);
    net2 = fitnet(neurons,'trainbr'); %Bayesian training optimization
    net2.trainParam.goal=1e-6;
    net2.performFcn='msereg'; %Mean squared error
    net2 = train(net2,input2,output2); %Train the model
    y = net2(input2); %Determine the output
    perf = perform(net2,y,output2); %Perform NN model
    c = sim(net2,input2); %Predict the output
    answer = output2;
    error = (answer - c)*100./answer; %Calculate the error
    ylim([-100,100])
    errorAbs = abs(error); %Calculate the absolute error
    error10Percentage = (sum(errorAbs>10)*100/1000);

end
```

Optimization function for MOO – Chapter 6

Main function

```
rng default % For reproducibility
clc
global x fval

FitnessFunction = @objfun8_variables;
ConstraintFunction = @volumeConstraint7;
numberOfVariables = 8;

%%%%%%%%%%%%%%%%%%%%
% Magnet Thickness
% Outer Diameter of the magnet
% Spacer
%%%%%%%%%%%%%%%%%%%%
lb = [25, 1, 80, 2, 2, 1, 20, 20];
ub = [500, 1, 80, 10, 10, 5, 500, 50];

mutationRate = 0.02; %Mutation ratio is 0.02
%Optimization is multi objective optimization
opts = optimoptions(@gamultiobj, 'MutationFcn', {@mutationadaptfeasible,
mutationRate},'CrossoverFcn',{@crossoverheuristic},'ParetoFraction',0.5, 'UseParallel', true ,
'UseVectorized', false,  'PopulationSize',350,'MaxGenerations',200,'MaxStallGenerations',10,
'Display','iter', 'PlotFcn', {@gaplotpareto});
[x,fval,exitflag, output] =
gamultiobj(FitnessFunction,numberOfVariables,[],[],[],[],lb,ub,ConstraintFunction,opts)
```

Objective function

```
function y = objfun6_variables(x)
global net
load('Global1net.mat') %load the NN model
%Parameters
OD = x(1); %Outer diameter
AG = x(2); %Air gap
freq = x(3);%Frequency
mt = x(4);%Magnet thickness
poles = ceil(x(5));%Poles
spacer = x(6);%Spacer
turns = x(7);%Turns
stroke = x(8);%Stroke
strokeLength = stroke;
OutermagnetDia = OD;
magnetthick = mt;
testInput1 = [OD AG freq mt poles spacer turns];
testErrorEfficiency  = 500
%Used to take account of the error in NN model
Plmax1 = stroke * 0.7* sim(net,testInput1')*0.70/33 - testErrorEfficiency ;
Plmax = Plmax1;
y(1) = 1000 - Plmax;%First variable in optimization

%Calculate the weight
magnetHeight = strokeLength - spacer;
InnermagnetDia = OutermagnetDia - 2*magnetthick;
densityMagnet = 7500; %Kg/m3
densityAlum = 2800; %Kg/m3
densitySteel = 7500; %Kg/m3
densityABSplastic = 1000; %Kg/m3
%Magnet mass
ODmagnetVolume = pi*(OutermagnetDia^2/4)*magnetHeight; %mm3
IDmagnetVolume = pi*(InnermagnetDia^2/4)*magnetHeight; %mm3
magnetVolume = ODmagnetVolume - IDmagnetVolume; %mm3
magnetMass = magnetVolume*densityMagnet*(poles+1)/10^9;

%ALuminium mass
alumDrumOD = InnermagnetDia;
alumThickness = 1;
alumDrumID = alumDrumOD - 2*alumThickness;
alumHeight = poles*strokeLength + magnetHeight;
ODalumDrumVolume =  pi*(alumDrumOD^2/4)*alumHeight; %mm3
IDalumDrumVolume =  pi*(alumDrumID^2/4)*alumHeight; %mm3
alumDrumVolume = ODalumDrumVolume - IDalumDrumVolume;
alumDrumMass = alumDrumVolume*densityMagnet/10^9;

%Aluminium shaft mass
if alumDrumID<15
    alumshaftDia = alumDrumID;
else
    alumshaftDia = 15;
end
alumShaftlength = strokeLength*4*poles;
alumshaftVolume = pi*alumshaftDia^2*alumShaftlength/4;
alumshaftMass = alumshaftVolume*densityAlum/10^9;
```

```
alumMass = alumDrumMass + alumshaftMass;

%Spacer mass
ODspacerVolume = pi*(OutermagnetDia^2/4)*spacer; %mm3
IDspacerVolume = pi*(InnermagnetDia^2/4)*spacer; %mm3
spacerVolume = ODspacerVolume - IDspacerVolume; %mm3
spacerMass = spacerVolume*densityABSplastic*(poles)/10^9;

%Total mass
totalMass = alumMass + magnetMass + spacerMass;
y(2) = totalMass; %Second variable in optimization

%Volume calculations
totalLength = (strokeLength*(poles+2))*3;

coilWidth = floor(strokeLength - 3);
coilHeight = (ceil(turns) * 4)/(coilWidth);

statorOD = OutermagnetDia + 2*AG + 2*coilHeight + 2*3;

volume = statorOD^2 * pi * totalLength/4;
y(3) = volume/1e9;%Third variable in optimization
end
```

Volume constraint – Chapter 6

```
function [c, ceq] = volumeConstraint7(x)

OD = x(1); %Outer diameter
AG = x(2); %Airgap
freq = x(3); %frequency
mt = x(4); %Magnet thickness
poles = ceil(x(5));%Poles
spacer = x(6);%spacer
turns = x(7);%Turns
strokeLength = x(8);%Stroke length
OutermagnetDia = OD;
magnetthick = mt;

magnetHeight = strokeLength - spacer;
InnermagnetDia = OutermagnetDia - 2*magnetthick;
%Densities of the materials
densityMagnet = 7500; %Kg/m3
densityAlum = 2800; %Kg/m3
densitySteel = 7500; %Kg/m3
densityABSplastic = 1000; %Kg/m3
%Magnet mass
ODmagnetVolume = pi*(OutermagnetDia^2/4)*magnetHeight; %mm3
IDmagnetVolume = pi*(InnermagnetDia^2/4)*magnetHeight; %mm3
magnetVolume = ODmagnetVolume - IDmagnetVolume; %mm3
magnetMass = magnetVolume*densityMagnet*(poles+1)/10^9;
```

```
%Aluminium drum mass
alumDrumOD = InnermagnetDia;
alumThickness = 1;
alumDrumID = alumDrumOD - 2*alumThickness;
alumHeight = poles*strokeLength + magnetHeight;
ODalumDrumVolume =  pi*(alumDrumOD^2/4)*alumHeight; %mm3
IDalumDrumVolume =  pi*(alumDrumID^2/4)*alumHeight; %mm3
alumDrumVolume = ODalumDrumVolume - IDalumDrumVolume;
alumDrumMass = alumDrumVolume*densityMagnet/10^9;
%Aluminium rod mass
if alumDrumID<15
    alumshaftDia = alumDrumID;
else
    alumshaftDia = 15;
end
alumShaftlength = strokeLength*4*poles;
alumshaftVolume = pi*alumshaftDia^2*alumShaftlength/4;
alumshaftMass = alumshaftVolume*densityAlum/10^9;
alumMass = alumDrumMass + alumshaftMass;

%Spacer mass
ODspacerVolume = pi*(OutermagnetDia^2/4)*spacer; %mm3
IDspacerVolume = pi*(InnermagnetDia^2/4)*spacer; %mm3
spacerVolume = ODspacerVolume - IDspacerVolume; %mm3
spacerMass = spacerVolume*densityABSplastic*(poles)/10^9;
totalMass = alumMass + magnetMass + spacerMass;

%Linear generator volume
totalLength = (strokeLength*(poles+2))*3;
coilWidth = floor(strokeLength - 3);
coilHeight = (ceil(turns) * 4)/(coilWidth);
statorOD = OutermagnetDia + 2*AG + 2*coilHeight + 2*6;
volume = statorOD^2 * pi * totalLength/4;
c(1) = totalMass - 2 ;
c(2) = -1*(InnermagnetDia-5);
c(3) = volume/1e9 - 10e-3;
ceq = [];
end
```

MATLAB GUI – Chapter 6

```
% Button pushed function: StartOptimizationButton
function OptimizationGA(app, event)
power1 = app.PowerEditField.Value; %Get the power value from the app
mass1 = app.MassEditField.Value; %Get the mass value from the app
a = app.MagnetThicknessCheckBox.Value; %Check if the magnet thickness is checked
b = app.OuterDiameterofthemagnetCheckBox.Value; %Check if the magnet thickness is checked
c = app.SpacerCheckBox.Value; %Check if the spacer is checked
d = app.PolesCheckBox.Value; %Check if the pole is checked
e = app.FrequencyCheckBox.Value; %Check if frequency is checked
f = app.StrokeLengthCheckBox.Value; %Check if stroke length is checked
g = app.TurnsCheckBox.Value; %Check if turn is checked
```

```
poles = app.PolesEditField.Value;
frequency = app.FrequencyEditField.Value;.
stroke = app.StrokeEditField.Value;

%Get the lower and upper bound for the variables
lb_magnetThickness = app.LBEditField.Value;
ub_magnetThickness = app.UBEditField.Value;
lb_OD = app.LBEditField_2.Value;
ub_OD = app.UBEditField_2.Value;
lb_spacer = app.LBEditField_3.Value;
ub_spacer = app.UBEditField_3.Value;
lb_poles = app.LBEditField_4.Value;
ub_poles = app.UBEditField_4.Value;
lb_frequency = app.LBEditField_5.Value;
ub_frequency = app.UBEditField_5.Value;

lb_Stroke = app.LBEditField_6.Value;
ub_Stroke = app.UBEditField_6.Value;

lb_turns = app.LBEditField_7.Value;
ub_turns = app.UBEditField_7.Value;
airgap = app.AirgapEditField.Value;

%Depending on the checked box, run the appropriate genetic algorithm
if d==1 && e==0 && f==0 && g==0
    geneticAlgorithm4VariablesAppPoles(power1, mass1, lb_magnetThickness, ub_magnetThickness,
lb_OD, ub_OD, lb_spacer, ub_spacer, lb_poles, ub_poles, frequency, stroke, airgap);

elseif d==0 && e==1 && f==0 && g==0
    geneticAlgorithm4VariablesAppFrequency(power1, mass1, lb_magnetThickness,
ub_magnetThickness, lb_OD, ub_OD, lb_spacer, ub_spacer, lb_frequency, ub_frequency, poles, stroke,
airgap);
elseif d==0 && e==0 && f==1 && g==0
    geneticAlgorithm4VariablesAppStroke(power1, mass1, lb_magnetThickness, ub_magnetThickness,
lb_OD, ub_OD, lb_spacer, ub_spacer, lb_Stroke, ub_Stroke, poles, frequency, airgap);
elseif d==1 && e==1 && f==0 && g==0
    geneticAlgorithm5VariablesAppPolesFrequency(power1, mass1, lb_magnetThickness,
ub_magnetThickness, lb_OD, ub_OD, lb_spacer, ub_spacer, lb_poles, ub_poles, lb_frequency,
ub_frequency, stroke, airgap);
elseif d==1 && e==0 && f==1 && g==0
    geneticAlgorithm5VariablesAppPolesStroke(power1, mass1, lb_magnetThickness,
ub_magnetThickness, lb_OD, ub_OD, lb_spacer, ub_spacer, lb_poles, ub_poles, lb_Stroke, ub_Stroke,
frequency, airgap);
elseif d==0 && e==1 && f==1 && g==0
    geneticAlgorithm5VariablesAppFrequencyStroke(power1, mass1, lb_magnetThickness,
ub_magnetThickness, lb_OD, ub_OD, lb_spacer, ub_spacer, lb_frequency, ub_frequency, lb_Stroke,
ub_Stroke, poles, airgap);
elseif d==1 && e==1 && f==1 && g==0
    geneticAlgorithm6VariablesApp(power1, mass1, lb_magnetThickness, ub_magnetThickness, lb_OD,
ub_OD, lb_spacer, ub_spacer, lb_poles, ub_poles, lb_frequency, ub_frequency, lb_Stroke, ub_Stroke,
airgap);
elseif d==1 && e==1 && f==1 && g==0
```

```
    geneticAlgorithm6VariablesAppTurns(power1, mass1, lb_magnetThickness, ub_magnetThickness,
lb_OD, ub_OD, lb_spacer, ub_spacer, lb_poles, ub_poles, lb_frequency, ub_frequency, lb_Stroke,
ub_Stroke, airgap);
else
    geneticAlgorithm3VariablesApp(power1, mass1, lb_magnetThickness, ub_magnetThickness, lb_OD,
ub_OD, lb_spacer, ub_spacer, poles, frequency, stroke, airgap);
end

end
```

Results from Case 2 - Airgap 1.5 mm – Chapter 6

MT	OD	Spacer	Pole	Stroke	Power	Mass
7.244569	25.45899	2.483244	4	29.49537	47.64958	0.5416
8.837701	25.04461	3.710583	4	35.68072	61.4526	0.608555
9.738007	25.09259	3.95122	4	37.85977	177.9299	0.642318
9.408508	25.11436	3.772382	5	38.96978	337.8982	0.804406
9.827532	25.13011	3.682999	5	39.97491	410.6539	0.826414
9.692041	25.58178	3.44166	5	42.60746	471.0162	0.924943
9.848069	25.2365	3.984972	6	40.99831	620.0072	0.993932
9.637354	25.45678	3.406503	6	42.39261	648.3215	1.065058
9.759626	25.06712	4.640563	7	40.5471	753.4118	1.092076
9.955286	25.08955	5.439765	8	39.8745	918.5234	1.183941
9.80261	25.09711	4.806332	8	40.43252	932.0796	1.223471
9.909402	25.15719	3.844072	9	36.76782	1778.014	1.258181
9.988451	25.04593	5.772005	9	39.10806	1056.642	1.271991
9.831346	25.06643	3.468005	10	39.40337	2200.555	1.496119
9.643484	25.13834	4.449117	9	43.91046	1229.248	1.509373
9.972571	25.08622	4.556676	9	45.007	1342.828	1.534556
9.952761	25.04985	4.704431	10	44.63508	1517.229	1.66357
9.987886	25.2216	2.68132	9	49.54046	1606.978	1.782053
9.989444	25.48682	4.318902	10	48.07433	1726.068	1.884392
9.948704	25.51801	4.009527	10	48.79001	1764.016	1.931511
9.997483	25.20572	2.560147	10	49.99164	1867.532	1.981

Results from Case 3 - Airgap 1 mm – Chapter 6

OD	AG	Frequency	MT	Poles	Spacer	Turns	Stroke length	Power	Mass	Volume

25.21	1	80	6.46	3	2.26	93.79	30.96	84.26	0.45	0.00136
25.19	1	80	6.4	3	2.87	105.26	34.28	125.96	0.49	0.001481
25.32	1	80	6.85	3	1.83	93.7	35.16	186.95	0.52	0.001337
25.36	1	80	7.84	3	2.24	111.77	37.07	229.93	0.54	0.001558
25.29	1	80	8.21	3	2.6	126.94	39.46	287.52	0.57	0.001759
25.31	1	80	8.61	3	2.19	134.64	41.21	352.68	0.6	0.00185
25.34	1	80	8.3	3	2.44	151.52	43.61	434.47	0.64	0.002087
25.23	1	80	8.75	6	4.09	175.61	24.58	547.43	0.57	0.004659
25.19	1	80	9.71	7	4.67	197.11	21.7	665.05	0.54	0.006758
26.06	1	80	9.72	8	4.99	185.93	20.89	722.73	0.61	0.007278
25.35	1	80	9.57	7	4.42	187.88	23.83	798.04	0.62	0.005954
25.37	1	80	9.56	3	2.43	177.89	48.32	860.98	0.7	0.002406
25.38	1	80	9.4	3	1.21	187.22	49.49	938.08	0.74	0.002545
25.87	1	80	9.89	3	2.26	180.27	49.78	1016.52	0.76	0.002504
25.1	1	80	8.14	9	1.19	76.09	40.44	1104.13	1.5	0.002594
25.14	1	80	9.88	4	3.05	180.53	44.79	1161.08	0.79	0.002968
25.21	1	80	9.94	7	3.5	175.19	28.87	1226.57	0.78	0.004908
25.24	1	80	9.83	4	2.81	187.98	46.52	1278.01	0.83	-0.00694
25.29	1	80	8.99	9	1.13	69.32	45.12	1371.01	1.69	0.002542
25.5	1	80	9.89	5	1.89	154.57	49.02	1428.55	1.1	0.002955
25.75	1	80	9.95	4	2.61	190.57	49.66	1472.6	0.93	0.003148
25.11	1	80	9.89	5	3.29	177.5	46.03	1542.64	0.97	0.003329
25.42	1	80	9.93	5	2.45	164.94	49.38	1600.49	1.09	0.003142
25.33	1	80	9.84	5	2.62	198.88	46.03	1651.03	1	0.003758
25.07	1	80	9.62	8	1.22	110.01	45.61	1731.83	1.5	0.003158
25.23	1	80	9.8	6	2.91	154.96	48.95	1805.53	1.23	0.003409
25.07	1	80	9.91	6	2.62	167.14	45.75	1863.02	1.13	0.003651
25.08	1	80	9.87	6	3.21	176.96	46.08	1914.72	1.13	0.003785
25.15	1	80	9.86	6	3.06	173.68	48.11	2004.21	1.19	0.003723
25.27	1	80	9.94	6	2.47	165.73	48.99	2042.22	1.24	0.003639
25.48	1	80	9.6	10	1.17	73.38	42.37	2205.53	1.76	0.002836
25.27	1	80	9.42	9	1.27	115.69	46.05	2311.33	1.71	0.00359
25.14	1	80	9.97	7	1.86	151.87	49.18	2369.94	1.43	0.003702
25.15	1	80	9.92	8	2.45	145.24	45.81	2455.68	1.48	0.004011

25.32	1	80	9.91	8	1.87	136.67	47.9	2500.78	1.58	0.003826
25.19	1	80	9.8	9	1.27	114.98	47.98	2570.94	1.77	0.00364
25.41	1	80	9.96	8	1.73	136.9	49.69	2651.84	1.66	0.003836
25.06	1	80	9.95	8	1.98	147.92	49.81	2773.84	1.61	0.004057
25.48	1	80	9.79	10	1.3	99.62	45.45	2825.68	1.88	0.003545
25.11	1	80	9.98	9	2.89	136.02	48.41	2886.47	1.72	0.004143
25.03	1	80	9.98	10	1.54	138.87	43.93	2959.59	1.74	0.004597
25.07	1	80	9.95	10	1.75	139.86	44.87	3000.57	1.78	0.004626
25.14	1	80	9.86	10	1.66	116.66	46.63	3092.01	1.86	0.003975
25.1	1	80	9.9	10	1.74	118.79	47.19	3163.26	1.88	0.003997
25.11	1	80	9.99	10	1.65	120.85	47.26	3235.71	1.88	0.004058
25.11	1	80	9.99	10	1.65	120.35	48.26	3311.51	1.93	0.004071

Results from Case 3 - Airgap 1.5 mm – Chapter 6

OD	AG	Frequency	MT	Poles	Spacer	Turns	Stroke length	Power	Mass	Volume
25.15758	1.5	80	7.099868	3	2.328083	85.65442	30.3314	52.4962	0.433333	0.001271
25.57731	1.5	80	8.312525	3	1.651968	113.1262	37.6418	221.809	0.564943	0.001672
25.25431	1.5	80	8.507224	3	2.426949	136.1073	38.83003	265.4109	0.558044	0.001967
25.55396	1.5	80	8.567669	3	1.564341	125.0822	41.89612	322.5548	0.629912	0.001841
25.64559	1.5	80	8.96542	3	1.354272	137.4856	43.04918	393.0801	0.653698	0.001965
25.10979	1.5	80	9.831817	3	1.681539	141.9475	42.12503	424.5618	0.605616	0.001985
25.29007	1.5	80	9.757226	3	1.805415	151.0616	42.64556	500.8311	0.620972	0.002153
25.06371	1.5	80	9.600581	3	1.401652	156.0204	44.61839	573.7978	0.644485	0.0022
25.35914	1	80	9.043664	3	2.271301	167.8327	45.88752	637.6656	0.670147	0.002309
25.99335	1.5	80	9.616028	3	1.301283	158.3175	48.03331	689.6049	0.750196	0.002265
25.40181	1.5	80	9.863408	3	1.84296	165.7573	47.14779	749.6738	0.694445	0.002317
25.46021	1.5	80	9.869726	3	1.875244	170.5193	48.15234	817.4846	0.71265	0.002386
25.86914	1.5	80	9.995592	3	1.288905	168.2088	48.8151	866.9649	0.754295	0.002423
25.24259	1.5	80	9.859724	3	2.732705	197.3856	47.05324	911.7756	0.672632	0.002735
25.24524	1.5	80	9.966656	3	3.025521	206.0915	47.08963	964.0255	0.669198	0.002866
26.07505	1.5	80	9.686695	4	1.1419	161.8755	49.04006	1040.12	0.969009	0.002773
25.13242	1.5	80	9.850625	4	1.564225	170.8854	47.06503	1102.963	0.853796	0.002831
25.71104	1.5	80	9.784835	4	1.491727	168.7573	49.5249	1152.258	0.944461	0.002877

25.04998	1.5	80	9.841481	5	1.484384	155.2557	47.0575	1221.177	1.020166	0.003023
25.24016	1.5	80	9.862115	4	2.759699	196.5104	47.08954	1264.758	0.842543	0.003267
25.34173	1.5	80	9.902587	4	1.76251	182.1776	49.32365	1311.506	0.907918	0.003053
25.03173	1.5	80	9.982919	4	2.157452	185.1175	49.50624	1354.736	0.881964	0.003084
25.44049	1.5	80	9.970234	4	1.523312	190.9869	49.82291	1433.4	0.928342	0.003224
25.05713	1.5	80	9.828453	5	3.110673	180.9937	47.22722	1502.907	0.993878	0.003493
25.43806	1.5	80	9.947553	5	1.334431	166.9552	49.33394	1544.687	1.107646	0.003279
25.22725	1.5	80	9.95188	5	3.095348	186.2289	47.22426	1591.864	1.007262	0.003626
25.24567	1.5	80	9.936222	5	1.855062	180.2745	49.27013	1678.563	1.07903	0.00351
25.39591	1.5	80	9.918996	8	1.458922	121.4406	47.17512	1728.43	1.581343	0.003558
25.55999	1.5	80	9.86059	6	1.589475	158.1378	49.61725	1782.167	1.30892	0.00362
25.25818	1.5	80	9.883242	6	2.135666	165.2099	49.18225	1855.161	1.253073	0.003694
25.41667	1.5	80	9.8042	7	1.790633	146.7898	48.57572	1905.741	1.443101	0.003777
25.48383	1.5	80	9.771073	7	1.343116	148.7101	49.07972	1963.143	1.478538	0.003797
25.00505	1.5	80	9.907835	7	2.533547	154.1038	48.52355	2040.146	1.373496	0.0039
25.34732	1.5	80	9.999007	7	4.249991	166.2722	47.91017	2132.888	1.349281	0.004254
25.40681	1.5	80	9.912341	7	1.701978	157.0357	49.84008	2190.53	1.481607	0.004048
25.22589	1.5	80	9.932884	7	3.403857	181.4738	48.52141	2225.932	1.37649	0.004561
25.09579	1.5	80	9.988253	7	1.989928	162.493	49.37017	2252.581	1.421988	0.004082
25.23168	1.5	80	9.994732	7	2.733316	175.0707	49.26573	2314.926	1.415916	0.004392
25.21635	1.5	80	9.988919	8	1.583638	145.0542	49.45138	2378.322	1.630821	0.00414
25.08523	1.5	80	9.983548	8	3.832197	162.7908	48.26943	2408.157	1.510056	0.004523
25.3583	1.5	80	9.962186	9	1.786333	137.8425	48.47096	2497.167	1.790588	0.004357
25.10901	1.5	80	9.963343	9	3.558714	154.99	48.40053	2547.704	1.695699	0.00477
25.2453	1.5	80	9.970561	9	1.661779	140.3491	49.2841	2578.062	1.80846	0.004411
25.30844	1.5	80	9.986745	9	1.752252	140.4533	49.77105	2618.46	1.833285	0.004465
25.23639	1.5	80	9.956205	9	1.821034	153.1896	49.94338	2678.177	1.827183	0.00482
25.16212	1.5	80	9.946762	10	2.945318	143.9235	48.5105	2701.217	1.90028	0.004899